

Electronic Theses and Dissertations, 2020-

2021

Documenting Outdoor Simulated Scenes with Photogrammetry: Methods for Improving Dappled Lighting Conditions

Caroline Jasiak
University of Central Florida

 Part of the [Archaeological Anthropology Commons](#), and the [Biological and Physical Anthropology Commons](#)

Find similar works at: <https://stars.library.ucf.edu/etd2020>

University of Central Florida Libraries <http://library.ucf.edu>

This Masters Thesis (Open Access) is brought to you for free and open access by STARS. It has been accepted for inclusion in Electronic Theses and Dissertations, 2020- by an authorized administrator of STARS. For more information, please contact STARS@ucf.edu.

STARS Citation

Jasiak, Caroline, "Documenting Outdoor Simulated Scenes with Photogrammetry: Methods for Improving Dappled Lighting Conditions" (2021). *Electronic Theses and Dissertations, 2020-*. 1141.
<https://stars.library.ucf.edu/etd2020/1141>

DOCUMENTING OUTDOOR SIMULATED SCENES WITH PHOTOGRAMMETRY:
METHODS FOR IMPROVING DAPPLED LIGHTING CONDITIONS

by

CAROLINE CATHRYN JASIAK
B.S. Tulane University, 2018

A thesis submitted in partial fulfillment of the requirements
for the degree of Master of Arts
in the Department of Anthropology
in the College of Sciences
at the University of Central Florida
Orlando, Florida

Summer Term
2021

©2021 Caroline Jasiak

ABSTRACT

The primary goal of a forensic archaeologist is to reconstruct the context of scenes involving skeletal remains using recording and mapping methods. However, the outdoor locations of most forensic archaeology scenes can result in difficulties when recording and mapping scenes. While close-range photogrammetry (CRP) has been considered for documenting context of forensic sciences, this method lacks a sufficient procedural basis to guide data recording when encountering problematic environmental conditions. The purpose of this research is to test how light correction tools, a sheet and artificial lights, could improve harsh lighting conditions. Photographs were taken of controlled scenes with skeletal remains in open, dappled, and shaded lighting environments, and the models were processed using Agisoft® Metashape® Professional. Phase 1 tested three different scenarios with four different iterations while varying the light correction tools: (1) no artificial lighting tool; (2) only a sheet over the scene; (3) artificial lights placed around the scene; and (4) a combination of lights and sheet. The accuracy was assessed quantitatively, using the root-mean square (RMS) reprojection error and total scale bar error, and qualitatively. The results indicated that no significant quantitative accuracy of the model changed between iterations. However, the visual accuracy of the scene did improve with the sheet by decreasing shadows across the scene. Phase 2 tested two larger scenarios using the same four iterations. While the models were all highly accurate quantitatively, the iterations that included the sheet appeared to have fewer qualitative errors. Guidelines are provided to successfully use light correction tools to improve harsh lighting conditions of outdoor scenes.

ACKNOWLEDGEMENTS

This thesis is the product of many people's hard work and encouragement. First, I want to thank my parents, for always providing encouragement, allowing me to use their credit card to order takeout when I was too tired to cook, and answering my phone calls for questions about word choice at all hours of the night. I could not have done it without you two. Secondly, I would like to thank my brothers, Jay and Michael, for always being able to make me laugh. I want to especially thank my committee chair, and mentor, Dr. John Schultz for his guidance and support throughout this process. Additionally, I want to thank my other committee members Dr. John Walker and Dr. Scott Branting for ensuring that my research considers all aspects of archaeology. Thank you to John Guziejka of UCF Landscape and Natural Resources for allowing us access to the UCF Natural Lands for data collection. Then, I would like to thank Dominique Langis-Barsetti for her instructions and recommendations involving Agisoft®. I also need to thank all the UCF graduate students that helped me as my field aides during this process, even as they were working on their own theses. They include, Kelly McGehee, Horvey Palacios, Emily Barron, Megann Phillips, Brenna Raisor, and Hannah Haynes. Special thanks go out to Morgan Ferrell, whose support and help extended through all aspects of this thesis and is a large reason that it is finished. Last, but certainly not least, I want to thank Sirius for staying up and keeping me company through long nights of research. I cannot thank everyone on this page, and many more people, enough. Thanks!

TABLE OF CONTENTS

| | |
|--|------|
| LIST OF FIGURES | viii |
| LIST OF TABLES | xiii |
| CHAPTER ONE | 1 |
| CHAPTER TWO | 5 |
| Introduction | 5 |
| Literature Review | 6 |
| Traditional Mapping | 7 |
| 3D Mapping Technologies | 8 |
| 3D Digital Mapping Technology Comparison | 9 |
| Light in Outdoor Settings | 11 |
| Materials and Methods | 12 |
| Scene Materials..... | 12 |
| Field Technology | 15 |
| Scene Preparation and Data Collection | 17 |
| Field Scenarios | 21 |
| Photograph Processing | 24 |
| Processing Steps | 26 |
| Exports | 32 |
| Evaluating Error | 33 |
| Results | 34 |
| RMS Reprojection and Scale Bar Error | 35 |
| Qualitative Visual Accuracy..... | 36 |

| | |
|--|----|
| Scenario 1 (Open)..... | 37 |
| Scenario 2 (Shaded)..... | 45 |
| Scenario 3 (Dappled)..... | 53 |
| Discussion | 60 |
| RMS Reprojection and Scale Bar Error | 61 |
| Visual Accuracy | 62 |
| Lighting Correction Tools | 69 |
| Challenges and Limitations | 70 |
| Conclusion..... | 72 |
| CHAPTER THREE | 73 |
| Introduction | 73 |
| Materials and Methods | 76 |
| Scene Materials..... | 78 |
| Field Technology | 78 |
| Field Scenarios | 79 |
| Photograph Processing | 81 |
| Processing Steps | 82 |
| Exports..... | 85 |
| Evaluating Error | 85 |
| Results | 86 |
| RMS Reprojection and Scale Bar Error | 86 |
| Qualitative Visual Accuracy..... | 88 |
| Scenario 1 (Dappled)..... | 89 |

| | |
|--|-----|
| Scenario 2 (Open)..... | 98 |
| Discussion | 105 |
| RMS Reprojection and Scale Bar Error | 106 |
| Visual Accuracy | 107 |
| Evaluation of Goals | 115 |
| Challenges and Limitations | 116 |
| Guidelines..... | 121 |
| Conclusion..... | 124 |
| CHAPTER FOUR..... | 126 |
| Summary of Results | 127 |
| Challenges and Guidelines | 128 |
| Archaeological and Crime Scene Applications..... | 129 |
| Conclusion..... | 130 |
| APPENDIX: PROCESSING REPORTS..... | 132 |
| LIST OF REFERENCES | 294 |

LIST OF FIGURES

| | |
|--|----|
| Figure 1: (A) An image showing the lights set up in the field with their heights at the shortest setting. (B) An image of the back of the light panel showing the settings used when the lights were in use. | 17 |
| Figure 2: Diagram of view angles. (A) Image of view angle 1, which is described as kneeling while holding the camera at about waist height. This image was taken when the artificial lights were in use. (B) Image of view angle 2, which is described as kneeling while holding the camera at about chest height. This image was taken when only the sheet was in use. (C) Image of view angle 3, which is described as standing with the camera at about waist height. This image was taken when neither the lights nor the sheet were in use. (D) Image of view angle 4, which is described as standing with the camera at about chest height. This image was taken when only the sheet was in use. (E) Image of view angle 5, which is described as standing with the camera above head. This image was taken when neither the lights nor the sheet were in use..... | 19 |
| Figure 3: (A) Image showing how the closeup photographs were taken to capture the details of the clothing and skeletal elements. This image was taken when both the lights and the sheet were in use. (B) Image demonstrating how the overhead shots were taken using an extension pole held parallel to the scene. This image was taken when only the sheet was in use. | 20 |
| Figure 4: Workflow describing the data collection process followed in the field | 24 |
| Figure 5: Camera positions for Model 2A-1, which did not use the artificial lights or the sheet. Each of the blue rectangles represent the position and view angle at which each photograph was taken. The white arrow indicates a 1-meter scale bar. | 26 |

| | |
|---|----|
| Figure 6: Workflow describing the pre-processing and processing steps of Chapter 2..... | 28 |
| Figure 7: The sparse point cloud of Model 2C-1, which used the artificial lights. The sparse point cloud is generated when feature points are detected in the image and then tracked throughout the set. Then, the scene geometry is constructed using these points. The white arrow identifies a 1-meter-long scale bar..... | 29 |
| Figure 8: The dense point cloud of Model 2C-2, which included the artificial lights. The dense point cloud contains an enormous number of X, Y, and Z data points located close to each other. The white arrow indicates a scale bar that is 1-meter long. | 30 |
| Figure 9: The solid polygonal mesh of Model 2A-1, which did not include the artificial lights or the sheet. This polygonal mesh model is created by Metashape® using the point cloud information..... | 31 |
| Figure 10: Model 1A-2 orthomosaic without using the lights and sheet correction tools, and shadows from the artificial lights that were turned off. | 38 |
| Figure 11: Model 1B-1 orthomosaic using the sheet. | 39 |
| Figure 12: Model 1C-1 orthomosaic using the artificial lights. | 40 |
| Figure 13: Model 1D-2 orthomosaic using the sheet and artificial lights..... | 42 |
| Figure 14: Images of the cranial closeups from Scenario 1. (A) Model 1A-2 without using the light correction tools. (B) Model 1B-1 using the sheet. (C) Model 1C-1 using the artificial lights. (D) Model 1D-2 using the sheet and artificial lights. | 45 |
| Figure 15: Model 2A-1 orthomosaic without using the light correction tools and sheet tools, and shadows from trees overhead..... | 46 |
| Figure 16: Model 2B-1 orthomosaic using the sheet. | 48 |

| | |
|--|----|
| Figure 17: Model 2C-1 orthomosaic using the artificial lights that resulted in a few bright spots throughout the model (arrows). Note the distortion of the left arm bones in the northwest corner that resulted in the appearance of doubling. | 49 |
| Figure 18: Model 2D-2 orthomosaic using the sheet and artificial lights..... | 50 |
| Figure 19: Images of the cranial closeups from Scenario 2. (A) Model 2A-1 without using the light correction tools. (B) Model 2B-1 using the sheet. (C) Model 2C-1 using the artificial lights. (D) Model 2D-2 using the sheet and artificial lights | 52 |
| Figure 20: Model 3A-1 orthomosaic without using the lights and sheet tools. | 53 |
| Figure 21: Model 3B-2 orthomosaic using the sheet. | 55 |
| Figure 22: Model 3C-2 orthomosaic using the artificial lights. | 56 |
| Figure 23: Model 3D-1 orthomosaic using the sheet and artificial lights..... | 57 |
| Figure 24: Images of the cranial closeups from Scenario 3. (A) Model 3A-1 without using the light correction tools. (B) Model 3B-2 using the sheet. (C) Model 3C-2 using the artificial lights. (D) Model 3D-1 using the sheet and artificial lights. | 59 |
| Figure 25: Workflow describing the data collection process followed in the field. | 81 |
| Figure 26: Workflow describing the steps of processing in Agisoft Metashape®. | 82 |
| Figure 27: Model 2A-1 sparse point cloud. | 83 |
| Figure 28: The dense point cloud of Model 2A-1. Note the targets marked out on the scale bars surrounding the scene. | 84 |
| Figure 29: Model 1A-1 orthomosaic using no lights or sheet. Note the rib located in the grey circle is almost unidentifiable due to the ground surface-subject interface distortion. | 90 |
| Figure 30: Model 1B-1 orthomosaic using the sheet. | 91 |

| | |
|--|-----|
| Figure 31: Model 1C-2 orthomosaic using the artificial lights, with highly dappled lighting caused by trees. Note the scale bar within the circle that has distortion due to bright patches of light on the targets. | 93 |
| Figure 32: Model 1D-1 orthomosaic using lights and sheet. Note the minor distortion of the left scapula caused by subject-subject interface distortion between the bone and shirt (arrow). | 94 |
| Figure 33: Model 1E-1 orthomosaic using the lights, but with 40 photographs being taken each round instead of 30..... | 95 |
| Figure 34: Images of the screenshots of the crania from Scenario 1. (A) Model 1A-11 using no light correction tools. (B) Model 1B-1 using the sheet. (C) Model 1C-2 using the artificial lights. (D) Model 1D-1 with the lights and sheet. (E) Model 1E—1 using the artificial lights and 40 photographs per view angle..... | 98 |
| Figure 35: Model 2A-1 orthomosaic using no lights or sheet. Note the severe distortion of the rib that makes it appear as two separate parts (arrow). | 99 |
| Figure 36: A closeup of the severely disjointed rib found in the Model 2B-1 and other models Scenario 2..... | 100 |
| Figure 37: Model 2B-1 orthomosaic using the sheet. Note the severely distorted rib that appears straight due to ground surface-subject distortion (arrow)..... | 100 |
| Figure 38: Model 2C-3 orthomosaic using the artificial lights..... | 101 |
| Figure 39: Model 2D-1 orthomosaic including the lights and sheet..... | 102 |
| Figure 40: Images of the screenshots of the crania in Scenario 2. (A) Model 2A-1 using no light correction tools. (B) Model 2B-1 using the sheet. (C) Model 2C-3 using the artificial lights. (D) Model 2D-1 with the lights and sheet..... | 104 |

| | |
|---|-----|
| Figure 41: Image of the ground surface-subject interface distortion exhibited in Model 2B-1. | 114 |
| Figure 42: Image of the brightness located on the northeastern 0.5-meter scale bar in Model 1B-1..... | 114 |
| Figure 43: The orthomosaic of the scenario that was discarded due to severe wind. Note the distortion of the north arrow, which was not seen in previous models (circle). | 117 |
| Figure 44: Closeup view of the windy model exhibiting the distortion of the right arm bones and ribs..... | 117 |
| Figure 45: Closeup view of the windy model that clearly shows the leaves present on the femur after the wind blew them onto the bone..... | 118 |
| Figure 46: A screengrab image of Model 1C-2, which achieved better qualitative and quantitative accuracy than Model 1C-1. | 120 |
| Figure 47: A screengrab image of Model 1C-1, which does appear more grainy overall than Model 1C-2. | 120 |
| Figure 48: Workflow guidelines for implementing a light correction in the field..... | 124 |

LIST OF TABLES

| | |
|---|-----|
| Table 1: Inventory of the human skeletal elements used in the three scenarios. | 14 |
| Table 2: Descriptions and number of photographs for each view angle..... | 18 |
| Table 3: Information showing the naming process of each model to promote easier identification of specific models throughout this research..... | 23 |
| Table 4: Table providing the RMS Reprojection and total scale bar errors for all of the models. | 36 |
| Table 5: Comparison of the visual accuracies as seen across each model. The “Ortho” rows indicate how the discussion applies to the orthomosaics of each model, while “C-SS” stands for the cranial screenshots..... | 63 |
| Table 6: Inventory of the human skeletal elements used in the two scenarios. | 77 |
| Table 7: Information showing the naming process of each model to promote easier identification of specific models throughout this research..... | 80 |
| Table 8: Table showing the RMS Reprojection and total scale bar errors for all models. | 87 |
| Table 9: Comparison of the visual accuracies as seen across each model. The “Ortho” rows indicates how the discussion applies to the orthomosaics of each model, while “C-SS” stands for the cranial screenshots..... | 110 |

CHAPTER ONE

Many archaeological methodologies have been adopted for forensic applications. The largest field of integration is that of forensic archaeology. This field of study applies established archaeological methodologies to forensic casework (Dirkmaat & Adovasio, 1997; Mikhail et al., 2001; Linder, 2003; Schultz & Dupras, 2008; Dupras et al., 2012; Dirkmaat & Cabo, 2012; Christensen et al., 2014; Dirkmaat, 2015). One of the most important methodologies in both traditional archaeology and forensic archaeology is the inclusion of maps and documentation of context. More recently, digital recording methods have been employed in archaeological research; one of the more notable of these methods is that of photogrammetry (Fussell, 1982; Burtch, 2008; Barazzetti et al., 2011a; Barsanti et al., 2013; Howland et al., 2014). The use of photogrammetry, and more specifically close-range photogrammetry (CRP), is now commonly employed by archaeologists to accurately document and record their excavations; CRP has become a relatively well-defined technique for the archaeological field (Fussell, 1982; Burtch, 2008; Barazzetti et al., 2011a; Barsanti et al., 2013). However, the use of photogrammetry has not been employed regularly and is not well defined in the context of forensic investigations (Barazzetti et al., 2011a; Gonzalez-Jorge et al., 2012). Despite CRP accuracy being comparable to that of a total station, something which is regularly utilized by law enforcement and anthropological teams, the use of this technology is not a standardized investigative practice (Randles et al., 2010; Edelman & Aalders, 2018). This technique, if utilized, can be advantageous to the analysis of crime scenes by investigators because photogrammetry can be used to create a three-dimensional (3D) model of the scene. The model will include the accurate position of the physical remains, as well as preserve the context and association of the evidence in relation to the remains and other pieces of evidence (Ferrell, 2020).

In the pursuit of high-quality forensic archaeology research, the documentation of a forensic scene remains one of the most important aspects of a proper recovery. For years, this documentation has occurred through the creation of maps, both digital and hand-drawn, of the scenes. The accurate documentation of the scenes is necessary to preserve the context of the original scene, as the analysis of archaeological sites and forensic scenes is a destructive process (Dirkmaat & Adovasio, 1997; Schultz & Dupras, 2008; Dupras et al., 2012; Dirkmaat & Cabo, 2012; Christensen et al., 2014; Dirkmaat, 2015). Therefore, the implementation of accurate documentation techniques is a necessity when processing a scene and, at a minimum, will include a hand-drawn map to ensure the preservation of the context and position of the subject matter before the excavation. The most recent techniques include digital mapping, which uses technology and computer software to generate accurate 3D reconstructions on a computer. Commonly used digital mapping techniques as cited by current forensic archaeological literature include the total station, TRIMBLE R8 GPS unit, and global imaging (GIS) software (Schultz & Dupras, 2008; Dupras et al., 2012; Christensen et al., 2014; Dirkmaat, 2015). In the field of forensic archaeology, the use of CRP as another digital mapping technique has become a useful, though rarely used tool.

The use of mock scenes as more realistic representations of actual forensic scenes can result in the improvement of current CRP guidelines, resulting in an improved understanding of the limitations and benefits of this technology (Barazzetti et al., 2012; Gidusko, 2018; Ferrell, 2020). By using staged mock crime scenes, CRP environmental variables are more easily controlled, and are able to be tested in an isolated environment resulting in specific guidelines that more explicitly address outdoor crime scene variables (Colwill, 2016; Gidusko, 2018; McCollum, 2020; Ferrell, 2020). These guidelines can be incorporated into future forensic

recovery protocols of human remains, and the creation of these guidelines will describe how to best map more complicated crime scenes. There are a large number of variables inherent in a crime scene; the number of variables is only exacerbated when the forensic scene is located outdoors. Weather, size and dispersal of the remains, and the scene's physical proximity to investigative resources can become problematic when documenting real-life scenes (Dirkmaat & Adovasio, 1997; Schultz & Dupras, 2008; Dupras et al., 2012; Dirkmaat, 2015). Therefore, as many variables as possible must be tested to determine how they affect the rendering of accurate models. However, the testing of multiple variables in one project is not scientifically sound; testing only one or two variables per study allows focus and variable control. A larger number of studies will allow for a complete set of guidelines to be written that address each of these numerous variables that investigators may encounter at actual forensic scenes (Gidusko, 2018; McCollum, 2020; Ferrell, 2020).

The variable that is directly tested in this research project is light. Natural light is a necessary, however unavoidable, component of outdoor crime scenes and therefore is something that must be addressed by photogrammetry users (Hochrein, 2003; Nedergaard et al., 2014; Colwill, 2016). Light is an important variable when recording scenes using CRP technology because the quality of available light can influence the positioning of shadows on detailed areas of the scene, can affect the shutter speed of the camera and therefore the number of objects that remain in focus in the photograph, and can influence the coloring of the overall model. By controlling for the volatility of the light source's influence, the CRP user can ensure a higher quality model and more accurate portrayal of the scene.

The purpose of this research is to improve the application of CRP to scenes involving uneven shadows that result from natural lighting. The lighting naturally occurring at the crime

scene cannot be easily controlled, but this research will attempt to provide guidance on how best to correct poor lighting in the field and during computer processing. Specifically, the first step of this project is an experimental phase, testing how the lighting correction tools of tarps and artificial lighting kits can be applied to small scenes. The second step of this project will be an application phase, where these lighting correction methods are applied to larger mock forensic scenes. Thirdly, the main overarching goal of this study is to develop improved guidelines to aid in the mitigation of problematic natural lighting effects experienced by CRP users in the field of crime scene investigation. To address these research goals, the data collection process of the thesis is divided into a Phase 1 experimental phase, and a Phase 2 application phase. The Phase 1 experimental phase involves smaller and more confined spaces to initially test how light correction tools affect scene quality. The Phase 2 application phase applies the light correction techniques to larger scenes that are more reminiscent of forensic outdoor scenes.

The thesis will be organized as two standalone chapters followed by a short discussion and conclusion chapter. Chapter 2 is a stand-alone chapter focusing on Phase 1 of the research project, while Chapter 3 addresses the Phase 2 aspect of the research project.

CHAPTER TWO

Introduction

The methodology of photogrammetry research has become an everchanging body of literature since its first applications. Initially, photogrammetry was conducted by taking overhead photographs and then developing these two-dimensional (2D) imaging sequences into 3D architectural reconstructions. These photographs could be taken from very tall ladders, using a hot-air balloon, or using an early airplane (Fussell, 1982). This provided the necessary overhead shots of large archaeological excavation sites that were then rendered into 3D models. The first documented application of photogrammetry methods was their use to record the ruins of Persepolis in 1885, and photogrammetry has proven to be a useful tool in preserving archaeological sites ever since (Carbonnell, 1968; Fussell, 1982). By 1961, close-range photogrammetry (CRP) was an emerging technique, which involved the photographs being taken on the ground and within a few feet of the scene instead of by airplanes or other long-distance photographic techniques (Burtch, 2008). The evolution of CRP technology has advanced along with computers, and now CRP models are rendered using computer software instead of hand-drawn maps. This allows for more accurate models and has expanded the technical applications of photogrammetry technology to address smaller objects.

Despite the advances made in the technology, methodology, and subjects of photogrammetry research, there is still a large gap in the literature when discussing the guidelines applied to smaller variables. Given that some photogrammetry settings are outdoors, the influence of natural variables must be addressed. Harsh lighting that affects the quality of produced models is a problem encountered by all users of photogrammetry, and there are a number of methods used in archaeology to control for lighting (Baltsavias, 1999; Ozbek et al.,

2010; Partsinevelos et al., 2014; Sapirstein, 2016). Artificial lights have been used to better illuminate indoor settings (Portalés et al., 2009; Teza et al., 2016). Tarps are also used by archaeologists to help block light when needed (McPherron et al., 2009). However, these practices have not extended to photogrammetry that is conducted at outdoor forensic scenes.

Outdoor forensic scenes are complex due to the number of environmental variables that exist, and because they are complicated by such variables, a degree of visual error will always occur when using photogrammetry. However, by continuing to investigate variables affecting photogrammetry model quality, the distortion caused may be minimized. The most tried and true method of scientific testing involves the experimentation of one variable in a small and controlled setting. Problems develop from a lack of published literature that directly addresses specific problematic variables encountered by outdoor photogrammetry users (Ferrell, 2020). The first phase of this thesis specifically addresses this lack of experimentation. By focusing on the isolated variable of light, this thesis will more accurately test how a white sheet, artificial lighting source, and both of these together affect the quality of a CRP model. Beyond producing high quality models, there are three goals of this research. The first is to experiment and determine if the light correction tools, sheet or artificial lights, are effective at reducing distortion caused by harsh lighting. The second goal is to test whether these techniques can then be realistically applied to large, real world forensic scenes. Third, guidelines will be produced to ensure that these practices can be easily integrated into photogrammetry practices when necessary.

Literature Review

Before the intricacies of current research can be addressed, the importance of traditional mapping and the evolution of 3D digital mapping technologies will be discussed. In addition to

discussing the origins of 3D mapping techniques, a comparison of three main technologies will occur: structure from motion technology, photogrammetry, and 3D scanners in archaeological settings. Then, the unique problem of lighting in outdoor settings will be discussed in archaeological and photogrammetry specific literature.

Traditional Mapping

The act of an archaeological excavation is an inherently destructive process, and harm to the site may occur during or after excavation (Al-kheder et al., 2008; Barazzetti et al., 2011b; Olson et al., 2013). Therefore, archaeologists must map the site throughout the excavation process to preserve the integrity of a site that may ultimately be ruined. Initially, this action involved hand-drawing maps and taking measurements of the scene to create an accurate scale (Dupras et al., 2012). This practice was adapted to forensic archaeology, as investigators realized that the context and association of the evidence in the initial scene was a vital aspect of the investigation process (Dirkmaat & Adovasio, 1997; Schultz & Dupras, 2008; Dupras et al., 2012; Dirkmaat & Cabo, 2012; Christensen et al., 2014; Dirkmaat, 2015). Therefore, methods involving meter tapes were developed and applied to archaeological and forensic scenes. One of the most commonly employed methods used to produce a plane view, or overhead view, is the baseline control-point method (Dupras et al., 2012; Christensen et al., 2014). This method involves placing a meter tape through the densely clustered, central aspect of the scene to act as a baseline. Then, another measuring tape is placed perpendicular to the scene and used to measure from the baseline to the piece of evidence. To achieve more accurate maps, multiple measurement points may be recorded on the same piece of evidence. This method produces a 2D bird's-eye view of the scene and the evidence. Limitations of this mapping method include the artistic talent of the mapmaker, as well as human error in the recorded measurements. If the

measurements are incorrectly recorded at the scene, the scale may appear off in the later map production and the map could be unreliable.

3D Mapping Technologies

There are a number of 3D documentation methods that are used to produce more accurate representations of archaeological sites and forensic scenes. The application of total stations and global positioning systems (GPS) allowed researchers to record individual points at a location in the context of the entire world (Howard, 2007; Dupras et al., 2012; Barazzetti et al., 2012; Dirkmaat, 2015). Therefore, smaller scale recordings of the local scene, using photogrammetry or laser scanners, could be geo-referenced on a global scale through the application of total station technology. This allows for a more complete understanding of the location of an archaeological site or forensic scene in relation to other areas of important context.

One commonly used type of visual recording technologies are structure from motion (SfM) technologies. Structure from motion technology is a general digital recording method that uses photographs to produce volumetric models (Benavides López et al., 2016). These photographs are then run through computer software such as Agisoft's Metashape after being processed in Photoshop (Howland et al., 2014). The software uses common points throughout the photograph catalogue and aligns the photographs to create a point cloud. This point cloud is rendered to create a 3D model that is scaled and includes the digital elevations of the site. This general method of SfM technology data collection and processing is the same for all variations on this method.

Photogrammetry is a specific variation of SfM technology that relies more on the complex non-linear 3D computer algorithms to align the photographs into a point cloud than other SfM technologies (Benavides López et al., 2016). While routine SfM motion technology

applications require the photographer to change camera settings and manually overlap photographs for alignment, photogrammetry can be performed either at close-range or from a distance using aerial photography methods (Mikhail et al., 2001; Linder, 2003; Burtch 2008; Portalés et al., 2009).

Three-dimensional scanners appear rather similar in their application to structure from motion technology, but the methodology itself is different. These 3D scanners use lasers to record three-dimensional points in space as x, y, and z coordinates, and then renders them into a model using computer software (Forte et al., 2012; Campana et al., 2012). The goals of this technological application include the reconstruction of stratigraphic sequences in excavation pits, the virtual visualization of artifacts in layers, the interpretation and contextualization of the site in time and space, and mitigation of the overall destructive technique of excavation. It has been a common practice to utilize laser scanning technology before the excavation of the site, and then again post-excavation. However, an article by Forte and others (2012) explored the application of three-dimensional laser scanning of the site of Çatalhöyük at more frequent frequencies than pre-excavation and post-excavation. The researchers attempted to record the excavation process in a manner that made the excavation process virtually reversible. They did this by taking 5-minute scans during every level of the excavation's stratigraphic layers, and the result is a highly accurate model that can be virtually visited and excavated by all archaeologists.

3D Digital Mapping Technology Comparison

Both 3D scanners and SfM technology methods are highly accurate, and both can be applied in close-range as well as aerial settings. However, the benefits and detriments of both visual recording methods have led to a group of investigative archaeological literature that

involves the recording of an archeological scene using more than one type of mapping technology (Baltsavias, 1999; Al-kheder et al., 2008; Porter et al., 2016).

Some of the benefits of photogrammetry, specifically, include that it is highly economical and involves easily portable equipment. The equipment required for most photogrammetry modeling is a camera, scaled targets, and computer software that is usually less expensive for academics. The limited equipment necessary means that photogrammetry technology equipment can be easily transported to remote locations. However, despite these benefits, photogrammetry requires a degree of specialized skills to record effectively, and it is easily affected by environmental weather conditions. The photography recording protocols as well as the software rendering, requires a specific technological knowledge. Additionally, the data collection itself is also relatively slow, depending on the size of the scene that you would like to record. Smaller, isolated aspects of archaeological sites, or contained forensic scenes, take hours to record properly. The application is also limited by the environment. The application of data collection for photogrammetry can be limited by environmental conditions including the location of the scene, low light levels, and other weather effects (rain and wind).

Three-dimensional scanning is beneficial to archaeologists because the technology can be more easily adapted to multiple weather environments, and it produces a model that is higher quality, or at least comparable to that of SfM technology. These scanners are especially useful when modeling homogenous surfaces, but the resolution can be insufficient when recording cracks or other breaks in an otherwise smooth surface (Al-kheder et al., 2008). Another challenge when using these scanners is that it is a highly specialized process, and the machines themselves are not easily transported to remote archaeological locations. Furthermore, any scene can take considerable time to scan and process, no matter the size. The process itself, is also

relatively expensive, and therefore is limited by the number of researchers who can afford the technology.

Light in Outdoor Settings

Despite the origin of many 3D digital recording technologies as archaeological techniques, there is a lack of literature directly addressing the environmental considerations necessary when using technology outside. However, the importance of quality lighting when using 3D digital recording technologies is a recognized concern in archaeology and related literature (Baltsavias, 1999; Ozbek et al., 2010; Partsinevelos et al., 2014; Sapirstein, 2016). It has been mentioned as a contributing factor in local 3D photogrammetry modeling error. Specifically, the shadows changed throughout the day and limited the time in which data collection could occur (Sapirstein, 2016).

Research has been conducted using unmanned aerial vehicles (UAVs) to conduct photogrammetry research in low levels of light (Burdziakowski & Bobkowska, 2021). As discussed in the article, the majority of photogrammetry research conducted in poor light occurred inside. Articles involving modeling the inside of religious buildings supported the use of artificial lighting as a corrective tool (Portalés et al., 2009; Teza et al., 2016). However, the general belief of the researchers was that “a photogrammetric product based on night-time photos will exhibit lower geometric accuracy and reduced interpretative quality” (Burdziakowski & Bobkowska, 2021, p. 3). Therefore, the goal of this research was to discover which steps of their research process had the greatest influence on the quality of the produced model. Their research process included data acquisition, processing using Agisoft® Metashape®, and spatial analysis of their results. This study did find a reduction in geometry and a poor absolute quality of the nighttime models; however, the nighttime geometry was still considered acceptable by the

photogrammetry software. The authors were not able to determine which step of the research process specifically had the largest impact on the lower quality nighttime model productions, and they do not recommend the use of nighttime photogrammetry models for surveying or cartographic projects. However, forensic investigators do not have the same luxury in choosing the time at which they are needed at a scene. Therefore, it is important to note that it is possible to use photogrammetry in poor lighting conditions, but that measures should be taken to improve lighting conditions when possible to ensure the models are high quality.

Materials and Methods

The methods were derived from previous research conducted by University of Central Florida students on the application of photogrammetry research to the field of forensic archaeology (Gidusko, 2018; McCollum, 2020; Ferrell, 2020). The data collection field site is located in the University of Central Florida's natural lands. The natural lands that were tested consisted of an oak hammock with pine flatwood matrix, and are relatively flat. The ground surface is generally covered in pine needles, live oak leaves, and grass. This tract of land has been consistently used in previous UCF Masters theses focusing on photogrammetry (McCollum, 2020; Ferrell, 2020). Three locations were specifically selected so that the lighting correction methods could be tested in an open, dappled, and shaded environment. These scenarios are discussed in more detail later in this section.

Scene Materials

Each of the staged forensic scenes included a composite human skeleton, and several clothing items that included a t-shirt, a pair of shorts, a tennis shoe, and a baseball cap (Table 1). These scenes were approximately 1 meter by 1.5 meters in size. In addition to the skeletal and

clothing material, four 1-meter Cultural Heritage Imaging calibrated photogrammetry scale bars with coded targets surrounded the scene. The scale bars were placed around the scene to ensure that they were visible in multiple overlapping images and from multiple angles (Cultural Heritage Imaging, 2021). These scale bars are used to ensure that the scale of model is validated, as the coded targets are automatically recognized as reference points by the software (Cultural Heritage Imaging, 2021; Edelman & Aalders, 2018). A north arrow was also included in each scene.

A queen-sized flat sheet was used as a cover for certain versions of the scene. The purpose of the sheet was to test how the elimination of shadows cast on the scene by people, the lights, and forest foliage affected final model quality. The sheet was held at an angle by volunteers to block the sunlight and ensure that the scene did not experience shadowing. The sheet was white to ensure that the light passing through the sheet was uncolored, and therefore did not influence the final coloring of the scene in the same manner that a blue tarp would. The white sheet also did not completely block the light in the same manner that a black tarp or sheet would (McPherron et al., 2009).

Table 1: Inventory of the human skeletal elements used in the three scenarios.

| <u>Skeletal Element Inventory</u> | | <u>Scenario 1</u> | <u>Scenario 2</u> | <u>Scenario 3</u> |
|--|-------|--------------------------|--------------------------|--------------------------|
| Cranium | | 1 | 1 | 1 |
| Mandible | | 1 | 1 | 1 |
| Scapula | Left | 1 | 1 | - |
| | Right | 1 | 1 | 1 |
| Humerus | Left | 1 | 1 | - |
| | Right | 1 | 1 | 1 |
| Radius | Left | 1 | 1 | - |
| | Right | - | 1 | - |
| Ulna | Left | - | 1 | - |
| | Right | 1 | 1 | 1 |
| Vertebrae | | 4 | 5 | 4 |
| Ribs | | 5 | 5 | 5 |
| Sternum | | 1 | 1 | 1 |
| Os Coxa | Left | 1 | 1 | 1 |
| | Right | 1 | 1 | 1 |
| Sacrum | | 1 | 1 | 1 |
| Femur | Left | 1 | 1 | 1 |
| | Right | 1 | 1 | 1 |
| Tibia | Left | 1 | 1 | 1 |
| | Right | 1 | 1 | 1 |
| Fibula | Left | - | 1 | 1 |
| | Right | 1 | 1 | 1 |
| Patella | Left | - | - | - |
| | Right | - | - | 1 |
| Tarsals | Left | - | - | - |
| | Right | 1 | 1 | 1 |
| <u>Total</u> | | 27 | 31 | 26 |

Field Technology

The camera used during photography is a NIKON D7200 model with a NIKKOR 18-140mm 1:3.5-5.6G ED lens and uses SanDisk 128GB and 64GB Extreme Pro SD cards. This lens is a zoom lens and not a fixed lens, the focal length was set to 18 mm to ensure stability when shooting the photographs (Agisoft LLC., 2019b; Nikon Inc., 201). Fixed lenses have a higher optical quality when compared to zoom lenses. Additionally, zoom lenses contain a higher number of movable parts and therefore are more internally unstable than fixed lenses (De Reu et al., 2014; Sapirstein & Murray, 2017). Both autofocus and manual focus were utilized during data collection. The autofocus setting was not changed during the first rounds of data collection, and the recorded focal lengths were either 18mm or 20 mm. When photographing using the manual focus, the focal length of the lens was set to 18 mm, and then was not adjusted during the data collection process (De Reu et al., 2014; Sapirstein & Murray, 2017). When photographing the manual setting rounds the lens needed to be set to autofocus during collection of the overhead photographs, because it was not easily possible to keep the overhead images focused while using the extension pole. Therefore, the model was photographed in the manual setting for every view except the overhead shots.

The aperture priority was kept consistent throughout photographing and was selected by shooting a couple of practice photographs before beginning data collection (Sapirstein & Murray 2017). The scene size itself was small, therefore, a lower aperture value of $f/8$ was chosen with an ISO of 400. This lower aperture allowed for an increased shutter speed and higher accuracy in recording the scene. The small size of the scene combatted the more limited depth of field that occurred due to the lower aperture.

To provide artificial lighting in an outdoor setting, two sets of Neewer 3-Pack Dimmable Bi-Color LED lights were purchased. Each of the sets contained three lights, so a total of six lights surrounded the scene itself. The lights themselves were placed around the scene approximately 0.3 meters (1 foot) from the scale bars. The settings could be altered to channel yellow or white light (Figure 1). Each of the lights also had a dimmer panel placed over the face of the light. The dimmer panel was kept in place during the scene's recording, as this panel appeared to reduce the opacity of the shadows produced by the lights themselves. It was noticed that when the lights were on, skeletal elements that extended vertically from the ground or were awkwardly shaped cast very dark shadows on certain aspects of the scene. The inclusion of the dimmer panels aided in the reduction of these dark shadows. Additionally, each light included a removable metal panel cover that protected the light and could be used to aim the light in smaller settings. When they were not removed, the lights could not be properly angled at the ground to point at the skeletal elements and evidence. Therefore, the metal panels were removed before data collection began. The lights included two shades of light, yellow and blue. To use the maximum brightness available, both of these light shades were turned to their highest settings. The highest intensity of light brightness was necessary in the outdoor setting because of the diffusion that occurred to the beams in the large expanse of open air. To mitigate this dispersal, the light stands were kept at their shortest settings (Figure 1).



Figure 1: (A) An image showing the lights set up in the field with their heights at the shortest setting. (B) An image of the back of the light panel showing the settings used when the lights were in use.

Scene Preparation and Data Collection

Prior to data collection, an appropriate area was located for each scene and the skeletal elements were set out as a confined scatter. After placing the remains, the scale bars were positioned around the remains before the careful cleaning of the scene began (Ferrell, 2020; McCollum, 2020). Cleaning the scene involved cutting grass and clearing leaves or other materials from around the skeletal elements and evidence. This was an important step, as material that covered or obstructed important aspects of the scene contributed to processing difficulties that resulted in visual discrepancies. After setting up and cleaning the scene, the photographing of the scene began.

Each scenario was photographed four times. First, the scene was shot without any lighting correction tools. Then, the scene was photographed using only the sheet. Next,

photographs were taken of the scene with the artificial lights turned on. Finally, both the artificial lights and the sheet were used to correct potential lighting problems.

The photographs were shot freehand from five different view angles (Figure 2). The five view angles were defined using the position of the photographer's body and the position in which the camera was being held (Table 2). These five view angles were consistent throughout all of the photography and ensured that consecutive images overlapped following the principle of ad hoc geometry at different heights (Barazzetti et al., 2012; Edelman & Aalders, 2018). Multiple photographs are also necessary to extract the 3D coordinates from the images, as a point must be visible in at least three images from different points of view to be included in the processing (Douglass et al., 2015; Willis et al., 2016; Edelman & Aalders, 2018).

Table 2: Descriptions and number of photographs for each view angle.

| <u>View Angle</u> | <u>Description</u> | <u>Number of Photographs</u> |
|--------------------------|---|-------------------------------------|
| View 1 | Kneeling while holding the camera at about waist height | 20 |
| View 2 | Kneeling while holding the camera at about chest height | 20 |
| View 3 | Standing with camera at about waist height | 20 |
| View 4 | Standing with camera at about chest height | 20 |
| View 5 | Standing with camera above head | 20 |
| Overheads | Parallel overhead shots using an extension pole | 10 |
| Closeups | Closeup photographs of complex areas and details of the scene | 10 |
| | | Total: 120 |



Figure 2: Diagram of view angles. (A) Image of view angle 1, which is described as kneeling while holding the camera at about waist height. This image was taken when the artificial lights were in use. (B) Image of view angle 2, which is described as kneeling while holding the camera at about chest height. This image was taken when only the sheet was in use. (C) Image of view angle 3, which is described as standing with the camera at about waist height. This image was taken when neither the lights nor the sheet were in use. (D) Image of view angle 4, which is described as standing with the camera at about chest height. This image was taken when only the sheet was in use. (E) Image of view angle 5, which is described as standing with the camera above head. This image was taken when neither the lights nor the sheet were in use.

Additionally, a smaller number of overhead shots were taken parallel to the scene (Figure 3). These photographs were taken by attaching the camera to an extension pole and holding it out over the scene. Close-up photographs were also taken of more complex areas of the scene.

Joint surfaces, the trunk region, the cranium, and areas where leaves and debris may have obscured part of the elements during photography were photographed again at a closer view. To ensure that the scene itself was not disturbed by leaves or other debris being moved on to the scale bars and evidence, an approximate radius of 0.6 meters (2 feet) was kept around the periphery of the scene. The number of photographs varies with the size of the scene, but all of the scenes for this phase were kept consistent. However, it is considered beneficial to take a larger number of photographs, as images may be deleted or not included during the computer processing phase.



Figure 3: (A) Image showing how the closeup photographs were taken to capture the details of the clothing and skeletal elements. This image was taken when both the lights and the sheet were in use. (B) Image demonstrating how the overhead shots were taken using an extension pole held parallel to the scene. This image was taken when only the sheet was in use.

Field Scenarios

The photography of one complete scene involved the recording of twelve complete models (Table 3). There were three different scenarios, and each scenario was recorded four times, using four iterations (Figure 4). The automatically focused scenes were chosen for close analysis, following the practices of prior research (Ferrell, 2020). However, each scene was photographed using both automatic and manual focus. All the scenes were approximately 1 meter by 1.5 meters in size. To better understand how the movement of the sun may have contributed to the lighting quality of each scene, it was recorded using approximate degrees throughout the data collection process. The scenes all were shot in the morning, and data collection began between 9 and 10 a.m., and ended between noon and 1 p.m. The consistency of starting times and tracking the sun's motion ensured that the angle of sun on the scenes was not drastically different. Despite the slight changes to the locations, the sun was always at approximately the same degree when recording each of the three scenes. All the scenes were located within the UCF natural lands, which has a latitude of 28.594° and longitude of -81.192° . An afternoon sun would be located differently in the sky and add another variable to the experimental process.

Scenario 1 was located in an open environment. This location had little tree cover, and therefore involved bright sunlight with little shadowing. The ground surface of this scene was grass, with a sandy base soil. There were few leaves that blew onto the scene, but the grass and other foliage was tall in certain areas and required careful grooming to prepare the scene. From 9 a.m. to 10:30 a.m. the sun's position moved from approximately a 45° angle to a 70° angle. There was one point during the day where the sky became incredibly overcast, and the sun was not easily visible between the time of 10 and 11 a.m.

For Scenario 2, a shaded location was chosen. This environment included heavy tree cover. The scene was almost completely shaded by tree branches, and the ground surface consisted of pine needles and oak leaves. Despite the heavy canopy, a few streaks of light did appear on the scene at certain points of the day. Data collection for this scenario took place between approximately 9 a.m. and ended at approximately noon. Within this time period, the sun moved from about a 40° angle to that of a 100° angle. Recording for the angles of movement was taken every 15 minutes throughout the data collection period, and the sun appeared to move approximately 5° each interval.

The location of Scenario 3 was in an area with dappled lighting. This place had a ground surface of grass, pine needles, and oak leaves. The positioning of the overhead branches contributed to partial lighting throughout the day. There were large patches of dark shadows and bright spots projected on the scene. The lighting fluctuated during this period of data collection, and there were periods of extreme sun as well as overcast skies. The data collection began slightly before 9 a.m., and at this time the sun was at an angle of about 40° . By 9:30 a.m., the sun was located at about 60° , and by noon it was located directly overhead.

Table 3: Information showing the naming process of each model to promote easier identification of specific models throughout this research.

| <u>Scenario Number</u> | <u>Scenario Description</u> | <u>Iteration ID</u> | <u>Iteration Description</u> | <u>Processing Settings</u> | <u>Model ID Notation</u> |
|------------------------|-----------------------------|---------------------|------------------------------|----------------------------|--------------------------|
| 1 | Open | A | No Lights or Sheet | 1 | 1A-1 |
| 1 | Open | A | No Lights or Sheet | 2 | 1A-2 |
| 1 | Open | B | Sheet Only | 1 | 1B-1 |
| 1 | Open | B | Sheet Only | 2 | 1B-2 |
| 1 | Open | C | Lights Only | 1 | 1C-1 |
| 1 | Open | C | Lights Only | 2 | 1C-2 |
| 1 | Open | D | Lights and Sheet | 1 | 1D-1 |
| 1 | Open | D | Lights and Sheet | 2 | 1D-2 |
| 2 | Shaded | A | No Lights or Sheet | 1 | 2A-1 |
| 2 | Shaded | A | No Lights or Sheet | 2 | 2A-2 |
| 2 | Shaded | B | Sheet Only | 1 | 2B-1 |
| 2 | Shaded | B | Sheet Only | 2 | 2B-2 |
| 2 | Shaded | C | Lights Only | 1 | 2C-1 |
| 2 | Shaded | C | Lights Only | 2 | 2C-2 |
| 2 | Shaded | D | Lights and Sheet | 1 | 2D-1 |
| 2 | Shaded | D | Lights and Sheet | 2 | 2D-2 |
| 3 | Dappled | A | No Lights or Sheet | 1 | 3A-1 |
| 3 | Dappled | A | No Lights or Sheet | 2 | 3A-2 |
| 3 | Dappled | B | Sheet Only | 1 | 3B-1 |
| 3 | Dappled | B | Sheet Only | 2 | 3B-2 |
| 3 | Dappled | C | Lights Only | 1 | 3C-1 |
| 3 | Dappled | C | Lights Only | 2 | 3C-2 |
| 3 | Dappled | D | Lights and Sheet | 1 | 3D-1 |
| 3 | Dappled | D | Lights and Sheet | 2 | 3D-2 |

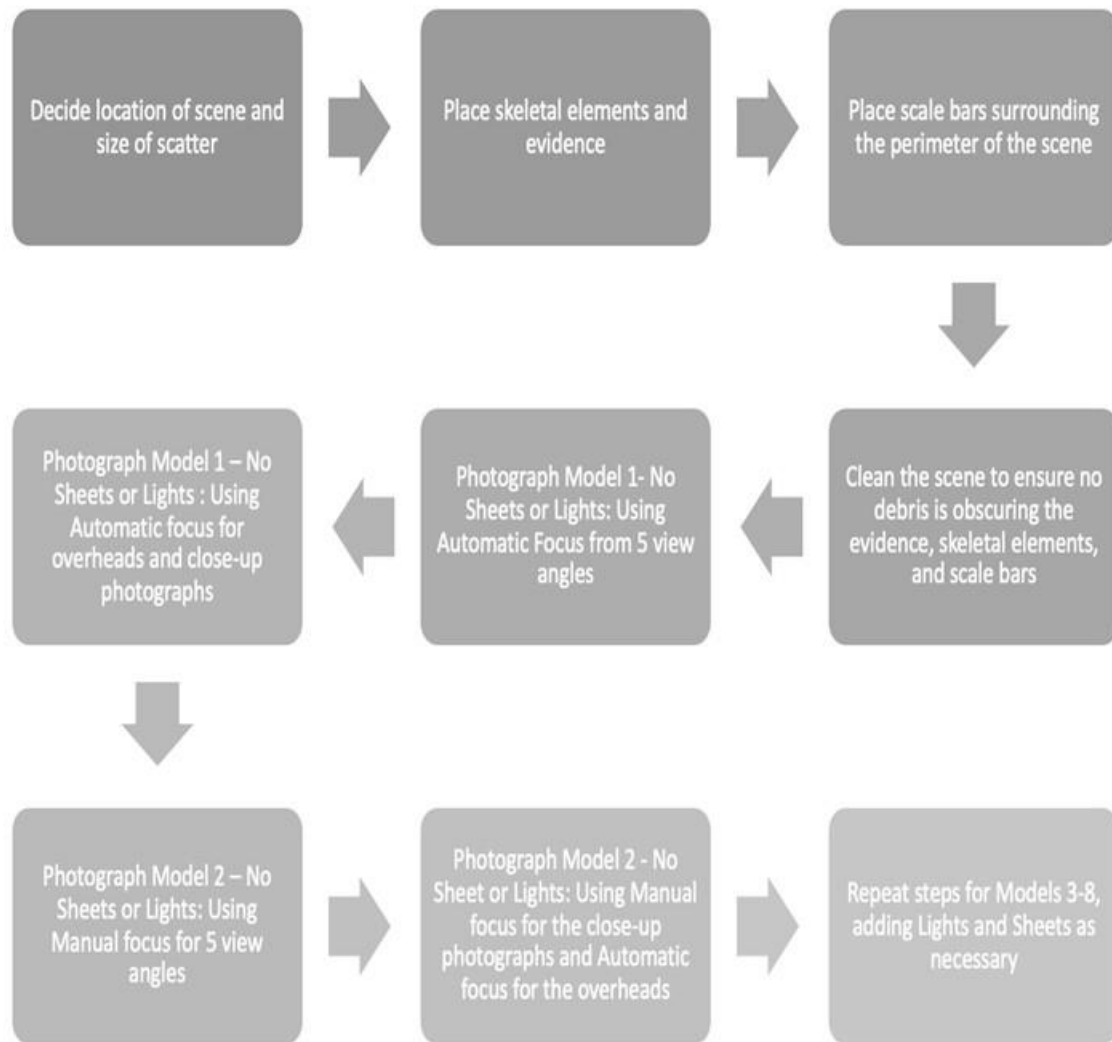


Figure 4: Workflow describing the data collection process followed in the field

Photograph Processing

After data collection in the field, preprocessing of the photographs occurred to prepare them for the modeling software. The scene was photographed using RAW to produce a higher quality file format than that of a compressed JPG image. These RAW images could then have their lighting and exposure altered before conversion to TIFF files (Agisoft LLC., 2019b). The program Adobe Bridge® was used to white balance the RAW photos; this was performed by

using the white balance tool to select a spot on the white region of the scale bar following Ferrell (2020) and Gidusko (2018). Then, images that were noticeably over or underexposed were manually adjusted using the shadow, exposure, and highlight tools following Ferrell (2020). After correction, the images were saved as TIFF files and imported to Agisoft® Metashape® Professional.

The processing of the 3D models occurred using Agisoft® Metashape® Professional Version 1.5.5 (Agisoft LLC., 2019a). This photogrammetry software application allows the user to manually set analysis parameters, while still employing a mostly automated workflow to develop the models (Green et al., 2014). Processing guides were used to determine the settings chosen for processing, but changes were made to the original settings during the second round of processing (USGS National UAS Project Office, 2017; Mayer et al., 2018; Ferrell, 2020). The Metashape® program also has the capability to automatically extract information regarding the camera used. This information includes the make, model, ISO setting, shutter speed, and aperture settings for each set of photographs. This extracted information is then used by the program to determine the camera position for each of the individual photographs taken during data collection (Figure 5) (Baier & Rando, 2016).



Figure 5: Camera positions for Model 2A-1, which did not use the artificial lights or the sheet. Each of the blue rectangles represent the position and view angle at which each photograph was taken. The white arrow indicates a 1-meter scale bar.

Processing Steps

Once the TIFF files were uploaded to Metashape®, the processing of the files into the development of 3D models began based on recommendations from Ferrell (2020) and McCollum (2020) (Figure 6). This process started with the application of the Detect Markers tool to register the coded targets present in the scale bars at the scene. The missing markers were manually selected to ensure that 12 markers were used when identifying the scale bars. After the targets were recognized, the photographs could then be aligned into a sparse point cloud. The inclusion of targets or markers is not necessary for the photogrammetry process, but is used to increase the accuracy of the model.

The sparse point cloud is constructed when the SfM algorithms in Metashape® detect unique feature points present in multiple images that can be identified throughout the photo set (Green et al., 2014; Douglass et al., 2015; Baier & Rando, 2016). From these feature points, the scene geometry is developed as the feature points are aligned across the images. The alignment of these points creates the sparse point cloud (Figure 7). The accuracy and precision is essential when generating an accurate 3D model, because this initial alignment of points is used as the basis from which the dense point cloud is developed (Douglass et al., 2015; Agisoft LLC., 2019b). Photographs that do not present with an adequate number of recognizable points are automatically deleted during this process.

To ensure that the sparse cloud is highly accurate, the Gradual Selection tool was used to refine and optimize the generated points as recommended in Ferrell (2020). First, the Reconstruction Uncertainty of the generated points was selected. This process selected and deleted points that significantly deviated from the object or scene surface, and their deletion reduced the number of extraneous points that existed in the sparse point cloud (Agisoft LLC., 2019b). To achieve the most accurate results, it is recommended that no more than 50% of the points be selected during this process. In general, this is the optimization tool that results in the largest point deletion (Agisoft LLC., 2019b; McCollum, 2020; Ferrell, 2020). Secondly, the Projection Accuracy of the model was refined. This step allowed for deletion of points that had poorly localized projections. Then, the Tie Point Accuracy was tightened from 1 pixel to 0.1 pixels. The tightening of the tie point accuracy signifies that the tie points will be detected at a smaller, more accurate scale of 0.1 pixels, not at only 1 pixel (Agisoft LLC., 2019b). Finally, the program was optimized to reduce the Reprojection Error. This involved removing all the points that were falsely matched across the model, or that had poor localization accuracy and large

residuals. As this optimization process occurred, the Optimize Camera tool was used to refine the camera locations after each round of point deletion. Throughout this process, the error (in pixels) of each camera production was monitored. Ideally, each of the cameras would end close to, or under, 0.3 pixels worth of error (Granshaw, 2016; Agisoft LLC., 2019b).

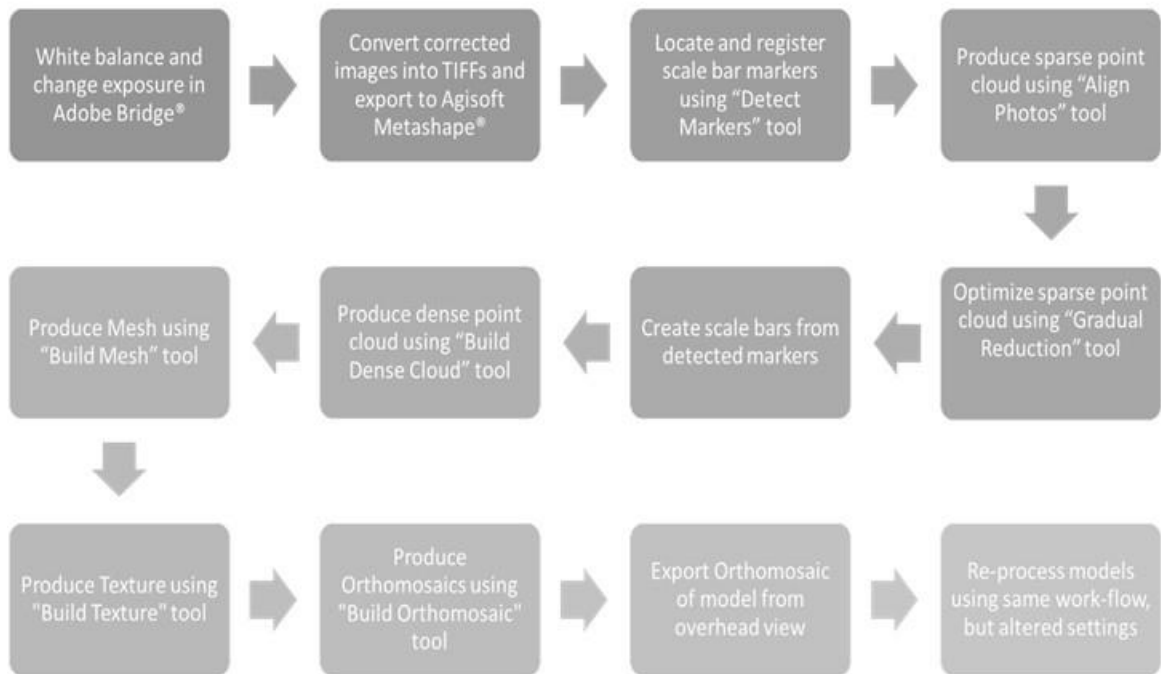


Figure 6: Workflow describing the pre-processing and processing steps of Chapter 2.



Figure 7: The sparse point cloud of Model 2C-1, which used the artificial lights. The sparse point cloud is generated when feature points are detected in the image and then tracked throughout the set. Then, the scene geometry is constructed using these points. The white arrow identifies a 1-meter-long scale bar.

After optimization, the scale bars themselves, of a known length, were identified using the registered targets on the CHI scale bars. The incorporation of scale bars with known lengths allowed for a more accurate scale production procedure within the software and does not require the individual measurement of coordinate points for each of the targets using a Total Station (Agisoft, LLC., 2019b). Four scale bars were used in total, as the CHI manual recommends this number for larger outdoor scenes as the bars are more easily compromised in an outdoor setting by the wind or other environmental influences (Cultural Heritage Imaging, 2021). For the primary running of the models, the Scale Bar Accuracy of the models was set to 0.001, as that is

the default setting in Metashape®. For the second processing of these models, this number was changed to 0.0001 as recommended in the CHI manual (Cultural Heritage Imaging, 2021).



Figure 8: The dense point cloud of Model 2C-2, which included the artificial lights. The dense point cloud contains an enormous number of X, Y, and Z data points located close to each other. The white arrow indicates a scale bar that is 1-meter long.

The final step of processing included running the processes to build a dense point cloud, mesh, and texture (Figure 8). The dense point cloud is developed from the original sparse point cloud and includes a higher number of X, Y, and Z data points located closer together (Douglass et al., 2015; Granshaw, 2016; Agisoft LLC., 2019b). This cloud of information then allows

Metashape® to produce the mesh. The mesh is a polygonal model that is used as a base for the texture development (Figure 9). Texture development occurs when the software creates a mosaic of all the photographed images and projects the photorealistic texture on the mesh. After adding the texture, an orthomosaic map of the scene is generated from geometrically accurate orthophotos that are stitched together by the software (Agisoft LLC., 2019b). The result is an accurate plane view map of the scene that can be exported.

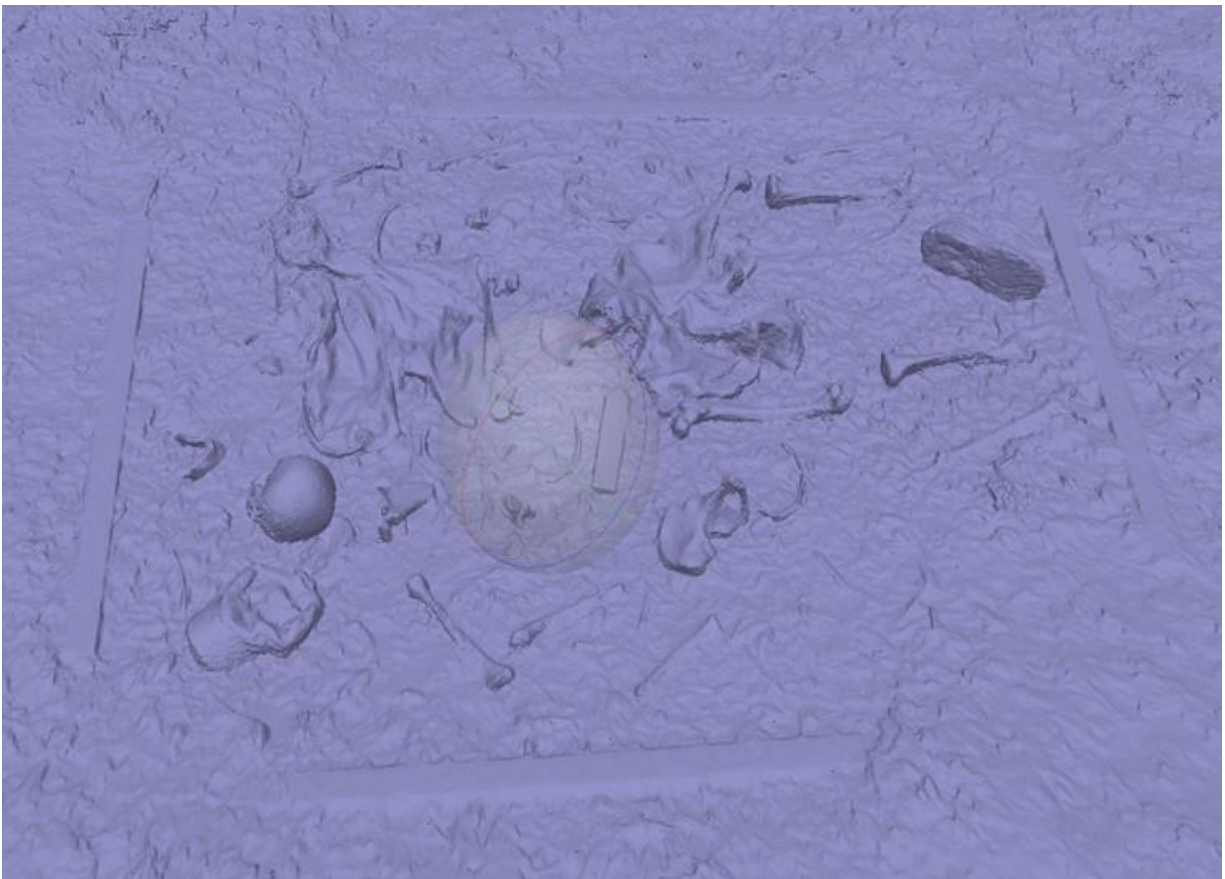


Figure 9: The solid polygonal mesh of Model 2A-1, which did not include the artificial lights or the sheet. This polygonal mesh model is created by Metashape® using the point cloud information.

In this chapter, the models were processed twice in order to determine whether the quality of the produced models could be improved through processing changes in addition to changes in field practices. Specifically, further accuracy refinement of the sparse point cloud and Scale Bar Accuracy resulted in additional deletion of photographs. For example, during the first round of processing, the photo alignment settings included Generic Preselection of photographs and a tie point limit of 40,000. When processing the second time, the Scale Bar Accuracy setting was increased from a setting of 0.001 to a setting of 0.0001. The setting of 0.001 is the setting automatically programmed into Agisoft Metashape®, however, the newest CHI guidelines suggested the setting be manually increased to 0.0001 (Agisoft LLC., 2019b; Cultural Heritage Imaging, 2021). Additionally, the Generic Preselection was not selected, and the tie point limit was increased from 40,000 to 50,000. Additionally, prior to alignment, photographs that contributed fewer than 300 projections to the sparse point cloud or had a pixel error over 5.0 were deleted. By reducing the number of images originally included in the sparse point cloud generation, the overall accuracy of the scene was improved. This also allowed for fewer generated points during the dense point cloud generation, and a more precise selection process. Only the automatic focus scenes were processed using these changed settings; the manual focus scenes were recorded and processed using only the initial settings. Once the scenes had been processed using the original, and then adjusted settings, the scene that displayed the higher qualitative and quantitative accuracy was chosen to be presented in the Results Section.

Exports

Imagery of the 3D model was exported using multiple formats. To ease viewing the results on all image viewing softwares, the final model orthomosaic images were exported in a

tagged image file format (TIFF). These files are lossless and preserve the quality across viewing platforms to ensure that anyone is able to view the models. Additionally, each model was saved as a Metashape® project on an external hard drive. This ensures that the researchers may edit and view the models to answer future research questions. For their presentation in this thesis, bird's-eye orthomosaic representations of the overall scene were included and used for visual comparisons between the models. Closeup screenshots of the cranium were used for comparison of detailed visual accuracy for each of the models. These screenshots were taken after the model was completely processed.

Evaluating Error

For the purpose of this project, the error was measured in two ways to determine the quantitative accuracy of the models. Based on previous studies, the root mean squared (RMS) reprojection error and scale bar error were used (McCollum, 2020; Ferrell, 2020). The RMS reprojection error measures the “distance between the point on the image where a reconstructed 3D point can be projected, and the original projection of that 3D point detected on the photo and used as a basis for the 3D point reconstruction procedure” (Agisoft LLC., 2019b, p. 51). The total RMS reprojection error is an average collected from all the feature points in the model, and models are considered highly accurate when this error value is close to 0.3 pixels (Mayer et al., 2018, Agisoft LLC., 2019b). This calculation is provided in the final report that is generated by Metashape®.

The scale bar error represents the difference between the manually input scale bar length and the distances that the software detects between a random sampling of points on the scale bars (Agisoft LLC., 2019b). Therefore, the total scale bar error of the model is calculated by Metashape® as the mean square root of the errors for the four reference scale bars used in the

model (Agisoft LLC., 2019b). Physically, the scale bars themselves have a built-in precision value of 0.1 mm. In a highly accurate model, the total scale bar error as calculated by Metashape® will be less than 0.1 mm (Cultural Heritage Imaging, 2020).

When examining the qualitative visual accuracy of the models, each model was examined for accuracy in the clothing and skeletal element geometry, the ground surface-subject interface points, the subject-subject interfaces, and the scale bar geometry based on Ferrell (2020). A visual examination of the orthomosaic generation of the model aided in the examination of the scale bar geometry and the overall accuracy of the skeletal geometry. The orthomosaic also shows clothing geometry, and subject-subject interfaces. For each of the models, a comparison of the anterior of the cranium was conducted. This area of the cranium is highly variable, and therefore the degree of accurate modeling seen of this bone was representative of the skeletal element geometry of the scene. Additionally, the cranium sometimes exhibited surface-subject interface distortion. Therefore, these close-up views of the anterior aspect of the cranium will provide a gauge of model distortion for each of the models.

Results

The results of this project were tested for using qualitative and quantitative accuracy. To better contextualize the results, each scenario is discussed separately, and then a comparison of the successfulness of the lighting correction tools is explained in the Discussion section. Each model was first examined for quantitative accuracy using the RMS reprojection errors and scale bar error. Then, a more detailed discussion of the visual accuracy of each model for each scenario will be addressed separately. To ensure that only the highest quality models were being evaluated, each model was processed twice, but only the more accurate model was selected for analysis. This selection is indicated by the number 1 or 2 that appears at the end of each model

number. For example, Model 1A-2 is the model from the second round of processing while Model 1B-1 is the model from the original processing set. Table 3 includes descriptions of the scenarios, iterations, and resulting model notation for reference.

RMS Reprojection and Scale Bar Error

The RMS reprojection errors for the entire dataset ranged from 0.283 (Model 1A-2) to 0.358 (Model 3B-2) (Table 4). When comparing only Scenario 1 (Open), the range of values was small. Model 1A-2 had the lowest RMS reprojection error with 0.283 pixels. The largest measure of RMS reprojection error in Scenario 1 was from 1D-2, with an error of 0.312 pixels. Within Scenario 2 (Shaded), the smallest error was 0.296 pixels (Model 2A-2), and Model 2D-2 recorded the largest error of 0.348 pixels. Scenario 3 (Dappled) showed Model 3A-1 had the smallest recorded error of 0.284 pixels. Model 3B-2 produced the largest RMS reprojection error with 0.358 pixels. The proximity of all the RMS reprojection error values to 0.3 pixels signifies that all of the models are considered highly accurate (Mayer et al., 2018). However, while the scale bar error was largest for Model 1C-1 at 0.1126 meters, it barely exceeded the recommended error as defined by Cultural Heritage Imaging (2021). The smallest scale bar error was found in Model 3C-2 at 0.0001 meters. Other than the high degree of error in Model 1C-1, the range for all total scale bar error was 0.0008 meters.

Table 4: Table providing the RMS Reprojection and total scale bar errors for all of the models.

| <u>Model Number</u> | <u>Iteration Description</u> | <u>RMS Reprojection Error (pixels)</u> | <u>Total Scale Bar Error (m)</u> |
|----------------------------|-------------------------------------|---|---|
| 1A-2 | No Lights or Sheet | 0.283 | 0.0009 |
| 1B-1 | Sheet Only | 0.286 | 0.0003 |
| 1C-1 | Lights Only | 0.288 | 0.1126 |
| 1D-2 | Lights and Sheet | 0.312 | 0.0002 |
| 2A-2 | No Lights or Sheet | 0.296 | 0.0002 |
| 2B-1 | Sheet Only | 0.346 | 0.0007 |
| 2C-2 | Lights Only | 0.327 | 0.0004 |
| 2D-2 | Lights and Sheet | 0.348 | 0.0006 |
| 3A-1 | No Lights or Sheet | 0.284 | 0.0003 |
| 3B-2 | Sheet Only | 0.358 | 0.0003 |
| 3C-2 | Lights Only | 0.303 | 0.0001 |
| 3D-1 | Lights and Sheet | 0.345 | 0.0003 |

Qualitative Visual Accuracy

As a representative of the scene upon its discovery, the accuracy of the visual appearance of the final models is important to investigators. To best evaluate the degree of visual accuracy, the model quality was measured using two approaches based off of recommendations from Ferrell (2020). First, each model's plane-view orthomosaic model was examined. This overview image is similar to hand drawn plane-view maps, as it provides a view of the scene that illustrates the original orientation and position of the remains and the evidence. Additionally, this view allows for the easy analysis of the scale bar geometry and general clothing and bone geometry. Then, the models were examined for detail. Close-up views of the anterior aspect of the cranium were evaluated to determine the level of fine detail achieved during modeling. The cranium has a highly complicated geometry that is difficult to capture during modeling. Ground

surface-subject interface distortion is commonly seen on the cranial vault, and there is a degree of noticeable distortion of the facial geometry. Then, a table summarized the degree of distortion observed.

Scenario 1 (Open)

Visual Accuracy of Orthomosaics

The Model 1A-2 orthomosaic without light correction tools exhibits minor distortion of some long bones and ribs, but only minimal distortion of the scale bar (Figure 10). There is noticeable grass covering the farthest right target of the northern scale bar. Distortions of the skeletal geometry of the model include minor distortion along the ribs, and the shafts of long bones including both tibiae, the left humerus, and the right femur. The mandible is visible, however, it somewhat blends into the ground surface due to its coloring. Beyond the color similarities, there is no ground surface-subject interface distortion of the mandible. The shadow of the light panel near the cranium appears on the scene and does cause a few dark shadows to be projected on the scene. The shorts, os coxa, long bones, and shoe especially create dark shadows. These shadows make it difficult to clearly see some of the skeletal materials. For example, the vertebrae that is located to the Northeast of the shirt is in the shadow cast by the light panel. There is no obvious visual distortion to the subject-subject interfaces.



Figure 10: Model 1A-2 orthomosaic without using the lights and sheet correction tools, and shadows from the artificial lights that were turned off.

Model 1B-1 with only a sheet produced an orthomosaic with minor distortion on a small number of skeletal elements and evidence when reviewing the orthomosaic and not closeup views (Figure 11). The scale bars have very minimal distortion, and only a few instances where there is grass or shadows obscuring sections of the scale bars or markers. The cranium has no obvious visual distortion to its geometry. The sutures, inferior aspect, teeth, and other features are clear. In comparison, the mandible is present and identifiable, but not easily visible. The coloring of the mandible continues to generate minor distortion at the ground surface-subject interface. All of the bones in the model are easily identifiable, and there is no obvious visible

distortion along the shafts of the long bones. There is no obvious visual distortion of the skeletal clothing geometry or subject-subject interface distortion. The use of the sheet to block the sun means that there are no bright patches or areas of shadows within the confines of the scale bars. The scene has a homogenous level of light, without much variation.



Figure 11: Model 1B-1 orthomosaic using the sheet.

The overall visual accuracy of Model 1C-1 with the artificial lights exhibited very minimal distortion (Figure 12). There is very minimal distortion of long bones in the orthomosaic. The ribs exhibit slight distortion and blending at the ground surface-subject interface. Additionally, the ribs located on top of the shirt experienced subject-subject interface distortion at their interface with the shirt. There are some instances of minimal distortion along

the scale bars, and the overall scale bar geometry is accurate. On the other scale bars, there are pieces of grass that appear to cover different aspects of the bar. The mandible is more visible in this orthomosaic and does not have as severe of a ground surface-subject distortion. The cranium has no noticeable distortion, and the inferior aspect, as well as the right half of the skull are extremely clear. There is minor distortion of the skeletal element and clothing geometry. One rib that is located between the shirt and the left os coxa is severely distorted. The bone appears disjointed, where sections of the bone have been moved or removed as a severe example of ground surface-subject interface distortion. Overall, there is still a degree of slight shadowing produced by the cranium and the shoe, but there is no noticeable shadow produced by the light panels themselves. The general level of light is more consistent throughout the entirety of this scene.



Figure 12: Model 1C-1 orthomosaic using the artificial lights.

When viewing the orthomosaic of 1D-2 with the inclusion of the lights and sheet, there is a minor degree of distortion across the model (Figure 13). Along the edges of each of the scale bars, there is minor distortion caused by pieces of grass or debris obscuring sections of the scale bar geometry. The black marker directly above the southern-most end target also appears to be minimally distorted. On the western scale bar, there is a large stick or piece of grass visible on the scale bar in-between the two southern-most targets. The southern scale bar exhibits minor distortion on the far-western target. There is also a piece of grass or a leaf covering a small portion of the scale bar near the far-eastern target. The skeletal elements are visible and identifiable, however there is evidence of minor distortion of much of the skeletal element geometry. The right scapula has minor distortion along its superior border. All of the ribs present in the scene exhibit distortion along their bodies to varying degrees. This includes ground surface-subject distortion along the interfaces of the ribs located on the ground, and subject-subject interface distortion where the shirt and the ribs interact. There is also a leaf present on one end of the rib placed under the shirt that was blown onto the scene during recording, and is now covering the sternal end. In addition to distortion of the ribs, there is distortion of the spinous processes of several vertebrae and along the edges of the vertebral bodies. The long bones have minimal distortion along their shafts, but there is additional evidence of distortion on the ischiopubic ramus of the left os coxa. The overall model is relatively dark in color. The coloring is even, and there are no obvious spots of shadow or brightness in the scene.



Figure 13: Model 1D-2 orthomosaic using the sheet and artificial lights.

Visual Accuracy of the Crania

Scenario 1 visual analysis includes an examination of the anterior view of the skulls using a closeup screenshot. This area of the cranium will be used as an example of distortion for each of the iterations (Figure 14).

When examining Model 1A-2 without using the light correction tools, there is minor distortion of the cranium. The inferior aspect of the skull has minimal distortion, and each of the main features are easily determined. The occipital portion and the accompanying sutures of the

cranial vault exhibit minor distortion, but the right squamosal suture has no obvious visual distortion. There is minimal distortion of the interorbital spaces. There is evidence of severe skeletal geometry distortion along the alveolar portion of the maxilla. The closeup view of the anterior aspect of the skull does not show the teeth. However, the teeth are visible and easily identifiable in the orthomosaic product. There is evidence of slight ground surface-subject interface distortion where the cranial vault interacts with the ground surface. Additionally, moderate subject-subject interface distortion exists along the right zygomatic arch. The leaves in the background are moderately distorting the integrity of the skeletal geometry of the bone. Therefore, the leaves and zygomatic arch are difficult to distinguish as separate elements in the closeup views.

In Model 1B-1 when using the sheet, the cranium exhibited slight distortion in the maxillary portion. The teeth are moderately distorted in this model, and the alveolar margin of the maxilla exhibited minimally distorted skeletal geometry. There was additional minor distortion along the parietal and occipital portions of the cranial vault. This distortion mostly occurred along the ground surface-subject interface. However, the squamosal suture is still easily identifiable in this rendering and there is no obvious visible distortion. There was severe distortion of the skeletal geometry of the bone along the right zygomatic. From this view, it appears as if the subject-subject interface between the temporal bone and the zygomatic are no longer distinct. It is highly distorted and difficult to identify the separation between the geometry of these two bones.

Overall, Model 1C-1 with the incorporation of the artificial lights exhibits less distortion than either of the two previous models. The cranium exhibits little to no distortion. From the inferior, overhead, and posterior views, there are no obvious visual distortions of the skeletal

element geometry. The screengrab of the anterior view of the skull does show moderate distortion in the right eye orbit and along the right mastoid process. Additionally, the right zygomatic process is severely distorted and does not appear as a distinct bone process in the model. However, the appearance of the teeth is less distorted than in previous models, and the alveolar process contains identifiable tooth sockets less distorted than in previous models.

In Model 1D-2, with the use of the lights and sheet, there appears to only exist minor distortion of the cranium. The sutures are visible, and there is very minimal distortion to the nasal area and eye orbits. The inferior aspect of the skull appears to have minor distortion, and both mastoid processes are visible. Along the cranial vault, where the frontal bone interacts with the ground surface, there is minor distortion at the ground surface-subject interface. Minimal distortion occurred on the maxilla and along the alveolar margin. The teeth are visible when present, and the alveolar sockets are identifiable within the maxilla. In general, this model appears to be the most visually accurate.

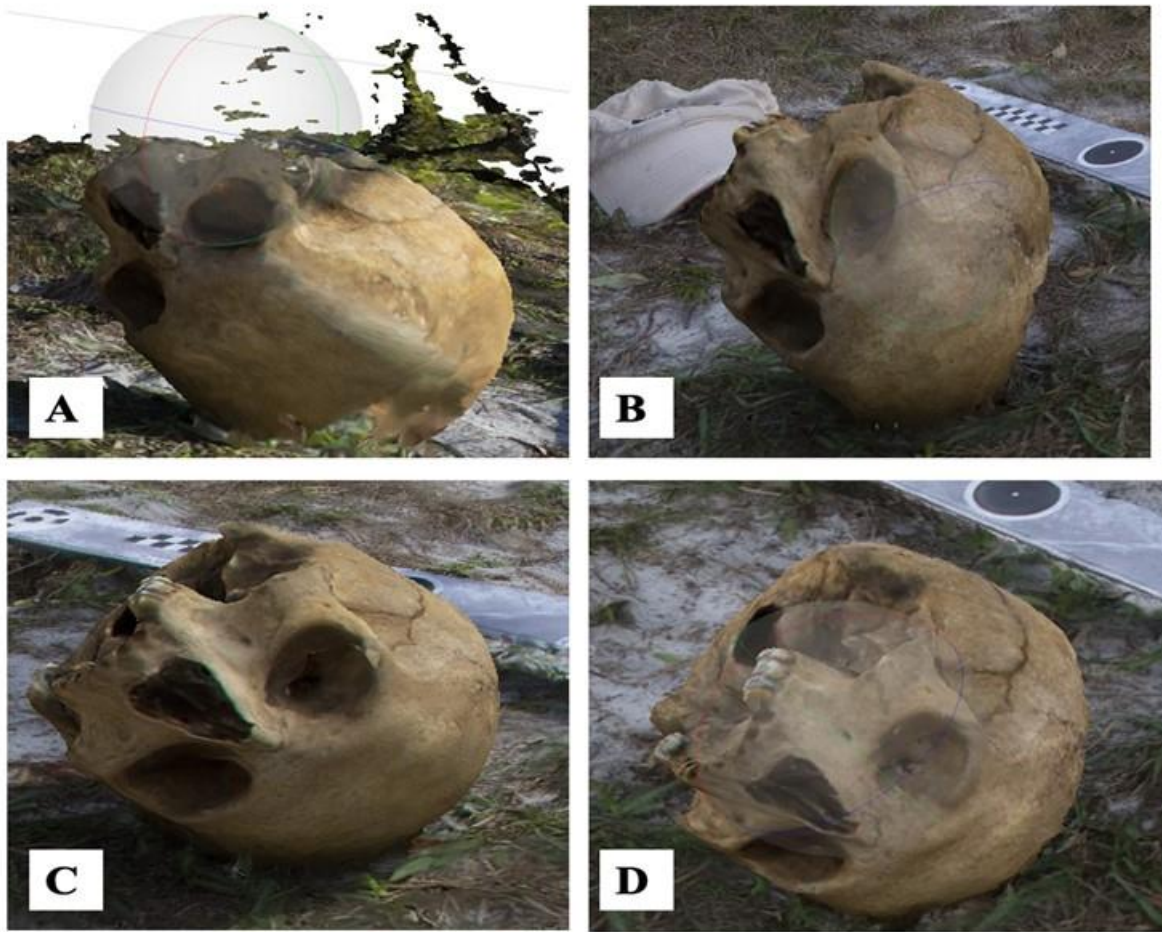


Figure 14: Images of the cranial closeups from Scenario 1. (A) Model 1A-2 without using the light correction tools. (B) Model 1B-1 using the sheet. (C) Model 1C-1 using the artificial lights. (D) Model 1D-2 using the sheet and artificial lights.

Scenario 2 (Shaded)

Visual Accuracy of the Orthomosaics

The orthomosaic of Model 2A -1, which used no lighting correction tools, has no obvious visual distortion of the skeletal geometry of the long bones in the scene (Figure 15). There is a very minimal degree of visual distortion along the superior angle of the left scapula.

Additionally, there is a very minimal degree of distortion along the shaft of the left tibia. There

is no obvious visual distortion caused by subject-subject interface corruption and the scale bar geometry has no obvious visual distortion. The lighting of the scene is highly uneven. There are large patches of dark shadows and bright sunlight throughout the scene. On the southern scale bar, the area is extremely bright, and the scale bar targets are difficult to identify.

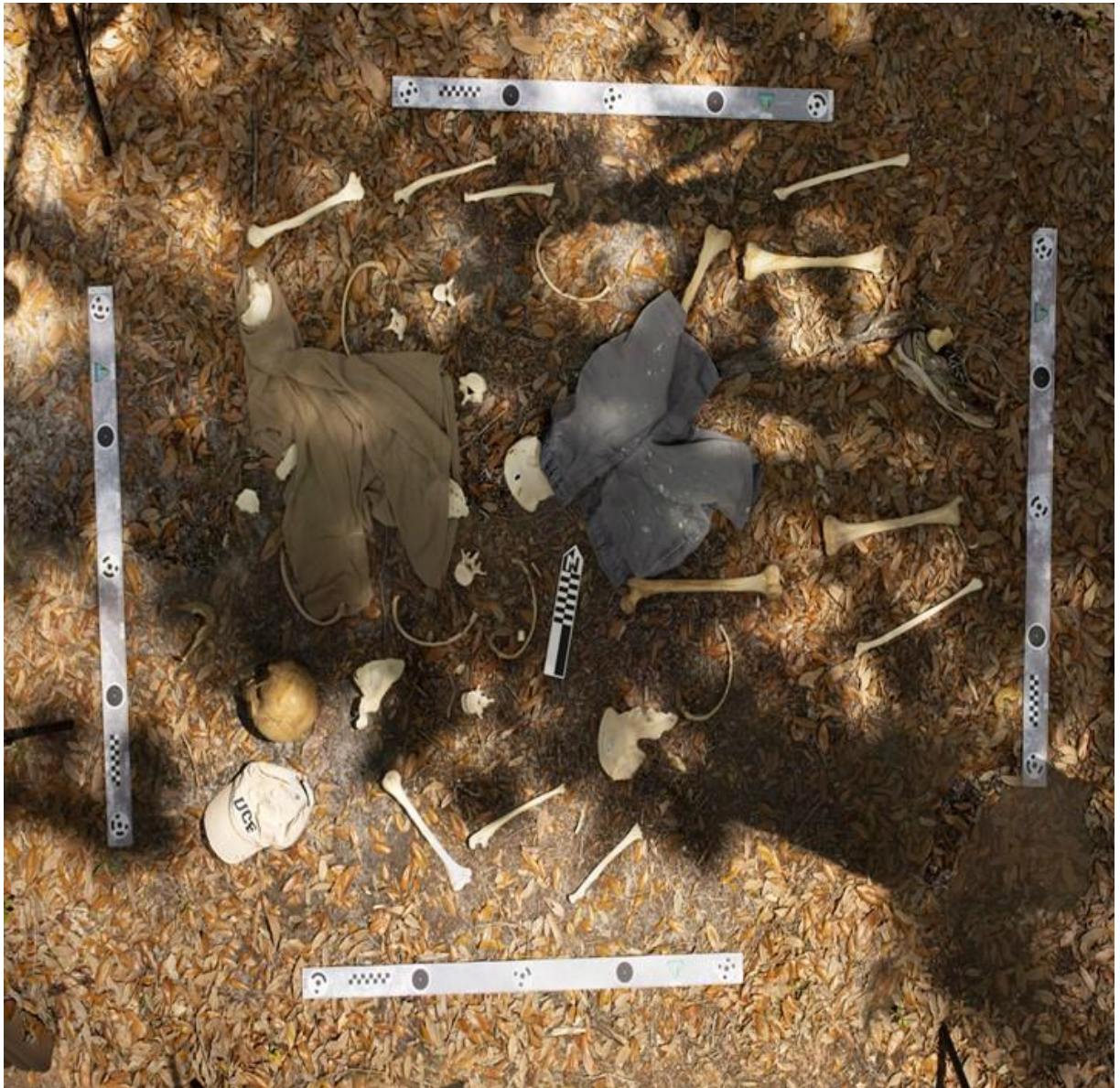


Figure 15: Model 2A-1 orthomosaic without using the light correction tools and sheet tools, and shadows from trees overhead.

This model, Model 2B-1 with the sheet, does exhibit minor to slight distortion of the skeletal elements throughout the scene (Figure 16). Long bones show moderate distortion along their shafts that sometimes make it appear as if the bone is slightly bent. This is best shown on the left humerus, radius, ulna, and femur. Severe distortion occurred on the left fibula, right tibia, right femur, and sacrum. These bones exhibited ground surface–subject distortion along their interfaces that resulted in a doubling effect. Moderate distortion occurred on the shaft of the left femur, as it appears that there is subject-subject interface distortion between the hem of the shorts and the shaft. Additionally, minor subject-subject interface distortion exists on the left scapula inside the shirt sleeve. In this model, the scale bar geometry is severely distorted throughout. The eastern scale bar shows severe distortion and doubling especially along the southern half. It also appears crooked. The northern scale bar exhibits severe distortion as well along the western portion of the bar. The western scale bar has only minor scale bar geometry distortion along the edges of the southern portion of the bar. The southern scale bar has no obvious visible errors, and the lighting is consistent throughout the scene.



Figure 16: Model 2B-1 orthomosaic using the sheet.

When examining Model 2C-1 which used the artificial lights, there is moderate distortion to the skeletal geometry of the left humerus, left ulna, and left radius (Figure 17). These three bones have a slight doubling effect occurring along the edges. There is also slight distortion along the shaft of the left tibia, and it appears to be slightly bent. Minor distortion exists on the edges of the left tibia and the left femur. Minor subject-subject distortion occurred at the interface of the left scapula and the shirt. Additionally, the edge distortion seen on the left femur may be contributed to subject-subject distortion with the hem of the shorts. However, there is no obvious visual distortion of the scale bars. Except, there is a leaf located on the eastern scale bar that is obscuring a portion of the bar. The lighting in this model is inconsistent. There are bright spots located on the bars as well as throughout the model itself. Additionally, one of the field

aides was positioned too close to the scene, and their leg was unable to be cropped out in the final model.



Figure 17: Model 2C-1 orthomosaic using the artificial lights that resulted in a few bright spots throughout the model (arrows). Note the distortion of the left arm bones in the northwest corner that resulted in the appearance of doubling.

The final model of Scenario 2, Model 2D-2 which used the artificial lights and sheet, had similar errors to Models 2B-1 and 2C-1 (Figure 18). There is severe distortion along the forearm bones of both sides of the body that have caused the bones to appear to double. However, there is only minimal distortion seen on the left and right humerus. The forearm bones are thinner, and a combination of distortion in the skeletal element geometry as well as distortion of the ground surface-subject interface may be contributing to the distortion of these bones. There is minimal distortion of both tibiae, and the left fibula. Slight subject-subject distortion occurred

where the left scapula is located inside of the shirt. There is also ground surface-subject distortion of multiple ribs. The scale bar geometry shows only minimal distortion along the edges and a leaf is located on the eastern bar near its most southern target. The lighting on the scene is consistent, without extreme patches of light.



Figure 18: Model 2D-2 orthomosaic using the sheet and artificial lights.

Visual Accuracy of the Crania

The orthomosaic exports of Scenario 2 showed evidence of having similar levels of distortion on the same locations within each model. This area of the cranium will be used as an example of distortion for each of the iterations. The crania appear to have modeled in the same manner, and the distortion appears similar in each model (Figure 19).

The crania of Model 2A-1 which did not include lighting correction tools, has minor distortion along the anterior portion of the nasal bones where it meets with the anterior nasal aperture. There is minimal distortion seen within the right eye socket, and there is an example of subject-subject interface distortion near the mastoid process. This severe distortion has the rib appear to be on top of or in line with of the mastoid process. However, the rib is located on the shirt further back in the frame. The sutures are clearly visible in this model, and there is no obvious visual distortion at the ground surface-subject interface. Also, there is no obvious visual distortion of the teeth or alveolar margin of the maxilla.

Model 2B-1, using the sheet, exhibits a cranium with slightly more distortion than in the previous model. The sutures are present, but not clearly visible, and there is moderate distortion of the anterior margin of the nasal bones. Minor distortion exists along the teeth and the alveolar margin. Ground surface-subject distortion exists on the cranial vault where a portion of the vault appears to be flattened and missing. Additionally, there is slight distortion of the skeletal geometry of the cranial vault as it appears bumpy and uneven near the mastoid process, and it should be smooth.

In general, Model 2C-1 which used the artificial lights, exhibits minimal distortion of the skeletal geometry. There is slight distortion along the ground surface-subject interface of the maxilla. Additionally, there is minimal distortion of the anterior nasal aperture's edge and the anterior portion of the nasal bone. There is no obvious visual distortion of the cranial vault or mastoid process, and all the sutures are clearly defined. However, there is severe skeletal geometry distortion along the maxilla under the anterior nasal aperture where a bone bridge appears to have been mistakenly modeled across the right corner of anterior nasal aperture.

Model 2D-2, using the artificial lights and the sheet, exhibited very minimal distortion of the overall skeletal geometry of the cranium. There is very minor distortion to the alveolar margin of the maxilla, but all of the teeth are identifiable. No obvious visual distortion due to ground surface-subject interfaces appears to exist. However, minor distortion does exist on the lateral edge of the left eye orbit. Minimal distortion is seen on the anterior edge of the nasal bones, and there is minimal distortion along the edges of the cranial vault. All of the sutures are visible and identifiable.

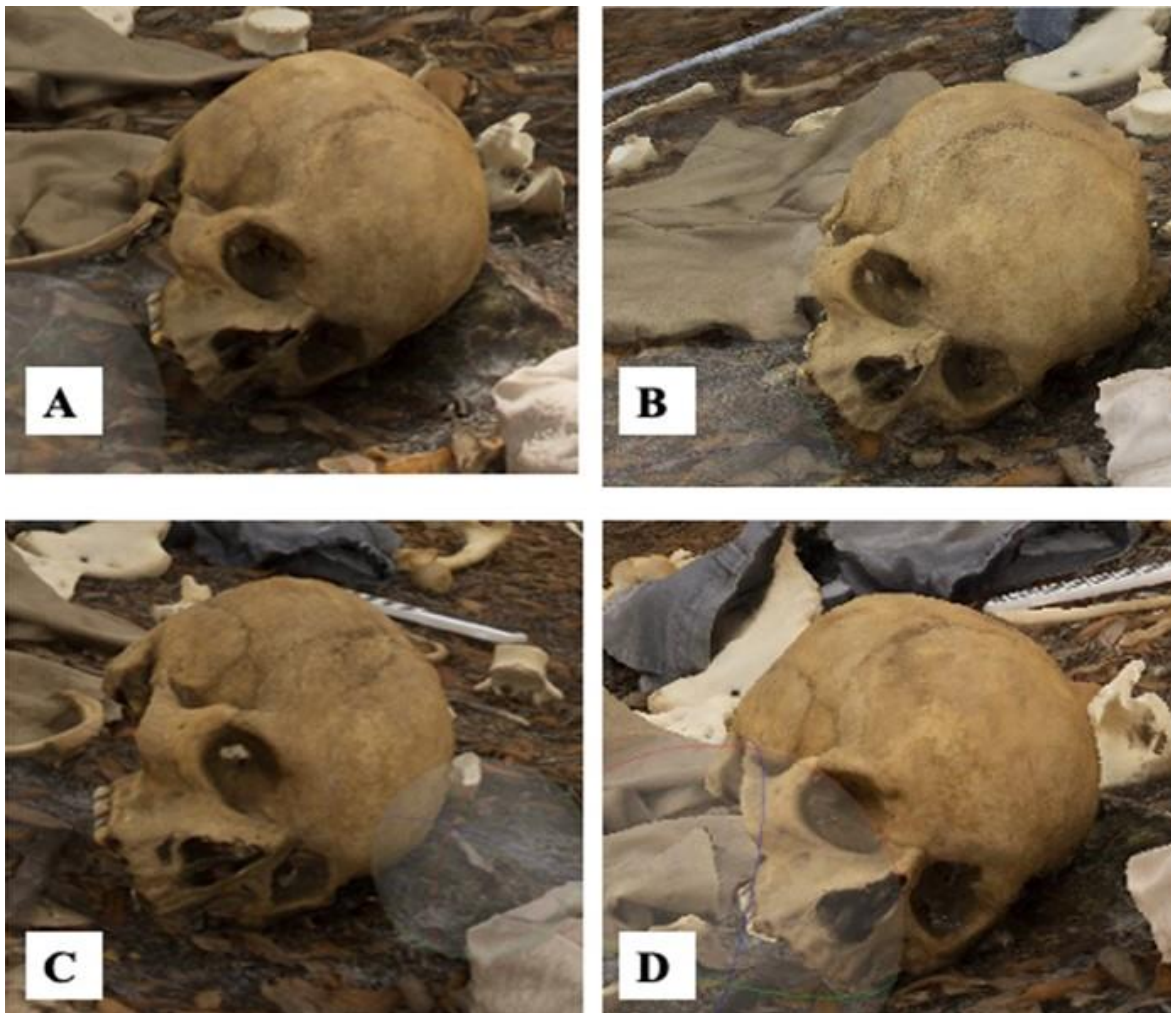


Figure 19: Images of the cranial closeups from Scenario 2. (A) Model 2A-1 without using the light correction tools. (B) Model 2B-1 using the sheet. (C) Model 2C-1 using the artificial lights. (D) Model 2D-2 using the sheet and artificial lights

Scenario 3 (Dappled)

Visual Accuracy of the Orthomosaics

The Model 3A-1 used no sheet or lights, and overall exhibited minor distortion of the skeletal geometry (Figure 20). There is minor distortion along the shaft of the left tibia. Slight subject-subject interface distortion is present on the ala of the left os coxa where it interacts with the shorts. Additionally, there is subject-subject interface distortion of the lower vertebrae on the left side of the shirt. Part of the body of the vertebrae exhibits subject-subject distortion with the shirt. There is no evidence of ground surface-subject interface distortion or distortion of the clothing geometry. No obvious visual distortion of the scale bars exists. There is a leaf on the southern scale bar located between the two western-most targets. The lighting throughout the scene is highly variable. Bones like the sacrum, right humerus, and right ulna are very bright white. Dark areas of shadow are seen on the shoe and the right os coxa.



Figure 20: Model 3A-1 orthomosaic without using the lights and sheet tools.

In general Model 3B-2, which incorporated the sheet, exhibited minor distortion throughout the skeletal and clothing geometry (Figure 21). Both tibiae had evidence of minimal distortion along the shafts. Slight ground surface-subject distortion occurred along the shaft and distal aspect of the left femur. The leaves located on the ground surface blended with the femur. Additionally, there is minor shaft distortion along the right femur. Slight distortion also occurred on the ala of the left os coxa. The distortion is attributed to the subject-subject distortion from the shirt and the shorts. There is also very minimal distortion to the manubrium where there is subject-subject interface with the tag of the shirt. A leaf is located on the head of the northern rib located between the shirt and the shorts. Scale bar geometry exhibits very minimal distortion, and there are a few leaves present on the scale bars. One is present on the northern scale bar near the western target, and another is on the southern bar near the eastern target. The light is consistent throughout the scene.



Figure 21: Model 3B-2 orthomosaic using the sheet.

Model 3C-2 incorporated the lighting correction tool of the artificial lights (Figure 22). Overall, there was minor to slight distortion of the skeletal geometry of the model. No obvious visual examples of subject-subject interface or clothing geometry is seen in this model. There is moderate distortion of the rib near the hat due to ground surface-subject interface between the anterior portion of the rib and the leafy ground surface. A leaf is present, partially obscuring the head of the rib located between the shirt and the shorts. Additional moderate ground surface-subject interface exists at the distal end of the right ulna, the distal end and shaft of the right humerus, and the edges of right scapula. Slight distortion exists on the ala of the left os coxa, and at the base of the sacrum. Minor distortion is shown on the shaft of the left femur. Both the left and right shafts of the tibiae exhibit minimal distortion. There also exists minor distortion of

the shaft of the right femur. The scale bars appear to have no obvious visual distortion of their geometry. There is one leaf present on the Western scale bar near the northern target. Throughout the scene, the light is very inconsistent. There are bright spots of light overexposing some of the bones, including the right humerus. This extreme presence of light may have contributed to the distortion of this bone.



Figure 22: Model 3C-2 orthomosaic using the artificial lights.

In general, the Model 3D-1 which included both the artificial lights and the sheet, showed minimal distortion throughout (Figure 23). When discussing skeletal geometry, the left os coxa exhibits slight distortion along the ala and the crest. The clothing geometry shows no obvious

visual distortion. Minor distortion is seen along the crest of the right os coxa as well. Along the superior and inferior angles of the scapula, there is minor distortion. Many long bones exhibit minimal distortion along the shafts. These bones include both tibiae, the left fibula, and both femora. Very minimal distortion is evident on the superior angle due to ground surface-subject interaction. No obvious visual distortion of the scene is seen as subject-subject interface distortion. There is no obvious visual distortion of the scale bar geometry, and the lighting is consistent throughout the scene.



Figure 23: Model 3D-1 orthomosaic using the sheet and artificial lights.

Visual Accuracy of the Crania

The orthomosaic representations of Scenario 3 exhibited similar levels of distortion. Examination of closeup views of the anterior aspect of the cranium shows similar distortions, making them gauges of distortion as seen in each of the iterations (Figure 24).

When examining the crania, Model 3A-1 which did not include the application of the sheet or artificial lights, has moderate distortion of the alveolar margin. The teeth are not identifiable, and the right side of the maxilla exhibits ground surface-subject distortion. The sutures are only slightly visible. The edges of the anterior nasal aperture, as well as the interior, exhibit minor distortion. Very minimal distortion exists around the cranial vault, and the rims of the eye orbits.

Model 3B-2, which used the sheet, also exhibited moderate skeletal geometry distortion along the alveolar margin. The teeth are not clearly defined or visible. Along the right portion of the cranium, where the lateral portion of the right orbit touches the ground, there is evidence of slight ground surface-subject distortion. The left zygomatic arch exhibits minor distortion, as well as along the inferior portion of the cranium near the mastoid process. There is no obvious visual distortion of the cranial vault. Around the anterior nasal aperture on the edges, there is minimal distortion.

The Model 3C-2, which included the artificial lights, exhibited less distortion than the previous two screenshot models. There are a small number of teeth visible, and only slight distortion of the alveolar margin. No obvious visual distortion is present along the cranial vault, or around the anterior nasal aperture. Minimal distortion exists along the left zygomatic arch. There does not appear to be evidence of ground surface-subject distortion.

In general, Model 3D-1 which used both light correction tools, shows slight distortion. There is evidence of slight ground surface-subject distortion along the right side of the maxilla

and zygomatic bone. Additionally, there is subject-subject distortion of the left zygomatic bone and the cranial vault. The distortion caused the two portions of the skull to combine and appear indistinct. Along the alveolar margin, only a small number of teeth are modeled and there is slight distortion. Around the anterior nasal aperture, including the nasal bones, there is minor distortion. Minimal distortion exists along the edges of both eye orbits and in the intraorbital space.

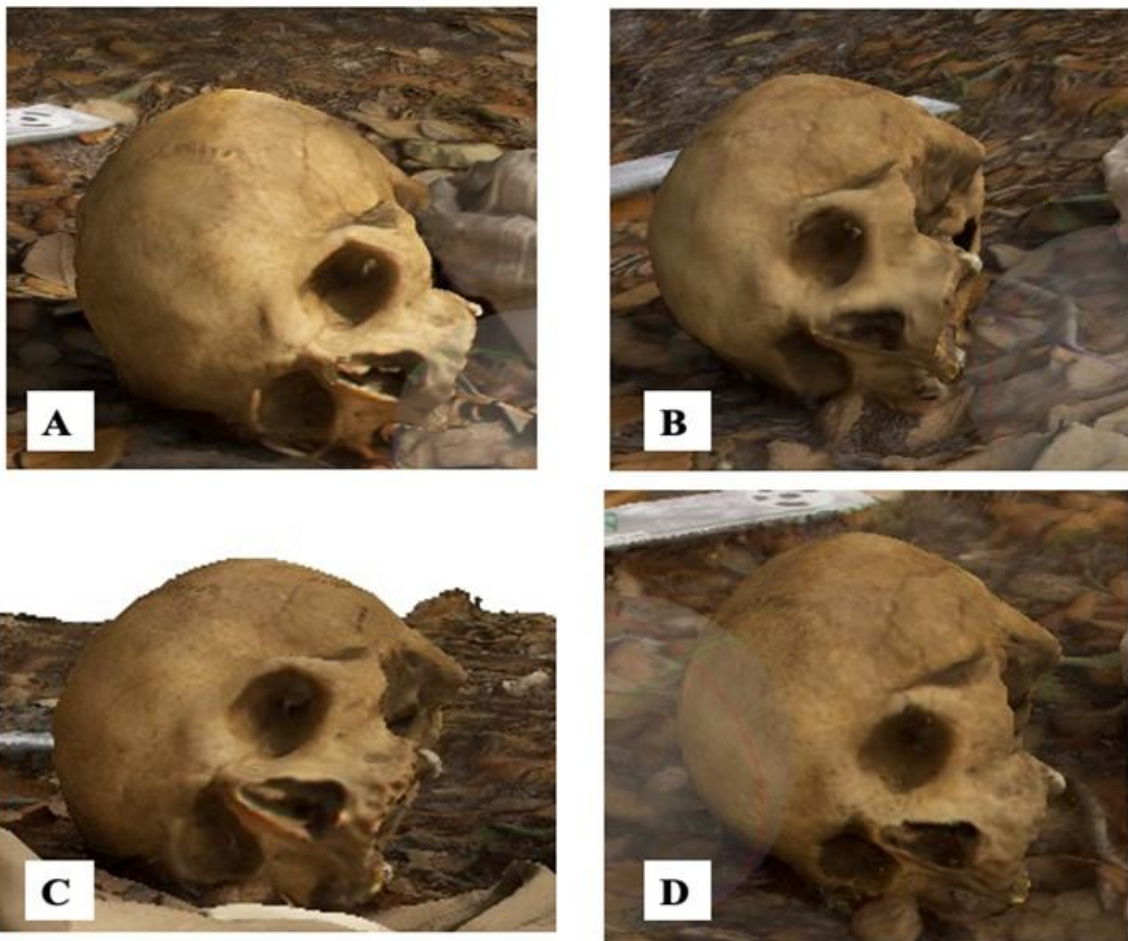


Figure 24: Images of the cranial closeups from Scenario 3. (A) Model 3A-1 without using the light correction tools. (B) Model 3B-2 using the sheet. (C) Model 3C-2 using the artificial lights. (D) Model 3D-1 using the sheet and artificial lights.

Discussion

The accurate mapping of a forensic scene is an important aspect of a forensic investigation, and a key aspect of a forensic archaeologist's work as these maps are vital to preserving the context of the scene. The preservation of the context of the scene beyond its initial observation can aid the forensic archaeologist in their task to recreate the series of events leading to the ultimate demise of the person (Dirkmaat & Adovasio, 1997; Dirkmaat & Cabo, 2012; Dupras et al., 2012; Dirkmaat, 2015). The successful integration of CRP into archaeology suggests that such a tool may be easily applied to forensic research as well. However, only a limited expanse of research exists that directly addresses specific guidelines for the application of this technology (McCollum, 2020; Ferrell, 2020). Even rarer is the degree of research that discusses problems, and their solutions, that photogrammetry users may encounter in the outdoor environments of traditional archaeology or forensic archaeology scenes (Ferrell, 2020; Burdziakowski & Bobkowska, 2021). Therefore, the current research seeks to develop guidelines for the correction of problematic lighting caused by shadows in wooded environments. This included a qualitative and quantitative investigation of the accuracy of the produced models. These models were tested under three different lighting scenarios and included four iterations of the scene that tested light correction tools. These tools included white sheets and artificial lights. Additionally, the improvement of the models continued into the processing phase, as the models were processed twice in Agisoft Metashape® utilizing different settings (Agisoft LLC., 2019b).

While the current and previous projects have demonstrated the applicability of photogrammetry to record skeletal remains, it is difficult to produce highly accurate models without visual errors (Church, 2018; McCollum, 2020; Ferrell, 2020). For example, closeup views of the skeletal elements in the orthomosaic models can exhibit distortion of the skeletal

geometry, scale bar geometry, subject-subject interfaces, and ground surface-subject interfaces. Therefore, this research seeks to overcome difficulties in lighting observed by Ferrell (2020) that resulted in distortions. To directly address the three main goals of this research study, the following discussion is organized to discuss each of these aspirations. First, this project sought to answer whether light correction tools of sheets and artificial lights could affect the quantitative and qualitative accuracy of the models. From the answer to this first question, the second goal was to test how these light correction tools could be applied to scenes that were more reminiscent of real-world forensic archaeology scenes. A final goal of the research was to develop guidelines explaining how to document and process forensic archaeology scenes in a wooded environment and in inconsistent lighting conditions. There were challenges and limitations that occurred during data collection and processing, and these affected the results of the research project. These circumstances helped contribute to the development of the final protocol guidelines included in this discussion.

RMS Reprojection and Scale Bar Error

All the models produced, were deemed highly accurate by their recorded RMS reprojection errors. The highest error rate was found during Scenario 3 (Dappled), while the lowest was found during Scenario 1 (Open). In total, the deviation of the RMS reprojection error was only 0.075 pixels. The scale bar error was relatively consistent throughout the scenarios, with a range of 0.0008 meters. The only exception was Model 1C-1. This model had the highest total scale bar error, with an error of 0.1126 meters. Including this outlier, the range of errors increases to 0.1125 meters. The large degree of error observed in this model may have been caused by the field aides disturbing the ground foliage and leaves as they walked around the scene, or while they were located close to the perimeter of the scene while holding the sheet.

Even with this wide variation, the National Forensic Science Technology Center (NFSTC) considers scenes accurate if the measurements of the scene fall within $\frac{1}{4}$ of an inch or 6.35 mm of the actual measurement (NFSTC, 2013).

Visual Accuracy

Each of the models did exhibit variations in their visual accuracy which are gauged using the orthomosaics, and a closeup screenshot of the anterior view of the cranium (Table 5). As discussed above, none of the models fell outside of the range of acceptable accuracy quantitatively. However, the variation in visual accuracy of the models was noticeable. Even when working in perfect lighting, photogrammetry models tend to experience a degree of visual distortion despite their quantitative measurements appearing perfect (Howland et al., 2014; McCollum, 2020; Ferrell, 2020). In general, none of these distorted details resulted in an inability of the viewer to identify the bones or the features of the skeletal material. However, it was noted that the models that included the sheet appeared more visually accurate than those without. Distortion was more obviously noticeable in the screenshots than in the orthomosaics. It has been noted that the orthomosaic renderings of the models are more visually precise than the in-program screenshots (Ferrell, 2020). However, detailed scrutinization was still conducted at the orthomosaic and closeup screengrab levels to ensure that the visual accuracy of the models was being analyzed thoroughly. All distortions observed in the orthomosaics and the screengrabs of the model were identified and described. There was also more noticeable distortion of the scale bars in Scenario 1 (Open). This location had a ground cover of grass, not leaves or pine needles. Without careful cleaning of the grass away from both sides of the scale bars, the distortion appeared worse than in the other locations (McCollum, 2020).

Table 5: Comparison of the visual accuracies as seen across each model. The “Ortho” rows indicate how the discussion applies to the orthomosaics of each model, while “C-SS” stands for the cranial screenshots.

| <u>Model Number</u> | | <u>Skeletal Element Geometry</u> | <u>Clothing Geometry</u> | <u>Scale Bar Geometry</u> | <u>Ground Surface-Subject Interface</u> | <u>Subject – Subject Interface</u> | <u>Overall Lighting</u> |
|----------------------------|-------|--|---------------------------------|--|--|---|---|
| 1A-2 | Ortho | Minor distortion of long bone and ribs | No obvious visual distortion | Minimal distortion of edges; some grass on bars | No obvious visual distortion | No obvious visual distortion | Severe shadowing from artificial lights |
| | C-SS | Minor distortion overall; severe distortion along alveolar margin | N/A | N/A | Slight distortion of cranial vault and ground | Moderate distortion of right zygomatic arch | N/A |
| 1B-1 | Ortho | Minor distortion of long bones and ribs | No obvious visual distortion | Minimal distortion of edges; few pieces of grass | Minor distortion due to color of mandible | No obvious visual distortion | Consistent |
| | C-SS | Slight distortion of splanchnocranium; minor distortion of cranial vault | N/A | N/A | No obvious visual distortion | Severe distortion of right temporal bone and zygomatic arch | N/A |
| 1C-1 | Ortho | Minimal distortion overall | Minor distortion of shoe | Minimal distortion of edges; few pieces of grass | Slight distortion of ribs | Slight distortion of ribs on shirt | Severe bright spots and shadows |

| <u>Model Number</u> | | <u>Skeletal Element Geometry</u> | <u>Clothing Geometry</u> | <u>Scale Bar Geometry</u> | <u>Ground Surface-Subject Interface</u> | <u>Subject – Subject Interface</u> | <u>Overall Lighting</u> |
|----------------------------|-------|--|---------------------------------|--|--|---|---------------------------------|
| | C-SS | Minimal distortion overall; moderate distortion of right eye orbit and mastoid process | N/A | N/A | No obvious visual distortion | Severe distortion of right zygomatic arch | N/A |
| 1D-2 | Ortho | Minor distortion of long bones and ribs | No obvious visual distortion | Minor distortion of edges; lots of pieces of grass/sticks; | Slight distortion of ribs | Slight distortion of ribs on shirt | Consistent |
| | C-SS | Minor distortion overall | N/A | N/A | Minor distortion between frontal bone and ground | No obvious visual distortion | N/A |
| 2A-2 | Ortho | No obvious visual distortion | No obvious visual distortion | Minimal distortion due to uneven lighting | No obvious visual distortion | No obvious visual distortion | Severe bright spots and shadows |
| | C-SS | Minor distortion overall; sutures are visible | N/A | N/A | No obvious visual distortion | Severe distortion of mastoid process due to rib | N/A |

| <u>Model Number</u> | | <u>Skeletal Element Geometry</u> | <u>Clothing Geometry</u> | <u>Scale Bar Geometry</u> | <u>Ground Surface-Subject Interface</u> | <u>Subject – Subject Interface</u> | <u>Overall Lighting</u> |
|----------------------------|-------|--|-----------------------------------|---|--|--|---------------------------------|
| 2B-1 | Ortho | Minor to slight general distortion; moderate distortion of long bone shafts | Slight distortion near left femur | Severe distortion of eastern and northern scale bars; minor distortion of edges of southern scale bar | Severe distortion of left fibula, right tibia, right femur, and sacrum for a doubling effect | Moderate distortion at interface of left femur and shorts; minor distortion at interface of shirt and left scapula | Consistent |
| | C-SS | Slight distortion overall; sutures are visible; moderate distortion of nasal bones | N/A | N/A | Severe distortion of cranial vault making it disappear and appear uneven | No obvious visual distortion | N/A |
| 2C-1 | Ortho | Moderate distortion of left arm bones for doubling effect | Slight distortion near left femur | No obvious visual distortion | No obvious visual distortion | Minor distortion at interface of shirt and left scapula; minor distortion at interface of left femur and shorts | Severe bright spots and shadows |

| <u>Model Number</u> | | <u>Skeletal Element Geometry</u> | <u>Clothing Geometry</u> | <u>Scale Bar Geometry</u> | <u>Ground Surface-Subject Interface</u> | <u>Subject – Subject Interface</u> | <u>Overall Lighting</u> |
|----------------------------|-------|---|--|--|--|--|---------------------------------|
| | C-SS | Minimal distortion overall; sutures are clearly defined; severe distortion of maxilla inferior to the anterior nasal aperture where bony bridge developed | N/A | N/A | Slight distortion at interface of maxilla and ground | No obvious visual distortion | N/A |
| 2D-2 | Ortho | Severe distortion along forearm bones of both sides for doubling effect; minimal distortion on both humeri | Slight distortion at left scapula location | Minimal distortion along edges; leaf present on eastern bar near southern target | Variable distortion of ribs with ground surface | Slight distortion of left scapula and shirt | Consistent |
| | C-SS | Minimal distortion overall; sutures are clearly defined | N/A | N/A | No obvious visual distortion | No obvious visual distortion | N/A |
| 3A-1 | Ortho | Minor distortion overall | No obvious visual distortion | No obvious visual distortion | No obvious visual distortion | Slight distortion of lower vertebrae on left side of shirt; Slight distortion of left os coxa at interface of shorts | Severe bright spots and shadows |

| <u>Model Number</u> | | <u>Skeletal Element Geometry</u> | <u>Clothing Geometry</u> | <u>Scale Bar Geometry</u> | <u>Ground Surface-Subject Interface</u> | <u>Subject – Subject Interface</u> | <u>Overall Lighting</u> |
|---------------------|-------|---|------------------------------|---|---|---|-------------------------|
| | C-SS | Minor distortion overall; ill-defined sutures; moderate distortion of alveolar margin | N/A | N/A | Slight distortion at interface of right lateral portion of the orbit and ground | No obvious visual distortion | N/A |
| 3B-2 | Ortho | Minor distortion overall | No obvious visual distortion | Very minimal distortion; leaves on bars | Slight distortion along shaft and distal aspect of the tibia | Slight distortion of left os coxa at interface of shorts; minimal distortion of manubrium at interface of shirt | Consistent |
| | C-SS | Moderate distortion overall | N/A | N/A | Slight distortion at interface of lateral portion of the right orbit and ground | No obvious visual distortion | N/A |

| <u>Model Number</u> | | <u>Skeletal Element Geometry</u> | <u>Clothing Geometry</u> | <u>Scale Bar Geometry</u> | <u>Ground Surface-Subject Interface</u> | <u>Subject – Subject Interface</u> | <u>Overall Lighting</u> |
|----------------------------|-------|---|---------------------------------|----------------------------------|---|---|---------------------------------|
| 3C-2 | Ortho | Slight distortion overall | No obvious visual distortion | No obvious visual distortion | Moderate distortion at distal end of right ulna, right scapula, and right humerus | No obvious visual distortion | Severe bright spots and shadows |
| | C-SS | Minimal distortion overall | N/A | N/A | No obvious visual distortion | No obvious visual distortion | N/A |
| 3D-1 | Ortho | Minimal distortion overall | No obvious visual distortion | No obvious visual distortion | No obvious visual distortion | No obvious visual distortion | Consistent |
| | C-SS | Slight distortion overall | N/A | N/A | Slight distortion of right maxilla | Slight distortion of left zygomatic | N/A |

Lighting Correction Tools

The lighting correction tools of the sheet and lights did not alter the RMS reprojection or scale bar error of the produced models to a significant degree. However, the light correction tools did influence the qualitative quality of the produced models. As outlined in Table 12, there are variations between each of the model's visual accuracies. In circumstances of dim lighting, the artificial lights may not appear to change the model quality drastically. Additionally, a non-visual contribution of the lights may be that their presence may contribute to a higher shutter speed during recording. This higher shutter speed contributes to the overall quality of the model by generating more accurate photographs during the initial data collection process.

Archaeologists employ artificial lighting in indoor settings to help increase shutter speed and improve model accuracy (Portalés et al., 2009; Teza et al., 2016). The application of the sheet to the scene eliminates dappled lighting from appearing on the scene because of trees or other objects creating shadows. Therefore, processing difficulties that could have been caused by inconsistent lighting within the scene are eliminated before the photographs are even uploaded to a computer. Tarps can, and have been, used as well, but a sheet was chosen to allow the light to not be completely blocked, only the shadows to be eliminated (McPherron et al., 2009). If the application of such tools is feasible for the documentation of a scene, their inclusion will prove beneficial to the overall visual quality of the model. The use of the sheet, especially, was helpful to the overall visual quality of the scene. Lighting issues that are not addressed in the field using the light correction tools can be partially corrected within the Adobe Bridge® processing step (McCollum, 2020; Ferrell, 2020). Using Bridge® photographs that have harsh lighting can be adjusted by changing the exposure of the image, or other settings (Ferrell, 2020). These pre-processing corrections are useful, however, are not a substitute for preparation and harsh lighting

corrections enacted in the field that are a part of better photogrammetry practices. However, both the lights and sheets as correction tools can result in challenges, as well as benefits, when employed in the field.

Challenges and Limitations

The challenges of this project occurred in the field, as well as in the processing phase of research. The outdoor nature of the data collection required specific weather (Ferrell, 2020). It could not be raining, as lights, camera, and skeletal materials could not be exposed to moisture. Additionally, the controlled scene could not be prepared for recording while the ground surface was wet. While the wet ground surface could damage skeletal material, rain could also be dripping from the trees causing further issues during data collection.

The need to clear the space on the outside of the scale bars, as well as inside the bounds of the scene was another challenge (Ferrell, 2020). Not adequately clearing the grass along the scale bars may have contributed to the distortion that occurred along the edges, and the heavy distortion of the scale bars. Grass and foliage needed to be cleared on both sides of the scale bars, not only along the interior edge. It was noted that the exterior edges of the bars often exhibited more distortion than the interior edges, especially when the ground foliage was not removed or cut. This distortion was exacerbated when accompanied by the movement of the ground surface foliage around the bars from field aides walking too close to the perimeter of the scene. Distortion that was caused by foliage next to the skeletal elements and evidence was noted by McCollum (2020) and Ferrell (2020), which produced the guideline of clearing the scene carefully. It was discovered that the cleanliness of the scene needed to be checked at the level of every view angle and from every side to ensure that the scene was completely cleared. The scene also needed to be re-checked at the beginning of every new model. This ensured that

stray material that may have blown onto the scene was removed before recording continued. After clearing, a 0.6-meter (2 foot) radius needed to be maintained by the photographer, the lights themselves, and additional people on the scene. The photographer taking photographs too close to the scale bars may have contributed to the distorted edges and the difficulty that Metashape® had in accurately reconstructing the geometry of the scale bars. Additionally, the ground surface of the Open location was a composition of grass and sand. Field aides walking too close to the perimeter of the scene may have disturbed the ground foliage or shifted the sandy surface. Another possibility is that the field aides may have unknowingly kicked ground foliage onto the bars. The lights being placed within an approximate 0.6-meter (2 foot) radius may have contributed to the projection of the shadows on to the scene itself, as well as making it more challenging for the photographer to keep a standardized distance around the scene.

The equipment necessary for photogrammetry, though relatively minimal, also contributed unique challenges to the data collection process. For example, the positioning of the lights around the scene required the photographer to maneuver carefully to ensure that they were not accidentally nudged out of position. The photographer also needed to be careful that no one, including themselves, was between the lights and the scene when they were in use. The lights also cast shadows themselves, and therefore may have contributed to some of the distortions seen on models where the lights had been placed there but were not turned on. Therefore, the addition of lights to the scene should only be enacted when the models involving the lights are occurring.

The use of the sheet also became challenging. Not only did the size of the sheet need to be adequate to cover the size of the scene, but several people were needed to hold the sheet. For these small scenes, a full-sized flat sheet was used, and three people were needed to hold the sheet. The people could angle the sheet in the early morning to block the sun, but as the day

progressed towards noon, the sun moved overhead. This became challenging, as the sheet was barely large enough to adequately cover the scene and holding the sheet at a more parallel angle put added strain on the additional team members. When holding the sheet, it was also necessary to position people so they were not standing in front of the lights or were within the 0.6-meter (2 foot) radius of the scene. These criteria severely limited locations in which people could stand.

Conclusion

The proper documentation of a forensic scene is vital to the analysis of the scene. However, these scenes are often complicated and often involve time constraints on data collection. This is especially true when the scenes are located outside, and weather patterns may shift suddenly and corrupt the scene. In archaeology, the recording of outdoor scenes has been successfully accomplished using CRP. This research has demonstrated that such technology can be applied successfully to forensic scenes to achieve fast and accurate scene documentation. Furthermore, it has attempted to directly mitigate difficulties caused by inconsistent lighting that is sometimes present in outdoor settings. The use of a white sheet or tarp, as well as artificial lighting, were tested as methods to eliminate lighting problems. Even though the use of lighting correction tools did not affect the overall quantitative quality of the models including the RMS reprojection and total scale bar errors, they are considered useful. The use of such tools did improve the overall visual appearance of the models by eliminating shadows and areas of bright sun that could affect the overall visual accuracy of the models. These tools can be easily integrated to current photogrammetry guidelines for forensic scenes, and the application of such practices utilized by current forensic investigators. The 3D modeling results of such CRP practices will create the benefit of accurate digital maps for the case reports and inclusion in courtroom presentations.

CHAPTER THREE

Introduction

The integration of archaeological techniques and tools into forensic investigations have resulted in the advancement of forensic archaeology as a field (Christensen, 2014; Dupras et al., 2012). This field incorporates the excavation expertise of traditional archaeological methods and applies it to forensic settings. These methods include ground search methods, evidence recovery, surveying, and mapping. Forensic archaeologists, in general, tend to work at outdoor scenes and the integration of modern forensic techniques with archaeological methods has made that easier. Forensic archaeologists are better able to analyze outdoor crime scenes because of their background in taphonomic processes that may scatter human remains. These agents can include animals, and through familiarity with the marks left by local animals, forensic archaeologists are able to identify these animals and refine the search parameters. (Dirkmaat & Adovasio, 1997; Schultz & Dupras, 2008; Dirkmaat & Cabo, 2012). Additionally, forensic archaeologists may easily identify nonhuman versus human remains, provide a trauma analysis profile, and ensure that all remains are handled appropriately and guarantee the chain of custody is maintained. Their experience with excavation techniques also allows forensic archaeologists to excavate human remains without damaging them or losing of the skeletal elements. These techniques have been adopted from bioarchaeological techniques to ensure the complete and careful recovery of ancient human remains. However, archaeologists do not experience the same stringent evidence documentation protocols that are necessary in legal forensic work (Dirkmaat & Adovasio, 1997; Schultz & Dupras, 2008; Dupras et al., 2012; Dirkmaat & Cabo, 2012; Christensen et al., 2014; Dirkmaat, 2015).

The protocols surrounding evidence collection at a forensic scene are strict. However, the majority of these protocols are written for indoor settings (Dirkmaat & Cabo, 2012). This is particularly true regarding guidelines on the recovery of human remains by law enforcement officers. When forensic professionals encounter a set of forensic remains in an outdoor location, the lack of established guidelines may lead to remains being collected quickly and their original position not being well recorded. Once the remains and evidence are collected, there is no procedure that can replace them in their original positions. If they are not properly documented before removal, information about the scene may be lost. Specific questions that cannot be answered through simple lab analysis include the postmortem interval, and the effects that animal scavenging, or other taphonomic agents, may have had on the remains. These questions cannot be properly addressed without knowledge of the original condition, position, and orientation of the remains (Dirkmaat & Cabo 2012; Dupras et al., 2012; Dirkmaat 2015). Therefore, the expansion of forensic archaeological protocols can only improve the quality of outdoor crime scene investigator practices.

Including the practices of forensic archaeology scene recovery protocols into outdoor crime scene investigation emphasizes the importance of documenting the original layout of the scene (Dirkmaat & Adavasio, 1997). Originally, such documentation was executed through the creation of a plane-view map. In more recent times, 3D digital documentation tools have been used. In the context of the present study, the technology that will be used is close-range photogrammetry (CRP). This technology has been applied when recording archaeological sites but only recently have its uses been explored in the context of outdoor crime scene investigations (Barazzetti et al., 2011a; Doneus et al., 2011; Green et al., 2014; Howland et al., 2014; Sapirstein, 2016). Despite the small number of examples of CRP appearing in a forensic context,

research has demonstrated that CRP can be successfully applied to outdoor scenes (Edelman & Aalders, 2018; Gidusko, 2018; Church 2019; McCollum, 2020; Ferrell, 2020). Specifically, these studies have tested the application of CRP on large, complex, staged outdoor scenes in a wooded environment. They have developed guidelines outlining the procedures necessary for data collection and processing, addressed the complications posed by partially obstructed wooden environments, and experimented with its accuracy on different ground surfaces. Specifically, Ferrell (2020) experimented with writing guidelines on how to correct model distortion before and during processing the photographs in Metashape®. The study concluded that one of the primary causes of visual distortion in the models originated from uneven lighting conditions that could not be fixed during processing. The resulting guidelines did not include recommendations on how to best correct these distortions beyond minor alteration during pre-processing.

Phase 1 of this research project included experimentation with four iterations of light correction tools per model. These iterations included using no light correction tools, using a sheet, using artificial lights, and finally using both the sheet and lights. In the experimental phase, it was found that the application of the sheet contributed to fewer visual errors and higher quality models. Additionally, the importance of preparing the scene before data collection and remaining far back from the scene during recording was emphasized. However, these were small scenes, not realistically sized scatters. The second phase of this research will test whether the application of these light correction tools will have corrective effects on a scene of approximately twice the size with scattering of skeletal elements.

The purpose of the Phase 2 research is to apply the procedures learned during Phase 1 to real-world sized outdoor scatters. Three goals were developed for this study to attempt and

correct lighting problems as encountered in large outdoor scenes. The first of these goals was to examine which of the lighting correction tools, the sheet or the artificial lights, aided in the qualitative and quantitative quality of the final models. Secondly, the learned procedures regarding cleaning the scene and remaining at a distance during data collection needed to be further tested on a real-world staged scene. Finally, guidelines needed to be adapted to incorporate all valuable procedures that were learned during Phase 1 and confirmed during Phase 2 on how best to eliminate harsh lighting in the field that may cause distortions during processing.

Materials and Methods

The natural lands located southeast of the University of Central Florida's main campus in Orlando were chosen as the field site for this project. Within the natural lands, two specific locations were chosen. These locations were selected so that one model could be recorded in dappled lighting, and the other in a primarily open location that involved little natural shadowing. It was noted during the Phase 1 research, that these two scenarios experienced the most drastic correction when the light correction tools were applied. Additionally, it is difficult for a completely shaded location to be found in the natural lands. The wooded nature of the area contributes itself more often to dappled scenes as the amount of time taken to properly record the scene results in changes in the sun's position throughout the day. A location that may be completely shaded at the beginning of recording becomes more dappled throughout the day. The dappled location, used for Scenario 1, had an oak hammock and pine flatwood matrix. The ground surface was flat and covered in live oak leaves and pine needles. The open location, used for Scenario 2, had a bottom surface that consisted of grasses and other plant matter and was sandy. After the location selection, the scenes were staged. These were larger scenes that were

approximately 4 m by 3.5 m in size, and involved more of a scatter than the smaller staged scenes. Therefore, more bones were used to stage these scenes in addition to the shirt, shorts, hat, and a pair of shoes. Approximately the same orientation and number of skeletal elements was utilized in both scenes (Table 6).

Table 6: Inventory of the human skeletal elements used in the two scenarios.

| <u>Skeletal Element Inventory</u> | | <u>Scenario 1</u> | <u>Scenario 2</u> |
|--|-------|--------------------------|--------------------------|
| Cranium | | 1 | 1 |
| Mandible | | 1 | 1 |
| Scapula | Left | 1 | 1 |
| | Right | 1 | 1 |
| Clavicles | Left | - | - |
| | Right | - | 1 |
| Humerus | Left | 1 | 1 |
| | Right | 1 | 1 |
| Radius | Left | 1 | 1 |
| | Right | 1 | 1 |
| Ulna | Left | 1 | 1 |
| | Right | 1 | 1 |
| Vertebrae | | 10 | 9 |
| Ribs | | 12 | 12 |
| Sternum | | 1 | 1 |
| Os Coxa | Left | 1 | 1 |
| | Right | 1 | 1 |
| Sacrum | | 1 | 1 |
| Femur | Left | 1 | 1 |
| | Right | 1 | 1 |
| Tibia | Left | 1 | 1 |
| | Right | 1 | 1 |
| Fibula | Left | - | 1 |
| | Right | 1 | 1 |
| Patella | Left | 1 | 1 |
| | Right | 1 | 1 |
| Tarsals | Left | 1 | 1 |
| | Right | 2 | 1 |
| Metatarsals | | 2 | 1 |
| <u>Total</u> | | 48 | 47 |

Scene Materials

In addition to the skeletal and clothing material, four 1-meter Cultural Heritage Imaging calibrated photogrammetry scale bars with coded targets surrounded the scene. Due to the larger nature of the scene, four additional 0.5-meter scale bars were included around the scene. The scale bars were placed around the scene to ensure that they were visible in multiple overlapping images and from multiple angles (Cultural Heritage Imaging, 2021). These scale bars are used to ensure that the scale of model is validated, as the coded targets are automatically recognized as reference points by the software (Cultural Heritage Imaging, 2021; Edelman & Aalders, 2018). A north arrow was also included in the scenes.

Two king-size flat sheets, sewn together, were used as a cover for certain versions of the scene. The sheet would be held at an angle by volunteers to ensure that the entirety of the scene was covered during these recording sessions. The sheet was white to ensure that there were no color changes occurring to the photographs. Due to the expanded size of the sheet, and the positioning of the sun during data collection, two tall stools were brought to the scene as well. Two of the field aides would stand on the stools while holding the sheet to better angle it over the scene. Sheet and tarps are successfully applied as a tool to limit sunlight exposure on the scene in archaeology; however, a sheet was chosen to allow the sun to pass through the material and not be completely blocked (McPherron et al., 200).

Field Technology

The camera used during photography is a NIKON D7200 model with a NIKKOR 18-140mm 1:3.5-5.6G ED lens. The aperture priority was kept consistent throughout photographing and was selected by shooting a couple of practice photographs before beginning data collection (Sapirstein & Murray 2017). The larger size of the scene required a higher aperture. Therefore,

an aperture of $f/11$ was chosen. To account for the higher aperture setting, a higher ISO was used as well. An ISO of 800 was used for the first scene because the dappled area was darker. Scenario 2 (Open) was located in direct sunlight, and therefore an ISO of 400 was used. These settings accounted for a scene that would remain in focus throughout the entirety of the area, while still maintaining a high shutter speed in low lights. Autofocus was used to document all of the models. To provide artificial lighting in an outdoor setting, two sets of Neewer 3-Pack Dimmable Bi-Color LED lights were purchased.

Field Scenarios

The first scenario was located in a setting with dappled lighting (Table 7) (Figure 25). The ground surface consisted of pine needles and oak leaves. There was a large log running along one side of the scene, which added an interesting element to its documentation and the processing. The lighting was consistently uneven throughout the day. Data collection began at around 11 a.m., as it had rained the night before and we needed to wait for the ground to dry before placing the skeletal remains. At the start of data collection, the sun was located at approximately 80° . We completed data collection at approximately 1:40 p.m., and at this point the sun had moved to approximately 100° . During data collection, only 30 photographs were taken from each viewpoint, except for the Model 1E-1. This model included 40 photographs each round. Therefore, this scenario includes five different iterations, instead of only four. For ease of comparison, this extra iteration will be referred to as Iteration E, which includes only the lights and additional photographs. After discussion, it was decided that we continue to take 40 photographs per view angle, while taking 20 closeups and 20 overhead photographs. During Scenario 2, 40 photos were taken at each view angle, with 20 overheads and 20 closeups.

Scenario 2 was positioned in an open area that did not contain tree coverings. Here, the ground surface consisted of grass and a sandy topsoil. Data collection for the day began at 11 a.m., and the sun was positioned at about 80°. Recording of Scenario 2 ended at approximately 1 p.m. At this time, the sun had moved to a position of about 100°.

Table 7: Information showing the naming process of each model to promote easier identification of specific models throughout this research.

| <u>Scenario Number</u> | <u>Scenario Description</u> | <u>Iteration ID</u> | <u>Iteration Description</u> | <u>Processing Settings</u> | <u>Model ID Notation</u> |
|-------------------------------|------------------------------------|----------------------------|-------------------------------------|-----------------------------------|---------------------------------|
| 1 | Dappled | A | No Lights or Sheet | 1 | 1A-1 |
| 1 | Dappled | B | Sheet Only | 1 | 1B-1 |
| 1 | Dappled | C | Lights Only | 1 | 1C-1 |
| 1 | Dappled | C | Lights Only | 2 | 1C-2 |
| 1 | Dappled | D | Lights and Sheet | 1 | 1D-1 |
| 1 | Dappled | E | Lights Only – Plus | 1 | 1E-1 |
| 2 | Open | A | No Lights or Sheet | 1 | 2A-1 |
| 2 | Open | A | No Lights or Sheet | 2 | 2A-2 |
| 2 | Open | B | Sheet Only | 1 | 2B-1 |
| 2 | Open | B | Sheet Only | 2 | 2B-2 |
| 2 | Open | C | Lights Only | 1 | 2C-1 |
| 2 | Open | C | Lights Only | 2 | 2C-2 |
| 2 | Open | C | Lights Only | 3 | 2C-3 |
| 2 | Open | D | Lights and Sheet | 1 | 2D-1 |
| 2 | Open | D | Lights and Sheet | 2 | 2D-2 |

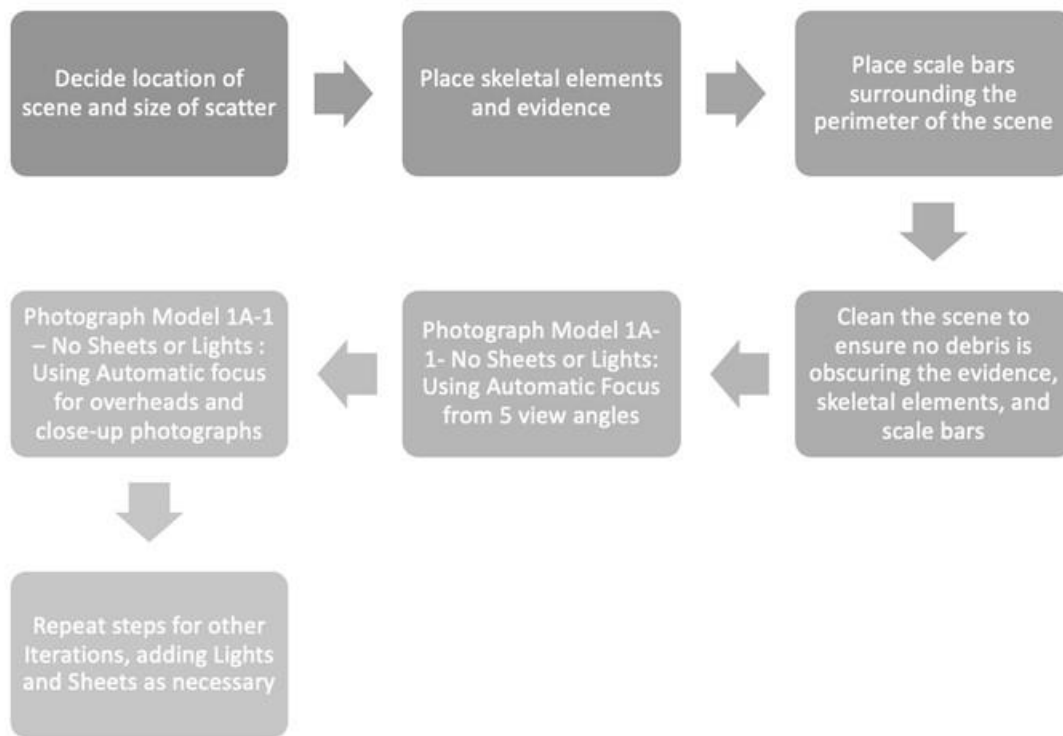


Figure 25: Workflow describing the data collection process followed in the field.

Photograph Processing

After data collection in the field, preprocessing of the photographs occurred to prepare them for the modeling software. The program Adobe Bridge® was used to white balance the RAW photos; this was performed by using the white balance tool to select a spot on the white region of the scale bar. Then, all images that were noticeably over or underexposed were manually adjusted using the shadow, exposure, and highlight tools. After correction, the images were saved as TIFF files and imported to Agisoft® Metashape® Professional Version 1.5.5 for processing (Agisoft LLC., 2019a). Processing guides were used to determine the settings chosen for processing, but changes were made to the original settings during the second round of processing (USGS National UAS Project Office, 2017; Mayer et al., 2018; Ferrell, 2020).

Processing Steps

Once the TIFF files were uploaded to Metashape®, the processing of the files into the development of 3D models began (Figure 26). This process started with the application of the Detect Markers tool to register the coded targets present in the scale bars at the scene. After the targets are recognized, the photographs can be aligned into a sparse point cloud.

To ensure that the sparse cloud is highly accurate, the Gradual Selection tool was used to refine and optimize the generated points (Figure 27). Throughout this process, the error (in pixels) of each camera production was monitored. Ideally, each of the cameras would end close to, or under, 0.3 pixels worth of error.

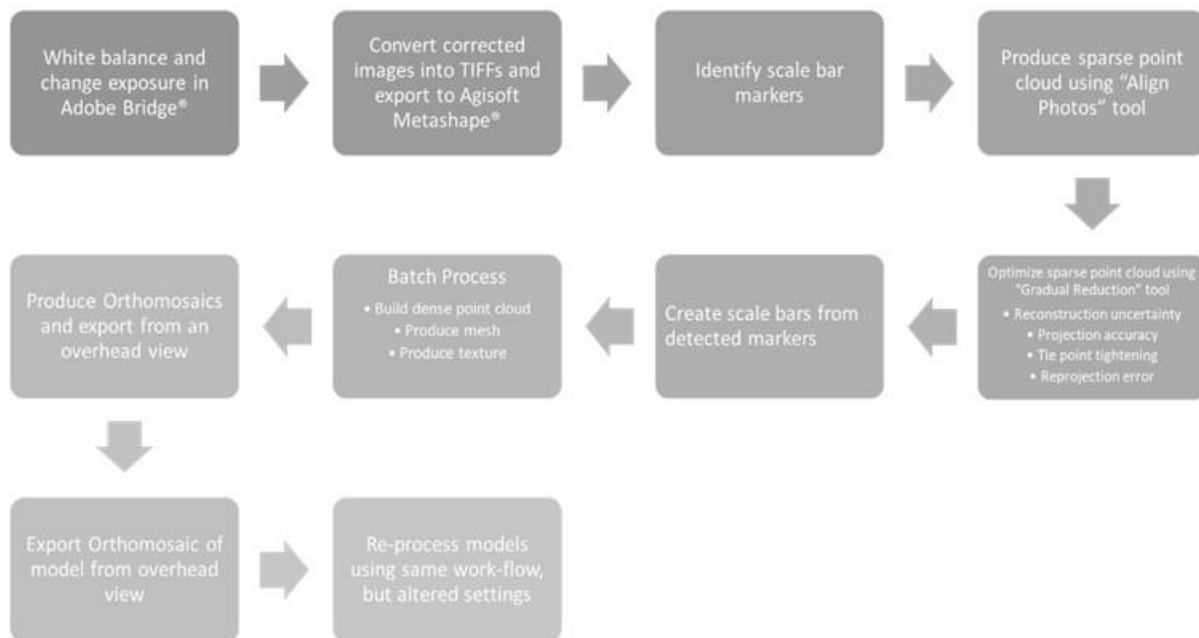


Figure 26: Workflow describing the steps of processing in Agisoft Metashape®.



Figure 27: Model 2A-1 sparse point cloud.

After optimization, the scale bars themselves were generated using the registered targets on the CHI scale bars (Figure 28). Four total scale bars were used in the processing stage, as the CHI compromised in an outdoor setting by the wind or other environmental influences (Cultural Heritage Imaging, 2021). However, six bars were included in each model. Only the 1-meter scale bars were included directly in the Metashape® program. The scale bar accuracy of the models was set to 0.0001 as recommended in the CHI manual (Cultural Heritage Imaging, 2021). The final step of processing included running a batch process to build a dense point cloud, mesh, and texture. This cloud of information then allows Metashape® to produce the mesh. The mesh is a polygonal model that is used as a base for the texture development. Texture development occurs when the software creates a mosaic of all the photographed images and projects the photorealistic texture on the mesh. After adding the texture, an orthomosaic map of the scene is

generated from geometrically accurate orthophotos that are stitched together by the software. The final result is an accurate plane view map of the scene that can be exported.



Figure 28: The dense point cloud of Model 2A-1. Note the targets marked out on the scale bars surrounding the scene.

The models of this chapter were processed multiple times in order to determine whether the quality of the produced models could be improved through processing changes in addition to changes in field practices. Specifically, changes were made to the settings when optimizing the sparse point cloud. In general, the largest number of points is deleted during the refinement of the Reconstruction Uncertainty. Changing the settings when optimizing the Reconstruction Uncertainty results in a larger number of feature points left for the creation of the dense point cloud. Therefore, a selection of models were processed more than once after altering the Reconstruction Uncertainty optimization settings. From the resulting models, only the highest quality one was selected for further analysis in this thesis. The determination of which processing session was used is represented by the final number in the Model Number codes.

Exports

The final results of this project were exported using multiple formats. To ease viewing the results on all image viewing softwares, the final model orthomosaic images were exported in a tagged image file format (TIFF). For their presentation in this thesis, bird's-eye orthomosaic representations of the overall scene were included and used for visual comparisons between the models. Screenshots of the anterior aspect of the cranium were used for comparison of closeup views.

Evaluating Error

For the purpose of this project, the error was measured in two ways to determine the quantitative accuracy of the models: the root mean squared (RMS) reprojection error and scale bar error. The scale bar error represents the difference between the manually input scale bar length and the distances that the software detects between the markers on the scale bars (Agisoft LLC., 2019b). In a highly accurate model, the total scale bar error as calculated by Metashape® will be less than 0.1 mm (Cultural Heritage Imaging, 2020). Additional accuracy criteria are applied to these models because they are forensic scenes. Forensic protocols recognize that measurements are highly accurate as long as they are within 6.35 mm of the true measurement (NFTSC, 2013).

The qualitative accuracy of the models was examined in addition to the quantitative error measurements that were mentioned previously. A thorough examination of the 3D models and the produced orthomosaics was conducted. Specifically, the models were examined for accuracy in the clothing and skeletal element geometry, the ground surface-subject interface points, the subject-subject interfaces, and the scale bar geometry. A general examination of the orthomosaic generation of the model aided in the examination of the scale bar geometry and the overall

accuracy of the skeletal geometry. The orthomosaic also shows clothing geometry, and subject-subject interfaces. For each of the models, a comparison was conducted between the anterior of the cranium. This area of the cranium is highly variable, and therefore the degree of accurate modeling seen of this bone was representative of the skeletal element geometry of the scene. Additionally, the cranium often exhibited surface-subject interface distortion. Therefore, these close-up views of the anterior aspect of the cranium will provide a gauge of model distortion for each of the models.

Results

The two scenarios in this chapter focused on identifying how effective the lighting correction tools discussed in Chapter 2 are on larger scenes. Therefore, the lighting correction tools were tested in two different types of lighting environments. Scenario 1(Dappled) was located in a darker area of tree cover, and the entire scene was immersed in dappled lighting throughout the day. In comparison, Scenario 2 (Open) was located in an open space. Here, the shadows cast upon the scene were not caused by overhanging trees, but by the equipment and data collectors themselves. To best analyze the results of the lighting correction tools on their respective scenes, the quantitative and qualitative integrity of the models was analyzed. The quantitative RMS reprojection and scale bar error are compared first. Then, the visual accuracy of the models will be described when viewing both orthomosaic exports and screenshots of the cranium.

RMS Reprojection and Scale Bar Error

When looking at the overall RMS reprojection errors for both scenarios, all the models fall within the highly accurate category (Table 8). All of the numbers are extremely close to 0.3

pixels, with the highest being 0.351 pixels for Model 1D-1. The lowest RMS reprojection error is 0.264 pixels for Model 2C-3. Looking only at the errors of Scenario 1 (Dappled), the lowest error number is 0.292 pixels for Model 1A-1. The highest range for Scenario 2 (Open) is 0.315 pixels for Model 2D-1. The total scale bar error also falls into the range of 0.1 meters for all of the collected models, which indicates a highly accurate model as defined by the Cultural Heritage Imaging and National Forensic Science Technology Center (Cultural Heritage Imaging, 2020; NFTSC, 2013). The smallest total scale bar error is found in Model 2B-1 with 0.00007 meters of error. Model 1D-1 has the highest overall RMS reprojection error and total scale bar error with a total scale bar error of 0.0005 meters. However, these numbers both fall within the acceptable limits of a model being considered highly accurate.

Table 8: Table showing the RMS Reprojection and total scale bar errors for all models.

| <u>Model Numbers</u> | <u>Iteration Description</u> | <u>RMS Reprojection Error (pixels)</u> | <u>Total Scale Bar Error (m)</u> |
|-----------------------------|-------------------------------------|---|---|
| 1A- 1 | No Lights or Sheet | 0.292 | 0.0002 |
| 1B- 1 | Lights Only | 0.334 | 0.0004 |
| 1C- 2 | Sheet Only | 0.275 | 0.0002 |
| 1D- 1 | Lights and Sheet | 0.351 | 0.0005 |
| 1E- 1 | Lights with 40 photos | 0.347 | 0.0004 |
| 2A- 1 | No Lights or Sheet | 0.269 | 0.0004 |
| 2B-1 | Lights Only | 0.289 | 0.00007 |
| 2C-3 | Sheet Only | 0.264 | 0.0001 |
| 2D-1 | Lights and Sheet | 0.315 | 0.0003 |

Qualitative Visual Accuracy

The visual accuracy of the models will be determined using two different techniques. First, the overall plane view orthomosaic image of the model will be evaluated. This image presents an excellent view of the overall scene but does not enable the viewer to closely turn and examine individual skeletal elements or pieces of evidence within the model. To closely analyze pieces of evidence, screengrabs were taken from within the Metashape® models. Specifically, closeup views of the anterior aspect of the cranium are analyzed. The cranium was chosen because it is an example of complex skeletal element geometry that often appears distorted after processing in Agisoft®. It is also one of the most critical bones to forensic archaeological investigations as it aids in the determination of sex, ancestry, and age for the biological profile.

To critically examine all aspects of distortion, specific criteria will be looked for in each exported image. General clothing and skeletal element geometry will be analyzed in the orthomosaic model. These more general observations will include an evaluation of the subject-subject interface of the scene. This refers to areas where pieces of evidence, or skeletal elements, are interfacing with each other. Additionally, the geometry of all the scale bars will be examined in the orthomosaic model. The closeup images of the cranium will be analyzed for skeletal geometry at a more detailed level. In a selection of models, the cranial vault distorts along the ground surface–subject interface, where the cranium and the ground interact. These four criteria will help guide the overall evaluation of the visual accuracy of the produced models. While the orthomosaics exhibited fewer errors than the closeup model images, both of these imagery options were evaluated for any distortions.

Scenario 1 (Dappled)

Visual Accuracy of Orthomosaics

The orthomosaic image of Model 1A-1, which did not include light correction tools, exhibits minor to slight distortion of the skeletal element and clothing geometry (Figure 29). There is also minor distortion observed along the shaft of the right femur, and the left tibia. Additionally, there is minimal distortion around the edges of the right humerus, right scapula, and right radius. Subject to subject distortion appears only minorly at the location where a rib crosses over the right radius. Another location includes where the left scapula interacts with the interface of the shirt. There also appears to be moderate ground surface-subject interface distortion of the ribs. The coloring of the ribs and the oak leaf matrix of the ground are very similar. Therefore, it is relatively easy for distortion to occur due to the texture aspect of the Agisoft® program not recognizing the two different colored geometries. Otherwise, there is no obvious visual distortion of the scale bars, other skeletal elements, or the clothing geometry. The lighting in this scene is relatively dark, and there are patches of bright light on the patella and ribs west of the shorts. More patches of light appear on a number of scale bars, but do not appear to affect the overall geometry of the scale bars.



Figure 29: Model 1A-1 orthomosaic using no lights or sheet. Note the rib located in the grey circle is almost unidentifiable due to the ground surface-subject interface distortion.

In general, there appears to be very minor distortion observed in the orthomosaic of Model 1B-1, which included the sheet (Figure 30). There is minor distortion along the right femur, but otherwise the model does not contain obvious visual distortion in the skeletal or clothing geometry. There is no obvious visual distortion caused at the subject-subject interfaces of the model materials. However, there is severe distortion caused by the light on northeastern 0.5-meter scale bar. This patch of very bright light completely obliterates the presence of the target that is located at that end of the scale bar. In general, there are many patches of bright white light that interact with the scale bars in this scene. The shade caused by the sheet also contributes to the similarity in coloring that contributes to the ground surface-subject interface distortion of the ribs as they blend into the background leaves.



Figure 30: Model 1B-1 orthomosaic using the sheet.

When examining Model 1C-2, which used the artificial lights, there is minor distortion of the skeletal element geography (Figure 31). The right femur has minor distortion along the shaft that makes the bone appear thinner than it is. On the left side, the femur has slight distortion that contributes to the distal end of the bone sticking out of the shorts to appear fuzzy and fractured. This is partially caused by subject-subject interface distortion caused by the interaction of the

shaft of the left femur and the leg of the shorts. There is minimal distortion along the edges of both tibiae. The coloring of the scene contributes to distortion of the ribs that results in them disappearing into the background because of ground surface-subject distortion. The scale bar geometry appears to be slightly distorted due to the severe patches of brightness and shadow that appear on the scale bars. A small number of the targets are difficult to identify because of the shadows. This inconsistent lighting endures throughout the model. Locations of very dark shadows and others of very bright light make the visual accuracy of the entire model appear slightly distorted. A few of the darkest shadows occurred because the light stands, and panels used in this iteration cast shadows directly onto the scene.



Figure 31: Model 1C-2 orthomosaic using the artificial lights, with highly dappled lighting caused by trees. Note the scale bar within the circle that has distortion due to bright patches of light on the targets.

Model 1D-1 used both the sheet and the artificial lights and does have the highest level of RMS reprojection area as well as total scale bar error (Figure 32). However, the orthomosaic model appears to be visually accurate. There is no obvious visual distortion of the long bones. Evidence of minor distortion does occur on the left scapula. At this location the distortion is subject-subject interface distortion occurring because of the shirt. The model appears to have no other evidence of subject-subject distortion. Minimal ground surface-subject distortion continues to occur between the ribs and the ground surface leaves. In this model, the mandible

also appears to be slightly distorted and blending into the leaf background. There is very minimal distortion to the outside edge of the southwestern 1-meter scale bar. The geometry of the scale bar may have been altered due to a leaf or other vegetation. However, the overall color of the model is very even, and there is no evidence of dark shadows or very bright patches of light.



Figure 32: Model 1D-1 orthomosaic using lights and sheet. Note the minor distortion of the left scapula caused by subject-subject interface distortion between the bone and shirt (arrow).

This model is of the same iteration as Model 1C-1; however, Model 1E-1 was included as a way to test whether more photographs of a scene did contribute to the quality of the model.

While all the other models in this scenario had 30 photographs taken per viewpoint, Model 1E-1 had 40 photographs taken per view angle (Figure 33). In comparison, this model does appear to

have higher visual accuracy than Model 1C-1. There is still minor distortion of the skeletal element geometry. Additionally, there is minimal distortion along the superior border of the right scapula and along the shaft of the right femur. There is no obvious visual distortion that could be contributed to subject-subject interface distortion or ground surface-subject distortion. On the scale bars, the geometry is moderately distorted due to the presence of very bright light and dark shadows on the targets of certain scale bars. This dappled lighting is evident throughout the model. The sacrum is brightly illuminated in this model, which has contributed to the distortion of its finer detail in the orthomosaic. Other bones, for example vertebrae, are highlighted in a similar manner.



Figure 33: Model 1E-1 orthomosaic using the lights, but with 40 photographs being taken each round instead of 30.

Visual Accuracy of Crania

Upon closer investigation, it becomes apparent that the above orthomosaics are not as perfect as they appear. The orthomosaic representations do appear of higher visual quality partially because they are generated as a process in Agisoft® that stitches the images together. The images of the crania appear less refined because they are merely screenshots of the anterior aspect of the skull after the texture had finished rendering (Figure 34).

In Model 1A-1, which included no sheet or lights, there is slight distortion of the skeletal geometry of the right zygomatic arch where it appears to be bumpy and uneven. There is minimal distortion to the mastoid process, but there is no obvious visual distortion of the sutures. On the front of the face, there is evidence of minor skeletal geometry distortion of the anterior nasal aperture and surrounding maxilla. The ground surface–subject interface of the cranial vault does exhibit slight distortion from leaves and sticks that are obscuring portions of the cranium.

Model 1B-1 used the sheet and in general, does not exhibit such severe distortion as Model 1A-1. There is minor distortion of the mastoid process and inferior aspect of the cranium. However, the distortion of the right zygomatic process is only minimal. Additionally, there is no obvious visual distortion of the anterior portion of the face near the anterior nasal aperture. There is no obvious visual distortion of the cranial vault at the ground surface-subject interface. The sutures appear clear and there is no obvious distortion of them. In this model, teeth are visible in the maxilla and are easily identified as teeth.

The general appearance of Model 1C-2, which used the artificial lights, is not as high quality as the previous model. There is slight distortion along the right zygomatic process and into the mastoid process. Around the right eye socket, there is minor distortion of the edge of the orbit. The maxilla, nasal bones, and anterior nasal aperture all exhibit minimal distortion. The maxillary teeth are present, but exhibit a moderate degree of distortion, as they are not able to be

easily identified. There appears to be very minimal distortion of the cranial vault at the ground surface–subject interface.

Model 1D-1 used both lighting correction tools, and there is minimal distortion along the occipital edge, but there is no obvious distortion of the cranial vault where it touches the ground at the ground surface-subject interface. There is minor distortion of the teeth. The teeth are identifiable as teeth but cannot be easily described due to their similarities in appearance and subject-subject interface distortion. Very minimal distortion exists along the edges of the anterior nasal aperture. Otherwise, there is no obvious visual distortion of the cranium.

When comparing Model 1E-1 and 1C-2, the visual appearance of Model 1E-1 is better. There is slight distortion of the inferior aspect of the cranium as well as the mastoid process. The distortion of the right eye orbit is minimal, and there is no obvious visual distortion of the cranial vault or the maxillary and anterior aspect of the face. The teeth are easily viewed and identified in this model. There is no obvious visual evidence of distortion to the cranial vault, and very minimal distortion occurred to the edges of the anterior nasal aperture.

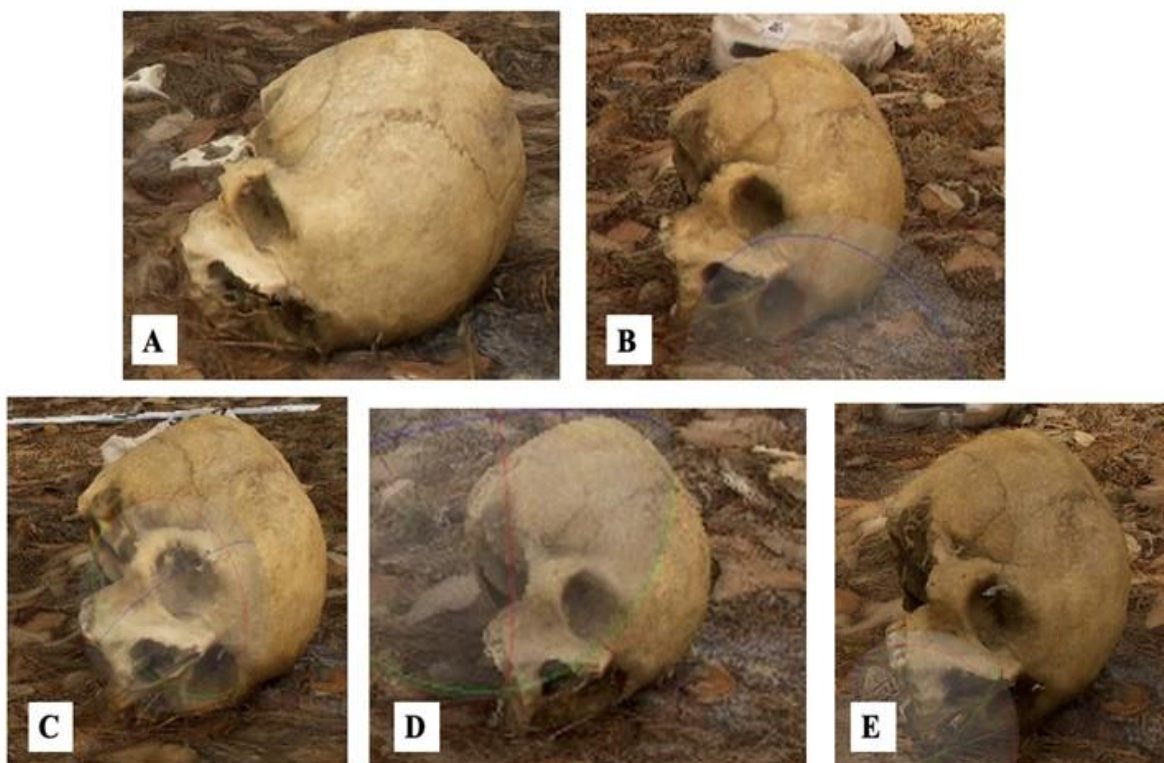


Figure 34: Images of the screenshots of the crania from Scenario 1. (A) Model 1A-11 using no light correction tools. (B) Model 1B-1 using the sheet. (C) Model 1C-2 using the artificial lights. (D) Model 1D-1 with the lights and sheet. (E) Model 1E—1 using the artificial lights and 40 photographs per view angle.

Scenario 2 (Open)

Visual Accuracy of Orthomosaics

In Model 2A-1 which included no light correction tools, there is evidence of minor distortion to the bodies of the ribs and the right femur (Figure 35). The left scapula exhibits minimal distortion to the superior border. No obvious visual distortion of ground surface-subject geometry or subject-subject distortion exists. There is no obvious visual distortion of the clothing geometry. Additionally, there is only very minimal distortion of the eastern scale bar on the outside edge. Throughout the model, there is only one slightly brighter spot. This location of light is near the 1-meter northeastern scale bar. Otherwise, the model exhibits no distortion.



Figure 35: Model 2A-1 orthomosaic using no lights or sheet. Note the severe distortion of the rib that makes it appear as two separate parts (arrow).

The general appearance of Model 2B-1, which is using the sheet, is also incredibly high quality (Figure 36). The right femur exhibits minor distortion at the subject-subject interface of the shorts. Severe ground surface-subject distortion exists for the one rib identified in the orthomosaic by an arrow (Figure 37). This rib appears to be disjointed in the model without its accurate continuous, curved appearance. There is no obvious visual distortion of the clothing geometry. Additionally, there is very minimal distortion of the outside edge of the eastern scale bar. The light is consistent throughout the scene.



Figure 36: A closeup of the severely disjuncted rib found in the Model 2B-1 and other models Scenario 2.



Figure 37: Model 2B-1 orthomosaic using the sheet. Note the severely distorted rib that appears straight due to ground surface-subject distortion (arrow).

Model 2C-3, which is using the artificial lights, exhibits very minimal distortion to the shaft of the right femur where it experiences subject-subject distortion at the interface of the shorts (Figure 38). There is also minor distortion of the left tibia. The right scapula does show minor distortion at the glenoid fossa. There is severe distortion seen in two ribs (arrow) that is caused by ground surface-subject distortion and causes the middle thirds of the rib bodies to appear disjointed. In this model, there is no other obvious visual distortion of the clothing geometry. There is no visible distortion of the scale bars. The light is not completely even throughout the scene. The northern half of the scene is distinctly brighter than the southern half. However, there do not appear to be distortions caused by this lighting unevenness.



Figure 38: Model 2C-3 orthomosaic using the artificial lights.

The final model of Scenario 2 that included the lights and the sheet, Model 2D-1 has very minimal distortion to the skeletal geometry of the left fibulas as well as the right femur (Figure 39). Additionally, there is very minimal distortion of a rib at the subject-subject interface that it has with the shorts. The rib that has consistently exhibited ground surface-subject distortion only shows slight distortion in this model. The scale bars bear no obvious visual distortion. Despite the inclusion of a sheet during this iteration, there does appear to be a bright spot of light on the 0.5-meter northeastern scale bar. On the far-right target, it is brighter white than the other targets.



Figure 39: Model 2D-1 orthomosaic including the lights and sheet.

Visual Accuracy of Crania

The appearance of the models for Scenario 2 was extremely grainy and reprocessing the models did not completely mitigate the problem. The closeup visuals of the anterior aspect of the skull continue to appear grainier than the orthomosaic exports (Figure 40).

In Model 2A-1 without the lights or sheet, there is moderate distortion along the ground surface-subject interface of the cranial vault. More minor distortion exists around the right eye orbit and on the anterior portion of the maxilla around the anterior nasal aperture. The anterior section of the alveolar margin of the maxilla is severely distorted and appears to be missing teeth, as well as the alveolar portion. Sutures are not clearly visible on the cranial vault. The teeth that are visible are indistinct. There is moderate distortion of the inferior aspect of the cranium and mastoid process.

Model 2B-1, which included the sheet, appears to be much higher quality than Model 2A-1. There is minor distortion along the anterior border of the nasal bones, and on the mastoid process. Otherwise, there is no obvious visible distortion caused by ground surface–subject interface distortion, or other areas of skeletal geometry distortion. The teeth in this model are clearly identifiable, and the sutures are highly visible.

When examining Model 2C-3, which included the artificial lights, there is slight distortion of the skeletal geometry of the right zygomatic arch where it appears to be bumpy and uneven. There is minimal distortion to the mastoid process. The sutures are not clearly visible on the cranial vault. The ground surface–subject interface quality is difficult to determine because the cranium cast a very opaque shadow. Therefore, other than minor distortion to the inner edge of the right eye orbit, it is difficult to evaluate more distortion.

Model 2D-1 included the lights and sheet, in general, exhibits minor distortion. This distortion is noticeable along the inferior aspect of the cranium, on the inner edge of the right eye

orbit, and on the anterior edge of the nasal bones. Slight distortion occurred along the alveolar margin of the maxilla. This resulted in teeth missing from the final image, and moderate distortion of the maxilla at the ground surface–subject interface. The sutures are visible, and there is no obvious visual distortion of the cranial vault.

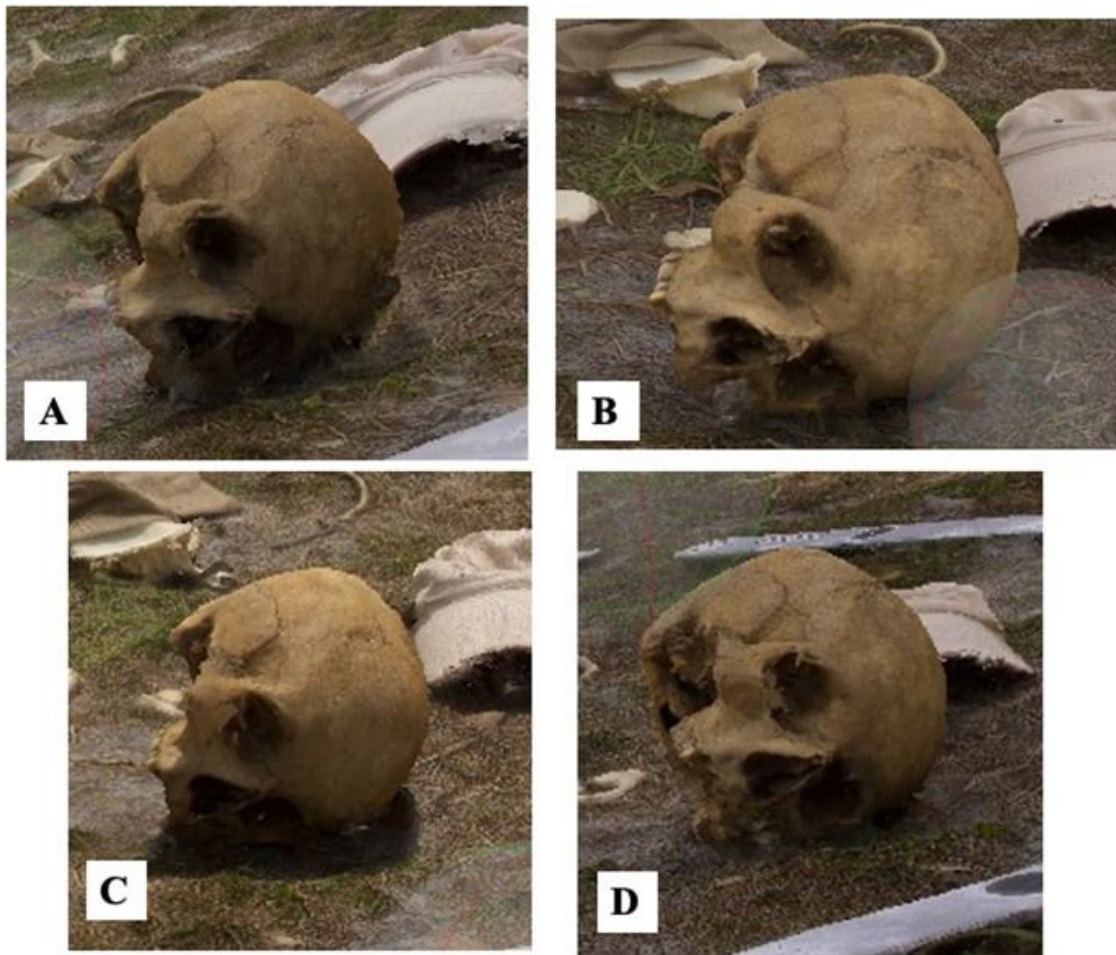


Figure 40: Images of the screenshots of the crania in Scenario 2. (A) Model 2A-1 using no light correction tools. (B) Model 2B-1 using the sheet. (C) Model 2C-3 using the artificial lights. (D) Model 2D-1 with the lights and sheet.

Discussion

Close range photogrammetry appears to be a successful tool when recording complex outdoor scenes in a wooded environment (Church, 2019; Gidusko, 2018; McCollum, 2020; Ferrell, 2020). However, it is the detailed accuracy of these models that allow them to prove useful to investigators as documentation of the original position, condition, and context is an essential aspect of forensic archaeology investigations (Dirkmaat & Adovasio, 1997; Dirkmaat & Cabo, 2012; Dirkmaat, 2015). Challenges exist with the routine application of CRP to outdoor crime scene recording because of the lack of guidelines present that detail how to counteract commonly seen natural processes. Recently, Ferrell (2020) focused on improving the production of high-quality models with harsh shadows, by lightening images pre-processing and testing a variety of processing procedures. However, these procedures did not include suggestions on how to directly combat harsh lighting conditions in the field. Therefore, this study attempted to mitigate distortion caused by harsh lighting through the application of light correction tools during data collection.

Phase 2 is the application portion of this research project, and the purpose of this phase was to understand how the knowledge gained during the experimental Phase 1 aided in combating harsh lighting. The discussion is organized around the three primary goals of this research project. The first goal was to determine whether the use of the sheet or the artificial lights contributed more to the overall qualitative and quantitative quality of the models. Part of this goal included the question of whether the use of these tools was practical in a staged outdoor forensic scene. Then, the second goal tested how improvements to procedures during Phase 1 affected the final model development of the larger scenes. These improvements include cleaning the scene and remaining at a distance during data collection. The third goal addressed providing guidelines to ensure that, if useful, such techniques can be integrated into current CRP practices.

The inclusion of these techniques will enable high quality CRP modeling to occur in situations of uneven lighting.

RMS Reprojection and Scale Bar Error

Overall, all of the RMS Reprojection and total scale bar errors fall within the acceptable levels for highly accurate modeling (Agisoft LLC., 2019b). However, when comparing the error totals of Scenario 1 (Dappled) and Scenario 2 (Open), differences become apparent. In Scenario 1 (Dappled), the highest RMS reprojection error is 0.351 pixels in Model 1D-1. The lowest score in Scenario 1 (Dappled) is 0.275 pixels (Model 1C-2), which creates a range of 0.076 pixels. The differences may appear minute, but the Scenario 2 (Open) range is only 0.051 pixels. In Scenario 2 (Open), the highest error is 0.315 pixels (Model 2D-1) and the lowest is 0.264 pixels (Model 2C-3). It is interesting to note that the lowest RMS reprojection error in both Scenario 1 (Dappled) and 2 (Open) is found in the iteration that involved only the sheet. These were also the only two models that had initial processing results more inaccurate than the reprocessing stages. All the other models achieved their highest accuracy scores with the initial processing settings. It is also interesting to note that all of the Scenario 2 (Open) RMS errors are smaller than the Scenario 1 (Dappled) errors. It does not appear that the answer simply depends on the higher numbers of photographs taken during Scenario 2 (Open), because Model 1E-1 falls within the ranges established by Scenario 1 (Dappled), not Scenario 2 (Open). Perhaps, the sunny nature of Scenario 2 (Open) benefitted the overall quantitative model accuracy.

The total scale bar error involved much less variation between scenarios. In Scenario 1 (Dappled), the total scale bar error range occurred between 0.0002 meters (Models 1A-1 and 1C-2), and 0.0005 meters (Model 1D-1). It is interesting to note that Model 1D-1 has the highest RMS reprojection error as well as the highest overall total scale bar error. Scenario 2 (Open) has

a range in total scale bar error of 0.0004. The lowest total scale bar error is 0.00007 (Model 2B-1). Similarly, to the RMS reprojection errors, all the total scale bar errors of Scenario 2 (Open) are smaller than those of Scenario 1 (Dappled). All scale bar errors fall within the acceptable range of high-quality models determined by the manufacturers (Cultural Heritage Imaging, 2021). Additionally, the National Forensic Technology Center, which sets the standards of data collection for digital mapping devices in forensic contexts, states that measurements of the scene should fall within 6.35 mm or ¼ of an inch (NFSTC, 2013). Therefore, all of the total scale bar errors for the models meet photogrammetry and forensic standards.

Visual Accuracy

When discussing the overall visual quality of the orthomosaic exports of the models, the inclusion of the sheet does appear to be an easy corrective tool for dappled lighting distortions observed in previous research (Table 9) (Ferrell, 2020). The use of the sheet did mitigate this problem, and in the iterations where the sheet was used, the lighting over the scene remained even. The only distortion found in the iterations that used the sheet developed from the sheet not covering the scale bars completely. Therefore, Model 2B-1 exhibited almost no distortion and the only severe distortion seen was caused by ground surface-subject interface distortion (Figure 41). Model 1B-1 exhibited distortion due to bright patches of light on the northeastern 0.5-meter scale bar (Figure 42). Within the covered confines of the scene, there was no distortion caused by uneven lighting. The artificial lights, however, were inconclusive in their contribution. Perhaps, in scenarios where the sky is overcast or it is later in the day, the lights would be more beneficial. Additionally, six lights may have been too few for the size of the scenes that was being tested. Further investigation into the application of more artificial lights, a different model

of lights, or during overcast days may contribute to a better understanding of the application of artificial lights to forensic archaeology scenes.

The models of Scenario 1 (Dappled) for this phase exhibited a grainy appearance, and therefore were processed multiple times to minimize the texture distortion. Since it was not possible to correct the graininess during processing, it is possible that the issue may have occurred during the initial data collection. The camera was used in an aperture priority mode, and therefore the aperture settings were consistent during recording. This odd texturing was more evident in the iterations that utilized the sheet light correction tool, however, it was noted to some degree in all of the models of this scenario. One possible cause of the grainy appearance of the models included the speed of the camera in the reduced light settings. For example, Ferrell (2020) noted that the models occurring in locations with reduced light, exhibited lower shutter speeds and were more visually distorted. The location of Scenario 1 (Dappled) exhibited increased shade when compared to Scenario 2 (Open). When combined with reduced lighting caused by the application of the sheet, the lower shutter speeds may explain the higher levels of distortion observed in these iterations.

Alternatively, another possible explanation for the grainy appearance of the models could be attributed to the sheet. The larger size of the sheet made it more difficult for the field aides to control, particularly when there was a gust of wind. To ensure that the sheet was not blocking the view of the camera, the field aides would wave the sheet up when the photographs were taken. The continued movement of the sheet, and the slight changes in light passing through the sheet, may have contributed to the grainy textures of these models when combined with the lower shutter speeds that were observed during these iterations. Future research should use a

fixed overhead sheet or tarp. This would eliminate the movement necessary to keep the sheet aloft and out of view of the camera.

Table 9: Comparison of the visual accuracies as seen across each model. The “Ortho” rows indicates how the discussion applies to the orthomosaics of each model, while “C-SS” stands for the cranial screenshots.

| <u>Model Number</u> | | <u>Skeletal Element Geometry</u> | <u>Clothing Geometry</u> | <u>Scale Bar Geometry</u> | <u>Ground Surface-Subject Interface</u> | <u>Subject – Subject Interface</u> | <u>Overall Lighting</u> |
|----------------------------|-------|--|---------------------------------|---|--|--|--|
| 1A-1 | Ortho | Minor to slight distortion of long bones | Minor distortion of clothing | No obvious visual distortion | Moderate distortion due to similar coloring of ribs and ground | Minor distortion at interface of rib and shirt; minor distortion of left scapula and shirt interface | Severe patches of light and shadow |
| | C-SS | Slight distortion of right zygomatic; sutures are highly visible | N/A | N/A | Slight distortion at interface of cranial vault and ground | No obvious visual distortion | N/A |
| 1B-1 | Ortho | Minor distortion overall | No obvious visual distortion | Severe distortion where spot of bright light is located on northeastern 0.5-meter scale bar | Slight distortion due to similar coloring of ribs and ground | No obvious visual distortion | Severe parch of light on scale bar target causing distortion |
| | C-SS | Minimal distortion throughout; sutures are highly visible | N/A | N/A | No obvious visual distortion | No obvious visual distortion | N/A |

| <u>Model Number</u> | | <u>Skeletal Element Geometry</u> | <u>Clothing Geometry</u> | <u>Scale Bar Geometry</u> | <u>Ground Surface-Subject Interface</u> | <u>Subject – Subject Interface</u> | <u>Overall Lighting</u> |
|----------------------------|-------|--|---------------------------------|---|---|---|--|
| 1C-2 | Ortho | Minor distortion overall | No obvious visual distortion | Slight distortion due to severe patches of light | Severe distortion due to similar coloring of ribs and ground | Slight distortion at interface of left femur and shorts | Severe patches of bright light and shadow throughout |
| | C-SS | Slight distortion throughout; sutures are visible | N/A | N/A | Minimal distortion at interface of cranial vault and ground | Moderate degree of distortion of teeth | N/A |
| 1D-1 | Ortho | Minimal distortion overall | No obvious visual distortion | Minimal distortion to edge of southwestern 1-meter bar; leaf on bar | Minimal distortion due to similar coloring of ribs and mandible to the ground | Minor distortion at interface of left scapula and shirt | Consistent |
| | C-SS | Minimal distortion throughout; sutures are visible | N/A | N/A | No obvious visual distortion | Minimal distortion of teeth | N/A |
| 1E-1 | Ortho | Minor distortion overall | No obvious visual distortion | Moderate distortion where spots of bright light appear | No obvious visual distortion | No obvious visual distortion | Severe patches of bright light and shadow throughout |

| <u>Model Number</u> | | <u>Skeletal Element Geometry</u> | <u>Clothing Geometry</u> | <u>Scale Bar Geometry</u> | <u>Ground Surface-Subject Interface</u> | <u>Subject – Subject Interface</u> | <u>Overall Lighting</u> |
|---------------------|-------|--|------------------------------|---|--|--|-----------------------------|
| | C-SS | Minor distortion throughout; sutures are visible | N/A | N/A | No obvious visual distortion | No obvious visual distortion | N/A |
| 2A-1 | Ortho | Minimal distortion overall | No obvious visual distortion | Minimal distortion to outer edge of eastern scale bar | No obvious visual distortion | No obvious visual distortion | Few patches of bright light |
| | C-SS | Moderate distortion throughout; severe distortion of alveolar process; sutures are not clearly visible | N/A | N/A | Moderate distortion at interface of cranial vault and ground | No obvious visual distortion | N/A |
| 2B-1 | Ortho | Minimal distortion overall | No obvious visual distortion | No obvious visual distortion | Severe distortion of rib that makes it appear disjointed | Minor distortion of right femur at interface of shorts | Consistent |
| | C-SS | Minor distortion throughout; highly visible sutures | N/A | N/A | No obvious visual distortion | No obvious visual distortion | N/A |

| <u>Model Number</u> | | <u>Skeletal Element Geometry</u> | <u>Clothing Geometry</u> | <u>Scale Bar Geometry</u> | <u>Ground Surface-Subject Interface</u> | <u>Subject – Subject Interface</u> | <u>Overall Lighting</u> |
|----------------------------|-------|---|---------------------------------|----------------------------------|--|---|--|
| 2C-3 | Ortho | Minor distortion overall | No obvious visual distortion | No obvious visual distortion | Severe distortion of two ribs that make them appear disjointed | Very minimal distortion of right femur at interface of shorts | Brighter in northern half than southern |
| | C-SS | Slight distortion throughout; sutures are not clearly visible | N/A | N/A | Difficult to determine due to shadowing | No obvious visual distortion | N/A |
| 2D-1 | Ortho | Minimal distortion overall | No obvious visual distortion | No obvious visual distortion | Slight distortion of one rib | Minimal distortion of rib at interface of shirt | Severe patches of bright light on scale bars |
| | C-SS | Minor distortion throughout; sutures are visible | N/A | N/A | Moderate distortion at interface of maxilla and ground | No obvious visual distortion | N/A |



Figure 41: Image of the ground surface-subject interface distortion exhibited in Model 2B-1.



Figure 42: Image of the brightness located on the northeastern 0.5-meter scale bar in Model 1B-1.

Evaluation of Goals

Procedures that can be applied in the field to combat processing distortions caused by lighting harshness are a necessity in forensic archaeology. Archeologists often use CRP successfully to record sites (Mikhail et al., 2001; Linder, 2003; Al-kheder et al, 2008; Burtch, 2008; Portalés et al., 2009; Howland et al., 2014; Benavides Lopez et al., 2016). However, archaeologists do not encounter the same difficulties with light in outdoor settings. Tarps and sheets are used when necessary, but if the lighting conditions are unfavorable then the data collection period can simply be moved to another time (McPherron et al, 2009). The medicolegal nature of forensic archaeology does not allow for data collection to be moved or the time changed. Therefore, the lighting correction tools for outdoor scenes need to be easily applicable to multiple scenarios, and definitively result in high visual accuracy of the produced models. Between the sheet and the artificial lights, the sheet is the more influential light correction tool when examining the visual accuracy of the final models.

Once the discrepancy is photographed, it becomes a part of the scene. The importance of cleaning the scene was established during Phase 1 and remains during Phase 2. In general, the degree of distortion caused by leaves and grass being present on the scene decreased. There was also a decrease in the degree of distortion of the scale bar geometry. By stepping farther back from the scene while taking photographs, and maintaining the distance throughout data collection, the scale bar geometry of the outside edge remained better preserved. This was determined to be a vital step in the application of CRP to real-world scenes.

The results of these goals, as well as knowledge gained from the limitations and challenges of this research, affected the guidelines. Guidelines were written from the information gathered during this project and can easily be applied to the recording of future scenes.

Challenges and Limitations

The challenges of this project included difficulties in both data collection in the field, and during processing. In the field, one of the most crippling environmental factors that was encountered was wind. Wind had been noted to contribute to difficulties in recording because of the movement it creates of leaves and other organic material (Ferrell, 2020; McCollum, 2020). When the wind blows, it can move leaves to obscure different aspects of the scene; and if a stray leaf is not removed before the data collection continues, it cannot be removed later in the process. Additionally, the wind provided added challenges to the field aides working with the white sheet.

While the sheet was the more successful lighting correction tool for qualitative visual accuracy, the incorporation of the sheet provided challenges. As mentioned above when it was windy the larger sheet became difficult to manage. This is shown most clearly in the orthomosaic below (Figure 43). Data collection began on a scene and was then abandoned because of the difficulties found in holding the sheet steady over the scene. The field aides would have to fight against the wind to hold the sheet still, because when it moved too much there were areas of the scene that were left uncovered. The RMS reprojection error for this model was the highest recorded at 0.374 pixels. The models total scale bar error was within the acceptable range at 0.0007 meters. Note the moderate distortion of the visual accuracy in the model's orthomosaic that results in leaves on the femur, a slight distortion of the hat, and moderate ground surface-subject distortion of the right shoe that makes it almost disappear into the background. There is also noticeable distortion of the north arrow that was not seen in previous models. Close up views of multiple elements exhibit the distortion observed in the right arm bones and shows a closer view of the leaves obscuring the femur (Figures 44 & 45).

Overall, the quality of the model was determined to be too poor to include in the final dataset because of distortions caused by the wind.



Figure 43: The orthomosaic of the scenario that was discarded due to severe wind. Note the distortion of the north arrow, which was not seen in previous models (circle).



Figure 44: Closeup view of the windy model exhibiting the distortion of the right arm bones and ribs.



Figure 45: Closeup view of the windy model that clearly shows the leaves present on the femur after the wind blew them onto the bone

The sheet also created challenges and limitations in terms of field equipment. With the larger sheet, stools were needed to better allow the field aides to angle the sheet appropriately and cover all of the scene. The field aides themselves were also considered elements of the sheet equipment, as a minimum of four people was necessary to hold the sheet at an appropriate angle. This required the coordination of multiple schedules to continue data collection. Additionally, the process of data collection takes time, and the field aides needed to rest their arms after holding up the sheet for more than a few minutes. Perhaps, in situations where people or time are limited, a white tent would be an acceptable alternative.

One issue noted after model creation was the appearance of a grainy texture in the models produced during Scenario 1 (Dappled). Changes to processing settings in Agisoft® partially mitigated the grainy texture appearance of the images. The improvement of the grainy image

texture required considerable time experimenting with Agisoft® settings. Two setting changes that contributed to a less grainy imagery texture was the inclusion of more photographs during alignment, as well as the deletion of more points during optimization. The models that included fewer points appeared to have a reduced grainy texture. For example, when comparing Models 1C-1 and 1C-2 the difference in graininess is notable (Figures 46 and 47). The only changes in the processing of these two models were the number of photographs and the deletion of points during optimization. Model 1C-1 used 173 images and began with 940,029 points before refinement. The number of tie points in the final model was 174,909 with 409,759 projections. The resulting errors of the model were a RMS reprojection error of 0.313 pixels and 0.0004 meters of total scale bar error. Conversely, Model 1C-2, which was the model chosen for use in this thesis, used 180 images. The model began with 941,989 points, and the final number of tie points was 69,724 with 166,502 projections. Quantitative errors for this model were 0.275 pixels of RMS reprojection error, and 0.0002 meters of total scale bar error. When comparing these two models, Model 1C-2 exhibits higher quantitative and qualitative accuracy that resulted from tweaking a number of settings when the images were reprocessed. Additional processing difficulties of Agisoft® included the size of the model files. The Agisoft® program does not warn the users before a processing stage begins how much memory will be necessary to complete the process. Therefore, a modeling process could appear to run normally and then fail partially through the action when the computer's memory reached capacity. This resulted in multiple processes needing to be repeated, and time taken to move files to allow enough space on the computer.



Figure 46: A screengrab image of Model 1C-2, which achieved better qualitative and quantitative accuracy than Model 1C-1.



Figure 47: A screengrab image of Model 1C-1, which does appear more grainy overall than Model 1C-2.

Guidelines

The guidelines of this thesis expand on the guidelines as established by previous UCF Masters students (Gidusko, 2018; McCollum, 2020; Ferrell, 2020). However, the challenges and limitations experienced during this project has led to an adjustment of previously outlined procedures (Figure 48). Previous research has mentioned that specific times of day, especially the early morning or when the weather is overcast, is the best time to record a scene due to the minimal shadows (Douglass et al., 2015; Ferrell, 2020). The inclusion of the light correction tools demonstrated in this research eliminates this limitation. Especially with the difficulties of shadows, an adequately sized sheet angled to cover the scene, mitigates the processing difficulties caused by moving shadows. Therefore, models can be recorded whenever it is necessary, which is incredibly important when attending to forensic casework. Additionally, problems with low-light conditions can be alleviated with the incorporation of artificial light sources. Even though the lights may not completely dispel with low light conditions, adding these additional light sources may result in improved shutter speed. An improved shutter speed allows the scene to be recorded freehanded, which increases the maneuverability of the photographer around obstacles results in a quicker recording speed. Another way to increase maneuverability and recording speed is to take the photographs using the automatic focus option. Traditionally, photogrammetry is performed with a manual focus lens that is set to a focal length and then not altered (Baltsavias, 1999; Al-kheder et al., 2008; Burtch, 2008; Porter et al., 2016). When applied to this research, it was found that the qualitative and quantitative quality of the orthomosaic models did not change, but the sum of time needed to document each model did increase when using manual focus.

Once the scene is declared to be applicable for photogrammetry recording, the preparation of the scene is the next vital step. Before preparation occurs, overall pictures of the

scene should be collected. Then, if there is time, it is recommended that the scene be completely recorded for modeling before scene preparation occurs to ensure that there is a visual record of the scene prior to intervention. This process should only involve placing scale bars and a north arrow where appropriate. After the recording of the unaffected scene, the scene should then be cleaned for an additional model. It is important to note that the fastidious removal of all grass and twigs is required to reduce visual errors. The photographer should circle the scene at the level of each of their view angles to check the scene. Grass that is tall enough to obscure the evidence, skeletal elements, or scale bars should be cut. Twigs, leaves, or pine needles that lay upon important element should be carefully removed. When cleaning, it is important to not move the elements or evidence in the scene. However, the scene should be cleaned as thoroughly as possible without disturbing the evidence from its provenance. Once the space within the scale bar perimeter is cleaned, an approximately 0.6 meter (2 foot) area on the outside of the scale bars should be cleared in a similar matter. Especially when recording from View angle 1 and View angle 2, tall grass or other environmental materials between the camera position and the scene may prevent the software from detecting the scene elements. It is especially important to clear the area between the camera position and the targets on the scale bars. Items blocking the targets may prevent the detection of the markers and cause the creation of inaccurate scale bars during processing. Once the first photograph is taken, no further changes can be made to the scene. Additional changes will result in inconsistent geometry development and distorted modeling. The only exception to this rule is if a leaf or other material blows on to an object during the recording process. As long as the material is carefully removed before the next photograph is taken, then the original geometry of the photographs will not be compromised.

After cleaning the scene, the photographer should determine whether a light correction tool is necessary. If deemed appropriate, the light correction tools should then be placed. It is important to note that the light correction tools should be placed approximately 0.6 meters (2 feet) from the scale bars. Then, photography will occur. No people, other than the photographer, should approach the scene after the light correction tools have been placed. The photographer should ensure that they maintain an appropriate distance from the scene, and that they are checking to ensure that no leaves have blown onto the scene after each view angle.

Finally, processing occurs in Metashape®. It is a good practice to re-process models while changing different settings. For example, some models that were processed in Scenario 2 (Dappled) after changes to the Reconstruction Uncertainty setting did appear more visually accurate. Processing the models more than once is one way to produce a higher quality final model. Experimentation with processing settings may contribute to new guidelines that greatly improve the overall accuracy of CRP forensic archaeology models.

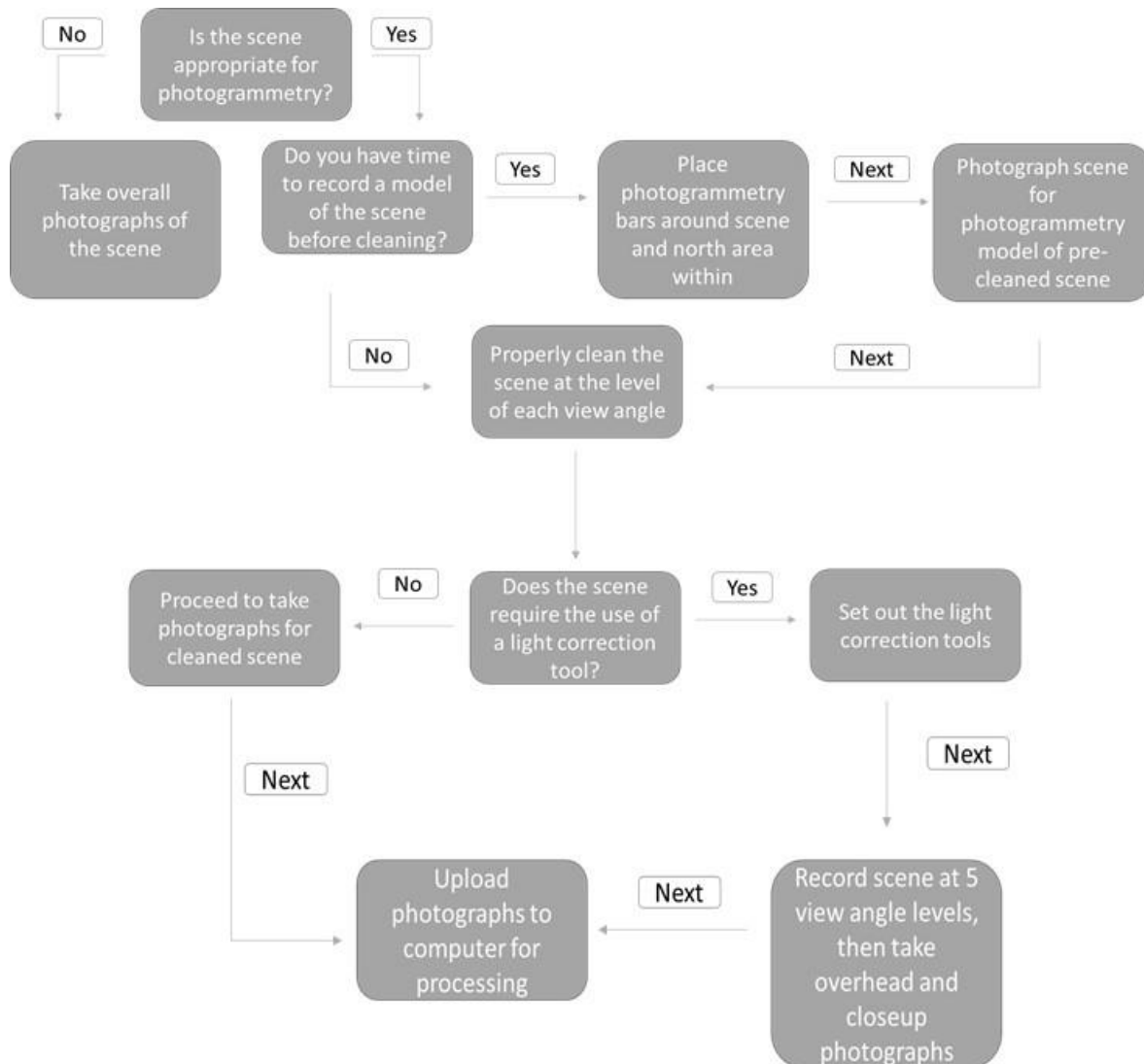


Figure 48: Workflow guidelines for implementing a light correction in the field.

Conclusion

The application of CRP to forensic investigations is something that can be easily accomplished, and has proven to be successful (Church, 2019; Gidusko, 2018; McCollum, 2020; Ferrell, 2020). However, guidelines must exist for the integration of such technology to be easily adapted to all scenes investigated by forensic anthropologists. Guidelines must be written that

specifically address problematic variables, including harsh lighting, that could be encountered in the field.

This study has demonstrated that light correction tools of a sheet and artificial lights are viable, and useful to the accurate recording of large and complex outdoor scenes. The sheet appears to be capable of limiting the volume of shadows cast on a scene and eliminating dappled lighting. The sheet is not the only solution to this problem, nor a perfect solution. Movement of the sheet may have resulted in grainy models, and further research needs to be conducted to explore this issue. The sheet has proven to be a relatively inexpensive fix to visual processing distortions caused by uneven lighting. Only further research involving CRP modeling at different levels of brightness will refine current guidelines and result in highly accurate 3D models.

CHAPTER FOUR

Without proper documentation and mapping, forensic investigators cannot recreate the context of the original scene and therefore may not be able to recreate the series of events that led to a person's death (Dirkmaat & Adovasio, 1997; Schultz & Dupras 2008, Dupras et al., 2012; Dirkmaat & Cabo, 2012; Christensen et al., 2014; Dirkmaat, 2015). Therefore, improvements by forensic archaeologists to document a scene quickly and accurately must be implemented. Close-range photogrammetry (CRP) is one of the most recent 3D digital mapping techniques that has been adopted by forensic investigators from archaeological techniques (Fussell, 1982; Burtch, 2008; Barazzetti et al., 2011a; Gonizzi Barsanti et al., 2013). When used by forensic archaeologists, the 3D models are scaled map representations of the scene. The models are beneficial in documenting a complete view of the scene more accurately than isolated photographs (Dupras et al., 2012). This allows for a more complete understanding of the original context of the scene, including the association of the skeletal elements and evidence (Dirkmaat & Cabo, 2012; Dirkmaat, 2015). The understanding of the context of the scene contributes to a better understanding of what agents may have influenced the deposition patterns (Schultz & Dupras, 2008; Dirkmaat, 2015). The application of this technology to large, complex, outdoor scenes has proven effective in preserving this context (Gidusko 2018; Church, 2019, McCollum, 2020; Ferrell & Schultz, 2021). However, the outdoor nature of many forensic archaeology scenes can lead to complications when collecting data and mapping the scenes. A sufficient procedural basis is necessary to guide photogrammetry users on how to best address problematic environmental conditions in the field, including light.

Therefore, the current study addressed how to best correct harsh lighting conditions using the lighting correction tools of a sheet and artificial lights. To best address this question, the

project was divided into two phases. Phase 1 was an experimental phase using smaller, contained scenes. Then, Phase 2 was the application phase, where these techniques were applied to real-world scenarios. Chapter 2 focused on Phase 1 of the project. There were three primary goals of this phase. The first goal was to examine which of the light correction tools were most effective at improving the qualitative and quantitative quality of the models of small scenes. Second, was to test whether these techniques can be applied to realistic forensic scenes. Third, was to write guidelines that explain how to best address lighting difficulties for photogrammetry users in outdoor settings. Chapter 3 applied the techniques learned in Chapter 2 to real-world modeled forensic scenes. Again, three goals were developed for Chapter 3, the first of which investigated how the lighting correction tools, the sheet or the artificial lights, aided in the qualitative and quantitative quality of the final models of large scenes. Secondly, the learned procedures regarding cleaning the scene and remaining at a distance during data collection needed to be further tested on a real-world staged scene. Finally, guidelines needed to be adapted to incorporate any valuable procedures that were learned during Phase 1 and confirmed during Phase 2 on how best to eliminate harsh lighting in the field that may cause distortions during processing.

Summary of Results

Throughout both phases, all the produced orthomosaic maps and models fell within the range of acceptable quantitative and qualitative errors. The RMS reprojection errors of all models were either under the limit of 0.3 pixels or were slightly over, indicating that the models are all highly accurate (Mayer et al., 2018). Scale bar error was expected to be less than 0.1 mm according to the Cultural Imaging Heritage criteria (2021). However, the acceptable level of measurement error for crime scene mapping is 6.35 mm or less (NFSTC, 2013). Visual errors

did occur both at the orthomosaic level, and on the screenshots of the crania. However, the visual errors appeared to be largely caused by distortions of the mesh geometry, not the texture overlay. The visual distortions were not extreme enough to render the models inaccurate or the skeletal elements unidentifiable. Therefore, as map-like representations of the scene, these models are accurate. More specific forensic anthropological analysis, such as biological profile creation, trauma analysis, or taphonomy analysis should be performed using the bones, not the models. However, possessing an accurate map contributes to understanding the original position, orientation, and context of the remains. This knowledge may improve the reconstruction of the death event, and provide accurate interpretation of taphonomic factors that influenced the final position of the remains (Schultz & Dupras, 2008; Dupras et al., 2012; Dirkmaat, 2015).

To specifically address the goals of Chapter 2, the sheet appears to have more of an effect than the artificial lights. This effect was only seen when evaluating the visual accuracy, but the application of the sheet and elimination of dappled lighting on the scene did improve the overall appearance of the model. Procedurally, it became apparent that proper clearing and cleaning of the scene prior to recording was necessary to enhance the overall final model accuracy. For Chapter 3, it is possible to apply these light correction tools and techniques to staged real-world scenarios. However, adjustments are necessary. For example, a much larger sheet and stools, or a tent, are necessary to adequately cover the larger scenes. This adjustment, as well as other specifics, were included in the final procedural guidelines of the chapter.

Challenges and Guidelines

Within the field data collection process, challenges were posed by the environment as well as by the experimental nature of the research process. The cleaning of the scene was a

vitality important step of data collection. The obvious materials that blocked pieces of evidence or skeletal materials did not only need to be removed, but all tall grass or plants need to be cut short. Cleaning of the scene needed to be performed from every angle, and at the level of each view angle before recording began. To preserve the pristine nature of the clear scene, people and material needed to be kept away from the scene. The photographer should be the only one near the scene and the lights. The field aides when they are holding the sheet, needed to be kept a minimum distance of 0.6 meters (2 feet) away from the scale bars. This not only kept people from accidentally knocking leaves or other debris onto the scene, but also helped with lighting discrepancies. The presence of people and the lights close to the scene during the recording of iterations in which they were unnecessary led to the projection of shadows on the scene. Specifically, the lights should not be added to the scene until they are necessary, as the large light panels cast static shadows on the scene when present.

Addressing these challenges in both phases resulted in updating guidelines for data acquisition that originated with Ferrell (2020). These guidelines included a description on how to decide whether a scene is appropriate for CRP documentation, how to properly set up and clear the scene, the process of data recording, and processing information. Key aspects of the field guidelines included cleaning the scene adequately during preparation, taking photographs from every level as well as overheads and closeups, and setting up the light correction tools. When processing, settings were altered to achieve the highest model quality. The guidelines recommend how to alter these settings, and to always process each set of images multiple times.

Archaeological and Crime Scene Applications

As with many forensic archaeology practices, CRP was originally utilized to record traditional archaeology sites (Fussell, 1982; Baltsavias, 1999; Al-kheder et al., 2008; Burtch,

2008; Barazzetti et al., 2011a; Barsanti et al., 2013; Benavides López et al., 2016; Porter et al., 2016). Archaeologists have already been using artificial lights and tarps as tools to correct poor light settings (McPherron et al., 2009; Portalés et al., 2009; Teza et al., 2016). While guidelines for applying these light correction tools have focused on forensic scenes, they can also be useful at archaeological sites. The importance of recording highly accurate maps of sites is not limited to only forensic scenes. Archaeologists require accurate maps of their sites to ensure its preservation, and encounter the same complex environmental factors found in all outdoor settings. Therefore, guidelines that integrate accepted light correction tools with protocols on recording complex scenes, can facilitate the more successful application of CRP technology in circumstances of dappled lighting.

Close-range photogrammetry has proven to be a reliable technique when recording outdoor forensic scenes. However, crime scene investigators do not have the same luxury as archaeologists when choosing the best time to use this technology. Forensic scenes must be recorded as quickly and accurately as possible, while working with whatever lighting situation is present. Therefore, the inclusion of the light correction tools may allow crime scene investigators the opportunity to employ this technology in many more lighting scenarios. Whatever the outdoor lighting situation is, the application of these tools can correct for all dappled or harsh lighting difficulties. Thus, the CRP technology can be used, and the produced models appear accurate enough for presentation in court.

Conclusion

In general, the application of CRP to forensic or archaeological scenes will result in highly accurate models. Even though not all environmental conditions can be mitigated, difficulties in harsh or dappled lighting will no longer be a limiting or challenging variable to

CRP users. The simple inclusion of artificial lights, a white sheet, or both can contribute to more even coloring and higher visual accuracy of the produced models. Further research may contribute procedures to better address other environmental causes of distortion in CRP models, and higher quality models in all conceivable outdoor data collection situations.

APPENDIX: PROCESSING REPORTS

Agisoft Metashape

Processing Report
30 May 2021



Survey Data

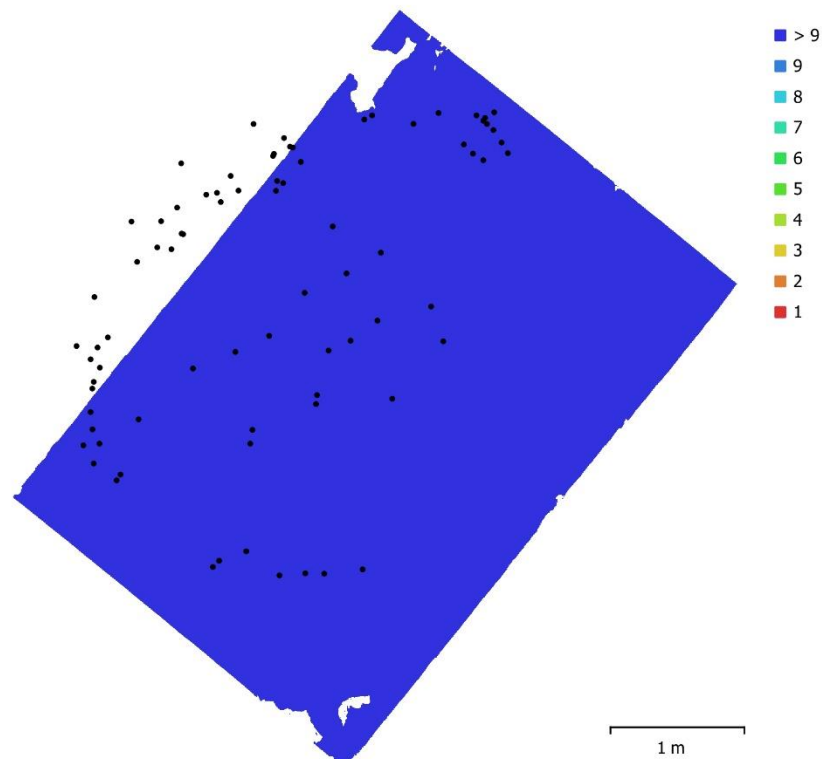


Fig. 1. Camera locations and image overlap.

| | | | |
|--------------------|---------------------|---------------------|-----------|
| Number of images: | 120 | Camera stations: | 79 |
| Flying altitude: | 1.85 m | Tie points: | 63,755 |
| Ground resolution: | 0.364 mm/pix | Projections: | 163,647 |
| Coverage area: | 14.8 m ² | Reprojection error: | 0.283 pix |

| Camera Model | Resolution | Focal Length | Pixel Size | Precalibrated |
|--------------------|-------------|--------------|---------------------|---------------|
| NIKON D7200 (20mm) | 6000 x 4000 | 20 mm | 3.91 x 3.91 μ m | No |
| NIKON D7200 (23mm) | 6000 x 4000 | 23 mm | 3.91 x 3.91 μ m | No |

Table 1. Cameras.

Camera Calibration

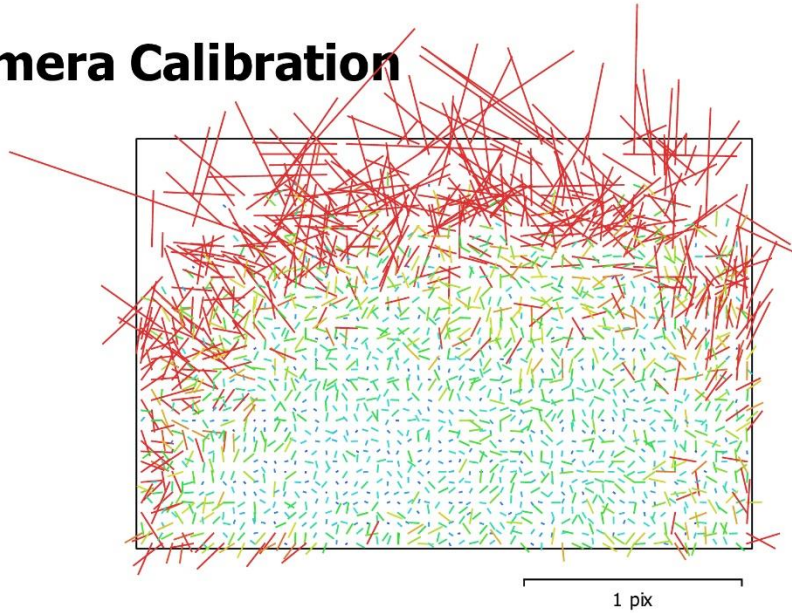


Fig. 2. Image residuals for NIKON D7200 (20mm).

NIKON D7200 (20mm)

110 images

| | | | |
|--------------|--------------------|--------------|---|
| Type | Resolution | Focal Length | Pixel Size |
| Frame | 6000 x 4000 | 20 mm | 3.91 x 3.91 μm |

| | Value | Error | F | Cx | Cy | B1 | B2 | K1 | K2 | K3 | K4 | P1 | P2 | P3 | P4 |
|-----------|----------------------|----------|------|------|-------|-------|-------|-------|-------|-------|-------|-------|-------|-------|-------|
| F | 5017.93 | 0.26 | 1.00 | 0.02 | 0.46 | -0.79 | -0.05 | -0.14 | 0.17 | -0.15 | 0.15 | 0.03 | 0.03 | -0.05 | 0.04 |
| Cx | 5.97099 | 0.34 | | 1.00 | -0.07 | 0.04 | 0.44 | 0.01 | -0.01 | 0.02 | -0.02 | 0.79 | -0.08 | 0.17 | -0.36 |
| Cy | 3.09333 | 0.45 | | | 1.00 | -0.78 | -0.03 | -0.11 | 0.09 | -0.08 | 0.08 | -0.07 | 0.47 | 0.00 | 0.03 |
| B1 | -7.21098 | 0.26 | | | | 1.00 | 0.07 | 0.13 | -0.11 | 0.09 | -0.10 | 0.02 | -0.11 | 0.04 | -0.03 |
| B2 | -0.300389 | 0.13 | | | | | 1.00 | -0.04 | 0.04 | -0.03 | 0.02 | 0.17 | 0.04 | 0.08 | 0.04 |
| K1 | -0.124619 | 0.00016 | | | | | | 1.00 | -0.97 | 0.92 | -0.86 | 0.03 | 0.00 | 0.00 | -0.03 |
| K2 | 0.119751 | 0.0012 | | | | | | | 1.00 | -0.98 | 0.95 | -0.02 | -0.02 | -0.01 | 0.04 |
| K3 | -0.0048053 | 0.0035 | | | | | | | | 1.00 | -0.99 | 0.01 | 0.01 | 0.04 | -0.06 |
| K4 | 0.0411786 | 0.0035 | | | | | | | | | 1.00 | -0.00 | -0.02 | -0.06 | 0.09 |
| P1 | 0.000322296 | 1.4e-005 | | | | | | | | | | 1.00 | -0.15 | -0.36 | -0.03 |
| P2 | -4.89187e-005 | 8.5e-006 | | | | | | | | | | | 1.00 | 0.08 | 0.03 |
| P3 | -0.17822 | 0.13 | | | | | | | | | | | | 1.00 | -0.85 |
| P4 | 3.61393 | 0.18 | | | | | | | | | | | | | 1.00 |

Table 2. Calibration coefficients and correlation matrix.

Camera Calibration

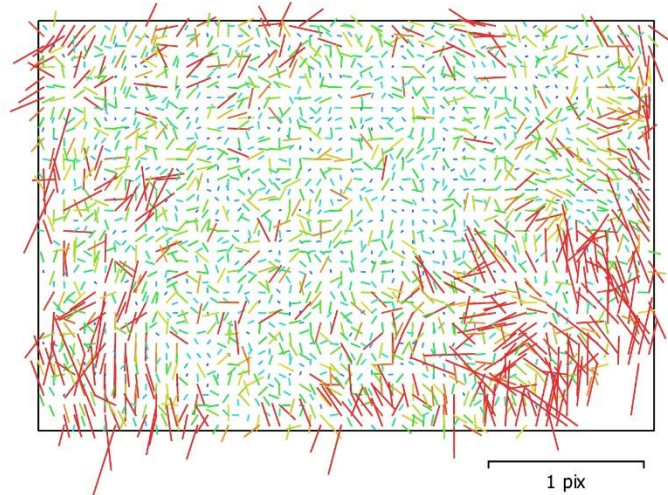


Fig. 3. Image residuals for NIKON D7200 (23mm).

NIKON D7200 (23mm)

10 images

| | | | |
|--------------|--------------------|--------------|---|
| Type | Resolution | Focal Length | Pixel Size |
| Frame | 6000 x 4000 | 23 mm | 3.91 x 3.91 μm |

| | Value | Error | F | Cx | Cy | B1 | B2 | K1 | K2 | K3 | K4 | P1 | P2 | P3 | P4 |
|-----------|--------------------|----------|------|-------|------|-------|-------|-------|-------|-------|-------|-------|-------|-------|-------|
| F | 5580.52 | 1.6 | 1.00 | -0.26 | 0.17 | -0.18 | 0.14 | -0.08 | 0.10 | -0.07 | 0.09 | 0.14 | 0.26 | -0.07 | 0.02 |
| Cx | 21.4615 | 0.31 | | 1.00 | 0.03 | 0.15 | 0.26 | 0.01 | -0.02 | 0.02 | -0.03 | 0.25 | -0.12 | 0.07 | 0.04 |
| Cy | 35.8806 | 0.41 | | | 1.00 | -0.46 | 0.43 | 0.04 | -0.02 | 0.03 | -0.04 | -0.02 | 0.32 | 0.01 | 0.01 |
| B1 | 1.78033 | 0.047 | | | | 1.00 | -0.28 | -0.02 | -0.01 | 0.01 | -0.01 | 0.02 | -0.36 | -0.02 | 0.04 |
| B2 | 4.4837 | 0.038 | | | | | 1.00 | -0.00 | -0.00 | 0.01 | -0.02 | 0.12 | 0.09 | 0.07 | -0.04 |
| K1 | -0.0849921 | 0.00038 | | | | | | 1.00 | -0.97 | 0.92 | -0.87 | -0.04 | -0.00 | 0.06 | -0.09 |
| K2 | 0.190229 | 0.0038 | | | | | | | 1.00 | -0.99 | 0.96 | 0.02 | 0.03 | -0.05 | 0.08 |
| K3 | -0.195757 | 0.015 | | | | | | | | 1.00 | -0.99 | -0.02 | -0.03 | 0.05 | -0.08 |
| K4 | 0.396617 | 0.02 | | | | | | | | | 1.00 | 0.02 | 0.04 | -0.06 | 0.09 |
| P1 | 0.000666125 | 1.4e-005 | | | | | | | | | | 1.00 | 0.69 | -0.75 | 0.64 |
| P2 | 0.000654113 | 1.4e-005 | | | | | | | | | | | 1.00 | -0.78 | 0.64 |
| P3 | 0.525504 | 0.13 | | | | | | | | | | | | 1.00 | -0.94 |
| P4 | 1.1437 | 0.26 | | | | | | | | | | | | | 1.00 |

Table 3. Calibration coefficients and correlation matrix.

Scale Bars

| Label | Distance (m) | Error (m) |
|---------------------|--------------|--------------------|
| target 49_target 51 | 0.998684 | -0.00129599 |
| target 57_target 59 | 0.999988 | -0.000112065 |
| target 73_target 75 | 1.0012 | 0.00100146 |
| Total | | 0.000947817 |

Table 4. Control scale bars.

Digital Elevation Model

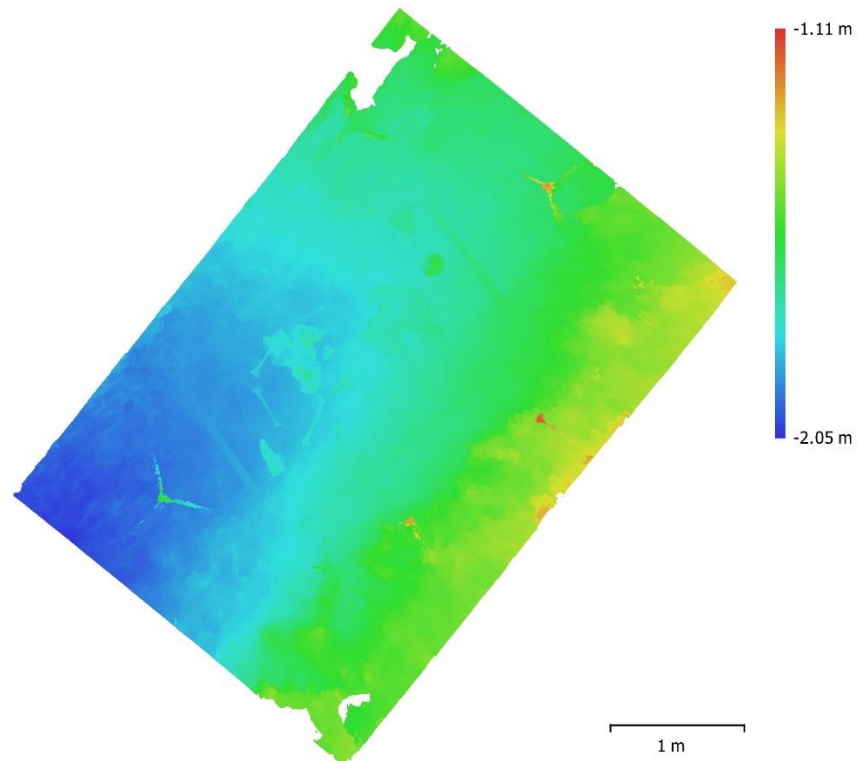


Fig. 4. Reconstructed digital elevation model.

Resolution: unknown
Point density: unknown

Processing Parameters

General

| | |
|-------------------|---------------------|
| Cameras | 120 |
| Aligned cameras | 79 |
| Markers | 12 |
| Scale bars | 4 |
| Coordinate system | WGS 84 (EPSG::4326) |
| Rotation angles | Yaw, Pitch, Roll |

Point Cloud

| | |
|--------------------------------|-------------------------|
| Points | 63,755 of 426,099 |
| RMS reprojection error | 0.117762 (0.282711 pix) |
| Max reprojection error | 0.355146 (2.38246 pix) |
| Mean key point size | 2.3576 pix |
| Point colors | 3 bands, uint8 |
| Key points | No |
| Average tie point multiplicity | 2.56982 |

Alignment parameters

| | |
|-------------------------------|----------------------|
| Accuracy | High |
| Generic preselection | No |
| Key point limit | 100,000 |
| Tie point limit | 50,000 |
| Adaptive camera model fitting | Yes |
| Matching time | 3 hours 32 minutes |
| Alignment time | 2 minutes 50 seconds |

Optimization parameters

| | |
|-------------------------------|---------------------------------|
| Parameters | f, b1, b2, cx, cy, k1-k4, p1-p4 |
| Adaptive camera model fitting | No |
| Optimization time | 2 seconds |
| Software version | 1.5.5.9097 |

Depth Maps

| | |
|-------|----|
| Count | 75 |
|-------|----|

Depth maps generation parameters

| | |
|------------------|--------------------|
| Quality | High |
| Filtering mode | Aggressive |
| Processing time | 3 hours 23 minutes |
| Software version | 1.5.5.9097 |

Dense Point Cloud

| | |
|--------------|----------------|
| Points | 28,614,984 |
| Point colors | 3 bands, uint8 |

Depth maps generation parameters

| | |
|-----------------|--------------------|
| Quality | High |
| Filtering mode | Aggressive |
| Processing time | 3 hours 23 minutes |

Dense cloud generation parameters

| | |
|------------------|----------------------|
| Processing time | 44 minutes 3 seconds |
| Software version | 1.5.5.9097 |

Model

| | |
|---------------|-------------------------------|
| Faces | 5,722,927 |
| Vertices | 2,872,556 |
| Vertex colors | 3 bands, uint8 |
| Texture | 8,192 x 8,192, 4 bands, uint8 |

General**Depth maps generation parameters**

| | |
|-----------------|--------------------|
| Quality | High |
| Filtering mode | Aggressive |
| Processing time | 3 hours 23 minutes |

Reconstruction parameters

| | |
|-------------------------|-------------------|
| Surface type | Arbitrary |
| Source data | Dense cloud |
| Interpolation | Enabled |
| Strict volumetric masks | No |
| Processing time | 1 hours 9 minutes |

Texturing parameters

| | |
|------------------------|-----------------------|
| Mapping mode | Generic |
| Blending mode | Mosaic |
| Texture size | 8,192 |
| Enable hole filling | Yes |
| Enable ghosting filter | Yes |
| UV mapping time | 11 minutes 21 seconds |
| Blending time | 24 minutes 9 seconds |
| Software version | 1.5.5.9097 |

Software

| | |
|----------|------------------|
| Version | 1.5.5 build 9097 |
| Platform | Windows 64 |

Model 1B-1

Agisoft Metashape

**Processing Report
31 May 2021**



Survey Data

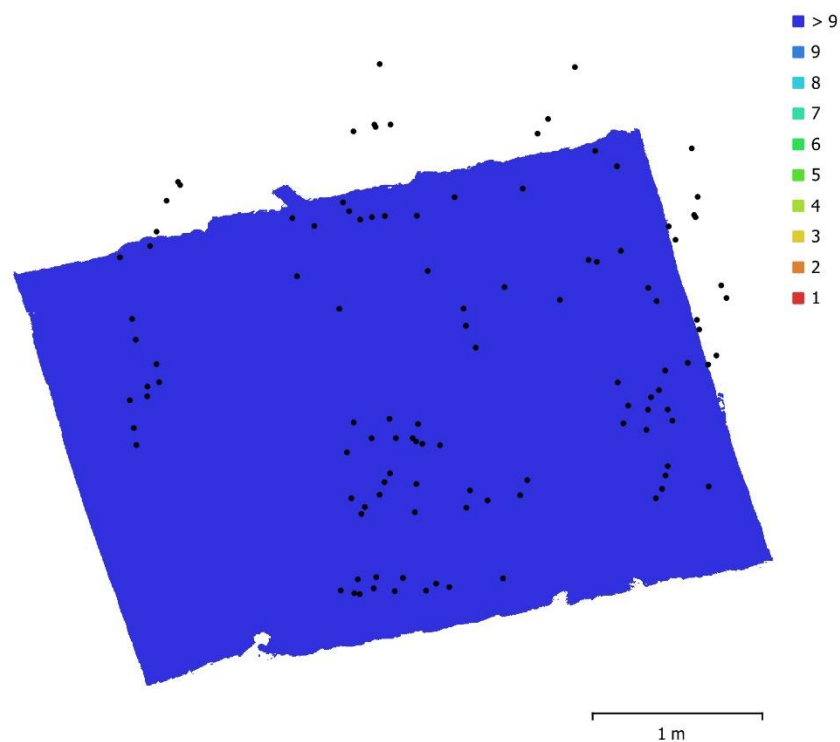


Fig. 1. Camera locations and image overlap.

| | | | |
|--------------------|--------------------|---------------------|-----------|
| Number of images: | 120 | Camera stations: | 111 |
| Flying altitude: | 1.8 m | Tie points: | 114,889 |
| Ground resolution: | 0.387 mm/pix | Projections: | 324,787 |
| Coverage area: | 9.8 m ² | Reprojection error: | 0.286 pix |

| Camera Model | Resolution | Focal Length | Pixel Size | Precalibrated |
|--------------------|-------------|--------------|----------------|---------------|
| NIKON D7200 (18mm) | 6000 x 4000 | 18 mm | 3.91 x 3.91 μm | No |

Table 1. Cameras.

Camera Calibration

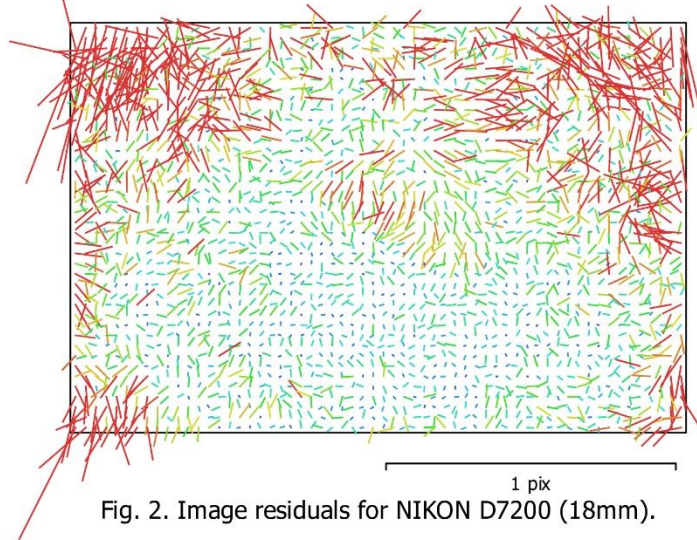


Fig. 2. Image residuals for NIKON D7200 (18mm).

NIKON D7200 (18mm)

120 images

| | | | |
|--------------|--------------------|--------------|---|
| Type | Resolution | Focal Length | Pixel Size |
| Frame | 6000 x 4000 | 18 mm | 3.91 x 3.91 μm |

| | Value | Error | F | Cx | Cy | B1 | B2 | K1 | K2 | K3 | K4 | P1 | P2 | P3 | P4 |
|-----------|----------------------|----------|------|------|-------|-------|-------|-------|-------|-------|-------|-------|-------|-------|-------|
| F | 4653.81 | 0.11 | 1.00 | 0.03 | -0.20 | -0.13 | -0.05 | -0.03 | 0.10 | -0.09 | 0.09 | 0.01 | 0.25 | -0.01 | 0.01 |
| Cx | 0.665976 | 0.12 | | 1.00 | -0.10 | 0.05 | 0.31 | 0.01 | -0.01 | 0.01 | -0.00 | 0.68 | -0.22 | 0.18 | -0.08 |
| Cy | 1.552 | 0.15 | | | 1.00 | -0.53 | -0.02 | -0.03 | 0.04 | -0.04 | 0.04 | -0.04 | 0.41 | 0.00 | -0.00 |
| B1 | 0.914408 | 0.021 | | | | 1.00 | -0.05 | 0.05 | -0.04 | 0.03 | -0.02 | 0.08 | -0.36 | -0.02 | -0.00 |
| B2 | -2.21899 | 0.02 | | | | | 1.00 | 0.02 | -0.01 | 0.01 | -0.00 | 0.12 | -0.19 | 0.06 | 0.01 |
| K1 | -0.152843 | 6.8e-005 | | | | | | 1.00 | -0.96 | 0.91 | -0.86 | -0.03 | -0.05 | 0.03 | -0.00 |
| K2 | 0.103735 | 0.00044 | | | | | | | 1.00 | -0.99 | 0.95 | 0.03 | 0.05 | -0.04 | 0.01 |
| K3 | -2.24109e-005 | 0.0011 | | | | | | | | 1.00 | -0.99 | -0.03 | -0.04 | 0.02 | 0.02 |
| K4 | -0.00146245 | 0.00092 | | | | | | | | | 1.00 | 0.01 | 0.02 | 0.02 | -0.05 |
| P1 | 0.000449688 | 4.8e-006 | | | | | | | | | | 1.00 | 0.13 | -0.40 | 0.35 |
| P2 | 0.00037169 | 4.5e-006 | | | | | | | | | | | 1.00 | -0.48 | 0.37 |
| P3 | -0.509932 | 0.03 | | | | | | | | | | | | 1.00 | -0.94 |
| P4 | 1.5913 | 0.039 | | | | | | | | | | | | | 1.00 |

Table 2. Calibration coefficients and correlation matrix.

Scale Bars

| Label | Distance (m) | Error (m) |
|---------------------|--------------|--------------------|
| target 57_target 59 | 0.999825 | -0.000175215 |
| target 49_target 51 | 0.999584 | -0.000415723 |
| target 65_target 67 | 1.00034 | 0.000335444 |
| target 73_target 75 | 1.00026 | 0.000261402 |
| Total | | 0.000309992 |

Table 3. Control scale bars.

Digital Elevation Model

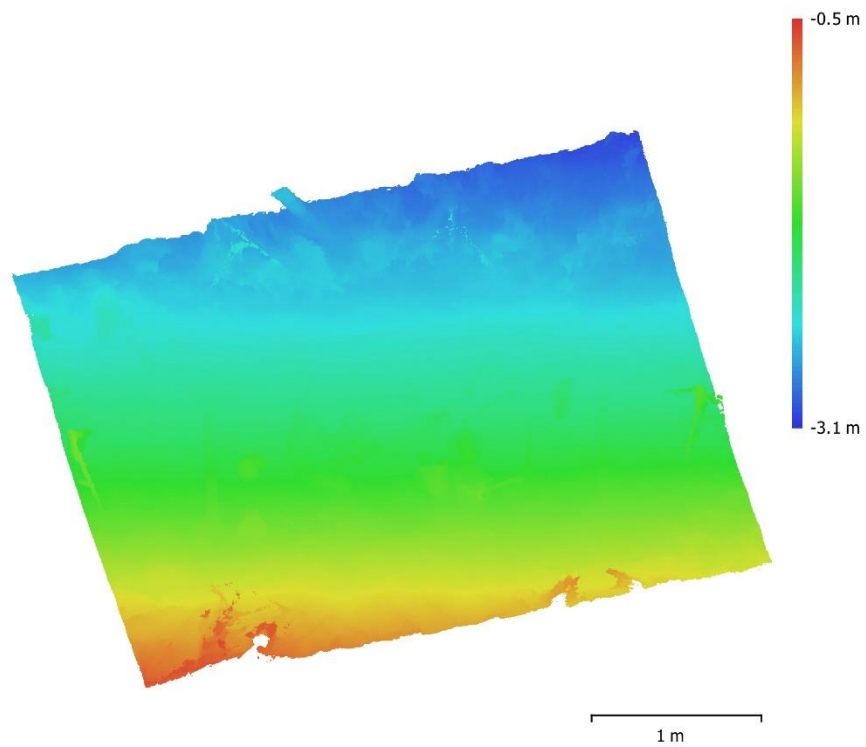


Fig. 3. Reconstructed digital elevation model.

Resolution: unknown
Point density: unknown

Processing Parameters

General

| | |
|-------------------|---------------------|
| Cameras | 120 |
| Aligned cameras | 111 |
| Markers | 12 |
| Scale bars | 4 |
| Coordinate system | WGS 84 (EPSG::4326) |
| Rotation angles | Yaw, Pitch, Roll |

Point Cloud

| | |
|--------------------------------|-------------------------|
| Points | 114,889 of 559,752 |
| RMS reprojection error | 0.120305 (0.286246 pix) |
| Max reprojection error | 0.390958 (2.60165 pix) |
| Mean key point size | 2.3489 pix |
| Point colors | 3 bands, uint8 |
| Key points | No |
| Average tie point multiplicity | 2.6339 |

Alignment parameters

| | |
|-------------------------------|-----------------------|
| Accuracy | High |
| Generic preselection | Yes |
| Key point limit | 100,000 |
| Tie point limit | 40,000 |
| Adaptive camera model fitting | Yes |
| Matching time | 15 minutes 35 seconds |
| Alignment time | 5 minutes 19 seconds |

Optimization parameters

| | |
|-------------------------------|---------------------------------|
| Parameters | f, b1, b2, cx, cy, k1-k4, p1-p4 |
| Adaptive camera model fitting | No |
| Optimization time | 8 seconds |
| Software version | 1.5.5.9097 |

Depth Maps

| | |
|-------|-----|
| Count | 111 |
|-------|-----|

Depth maps generation parameters

| | |
|------------------|--------------------|
| Quality | High |
| Filtering mode | Aggressive |
| Processing time | 8 hours 29 minutes |
| Software version | 1.5.5.9097 |

Dense Point Cloud

| | |
|--------------|----------------|
| Points | 26,131,134 |
| Point colors | 3 bands, uint8 |

Depth maps generation parameters

| | |
|-----------------|--------------------|
| Quality | High |
| Filtering mode | Aggressive |
| Processing time | 8 hours 29 minutes |

Dense cloud generation parameters

| | |
|------------------|--------------------|
| Processing time | 2 hours 37 minutes |
| Software version | 1.5.5.9097 |

Model

| | |
|---------------|-------------------------------|
| Faces | 5,226,086 |
| Vertices | 2,623,623 |
| Vertex colors | 3 bands, uint8 |
| Texture | 8,192 x 8,192, 4 bands, uint8 |

General**Depth maps generation parameters**

| | |
|-----------------|--------------------|
| Quality | High |
| Filtering mode | Aggressive |
| Processing time | 8 hours 29 minutes |

Reconstruction parameters

| | |
|-------------------------|--------------------|
| Surface type | Arbitrary |
| Source data | Dense cloud |
| Interpolation | Enabled |
| Strict volumetric masks | No |
| Processing time | 2 hours 40 minutes |

Texturing parameters

| | |
|------------------------|-----------------------|
| Mapping mode | Generic |
| Blending mode | Mosaic |
| Texture size | 8,192 |
| Enable hole filling | Yes |
| Enable ghosting filter | Yes |
| UV mapping time | 11 minutes 4 seconds |
| Blending time | 21 minutes 40 seconds |
| Software version | 1.5.5.9097 |

Orthomosaic

| | |
|-------------------|---------------------|
| Size | 10,102 x 7,743 |
| Coordinate system | WGS 84 (EPSG::4978) |
| Colors | 3 bands, uint8 |

Reconstruction parameters

| | |
|---------------------|-----------------------|
| Blending mode | Mosaic |
| Surface | Mesh |
| Enable hole filling | Yes |
| Processing time | 21 minutes 19 seconds |
| Software version | 1.5.5.9097 |

Software

| | |
|----------|------------------|
| Version | 1.5.5 build 9097 |
| Platform | Windows 64 |

Model 1C-1

Agisoft Metashape

Processing Report
09 June 2021



Survey Data

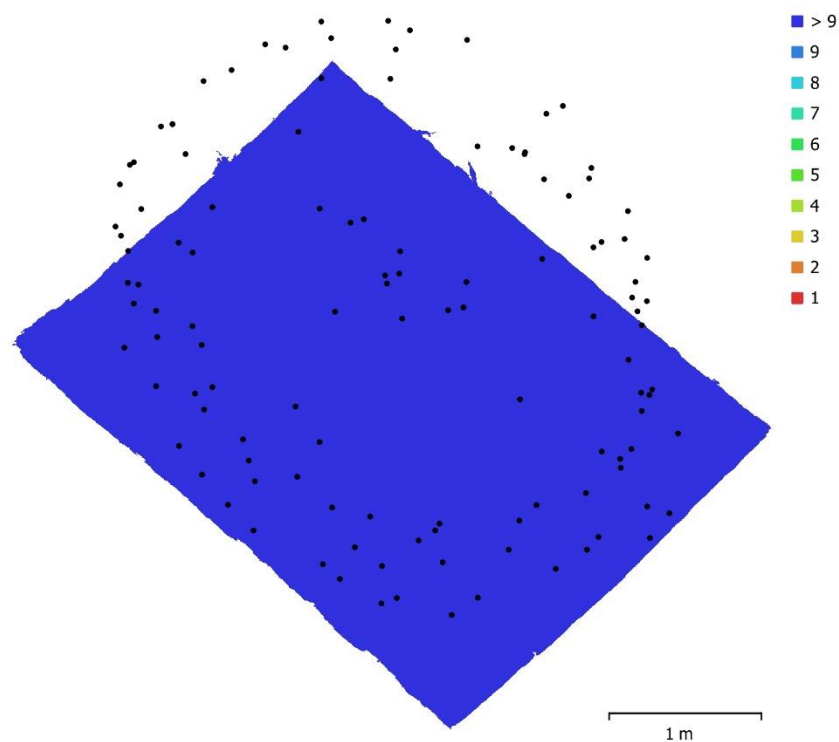


Fig. 1. Camera locations and image overlap.

| | | | |
|--------------------|---------------------|---------------------|-----------|
| Number of images: | 120 | Camera stations: | 118 |
| Flying altitude: | 1.76 m | Tie points: | 144,833 |
| Ground resolution: | 0.379 mm/pix | Projections: | 412,017 |
| Coverage area: | 10.7 m ² | Reprojection error: | 0.288 pix |

| Camera Model | Resolution | Focal Length | Pixel Size | Precalibrated |
|--------------------|-------------|--------------|----------------|---------------|
| NIKON D7200 (18mm) | 6000 x 4000 | 18 mm | 3.91 x 3.91 μm | No |

Table 1. Cameras.

Camera Calibration

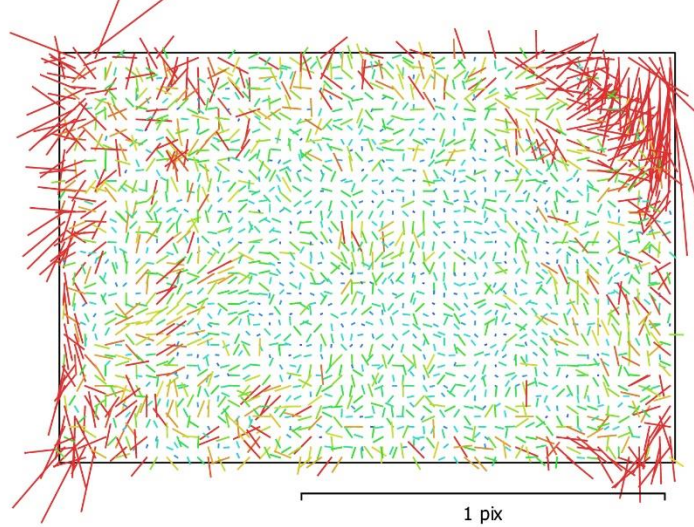


Fig. 2. Image residuals for NIKON D7200 (18mm).

NIKON D7200 (18mm)

120 images

| | | | |
|--------------|--------------------|--------------|--------------------------------------|
| Type | Resolution | Focal Length | Pixel Size |
| Frame | 6000 x 4000 | 18 mm | 3.91 x 3.91 μm |

| | Value | Error | F | Cx | Cy | B1 | B2 | K1 | K2 | K3 | K4 | P1 | P2 | P3 | P4 |
|-----------|--------------------|----------|------|-------|-------|-------|-------|-------|-------|-------|-------|-------|-------|-------|-------|
| F | 4656.99 | 0.12 | 1.00 | -0.08 | -0.65 | 0.05 | 0.01 | -0.18 | 0.15 | -0.11 | 0.10 | 0.08 | 0.23 | -0.09 | 0.03 |
| Cx | 4.88359 | 0.074 | | 1.00 | 0.14 | -0.06 | 0.19 | -0.00 | 0.01 | -0.01 | 0.00 | 0.23 | -0.03 | -0.05 | 0.10 |
| Cy | 12.4087 | 0.1 | | | 1.00 | -0.26 | -0.05 | 0.01 | 0.01 | -0.02 | 0.02 | -0.01 | -0.20 | 0.01 | 0.06 |
| B1 | -0.883867 | 0.0094 | | | | 1.00 | 0.00 | 0.02 | -0.03 | 0.03 | -0.03 | 0.08 | 0.10 | -0.06 | 0.02 |
| B2 | -0.18342 | 0.0095 | | | | | 1.00 | 0.00 | -0.01 | 0.01 | -0.01 | -0.02 | -0.03 | -0.01 | 0.04 |
| K1 | -0.155718 | 8.7e-005 | | | | | | 1.00 | -0.96 | 0.90 | -0.84 | -0.06 | -0.06 | 0.06 | -0.06 |
| K2 | 0.107404 | 0.00055 | | | | | | | 1.00 | -0.98 | 0.95 | 0.07 | 0.06 | -0.08 | 0.09 |
| K3 | -0.00162079 | 0.0014 | | | | | | | | 1.00 | -0.99 | -0.07 | -0.05 | 0.08 | -0.09 |
| K4 | -0.00171805 | 0.0012 | | | | | | | | | 1.00 | 0.06 | 0.04 | -0.07 | 0.08 |
| P1 | 0.000427704 | 3.9e-006 | | | | | | | | | | 1.00 | 0.79 | -0.83 | 0.71 |
| P2 | 0.000499049 | 4.3e-006 | | | | | | | | | | | 1.00 | -0.86 | 0.72 |
| P3 | 0.691157 | 0.042 | | | | | | | | | | | | 1.00 | -0.95 |
| P4 | 0.0921214 | 0.052 | | | | | | | | | | | | | 1.00 |

Table 2. Calibration coefficients and correlation matrix.

Scale Bars

| Label | Distance (m) | Error (m) |
|---------------------|--------------|-----------------|
| target 49_target 51 | 1.11119 | 0.111205 |
| target 73_target 75 | 1.11235 | 0.112152 |
| target 59_target 57 | 1.1144 | 0.114299 |
| Total | | 0.112559 |

Table 3. Control scale bars.

Digital Elevation Model

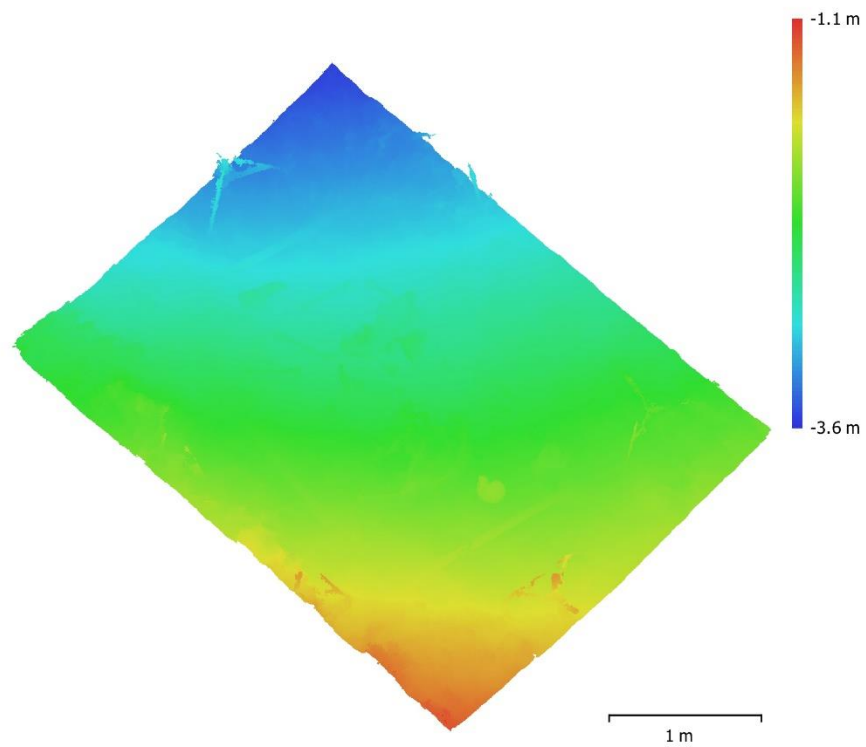


Fig. 3. Reconstructed digital elevation model.

Resolution: unknown
Point density: unknown

Processing Parameters

General

| | |
|-------------------|---------------------|
| Cameras | 120 |
| Aligned cameras | 118 |
| Markers | 12 |
| Scale bars | 4 |
| Coordinate system | WGS 84 (EPSG::4326) |
| Rotation angles | Yaw, Pitch, Roll |

Point Cloud

| | |
|--------------------------------|-------------------------|
| Points | 144,833 of 467,383 |
| RMS reprojection error | 0.121614 (0.287841 pix) |
| Max reprojection error | 0.404199 (1.69883 pix) |
| Mean key point size | 2.33828 pix |
| Point colors | 3 bands, uint8 |
| Key points | No |
| Average tie point multiplicity | 2.87347 |

Alignment parameters

| | |
|-------------------------------|-----------------------|
| Accuracy | High |
| Generic preselection | Yes |
| Key point limit | 100,000 |
| Tie point limit | 40,000 |
| Adaptive camera model fitting | Yes |
| Matching time | 15 minutes 14 seconds |
| Alignment time | 3 minutes 19 seconds |

Optimization parameters

| | |
|-------------------------------|---------------------------------|
| Parameters | f, b1, b2, cx, cy, k1-k4, p1-p4 |
| Adaptive camera model fitting | No |
| Optimization time | 4 seconds |
| Software version | 1.5.5.9097 |

Depth Maps

| | |
|-------|-----|
| Count | 109 |
|-------|-----|

Depth maps generation parameters

| | |
|------------------|---------------------|
| Quality | High |
| Filtering mode | Aggressive |
| Processing time | 14 hours 53 minutes |
| Software version | 1.5.5.9097 |

Dense Point Cloud

| | |
|--------------|----------------|
| Points | 22,326,869 |
| Point colors | 3 bands, uint8 |

Depth maps generation parameters

| | |
|-----------------|---------------------|
| Quality | High |
| Filtering mode | Aggressive |
| Processing time | 14 hours 53 minutes |

Dense cloud generation parameters

| | |
|------------------|--------------------|
| Processing time | 3 hours 22 minutes |
| Software version | 1.5.5.9097 |

Model

| | |
|---------------|-------------------------------|
| Faces | 4,465,266 |
| Vertices | 2,240,528 |
| Vertex colors | 3 bands, uint8 |
| Texture | 8,192 x 8,192, 4 bands, uint8 |

General**Depth maps generation parameters**

| | |
|-----------------|---------------------|
| Quality | High |
| Filtering mode | Aggressive |
| Processing time | 14 hours 53 minutes |

Reconstruction parameters

| | |
|-------------------------|-----------------------|
| Surface type | Arbitrary |
| Source data | Dense cloud |
| Interpolation | Enabled |
| Strict volumetric masks | No |
| Processing time | 29 minutes 10 seconds |

Texturing parameters

| | |
|------------------------|-----------------------|
| Mapping mode | Generic |
| Blending mode | Mosaic |
| Texture size | 8,192 |
| Enable hole filling | Yes |
| Enable ghosting filter | Yes |
| UV mapping time | 7 minutes 17 seconds |
| Blending time | 55 minutes 48 seconds |
| Software version | 1.5.5.9097 |

Orthomosaic

| | |
|-------------------|---------------------|
| Size | 10,032 x 8,459 |
| Coordinate system | WGS 84 (EPSG::4978) |
| Colors | 3 bands, uint8 |

Reconstruction parameters

| | |
|---------------------|-----------------------|
| Blending mode | Mosaic |
| Surface | Mesh |
| Enable hole filling | Yes |
| Processing time | 19 minutes 22 seconds |
| Software version | 1.5.5.9097 |

Software

| | |
|----------|------------------|
| Version | 1.5.5 build 9097 |
| Platform | Windows 64 |

Model 1D-2

Agisoft Metashape

Processing Report
30 May 2021



Survey Data

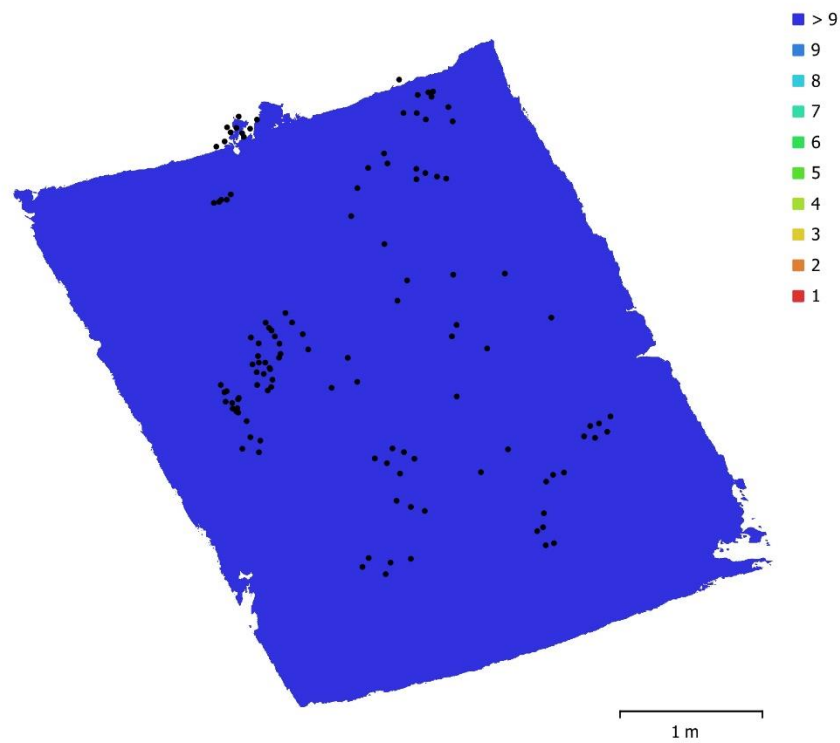


Fig. 1. Camera locations and image overlap.

| | | | |
|--------------------|---------------------|---------------------|-----------|
| Number of images: | 120 | Camera stations: | 120 |
| Flying altitude: | 1.95 m | Tie points: | 165,322 |
| Ground resolution: | 0.42 mm/pix | Projections: | 471,727 |
| Coverage area: | 14.2 m ² | Reprojection error: | 0.312 pix |

| Camera Model | Resolution | Focal Length | Pixel Size | Precalibrated |
|--------------------|-------------|--------------|----------------|---------------|
| NIKON D7200 (18mm) | 6000 x 4000 | 18 mm | 3.91 x 3.91 μm | No |

Table 1. Cameras.

Camera Calibration

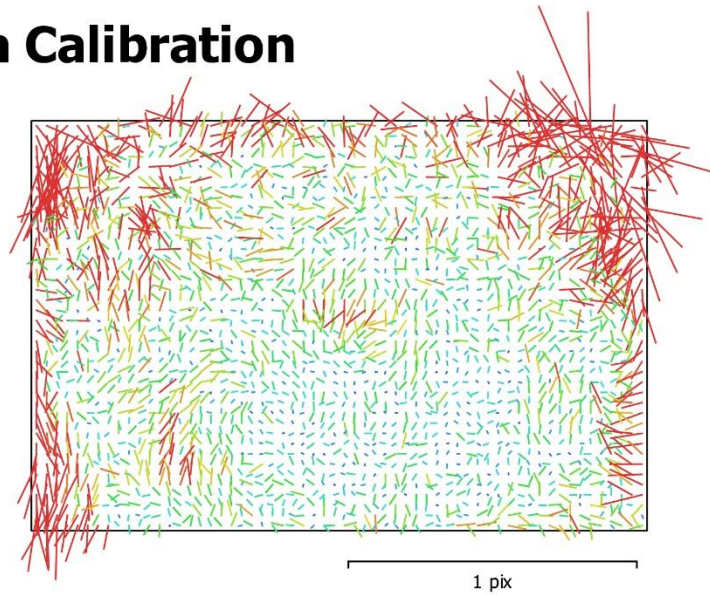


Fig. 2. Image residuals for NIKON D7200 (18mm).

NIKON D7200 (18mm)

120 images

| | | | |
|--------------|--------------------|--------------|---|
| Type | Resolution | Focal Length | Pixel Size |
| Frame | 6000 x 4000 | 18 mm | 3.91 x 3.91 μm |

| | Value | Error | F | Cx | Cy | B1 | B2 | K1 | K2 | K3 | K4 | P1 | P2 | P3 | P4 |
|-----------|---------------------|----------|------|------|-------|-------|-------|-------|-------|-------|-------|-------|-------|-------|-------|
| F | 4648.23 | 0.076 | 1.00 | 0.04 | -0.28 | 0.05 | 0.03 | -0.08 | 0.14 | -0.13 | 0.12 | 0.08 | 0.11 | -0.04 | 0.01 |
| Cx | 6.8323 | 0.088 | | 1.00 | 0.01 | -0.06 | 0.23 | 0.02 | -0.01 | 0.01 | -0.01 | 0.67 | -0.04 | 0.03 | 0.00 |
| Cy | 12.7584 | 0.1 | | | 1.00 | -0.47 | -0.07 | -0.03 | 0.03 | -0.02 | 0.02 | -0.01 | 0.34 | -0.01 | 0.04 |
| B1 | 0.604742 | 0.015 | | | | 1.00 | 0.08 | 0.03 | -0.04 | 0.04 | -0.03 | 0.01 | 0.19 | -0.02 | -0.04 |
| B2 | 0.173224 | 0.014 | | | | | 1.00 | 0.02 | -0.02 | 0.02 | -0.02 | 0.01 | 0.05 | -0.00 | 0.03 |
| K1 | -0.153686 | 5.8e-005 | | | | | | 1.00 | -0.97 | 0.92 | -0.87 | -0.04 | -0.07 | 0.09 | -0.07 |
| K2 | 0.104037 | 0.00037 | | | | | | | 1.00 | -0.99 | 0.95 | 0.05 | 0.04 | -0.10 | 0.09 |
| K3 | -0.000965039 | 0.00092 | | | | | | | | 1.00 | -0.99 | -0.04 | -0.03 | 0.08 | -0.07 |
| K4 | -0.00165612 | 0.00077 | | | | | | | | | 1.00 | 0.03 | 0.02 | -0.06 | 0.05 |
| P1 | 0.000557102 | 3.5e-006 | | | | | | | | | | 1.00 | 0.37 | -0.60 | 0.50 |
| P2 | 0.00053088 | 3.6e-006 | | | | | | | | | | | 1.00 | -0.56 | 0.44 |
| P3 | 0.159102 | 0.021 | | | | | | | | | | | | 1.00 | -0.94 |
| P4 | 1.01862 | 0.025 | | | | | | | | | | | | | 1.00 |

Table 2. Calibration coefficients and correlation matrix.

Scale Bars

| Label | Distance (m) | Error (m) |
|---------------------|--------------|--------------------|
| target 49_target 51 | 0.999915 | -6.45002e-005 |
| target 57_target 59 | 0.999896 | -0.000203794 |
| target 65_target 67 | 1.00016 | 0.000251687 |
| target 73_target 75 | 1.0002 | 4.12001e-006 |
| Total | | 0.000165118 |

Table 3. Control scale bars.

Digital Elevation Model

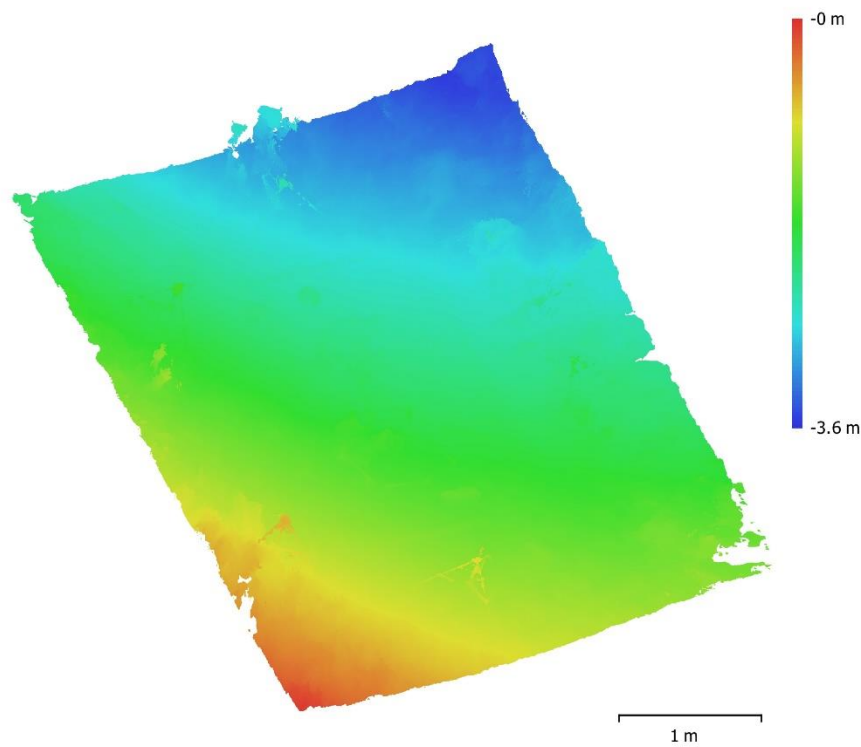


Fig. 3. Reconstructed digital elevation model.

Resolution: unknown
Point density: unknown

Processing Parameters

General

| | |
|-------------------|---------------------|
| Cameras | 120 |
| Aligned cameras | 120 |
| Markers | 12 |
| Scale bars | 4 |
| Coordinate system | WGS 84 (EPSG::4326) |
| Rotation angles | Yaw, Pitch, Roll |

Point Cloud

| | |
|--------------------------------|-------------------------|
| Points | 165,322 of 812,095 |
| RMS reprojection error | 0.131042 (0.311667 pix) |
| Max reprojection error | 0.887563 (2.51333 pix) |
| Mean key point size | 2.34174 pix |
| Point colors | 3 bands, uint8 |
| Key points | No |
| Average tie point multiplicity | 3.04537 |

Alignment parameters

| | |
|-------------------------------|----------------------|
| Accuracy | High |
| Generic preselection | No |
| Key point limit | 100,000 |
| Tie point limit | 50,000 |
| Adaptive camera model fitting | Yes |
| Matching time | 3 hours 40 minutes |
| Alignment time | 6 minutes 22 seconds |

Optimization parameters

| | |
|-------------------------------|---------------------------------|
| Parameters | f, b1, b2, cx, cy, k1-k4, p1-p4 |
| Adaptive camera model fitting | No |
| Optimization time | 7 seconds |
| Software version | 1.5.5.9097 |

Depth Maps

| | |
|-------|-----|
| Count | 115 |
|-------|-----|

Depth maps generation parameters

| | |
|------------------|--------------------|
| Quality | High |
| Filtering mode | Aggressive |
| Processing time | 10 hours 3 minutes |
| Software version | 1.5.5.9097 |

Dense Point Cloud

| | |
|--------------|----------------|
| Points | 39,018,417 |
| Point colors | 3 bands, uint8 |

Depth maps generation parameters

| | |
|-----------------|--------------------|
| Quality | High |
| Filtering mode | Aggressive |
| Processing time | 10 hours 3 minutes |

Dense cloud generation parameters

| | |
|------------------|-------------------|
| Processing time | 3 hours 0 minutes |
| Software version | 1.5.5.9097 |

Model

| | |
|---------------|-------------------------------|
| Faces | 7,803,577 |
| Vertices | 3,918,863 |
| Vertex colors | 3 bands, uint8 |
| Texture | 8,192 x 8,192, 4 bands, uint8 |

General**Depth maps generation parameters**

| | |
|-----------------|--------------------|
| Quality | High |
| Filtering mode | Aggressive |
| Processing time | 10 hours 3 minutes |

Reconstruction parameters

| | |
|-------------------------|--------------------|
| Surface type | Arbitrary |
| Source data | Dense cloud |
| Interpolation | Enabled |
| Strict volumetric masks | No |
| Processing time | 1 hours 34 minutes |

Texturing parameters

| | |
|------------------------|-----------------------|
| Mapping mode | Generic |
| Blending mode | Mosaic |
| Texture size | 8,192 |
| Enable hole filling | Yes |
| Enable ghosting filter | Yes |
| UV mapping time | 14 minutes 51 seconds |
| Blending time | 25 minutes 51 seconds |
| Software version | 1.5.5.9097 |

Software

| | |
|----------|------------------|
| Version | 1.5.5 build 9097 |
| Platform | Windows 64 |

Model 2A-2

Agisoft Metashape

Processing Report
15 June 2021



Survey Data

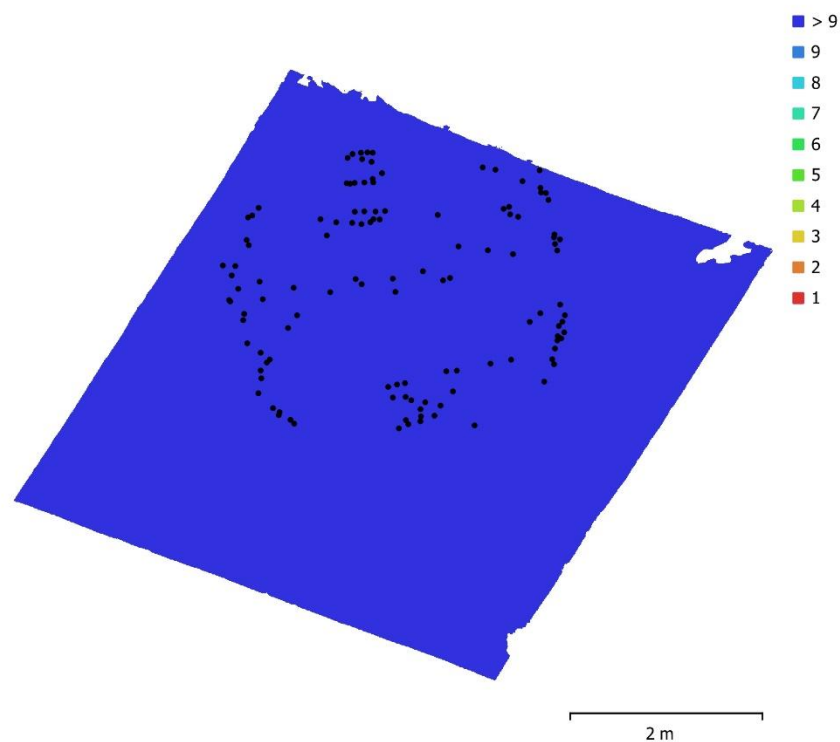


Fig. 1. Camera locations and image overlap.

| | | | |
|--------------------|---------------------|---------------------|-----------|
| Number of images: | 120 | Camera stations: | 120 |
| Flying altitude: | 1.83 m | Tie points: | 137,506 |
| Ground resolution: | 0.393 mm/pix | Projections: | 390,251 |
| Coverage area: | 27.6 m ² | Reprojection error: | 0.296 pix |

| Camera Model | Resolution | Focal Length | Pixel Size | Precalibrated |
|--------------------|-------------|--------------|----------------|---------------|
| NIKON D7200 (18mm) | 6000 x 4000 | 18 mm | 3.91 x 3.91 μm | No |

Table 1. Cameras.

Camera Calibration

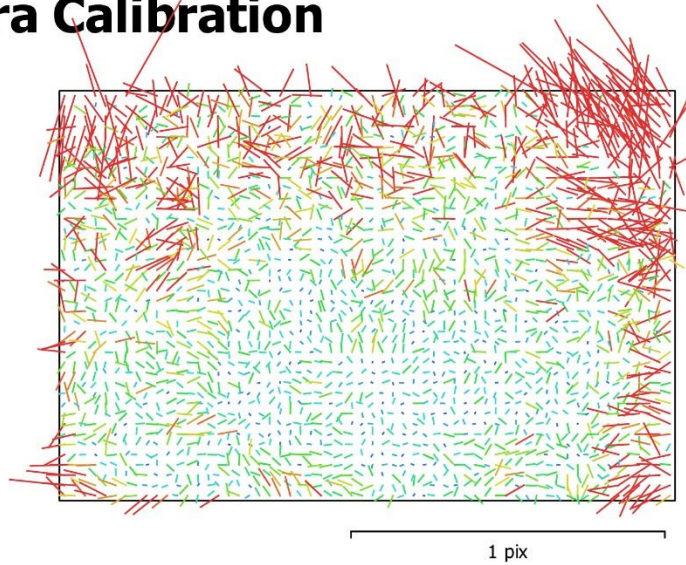


Fig. 2. Image residuals for NIKON D7200 (18mm).

NIKON D7200 (18mm)

120 images

| | | | |
|--------------|--------------------|--------------|--------------------------------------|
| Type | Resolution | Focal Length | Pixel Size |
| Frame | 6000 x 4000 | 18 mm | 3.91 x 3.91 μm |

| | Value | Error | F | Cx | Cy | B1 | B2 | K1 | K2 | K3 | K4 | P1 | P2 | P3 | P4 |
|-----------|---------------------|----------|------|------|-------|-------|-------|-------|-------|-------|-------|-------|-------|-------|-------|
| F | 4662.15 | 0.074 | 1.00 | 0.00 | -0.07 | -0.11 | -0.01 | -0.11 | 0.17 | -0.15 | 0.14 | -0.04 | 0.19 | -0.01 | 0.01 |
| Cx | -5.813 | 0.057 | | 1.00 | 0.02 | 0.06 | 0.13 | 0.04 | -0.03 | 0.03 | -0.03 | 0.78 | -0.04 | 0.06 | 0.01 |
| Cy | 2.83332 | 0.1 | | | 1.00 | -0.44 | 0.20 | -0.02 | 0.04 | -0.03 | 0.03 | 0.08 | 0.22 | 0.01 | 0.09 |
| B1 | 0.0855284 | 0.016 | | | | 1.00 | -0.08 | 0.01 | -0.02 | 0.02 | -0.01 | 0.00 | 0.07 | 0.01 | -0.04 |
| B2 | -0.785131 | 0.015 | | | | | 1.00 | 0.00 | 0.00 | 0.00 | -0.01 | -0.06 | 0.03 | 0.00 | 0.02 |
| K1 | -0.154073 | 6.3e-005 | | | | | | 1.00 | -0.97 | 0.92 | -0.87 | 0.02 | -0.20 | 0.16 | -0.12 |
| K2 | 0.110937 | 0.00041 | | | | | | | 1.00 | -0.99 | 0.95 | 0.00 | 0.18 | -0.19 | 0.16 |
| K3 | -0.0146983 | 0.001 | | | | | | | | 1.00 | -0.99 | -0.00 | -0.15 | 0.16 | -0.14 |
| K4 | 0.0112664 | 0.00083 | | | | | | | | | 1.00 | -0.01 | 0.11 | -0.11 | 0.08 |
| P1 | 9.29829e-005 | 2.9e-006 | | | | | | | | | | 1.00 | 0.02 | -0.12 | 0.16 |
| P2 | 0.000790558 | 5.7e-006 | | | | | | | | | | | 1.00 | -0.55 | 0.52 |
| P3 | -0.843869 | 0.024 | | | | | | | | | | | | 1.00 | -0.96 |
| P4 | 0.645557 | 0.037 | | | | | | | | | | | | | 1.00 |

Table 2. Calibration coefficients and correlation matrix.

Scale Bars

| Label | Distance (m) | Error (m) |
|---------------------|--------------|--------------------|
| target 73_target 75 | 0.999872 | -0.000347596 |
| target 65_target 67 | 1.00001 | 0.000102319 |
| target 57_target 59 | 1.00013 | 2.94351e-005 |
| target 49_target 51 | 0.999934 | 0.000133684 |
| Total | | 0.000193669 |

Table 3. Control scale bars.

Digital Elevation Model

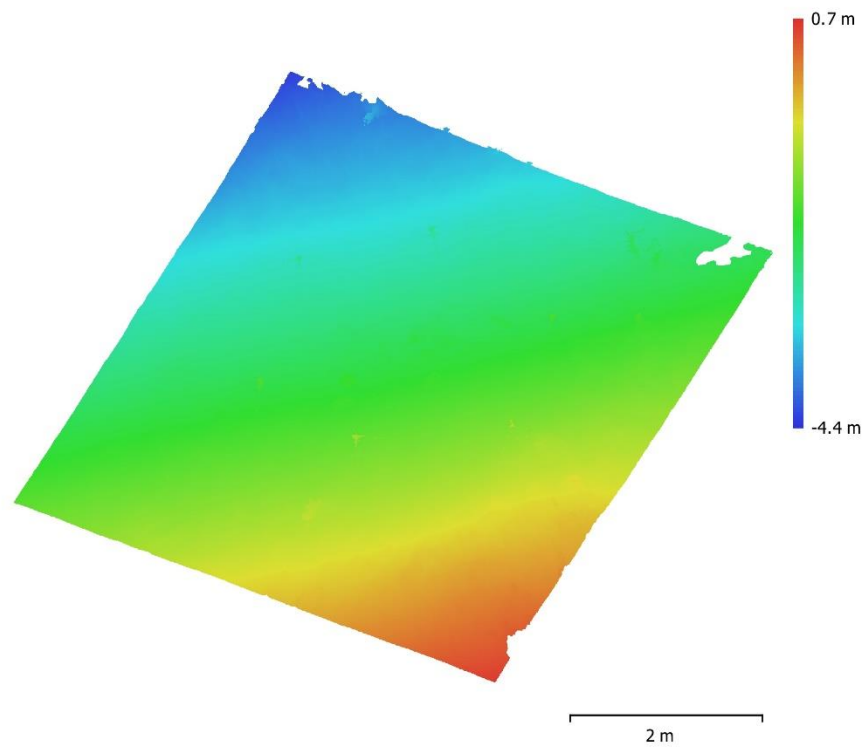


Fig. 3. Reconstructed digital elevation model.

Resolution: unknown
Point density: unknown

Processing Parameters

General

| | |
|-------------------|-----------------------|
| Cameras | 120 |
| Aligned cameras | 120 |
| Markers | 12 |
| Scale bars | 4 |
| Coordinate system | Local Coordinates (m) |
| Rotation angles | Yaw, Pitch, Roll |

Point Cloud

| | |
|--------------------------------|-------------------------|
| Points | 137,506 of 878,466 |
| RMS reprojection error | 0.113513 (0.295888 pix) |
| Max reprojection error | 0.441685 (2.73431 pix) |
| Mean key point size | 2.57152 pix |
| Point colors | 3 bands, uint8 |
| Key points | No |
| Average tie point multiplicity | 2.67027 |

Alignment parameters

| | |
|-------------------------------|----------------------|
| Accuracy | High |
| Generic preselection | No |
| Key point limit | 100,000 |
| Tie point limit | 40,000 |
| Adaptive camera model fitting | Yes |
| Matching time | 3 hours 37 minutes |
| Alignment time | 15 minutes 7 seconds |

Optimization parameters

| | |
|-------------------------------|---------------------------------|
| Parameters | f, b1, b2, cx, cy, k1-k4, p1-p4 |
| Adaptive camera model fitting | No |
| Optimization time | 7 seconds |
| Software version | 1.5.5.9097 |

Depth Maps

| | |
|-------|-----|
| Count | 120 |
|-------|-----|

Depth maps generation parameters

| | |
|------------------|--------------------|
| Quality | High |
| Filtering mode | Aggressive |
| Processing time | 6 hours 17 minutes |
| Software version | 1.5.5.9097 |

Dense Point Cloud

| | |
|--------------|----------------|
| Points | 42,415,877 |
| Point colors | 3 bands, uint8 |

Depth maps generation parameters

| | |
|-----------------|--------------------|
| Quality | High |
| Filtering mode | Aggressive |
| Processing time | 6 hours 17 minutes |

Dense cloud generation parameters

| | |
|------------------|--------------------|
| Processing time | 4 hours 30 minutes |
| Software version | 1.5.5.9097 |

Model

| | |
|---------------|-------------------------------|
| Faces | 8,483,109 |
| Vertices | 4,250,854 |
| Vertex colors | 3 bands, uint8 |
| Texture | 8,192 x 8,192, 4 bands, uint8 |

General**Depth maps generation parameters**

| | |
|-----------------|--------------------|
| Quality | High |
| Filtering mode | Aggressive |
| Processing time | 6 hours 17 minutes |

Reconstruction parameters

| | |
|-------------------------|--------------------|
| Surface type | Arbitrary |
| Source data | Dense cloud |
| Interpolation | Enabled |
| Strict volumetric masks | No |
| Processing time | 1 hours 18 minutes |

Texturing parameters

| | |
|------------------------|-----------------------|
| Mapping mode | Generic |
| Blending mode | Mosaic |
| Texture size | 8,192 |
| Enable hole filling | Yes |
| Enable ghosting filter | No |
| UV mapping time | 6 minutes 10 seconds |
| Blending time | 16 minutes 26 seconds |
| Software version | 1.5.5.9097 |

Orthomosaic

| | |
|-------------------|-----------------------|
| Size | 17,326 x 17,638 |
| Coordinate system | Local Coordinates (m) |
| Colors | 3 bands, uint8 |

Reconstruction parameters

| | |
|---------------------|--------------------|
| Blending mode | Mosaic |
| Surface | Mesh |
| Enable hole filling | Yes |
| Processing time | 5 hours 33 minutes |
| Software version | 1.5.5.9097 |

Software

| | |
|----------|------------------|
| Version | 1.5.5 build 9097 |
| Platform | Windows 64 |

Model 2B-1

Agisoft Metashape

Processing Report
15 June 2021



Survey Data

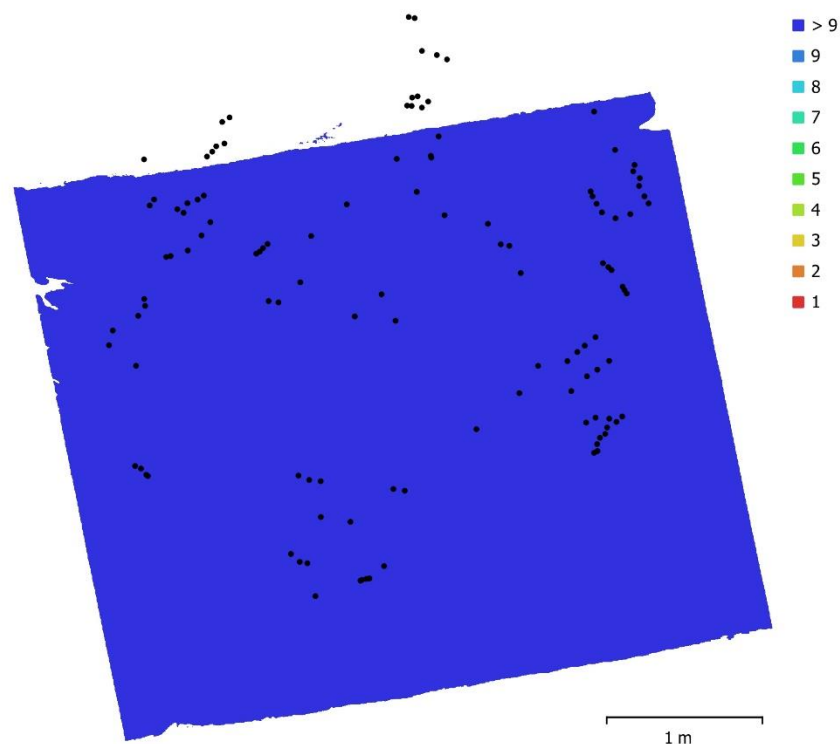


Fig. 1. Camera locations and image overlap.

| | | | |
|--------------------|-------------------|---------------------|-----------|
| Number of images: | 120 | Camera stations: | 120 |
| Flying altitude: | 1.61 m | Tie points: | 92,716 |
| Ground resolution: | 0.331 mm/pix | Projections: | 267,019 |
| Coverage area: | 15 m ² | Reprojection error: | 0.346 pix |

| Camera Model | Resolution | Focal Length | Pixel Size | Precalibrated |
|--------------------|-------------|--------------|----------------|---------------|
| NIKON D7200 (18mm) | 6000 x 4000 | 18 mm | 3.91 x 3.91 μm | No |

Table 1. Cameras.

Camera Calibration

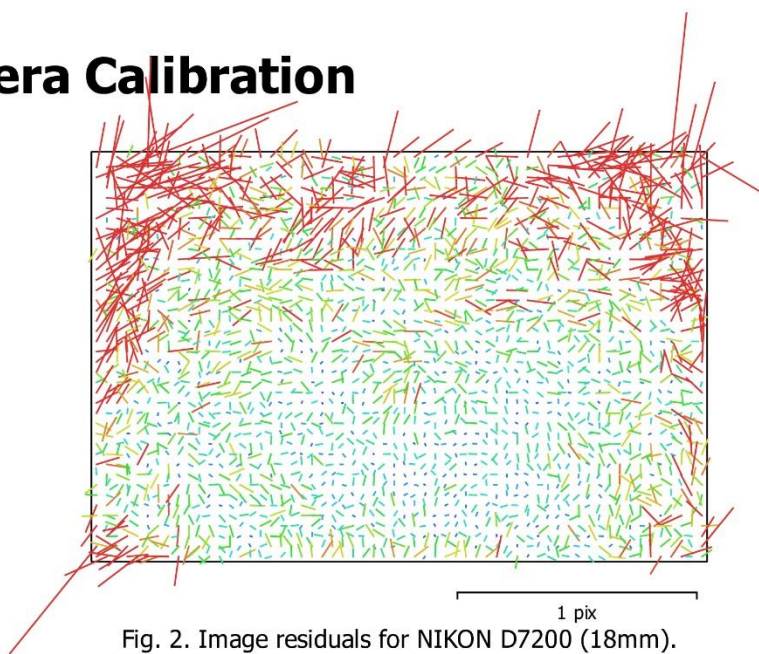


Fig. 2. Image residuals for NIKON D7200 (18mm).

NIKON D7200 (18mm)

120 images

| Type | Resolution | Focal Length | Pixel Size |
|-------|-------------|--------------|----------------|
| Frame | 6000 x 4000 | 18 mm | 3.91 x 3.91 μm |
| F: | 4856.24 | | |
| Cx: | -3.83637 | B1: | -0.297312 |
| Cy: | 8.85437 | B2: | -2.08186 |
| K1: | -0.135893 | P1: | -0.000173878 |
| K2: | 0.11464 | P2: | 0.000513758 |
| K3: | -0.00938651 | P3: | -2.07086 |
| K4: | 0.0279987 | P4: | 1.5302 |

Scale Bars

| Label | Distance (m) | Error (m) |
|---------------------|--------------|--------------------|
| target 73_target 75 | 1.00065 | 0.000431587 |
| target 65_target 67 | 0.998867 | -0.00104332 |
| target 57_target 59 | 0.999928 | -0.000172017 |
| target 49_target 51 | 1.00061 | 0.000806169 |
| Total | | 0.000698978 |

Table 2. Control scale bars.

Digital Elevation Model

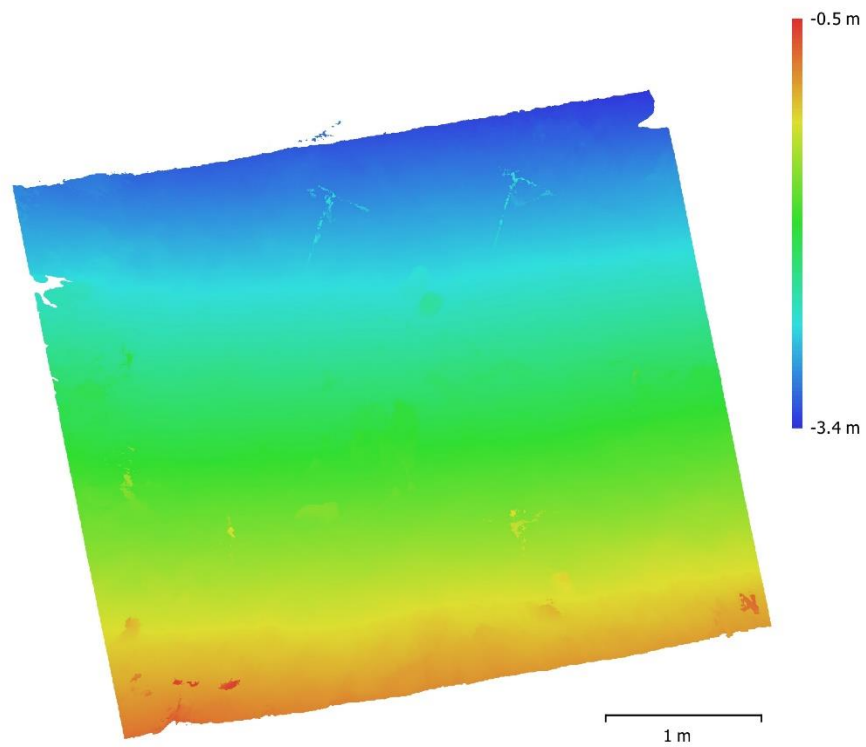


Fig. 3. Reconstructed digital elevation model.

Resolution: unknown
Point density: unknown

Processing Parameters

General

| | |
|-------------------|-----------------------|
| Cameras | 120 |
| Aligned cameras | 120 |
| Markers | 12 |
| Scale bars | 4 |
| Coordinate system | Local Coordinates (m) |
| Rotation angles | Yaw, Pitch, Roll |

Point Cloud

| | |
|--------------------------------|-------------------------|
| Points | 92,716 of 1,154,625 |
| RMS reprojection error | 0.113113 (0.345809 pix) |
| Max reprojection error | 0.866451 (2.61024 pix) |
| Mean key point size | 3.0024 pix |
| Point colors | 3 bands, uint8 |
| Key points | No |
| Average tie point multiplicity | 2.68956 |

Alignment parameters

| | |
|-------------------------------|-----------------------|
| Accuracy | High |
| Generic preselection | No |
| Key point limit | 100,000 |
| Tie point limit | 40,000 |
| Adaptive camera model fitting | Yes |
| Matching time | 3 hours 21 minutes |
| Alignment time | 24 minutes 44 seconds |

Optimization parameters

| | |
|-------------------------------|---------------------------------|
| Parameters | f, b1, b2, cx, cy, k1-k4, p1-p4 |
| Adaptive camera model fitting | No |
| Optimization time | 4 seconds |
| Software version | 1.5.5.9097 |

Depth Maps

| | |
|-------|-----|
| Count | 120 |
|-------|-----|

Depth maps generation parameters

| | |
|------------------|--------------------|
| Quality | High |
| Filtering mode | Aggressive |
| Processing time | 4 hours 37 minutes |
| Software version | 1.5.5.9097 |

Dense Point Cloud

| | |
|--------------|----------------|
| Points | 38,065,719 |
| Point colors | 3 bands, uint8 |

Depth maps generation parameters

| | |
|-----------------|--------------------|
| Quality | High |
| Filtering mode | Aggressive |
| Processing time | 4 hours 37 minutes |

Dense cloud generation parameters

| | |
|------------------|--------------------|
| Processing time | 3 hours 56 minutes |
| Software version | 1.5.5.9097 |

Model

| | |
|---------------|-------------------------------|
| Faces | 7,613,055 |
| Vertices | 3,817,046 |
| Vertex colors | 3 bands, uint8 |
| Texture | 8,192 x 8,192, 4 bands, uint8 |

General**Depth maps generation parameters**

| | |
|-----------------|--------------------|
| Quality | High |
| Filtering mode | Aggressive |
| Processing time | 4 hours 37 minutes |

Reconstruction parameters

| | |
|-------------------------|-------------------|
| Surface type | Arbitrary |
| Source data | Dense cloud |
| Interpolation | Enabled |
| Strict volumetric masks | No |
| Processing time | 5 hours 2 minutes |

Texturing parameters

| | |
|------------------------|-----------------------|
| Mapping mode | Generic |
| Blending mode | Mosaic |
| Texture size | 8,192 |
| Enable hole filling | Yes |
| Enable ghosting filter | No |
| UV mapping time | 5 minutes 8 seconds |
| Blending time | 19 minutes 40 seconds |
| Software version | 1.5.5.9097 |

Orthomosaic

| | |
|-------------------|-----------------------|
| Size | 15,510 x 15,678 |
| Coordinate system | Local Coordinates (m) |
| Colors | 3 bands, uint8 |

Reconstruction parameters

| | |
|---------------------|--------------------|
| Blending mode | Mosaic |
| Surface | Mesh |
| Enable hole filling | Yes |
| Processing time | 3 hours 55 minutes |
| Software version | 1.5.5.9097 |

Software

| | |
|----------|------------------|
| Version | 1.5.5 build 9097 |
| Platform | Windows 64 |

Model 2C-2

Agisoft Metashape

Processing Report
16 June 2021



Survey Data

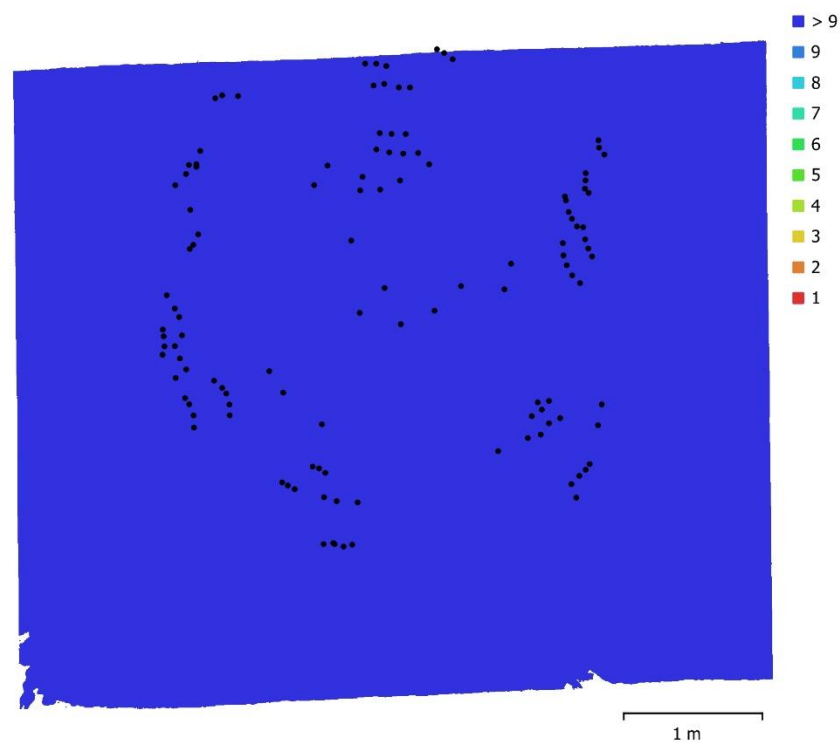


Fig. 1. Camera locations and image overlap.

| | | | |
|--------------------|---------------------|---------------------|-----------|
| Number of images: | 120 | Camera stations: | 120 |
| Flying altitude: | 2.06 m | Tie points: | 270,744 |
| Ground resolution: | 0.443 mm/pix | Projections: | 727,624 |
| Coverage area: | 25.1 m ² | Reprojection error: | 0.327 pix |

| Camera Model | Resolution | Focal Length | Pixel Size | Precalibrated |
|--------------------|-------------|--------------|---------------------|---------------|
| NIKON D7200 (18mm) | 6000 x 4000 | 18 mm | 3.91 x 3.91 μ m | No |

Table 1. Cameras.

Camera Calibration

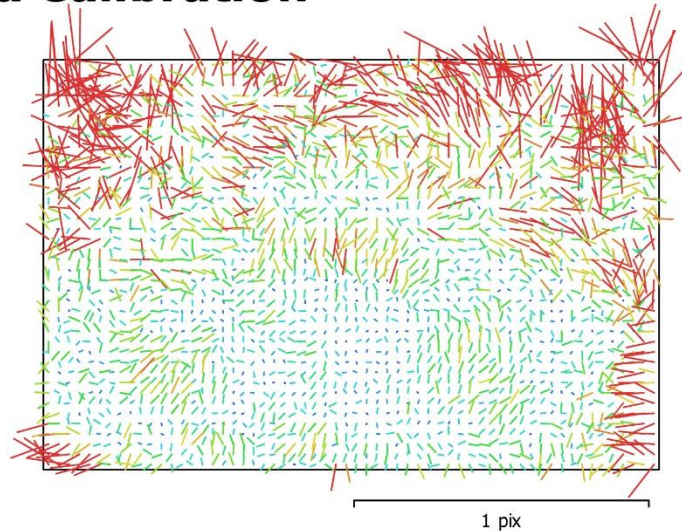


Fig. 2. Image residuals for NIKON D7200 (18mm).

NIKON D7200 (18mm)

120 images

| | | | |
|--------------|--------------------|--------------|---|
| Type | Resolution | Focal Length | Pixel Size |
| Frame | 6000 x 4000 | 18 mm | 3.91 x 3.91 μm |

| | Value | Error | F | Cx | Cy | B1 | B2 | K1 | K2 | K3 | K4 | P1 | P2 | P3 | P4 |
|-----------|---------------------|----------|------|------|-------|-------|-------|-------|-------|-------|-------|-------|-------|-------|-------|
| F | 4666.52 | 0.075 | 1.00 | 0.06 | -0.08 | -0.13 | 0.04 | -0.09 | 0.15 | -0.13 | 0.12 | 0.04 | 0.21 | -0.04 | 0.03 |
| Cx | -4.44184 | 0.057 | | 1.00 | 0.01 | -0.08 | 0.09 | 0.02 | -0.01 | 0.00 | -0.00 | 0.75 | -0.03 | 0.04 | -0.01 |
| Cy | 9.97331 | 0.11 | | | 1.00 | -0.22 | -0.12 | 0.00 | 0.02 | -0.03 | 0.02 | 0.09 | 0.31 | 0.01 | 0.13 |
| B1 | -0.706253 | 0.018 | | | | 1.00 | 0.02 | 0.01 | -0.02 | 0.02 | -0.01 | -0.08 | 0.19 | -0.01 | -0.02 |
| B2 | -1.12068 | 0.018 | | | | | 1.00 | -0.01 | 0.00 | -0.00 | 0.00 | -0.15 | 0.05 | 0.01 | -0.02 |
| K1 | -0.153264 | 5.3e-005 | | | | | | 1.00 | -0.97 | 0.92 | -0.87 | 0.00 | -0.16 | 0.20 | -0.16 |
| K2 | 0.108263 | 0.00034 | | | | | | | 1.00 | -0.99 | 0.95 | 0.02 | 0.15 | -0.22 | 0.20 |
| K3 | -0.00581291 | 0.00086 | | | | | | | | 1.00 | -0.99 | -0.02 | -0.12 | 0.19 | -0.17 |
| K4 | 0.00418336 | 0.00073 | | | | | | | | | 1.00 | 0.01 | 0.10 | -0.13 | 0.11 |
| P1 | 3.67178e-005 | 2.6e-006 | | | | | | | | | | 1.00 | -0.02 | -0.04 | 0.06 |
| P2 | 0.000801036 | 5.4e-006 | | | | | | | | | | | 1.00 | -0.55 | 0.54 |
| P3 | -0.19532 | 0.022 | | | | | | | | | | | | 1.00 | -0.96 |
| P4 | -0.115668 | 0.033 | | | | | | | | | | | | | 1.00 |

Table 2. Calibration coefficients and correlation matrix.

Scale Bars

| Label | Distance (m) | Error (m) |
|---------------------|--------------|--------------------|
| target 49_target 51 | 0.999634 | -0.000346049 |
| target 57_target 59 | 0.999777 | -0.00032322 |
| target 65_target 67 | 1.00022 | 0.000307859 |
| target 73_target 75 | 1.00069 | 0.000485228 |
| Total | | 0.000372305 |

Table 3. Control scale bars.

Digital Elevation Model

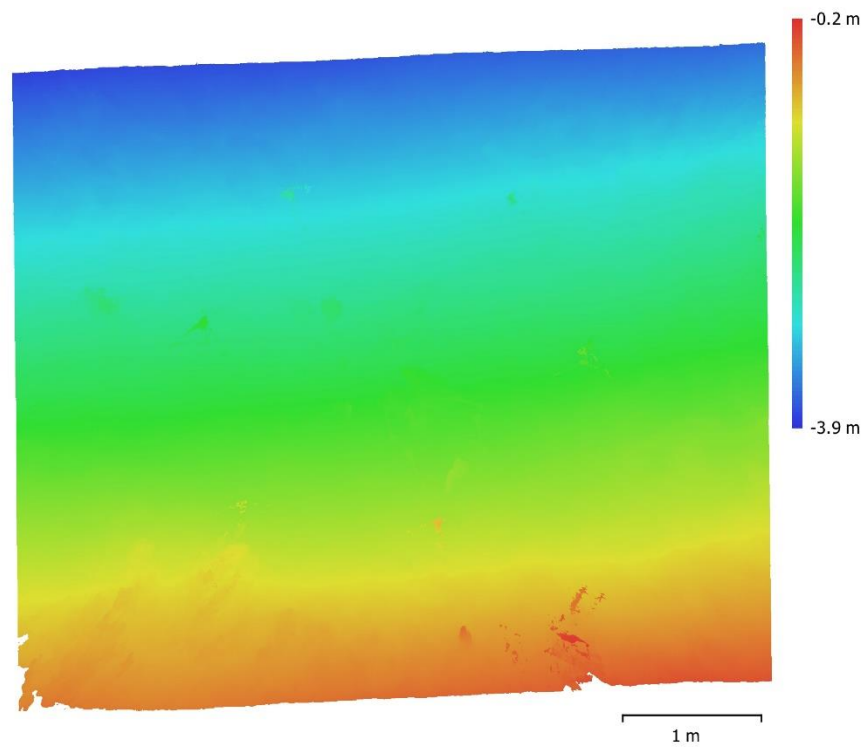


Fig. 3. Reconstructed digital elevation model.

Resolution: unknown
Point density: unknown

Processing Parameters

General

| | |
|-------------------|---------------------|
| Cameras | 120 |
| Aligned cameras | 120 |
| Markers | 12 |
| Scale bars | 4 |
| Coordinate system | WGS 84 (EPSG::4326) |
| Rotation angles | Yaw, Pitch, Roll |

Point Cloud

| | |
|--------------------------------|-------------------------|
| Points | 270,744 of 925,610 |
| RMS reprojection error | 0.117719 (0.326677 pix) |
| Max reprojection error | 0.691329 (3.02072 pix) |
| Mean key point size | 2.7393 pix |
| Point colors | 3 bands, uint8 |
| Key points | No |
| Average tie point multiplicity | 2.59366 |

Alignment parameters

| | |
|-------------------------------|----------------------|
| Accuracy | High |
| Generic preselection | Yes |
| Key point limit | 100,000 |
| Tie point limit | 40,000 |
| Adaptive camera model fitting | No |
| Matching time | 20 minutes 1 seconds |
| Alignment time | 8 minutes 21 seconds |

Optimization parameters

| | |
|-------------------------------|---------------------------------|
| Parameters | f, b1, b2, cx, cy, k1-k4, p1-p4 |
| Adaptive camera model fitting | No |
| Optimization time | 19 seconds |
| Software version | 1.5.5.9097 |

Depth Maps

| | |
|-------|-----|
| Count | 118 |
|-------|-----|

Depth maps generation parameters

| | |
|------------------|--------------------|
| Quality | High |
| Filtering mode | Aggressive |
| Processing time | 5 hours 56 minutes |
| Software version | 1.5.5.9097 |

Dense Point Cloud

| | |
|--------------|----------------|
| Points | 43,798,240 |
| Point colors | 3 bands, uint8 |

Depth maps generation parameters

| | |
|-----------------|--------------------|
| Quality | High |
| Filtering mode | Aggressive |
| Processing time | 5 hours 56 minutes |

Dense cloud generation parameters

| | |
|------------------|--------------------|
| Processing time | 5 hours 15 minutes |
| Software version | 1.5.5.9097 |

Model

| | |
|---------------|-------------------------------|
| Faces | 8,759,572 |
| Vertices | 4,390,281 |
| Vertex colors | 3 bands, uint8 |
| Texture | 8,192 x 8,192, 4 bands, uint8 |

General**Depth maps generation parameters**

| | |
|-----------------|--------------------|
| Quality | High |
| Filtering mode | Aggressive |
| Processing time | 5 hours 56 minutes |

Reconstruction parameters

| | |
|-------------------------|--------------------|
| Surface type | Arbitrary |
| Source data | Dense cloud |
| Interpolation | Enabled |
| Strict volumetric masks | No |
| Processing time | 2 hours 11 minutes |

Texturing parameters

| | |
|------------------------|-----------------------|
| Mapping mode | Generic |
| Blending mode | Mosaic |
| Texture size | 8,192 |
| Enable hole filling | Yes |
| Enable ghosting filter | Yes |
| UV mapping time | 7 minutes 11 seconds |
| Blending time | 24 minutes 44 seconds |
| Software version | 1.5.5.9097 |

Orthomosaic

| | |
|-------------------|---------------------|
| Size | 13,311 x 12,920 |
| Coordinate system | WGS 84 (EPSG::4978) |
| Colors | 3 bands, uint8 |

Reconstruction parameters

| | |
|---------------------|-----------------------|
| Blending mode | Mosaic |
| Surface | Mesh |
| Enable hole filling | Yes |
| Processing time | 19 minutes 48 seconds |
| Software version | 1.5.5.9097 |

Software

| | |
|----------|------------------|
| Version | 1.5.5 build 9097 |
| Platform | Windows 64 |

Agisoft Metashape

Processing Report
08 June 2021



Survey Data

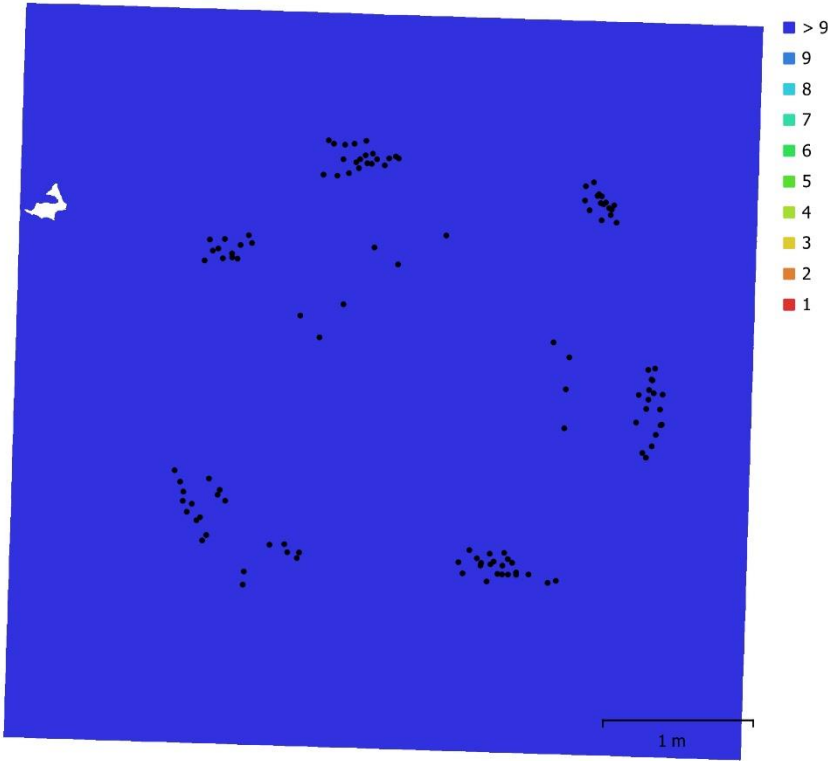


Fig. 1. Camera locations and image overlap.

| | | | |
|--------------------|---------------------|---------------------|-----------|
| Number of images: | 120 | Camera stations: | 120 |
| Flying altitude: | 1.78 m | Tie points: | 287,316 |
| Ground resolution: | 0.371 mm/pix | Projections: | 846,682 |
| Coverage area: | 23.9 m ² | Reprojection error: | 0.348 pix |

| Camera Model | Resolution | Focal Length | Pixel Size | Precalibrated |
|--------------------|-------------|--------------|----------------|---------------|
| NIKON D7200 (18mm) | 6000 x 4000 | 18 mm | 3.91 x 3.91 μm | No |

Table 1. Cameras.

Camera Calibration

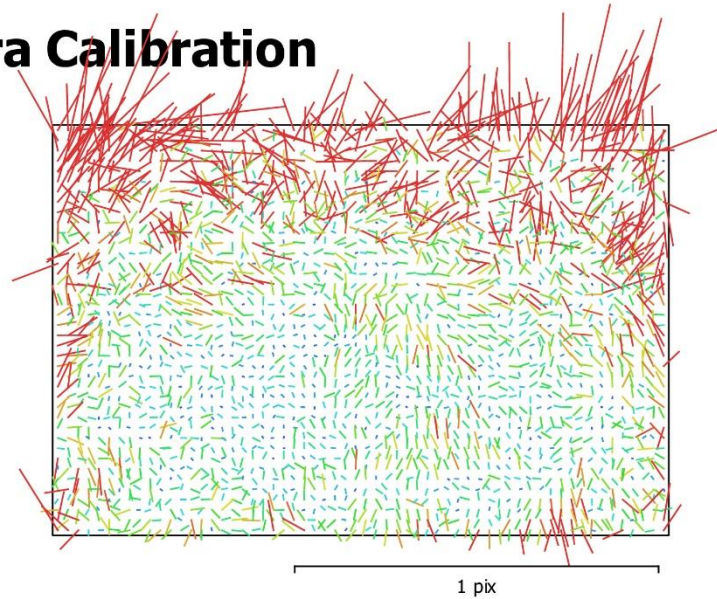


Fig. 2. Image residuals for NIKON D7200 (18mm).

NIKON D7200 (18mm)

120 images

| | | | |
|--------------|--------------------|--------------|---|
| Type | Resolution | Focal Length | Pixel Size |
| Frame | 6000 x 4000 | 18 mm | 3.91 x 3.91 μm |

| | Value | Error | F | Cx | Cy | B1 | B2 | K1 | K2 | K3 | K4 | P1 | P2 | P3 | P4 |
|-----------|---------------------|----------|------|-------|-------|-------|-------|-------|-------|-------|-------|-------|-------|-------|-------|
| F | 4801.16 | 0.075 | 1.00 | -0.05 | 0.40 | -0.67 | -0.06 | -0.13 | 0.16 | -0.15 | 0.16 | -0.01 | 0.15 | -0.03 | 0.01 |
| Cx | 1.02248 | 0.11 | | 1.00 | -0.03 | 0.05 | 0.31 | 0.02 | -0.01 | 0.01 | -0.01 | 0.80 | -0.01 | 0.08 | -0.09 |
| Cy | 2.37379 | 0.17 | | | 1.00 | -0.73 | -0.10 | -0.09 | 0.08 | -0.08 | 0.09 | 0.03 | 0.62 | -0.07 | 0.04 |
| B1 | -6.22074 | 0.067 | | | | 1.00 | 0.14 | 0.11 | -0.10 | 0.10 | -0.11 | -0.04 | -0.13 | 0.08 | -0.01 |
| B2 | -2.3435 | 0.033 | | | | | 1.00 | 0.01 | -0.02 | 0.02 | -0.02 | -0.01 | 0.08 | 0.05 | 0.10 |
| K1 | -0.142335 | 4.9e-005 | | | | | | 1.00 | -0.97 | 0.92 | -0.87 | 0.03 | -0.03 | -0.02 | 0.02 |
| K2 | 0.115336 | 0.00034 | | | | | | | 1.00 | -0.99 | 0.96 | -0.02 | -0.00 | 0.02 | -0.02 |
| K3 | -0.0151382 | 0.00094 | | | | | | | | 1.00 | -0.99 | 0.01 | 0.01 | -0.00 | 0.00 |
| K4 | 0.0247147 | 0.00087 | | | | | | | | | 1.00 | -0.00 | -0.01 | -0.02 | 0.02 |
| P1 | 0.000332687 | 4.1e-006 | | | | | | | | | | 1.00 | -0.17 | -0.42 | 0.27 |
| P2 | -0.000142082 | 3.7e-006 | | | | | | | | | | | 1.00 | 0.20 | -0.10 |
| P3 | 0.26171 | 0.037 | | | | | | | | | | | | 1.00 | -0.93 |
| P4 | 1.60971 | 0.048 | | | | | | | | | | | | | 1.00 |

Table 2. Calibration coefficients and correlation matrix.

Scale Bars

| Label | Distance (m) | Error (m) |
|---------------------|--------------|--------------------|
| target 49_target 51 | 0.999022 | -0.000957925 |
| target 57_target 59 | 1.00026 | 0.000159302 |
| target 65_target 67 | 1.00055 | 0.000641238 |
| target 73_target 75 | 1.00036 | 0.000156988 |
| Total | | 0.000587118 |

Table 3. Control scale bars.

Digital Elevation Model

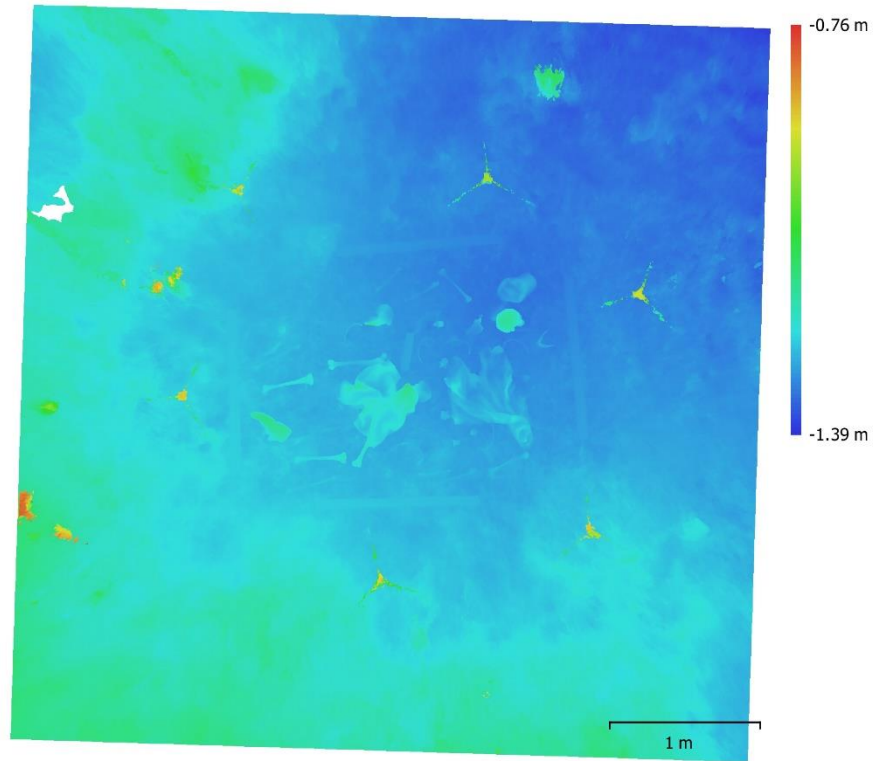


Fig. 3. Reconstructed digital elevation model.

Resolution: unknown
Point density: unknown

Processing Parameters

General

| | |
|-------------------|---------------------|
| Cameras | 120 |
| Aligned cameras | 120 |
| Markers | 12 |
| Scale bars | 4 |
| Coordinate system | WGS 84 (EPSG::4326) |
| Rotation angles | Yaw, Pitch, Roll |

Point Cloud

| | |
|--------------------------------|-------------------------|
| Points | 287,316 of 1,070,185 |
| RMS reprojection error | 0.124508 (0.348272 pix) |
| Max reprojection error | 0.857735 (2.92805 pix) |
| Mean key point size | 2.75156 pix |
| Point colors | 3 bands, uint8 |
| Key points | No |
| Average tie point multiplicity | 2.90502 |

Alignment parameters

| | |
|-------------------------------|----------------------|
| Accuracy | High |
| Generic preselection | No |
| Key point limit | 100,000 |
| Tie point limit | 50,000 |
| Adaptive camera model fitting | Yes |
| Matching time | 2 hours 21 minutes |
| Alignment time | 11 minutes 5 seconds |

Optimization parameters

| | |
|-------------------------------|---------------------------------|
| Parameters | f, b1, b2, cx, cy, k1-k4, p1-p4 |
| Adaptive camera model fitting | No |
| Optimization time | 30 seconds |
| Software version | 1.5.5.9097 |

Depth Maps

| | |
|-------|-----|
| Count | 120 |
|-------|-----|

Depth maps generation parameters

| | |
|------------------|--------------------|
| Quality | High |
| Filtering mode | Aggressive |
| Processing time | 6 hours 57 minutes |
| Software version | 1.5.5.9097 |

Dense Point Cloud

| | |
|--------------|----------------|
| Points | 42,899,928 |
| Point colors | 3 bands, uint8 |

Depth maps generation parameters

| | |
|-----------------|--------------------|
| Quality | High |
| Filtering mode | Aggressive |
| Processing time | 6 hours 57 minutes |

Dense cloud generation parameters

| | |
|------------------|-------------------|
| Processing time | 3 hours 1 minutes |
| Software version | 1.5.5.9097 |

Model

| | |
|---------------|-------------------------------|
| Faces | 8,579,893 |
| Vertices | 4,301,268 |
| Vertex colors | 3 bands, uint8 |
| Texture | 8,192 x 8,192, 4 bands, uint8 |

General**Depth maps generation parameters**

| | |
|-----------------|--------------------|
| Quality | High |
| Filtering mode | Aggressive |
| Processing time | 6 hours 57 minutes |

Reconstruction parameters

| | |
|-------------------------|--------------------|
| Surface type | Arbitrary |
| Source data | Dense cloud |
| Interpolation | Enabled |
| Strict volumetric masks | No |
| Processing time | 1 hours 32 minutes |

Texturing parameters

| | |
|------------------------|-----------------------|
| Mapping mode | Generic |
| Blending mode | Mosaic |
| Texture size | 8,192 |
| Enable hole filling | Yes |
| Enable ghosting filter | Yes |
| UV mapping time | 5 minutes 1 seconds |
| Blending time | 44 minutes 37 seconds |
| Software version | 1.5.5.9097 |

Orthomosaic

| | |
|-------------------|---------------------|
| Size | 12,557 x 12,527 |
| Coordinate system | WGS 84 (EPSG::4978) |
| Colors | 3 bands, uint8 |

Reconstruction parameters

| | |
|---------------------|-----------------------|
| Blending mode | Mosaic |
| Surface | Mesh |
| Enable hole filling | Yes |
| Processing time | 29 minutes 44 seconds |
| Software version | 1.5.5.9097 |

Software

| | |
|----------|------------------|
| Version | 1.5.5 build 9097 |
| Platform | Windows 64 |

Model 3A-1

Agisoft Metashape

Processing Report
09 June 2021



Survey Data

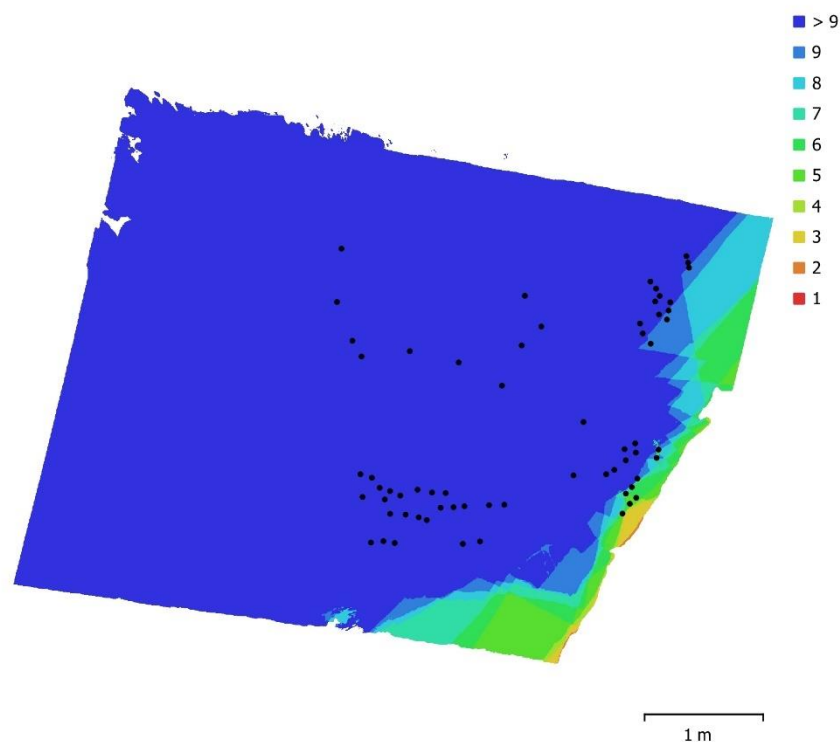


Fig. 1. Camera locations and image overlap.

| | | | |
|--------------------|---------------------|---------------------|-----------|
| Number of images: | 120 | Camera stations: | 64 |
| Flying altitude: | 2.06 m | Tie points: | 134,466 |
| Ground resolution: | 0.441 mm/pix | Projections: | 322,205 |
| Coverage area: | 21.4 m ² | Reprojection error: | 0.284 pix |

| Camera Model | Resolution | Focal Length | Pixel Size | Precalibrated |
|--------------------|-------------|--------------|----------------|---------------|
| NIKON D7200 (18mm) | 6000 x 4000 | 18 mm | 3.91 x 3.91 μm | No |

Table 1. Cameras.

Camera Calibration

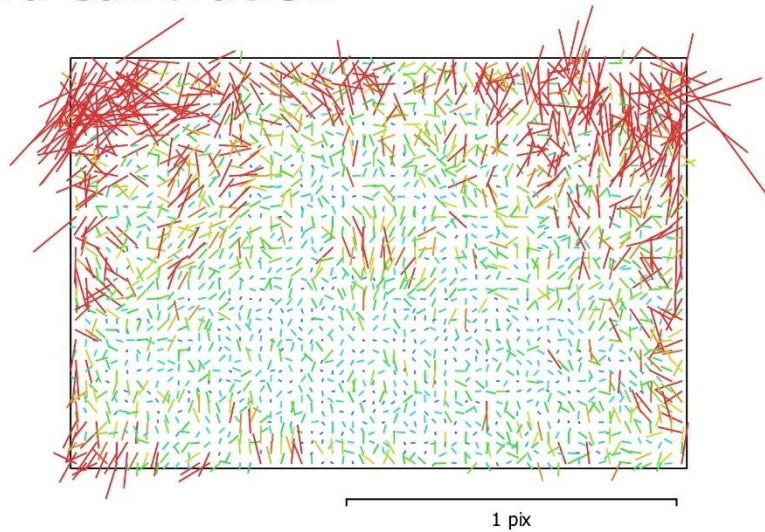


Fig. 2. Image residuals for NIKON D7200 (18mm).

NIKON D7200 (18mm)

120 images

| | | | |
|--------------|--------------------|--------------|---|
| Type | Resolution | Focal Length | Pixel Size |
| Frame | 6000 x 4000 | 18 mm | 3.91 x 3.91 μm |

| | Value | Error | F | Cx | Cy | B1 | B2 | K1 | K2 | K3 | K4 | P1 | P2 | P3 | P4 |
|-----------|---------------------|----------|------|------|-------|-------|-------|-------|-------|-------|-------|-------|-------|-------|-------|
| F | 4664.28 | 0.13 | 1.00 | 0.02 | -0.17 | -0.11 | 0.08 | -0.06 | 0.12 | -0.10 | 0.11 | -0.01 | 0.20 | 0.02 | -0.04 |
| Cx | -13.6452 | 0.1 | | 1.00 | -0.11 | -0.24 | 0.05 | 0.01 | -0.00 | 0.00 | -0.01 | 0.78 | -0.21 | 0.02 | 0.02 |
| Cy | 17.0517 | 0.17 | | | 1.00 | 0.07 | -0.22 | 0.00 | 0.03 | -0.03 | 0.02 | -0.03 | 0.38 | -0.07 | 0.15 |
| B1 | -0.193305 | 0.015 | | | | 1.00 | 0.08 | 0.04 | -0.03 | 0.02 | -0.02 | -0.20 | 0.11 | 0.03 | -0.03 |
| B2 | 0.026301 | 0.016 | | | | | 1.00 | -0.01 | -0.00 | 0.01 | -0.01 | -0.03 | 0.05 | -0.03 | -0.00 |
| K1 | -0.152348 | 8.3e-005 | | | | | | 1.00 | -0.96 | 0.91 | -0.86 | -0.04 | -0.08 | 0.13 | -0.11 |
| K2 | 0.103327 | 0.00055 | | | | | | | 1.00 | -0.98 | 0.95 | 0.06 | 0.09 | -0.15 | 0.13 |
| K3 | -0.000518065 | 0.0014 | | | | | | | | 1.00 | -0.99 | -0.05 | -0.07 | 0.12 | -0.11 |
| K4 | 0.00311241 | 0.0012 | | | | | | | | | 1.00 | 0.04 | 0.05 | -0.08 | 0.06 |
| P1 | 0.000199858 | 4.2e-006 | | | | | | | | | | 1.00 | 0.04 | -0.34 | 0.33 |
| P2 | 0.000710828 | 7.9e-006 | | | | | | | | | | | 1.00 | -0.66 | 0.59 |
| P3 | 0.367101 | 0.039 | | | | | | | | | | | | 1.00 | -0.96 |
| P4 | -0.240557 | 0.053 | | | | | | | | | | | | | 1.00 |

Table 2. Calibration coefficients and correlation matrix.

Scale Bars

| Label | Distance (m) | Error (m) |
|---------------------|--------------|-------------------|
| target 49_target 51 | 1.00007 | 9.12832e-005 |
| target 57_target 59 | 1.00005 | -5.37882e-005 |
| target 65_target 67 | 0.999585 | -0.000325251 |
| target 73_target 75 | 1.00064 | 0.00044454 |
| Total | | 0.00028046 |

Table 3. Control scale bars.

Digital Elevation Model

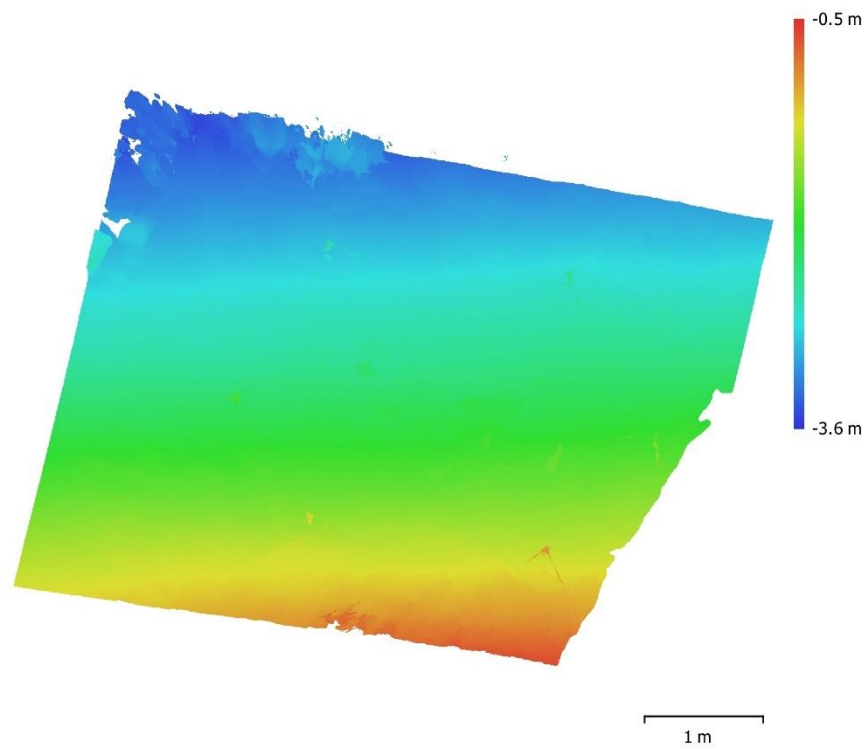


Fig. 3. Reconstructed digital elevation model.

Resolution: unknown
Point density: unknown

Processing Parameters

General

| | |
|-------------------|---------------------|
| Cameras | 120 |
| Aligned cameras | 64 |
| Markers | 12 |
| Scale bars | 4 |
| Coordinate system | WGS 84 (EPSG::4326) |
| Rotation angles | Yaw, Pitch, Roll |

Point Cloud

| | |
|--------------------------------|-------------------------|
| Points | 134,466 of 882,349 |
| RMS reprojection error | 0.100749 (0.283902 pix) |
| Max reprojection error | 0.299987 (2.00679 pix) |
| Mean key point size | 2.78138 pix |
| Point colors | 3 bands, uint8 |
| Key points | No |
| Average tie point multiplicity | 2.41102 |

Alignment parameters

| | |
|-------------------------------|-----------------------|
| Accuracy | High |
| Generic preselection | Yes |
| Key point limit | 100,000 |
| Tie point limit | 40,000 |
| Adaptive camera model fitting | No |
| Matching time | 17 minutes 51 seconds |
| Alignment time | 6 minutes 0 seconds |

Optimization parameters

| | |
|-------------------------------|---------------------------------|
| Parameters | f, b1, b2, cx, cy, k1-k4, p1-p4 |
| Adaptive camera model fitting | No |
| Optimization time | 10 seconds |
| Software version | 1.5.5.9097 |

Depth Maps

| | |
|-------|----|
| Count | 64 |
|-------|----|

Depth maps generation parameters

| | |
|------------------|--------------------|
| Quality | High |
| Filtering mode | Aggressive |
| Processing time | 2 hours 55 minutes |
| Software version | 1.5.5.9097 |

Dense Point Cloud

| | |
|--------------|----------------|
| Points | 31,405,248 |
| Point colors | 3 bands, uint8 |

Depth maps generation parameters

| | |
|-----------------|--------------------|
| Quality | High |
| Filtering mode | Aggressive |
| Processing time | 2 hours 55 minutes |

Dense cloud generation parameters

| | |
|------------------|----------------------|
| Processing time | 50 minutes 8 seconds |
| Software version | 1.5.5.9097 |

Model

| | |
|---------------|-------------------------------|
| Faces | 6,280,976 |
| Vertices | 3,149,876 |
| Vertex colors | 3 bands, uint8 |
| Texture | 8,192 x 8,192, 4 bands, uint8 |

General**Depth maps generation parameters**

| | |
|-----------------|--------------------|
| Quality | High |
| Filtering mode | Aggressive |
| Processing time | 2 hours 55 minutes |

Reconstruction parameters

| | |
|-------------------------|--------------------|
| Surface type | Arbitrary |
| Source data | Dense cloud |
| Interpolation | Enabled |
| Strict volumetric masks | No |
| Processing time | 1 hours 15 minutes |

Texturing parameters

| | |
|------------------------|-----------------------|
| Mapping mode | Generic |
| Blending mode | Mosaic |
| Texture size | 8,192 |
| Enable hole filling | Yes |
| Enable ghosting filter | Yes |
| UV mapping time | 6 minutes 35 seconds |
| Blending time | 23 minutes 35 seconds |
| Software version | 1.5.5.9097 |

Software

| | |
|----------|------------------|
| Version | 1.5.5 build 9097 |
| Platform | Windows 64 |

Model 3B-2

Agisoft Metashape

Processing Report
23 July 2021



Survey Data

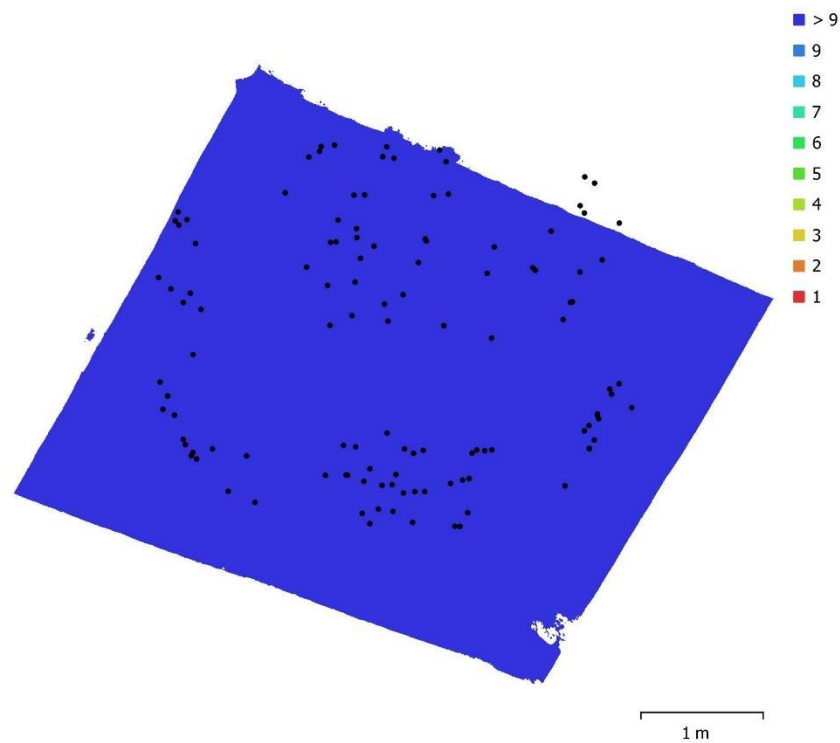


Fig. 1. Camera locations and image overlap.

| | | | |
|--------------------|---------------------|---------------------|-----------|
| Number of images: | 120 | Camera stations: | 118 |
| Flying altitude: | 1.91 m | Tie points: | 192,514 |
| Ground resolution: | 0.41 mm/pix | Projections: | 499,507 |
| Coverage area: | 17.5 m ² | Reprojection error: | 0.358 pix |

| Camera Model | Resolution | Focal Length | Pixel Size | Precalibrated |
|--------------------|-------------|--------------|----------------|---------------|
| NIKON D7200 (18mm) | 6000 x 4000 | 18 mm | 3.91 x 3.91 μm | No |

Table 1. Cameras.

Camera Calibration

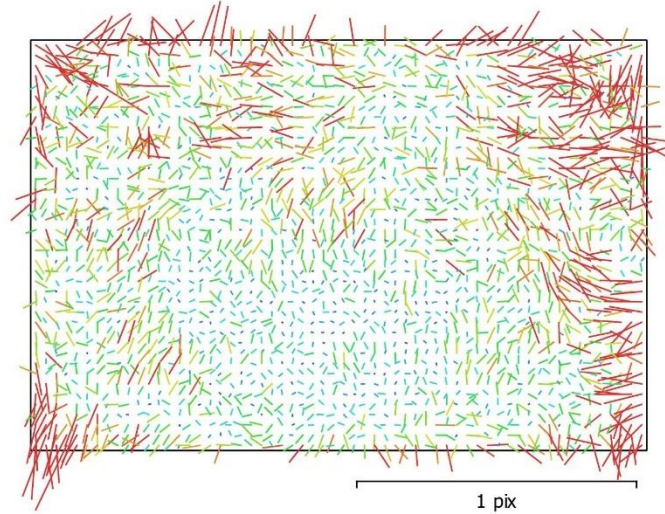


Fig. 2. Image residuals for NIKON D7200 (18mm).

NIKON D7200 (18mm)

120 images

| | | | |
|--------------|--------------------|--------------|---|
| Type | Resolution | Focal Length | Pixel Size |
| Frame | 6000 x 4000 | 18 mm | 3.91 x 3.91 μm |

| | Value | Error | F | Cx | Cy | B1 | B2 | K1 | K2 | K3 | K4 | P1 | P2 | P3 | P4 |
|-----------|--------------------|----------|------|------|-------|-------|-------|-------|-------|-------|-------|-------|-------|-------|-------|
| F | 4645.57 | 0.073 | 1.00 | 0.09 | 0.04 | -0.33 | 0.02 | -0.21 | 0.23 | -0.21 | 0.20 | 0.05 | 0.22 | 0.00 | -0.02 |
| Cx | 2.99993 | 0.12 | | 1.00 | -0.04 | 0.04 | 0.13 | -0.01 | 0.01 | -0.01 | 0.01 | 0.64 | 0.02 | -0.01 | -0.00 |
| Cy | 2.27099 | 0.12 | | | 1.00 | -0.43 | -0.06 | -0.03 | 0.02 | -0.01 | 0.01 | 0.03 | 0.48 | -0.05 | 0.06 |
| B1 | -0.444206 | 0.028 | | | | 1.00 | 0.05 | 0.02 | -0.03 | 0.02 | -0.02 | 0.05 | -0.03 | 0.00 | -0.03 |
| B2 | 1.27348 | 0.024 | | | | | 1.00 | 0.01 | -0.01 | 0.01 | -0.00 | -0.02 | 0.05 | 0.02 | 0.00 |
| K1 | -0.154628 | 8.1e-005 | | | | | | 1.00 | -0.97 | 0.92 | -0.87 | -0.01 | -0.00 | 0.01 | 0.00 |
| K2 | 0.106393 | 0.00052 | | | | | | | 1.00 | -0.99 | 0.96 | 0.03 | -0.01 | -0.02 | 0.01 |
| K3 | -0.00530045 | 0.0013 | | | | | | | | 1.00 | -0.99 | -0.03 | 0.00 | 0.03 | -0.02 |
| K4 | 0.00241619 | 0.0011 | | | | | | | | | 1.00 | 0.03 | -0.00 | -0.03 | 0.03 |
| P1 | 0.000328373 | 5.2e-006 | | | | | | | | | | 1.00 | 0.39 | -0.69 | 0.56 |
| P2 | 0.000178171 | 3.9e-006 | | | | | | | | | | | 1.00 | -0.49 | 0.38 |
| P3 | 0.349668 | 0.06 | | | | | | | | | | | | 1.00 | -0.95 |
| P4 | 0.981294 | 0.07 | | | | | | | | | | | | | 1.00 |

Table 2. Calibration coefficients and correlation matrix.

Scale Bars

| Label | Distance (m) | Error (m) |
|---------------------|--------------|--------------------|
| target 49_target 51 | 1.00009 | 0.000112015 |
| target 57_target 59 | 1.00002 | -8.18858e-005 |
| target 65_target 67 | 1.00002 | 0.000105518 |
| target 73_target 75 | 1.00005 | -0.000153267 |
| Total | | 0.000274893 |

Table 3. Control scale bars.

Digital Elevation Model

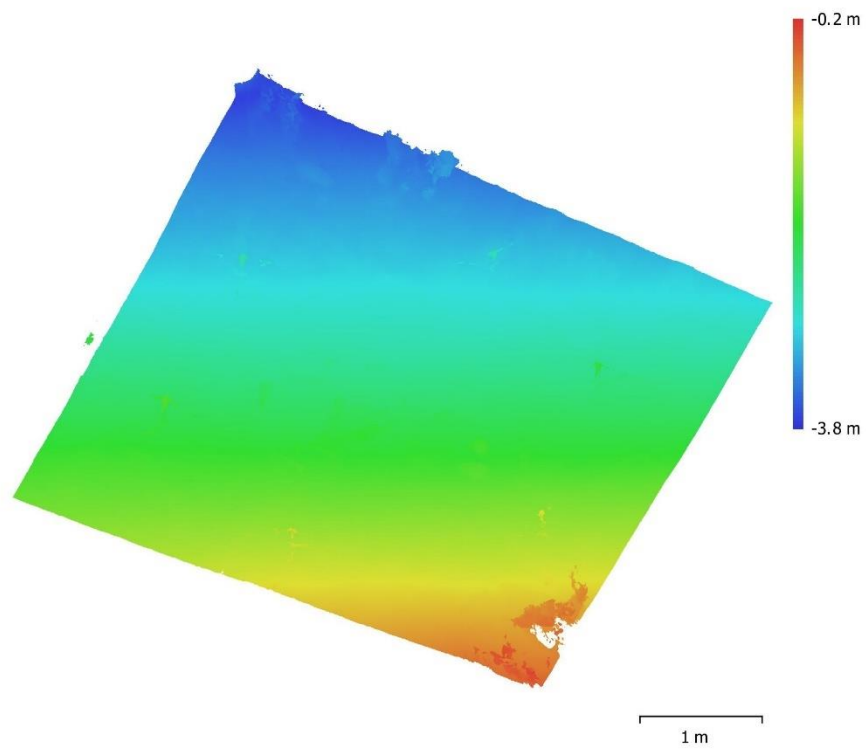


Fig. 3. Reconstructed digital elevation model.

Resolution: unknown
Point density: unknown

Processing Parameters

General

| | |
|-------------------|---------------------|
| Cameras | 120 |
| Aligned cameras | 118 |
| Markers | 12 |
| Scale bars | 4 |
| Coordinate system | WGS 84 (EPSG::4326) |
| Rotation angles | Yaw, Pitch, Roll |

Point Cloud

| | |
|--------------------------------|-------------------------|
| Points | 192,514 of 651,403 |
| RMS reprojection error | 0.125031 (0.427161 pix) |
| Max reprojection error | 0.597356 (6.27011 pix) |
| Mean key point size | 3.32421 pix |
| Point colors | 3 bands, uint8 |
| Key points | No |
| Average tie point multiplicity | 2.75636 |

Alignment parameters

| | |
|-------------------------------|----------------------|
| Accuracy | High |
| Generic preselection | No |
| Key point limit | 100,000 |
| Tie point limit | 50,000 |
| Adaptive camera model fitting | No |
| Matching time | 2 hours 10 minutes |
| Alignment time | 4 minutes 11 seconds |

Optimization parameters

| | |
|-------------------------------|---------------------------------|
| Parameters | f, b1, b2, cx, cy, k1-k4, p1-p4 |
| Adaptive camera model fitting | No |
| Optimization time | 13 seconds |
| Software version | 1.5.5.9097 |

Depth Maps

| | |
|-------|-----|
| Count | 107 |
|-------|-----|

Depth maps generation parameters

| | |
|------------------|-------------------|
| Quality | High |
| Filtering mode | Aggressive |
| Processing time | 7 hours 3 minutes |
| Software version | 1.5.5.9097 |

Dense Point Cloud

| | |
|--------------|----------------|
| Points | 31,891,169 |
| Point colors | 3 bands, uint8 |

Depth maps generation parameters

| | |
|-----------------|-------------------|
| Quality | High |
| Filtering mode | Aggressive |
| Processing time | 7 hours 3 minutes |

Dense cloud generation parameters

| | |
|------------------|--------------------|
| Processing time | 2 hours 17 minutes |
| Software version | 1.5.5.9097 |

Model

| | |
|---------------|-------------------------------|
| Faces | 6,378,142 |
| Vertices | 3,198,543 |
| Vertex colors | 3 bands, uint8 |
| Texture | 4,096 x 4,096, 4 bands, uint8 |

General**Depth maps generation parameters**

| | |
|-----------------|-------------------|
| Quality | High |
| Filtering mode | Aggressive |
| Processing time | 7 hours 3 minutes |

Reconstruction parameters

| | |
|-------------------------|----------------------|
| Surface type | Arbitrary |
| Source data | Dense cloud |
| Interpolation | Enabled |
| Strict volumetric masks | No |
| Processing time | 44 minutes 9 seconds |

Texturing parameters

| | |
|------------------------|-----------------------|
| Mapping mode | Generic |
| Blending mode | Mosaic |
| Texture size | 8,192 |
| Enable hole filling | Yes |
| Enable ghosting filter | Yes |
| UV mapping time | 3 minutes 26 seconds |
| Blending time | 18 minutes 17 seconds |
| Software version | 1.5.5.9097 |

Orthomosaic

| | |
|-------------------|---------------------|
| Size | 14,506 x 14,122 |
| Coordinate system | WGS 84 (EPSG::4978) |
| Colors | 3 bands, uint8 |

Reconstruction parameters

| | |
|---------------------|-------------------|
| Blending mode | Mosaic |
| Surface | Mesh |
| Enable hole filling | Yes |
| Processing time | 5 hours 0 minutes |
| Software version | 1.5.5.9097 |

Software

| | |
|----------|------------------|
| Version | 1.5.5 build 9097 |
| Platform | Windows 64 |

Model 3C-2

Agisoft Metashape

**Processing Report
09 June 2021**



Survey Data

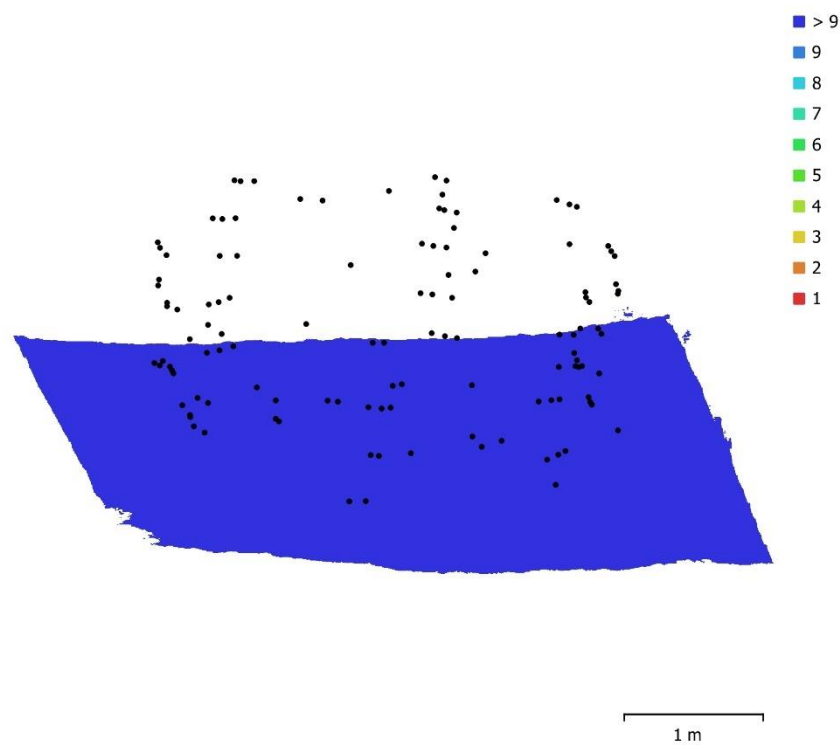


Fig. 1. Camera locations and image overlap.

| | | | |
|--------------------|---------------------|---------------------|-----------|
| Number of images: | 120 | Camera stations: | 120 |
| Flying altitude: | 2.01 m | Tie points: | 260,339 |
| Ground resolution: | 0.43 mm/pix | Projections: | 637,673 |
| Coverage area: | 7.63 m ² | Reprojection error: | 0.303 pix |

| Camera Model | Resolution | Focal Length | Pixel Size | Precalibrated |
|--------------------|-------------|--------------|---------------------|---------------|
| NIKON D7200 (18mm) | 6000 x 4000 | 18 mm | 3.91 x 3.91 μ m | No |

Table 1. Cameras.

Camera Calibration

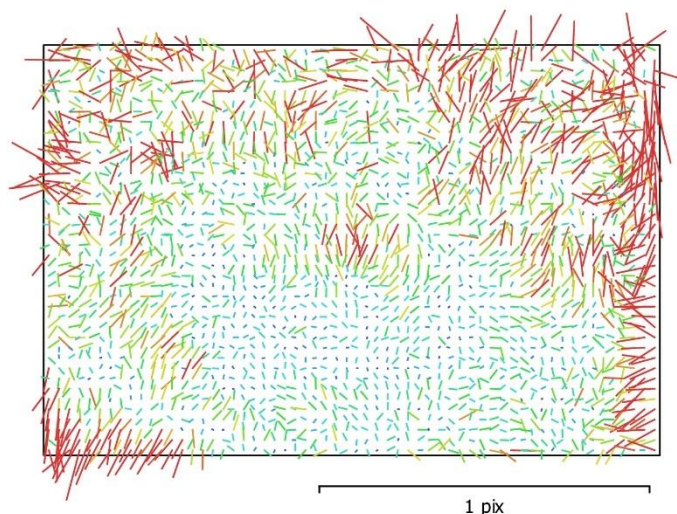


Fig. 2. Image residuals for NIKON D7200 (18mm).

NIKON D7200 (18mm)

120 images

| | | | |
|--------------|--------------------|--------------|---|
| Type | Resolution | Focal Length | Pixel Size |
| Frame | 6000 x 4000 | 18 mm | 3.91 x 3.91 μm |

| | Value | Error | F | Cx | Cy | B1 | B2 | K1 | K2 | K3 | K4 | P1 | P2 | P3 | P4 |
|-----------|--------------------|----------|------|------|------|-------|-------|-------|-------|-------|-------|-------|-------|-------|-------|
| F | 4676.01 | 0.073 | 1.00 | 0.00 | 0.00 | -0.22 | 0.01 | -0.11 | 0.16 | -0.14 | 0.14 | -0.02 | 0.25 | 0.02 | -0.03 |
| Cx | -4.92795 | 0.083 | | 1.00 | 0.01 | -0.17 | 0.15 | 0.03 | -0.01 | -0.00 | 0.01 | 0.80 | -0.22 | 0.10 | 0.02 |
| Cy | 7.96815 | 0.11 | | | 1.00 | -0.19 | -0.20 | -0.01 | 0.02 | -0.01 | 0.01 | 0.04 | 0.54 | 0.01 | 0.06 |
| B1 | -0.0627052 | 0.021 | | | | 1.00 | 0.09 | 0.01 | -0.01 | 0.01 | -0.01 | -0.13 | 0.14 | -0.03 | -0.02 |
| B2 | -0.897998 | 0.019 | | | | | 1.00 | -0.00 | 0.01 | -0.01 | 0.00 | -0.02 | -0.06 | -0.00 | 0.00 |
| K1 | -0.151054 | 5.8e-005 | | | | | | 1.00 | -0.97 | 0.92 | -0.87 | -0.00 | -0.07 | 0.06 | -0.03 |
| K2 | 0.102593 | 0.00038 | | | | | | | 1.00 | -0.99 | 0.96 | 0.03 | 0.06 | -0.08 | 0.05 |
| K3 | 0.00508407 | 0.00096 | | | | | | | | 1.00 | -0.99 | -0.04 | -0.05 | 0.06 | -0.04 |
| K4 | -0.0033921 | 0.00081 | | | | | | | | | 1.00 | 0.03 | 0.04 | -0.03 | 0.01 |
| P1 | 0.000286856 | 3.6e-006 | | | | | | | | | | 1.00 | 0.02 | -0.35 | 0.39 |
| P2 | 0.000503922 | 5.3e-006 | | | | | | | | | | | 1.00 | -0.47 | 0.40 |
| P3 | -0.252723 | 0.028 | | | | | | | | | | | | 1.00 | -0.96 |
| P4 | 0.571659 | 0.04 | | | | | | | | | | | | | 1.00 |

Table 2. Calibration coefficients and correlation matrix.

Scale Bars

| Label | Distance (m) | Error (m) |
|---------------------|--------------|--------------------|
| target 49_target 51 | 1.00008 | 0.000100644 |
| target 57_target 59 | 1.00005 | -5.21981e-005 |
| target 65_target 67 | 0.999714 | -0.000195644 |
| target 73_target 75 | 1.00035 | 0.000151156 |
| Total | | 0.000135995 |

Table 3. Control scale bars.

Digital Elevation Model

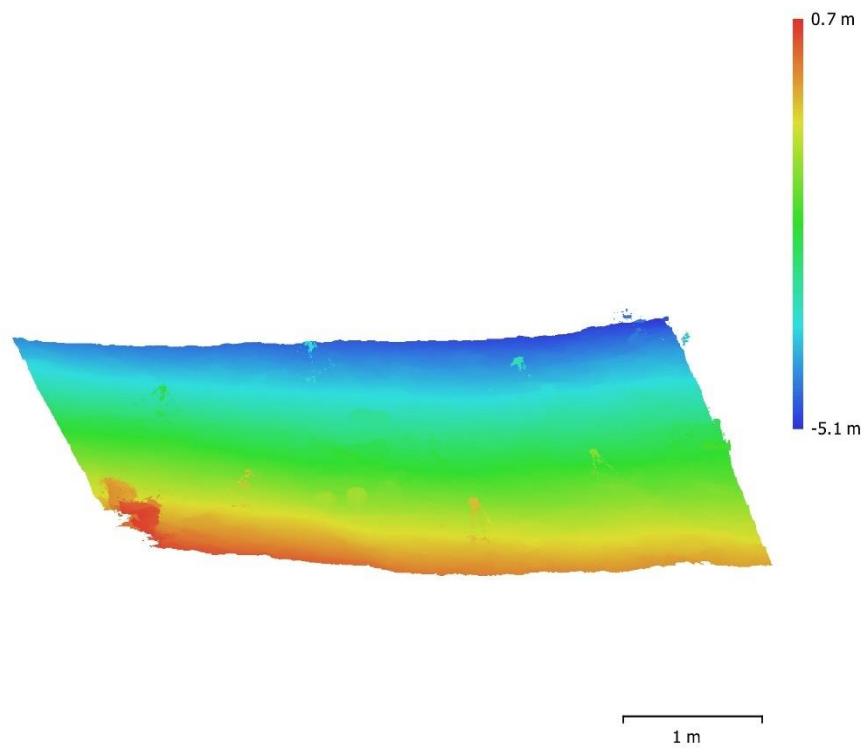


Fig. 3. Reconstructed digital elevation model.

Resolution: unknown
Point density: unknown

Processing Parameters

General

| | |
|-------------------|---------------------|
| Cameras | 120 |
| Aligned cameras | 120 |
| Markers | 12 |
| Scale bars | 4 |
| Coordinate system | WGS 84 (EPSG::4326) |
| Rotation angles | Yaw, Pitch, Roll |

Point Cloud

| | |
|--------------------------------|------------------------|
| Points | 260,339 of 866,006 |
| RMS reprojection error | 0.108092 (0.30345 pix) |
| Max reprojection error | 0.987668 (2.99406 pix) |
| Mean key point size | 2.76405 pix |
| Point colors | 3 bands, uint8 |
| Key points | No |
| Average tie point multiplicity | 2.46663 |

Alignment parameters

| | |
|-------------------------------|-----------------------|
| Accuracy | High |
| Generic preselection | No |
| Key point limit | 100,000 |
| Tie point limit | 50,000 |
| Adaptive camera model fitting | No |
| Matching time | 3 hours 34 minutes |
| Alignment time | 15 minutes 21 seconds |

Optimization parameters

| | |
|-------------------------------|---------------------------------|
| Parameters | f, b1, b2, cx, cy, k1-k4, p1-p4 |
| Adaptive camera model fitting | No |
| Optimization time | 28 seconds |
| Software version | 1.5.5.9097 |

Depth Maps

| | |
|-------|-----|
| Count | 120 |
|-------|-----|

Depth maps generation parameters

| | |
|------------------|--------------------|
| Quality | High |
| Filtering mode | Aggressive |
| Processing time | 7 hours 46 minutes |
| Software version | 1.5.5.9097 |

Dense Point Cloud

| | |
|--------------|----------------|
| Points | 35,977,509 |
| Point colors | 3 bands, uint8 |

Depth maps generation parameters

| | |
|-----------------|--------------------|
| Quality | High |
| Filtering mode | Aggressive |
| Processing time | 7 hours 46 minutes |

Dense cloud generation parameters

| | |
|------------------|--------------------|
| Processing time | 3 hours 12 minutes |
| Software version | 1.5.5.9097 |

Model

| | |
|---------------|-------------------------------|
| Faces | 7,195,416 |
| Vertices | 3,606,600 |
| Vertex colors | 3 bands, uint8 |
| Texture | 8,192 x 8,192, 4 bands, uint8 |

General**Depth maps generation parameters**

| | |
|-----------------|--------------------|
| Quality | High |
| Filtering mode | Aggressive |
| Processing time | 7 hours 46 minutes |

Reconstruction parameters

| | |
|-------------------------|-----------------------|
| Surface type | Arbitrary |
| Source data | Dense cloud |
| Interpolation | Enabled |
| Strict volumetric masks | No |
| Processing time | 46 minutes 53 seconds |

Texturing parameters

| | |
|------------------------|-----------------------|
| Mapping mode | Generic |
| Blending mode | Mosaic |
| Texture size | 8,192 |
| Enable hole filling | Yes |
| Enable ghosting filter | Yes |
| UV mapping time | 3 minutes 44 seconds |
| Blending time | 22 minutes 48 seconds |
| Software version | 1.5.5.9097 |

Orthomosaic

| | |
|-------------------|---------------------|
| Size | 12,830 x 11,733 |
| Coordinate system | WGS 84 (EPSG::4978) |
| Colors | 3 bands, uint8 |

Reconstruction parameters

| | |
|---------------------|-----------------------|
| Blending mode | Mosaic |
| Surface | Mesh |
| Enable hole filling | Yes |
| Processing time | 19 minutes 39 seconds |
| Software version | 1.5.5.9097 |

Software

| | |
|----------|------------------|
| Version | 1.5.5 build 9097 |
| Platform | Windows 64 |

4.30 Lights and Sheet

Processing Report
13 June 2021



Survey Data

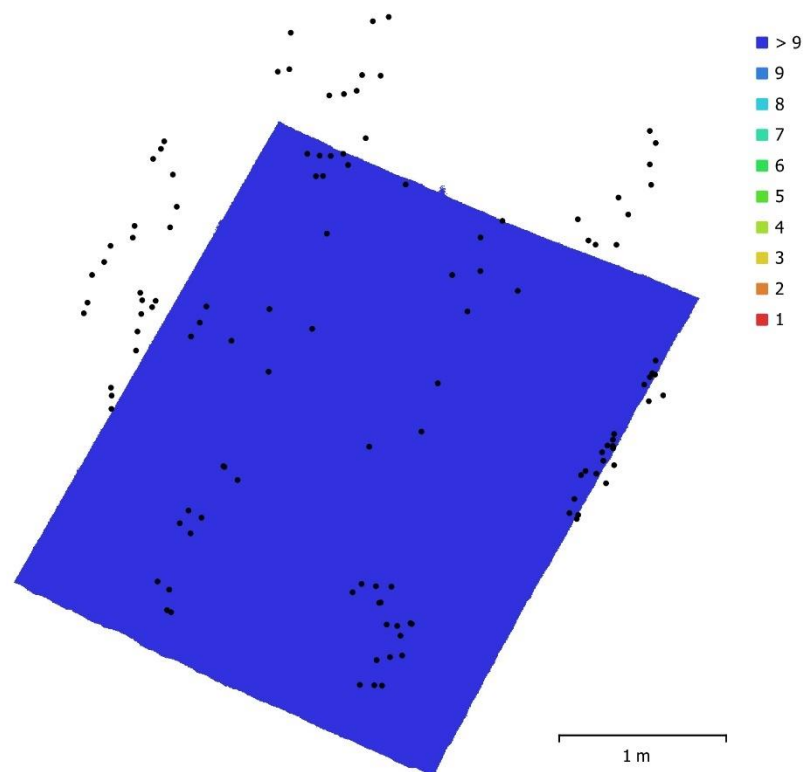


Fig. 1. Camera locations and image overlap.

| | | | |
|--------------------|---------------------|---------------------|-----------|
| Number of images: | 120 | Camera stations: | 120 |
| Flying altitude: | 1.84 m | Tie points: | 64,636 |
| Ground resolution: | 0.393 mm/pix | Projections: | 193,944 |
| Coverage area: | 8.83 m ² | Reprojection error: | 0.345 pix |

| Camera Model | Resolution | Focal Length | Pixel Size | Precalibrated |
|--------------------|-------------|--------------|----------------|---------------|
| NIKON D7200 (18mm) | 6000 x 4000 | 18 mm | 3.91 x 3.91 μm | No |

Table 1. Cameras.

Camera Calibration

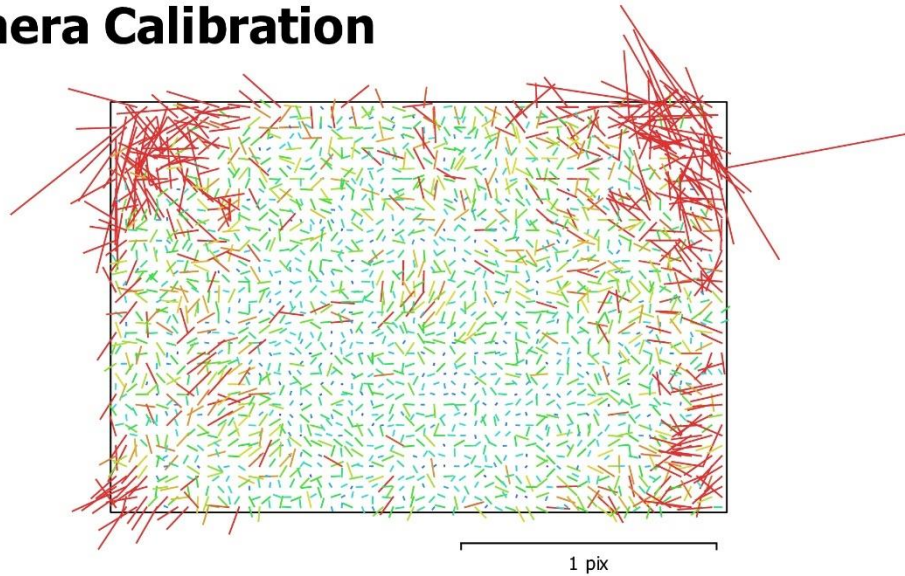


Fig. 2. Image residuals for NIKON D7200 (18mm).

NIKON D7200 (18mm)

120 images

| | | | |
|--------------|--------------------|--------------|--------------------------------------|
| Type | Resolution | Focal Length | Pixel Size |
| Frame | 6000 x 4000 | 18 mm | 3.91 x 3.91 μm |

| | Value | Error | F | Cx | Cy | B1 | B2 | K1 | K2 | K3 | K4 | P1 | P2 | P3 | P4 |
|-----------|--------------------|----------|------|------|-------|-------|-------|-------|-------|-------|-------|-------|-------|-------|-------|
| F | 4669.9 | 0.11 | 1.00 | 0.05 | -0.37 | 0.00 | 0.04 | -0.12 | 0.16 | -0.14 | 0.14 | 0.01 | 0.15 | -0.01 | -0.03 |
| Cx | -3.24281 | 0.11 | | 1.00 | -0.05 | -0.04 | 0.21 | 0.02 | 0.00 | -0.01 | 0.01 | 0.76 | -0.09 | -0.00 | 0.08 |
| Cy | 6.76294 | 0.14 | | | 1.00 | -0.45 | -0.20 | 0.00 | 0.02 | -0.01 | 0.01 | 0.05 | -0.05 | -0.06 | 0.13 |
| B1 | -0.252125 | 0.022 | | | | 1.00 | 0.06 | 0.01 | -0.03 | 0.03 | -0.03 | -0.04 | 0.17 | 0.01 | -0.04 |
| B2 | -1.48193 | 0.018 | | | | | 1.00 | -0.02 | 0.01 | -0.01 | 0.01 | 0.00 | 0.04 | -0.01 | -0.00 |
| K1 | -0.152872 | 9.6e-005 | | | | | | 1.00 | -0.97 | 0.92 | -0.86 | -0.00 | -0.11 | 0.06 | -0.03 |
| K2 | 0.105723 | 0.00063 | | | | | | | 1.00 | -0.99 | 0.95 | 0.02 | 0.09 | -0.07 | 0.04 |
| K3 | -0.00105868 | 0.0016 | | | | | | | | 1.00 | -0.99 | -0.02 | -0.06 | 0.04 | -0.01 |
| K4 | 0.00105916 | 0.0014 | | | | | | | | | 1.00 | 0.01 | 0.03 | 0.02 | -0.05 |
| P1 | 0.000212733 | 4.5e-006 | | | | | | | | | | 1.00 | 0.09 | -0.27 | 0.31 |
| P2 | 0.000912302 | 7.6e-006 | | | | | | | | | | | 1.00 | -0.72 | 0.60 |
| P3 | -0.238057 | 0.033 | | | | | | | | | | | | 1.00 | -0.96 |
| P4 | 0.339456 | 0.05 | | | | | | | | | | | | | 1.00 |

Table 2. Calibration coefficients and correlation matrix.

Scale Bars

| Label | Distance (m) | Error (m) |
|---------------------|--------------|--------------------|
| target 49_target 51 | 0.999447 | -0.000352584 |
| target 57_target 59 | 0.999877 | -0.000223128 |
| target 65_target 67 | 1.00025 | 0.000341308 |
| target 73_target 75 | 1.00043 | 0.000209069 |
| Total | | 0.000289094 |

Table 3. Control scale bars.

Digital Elevation Model

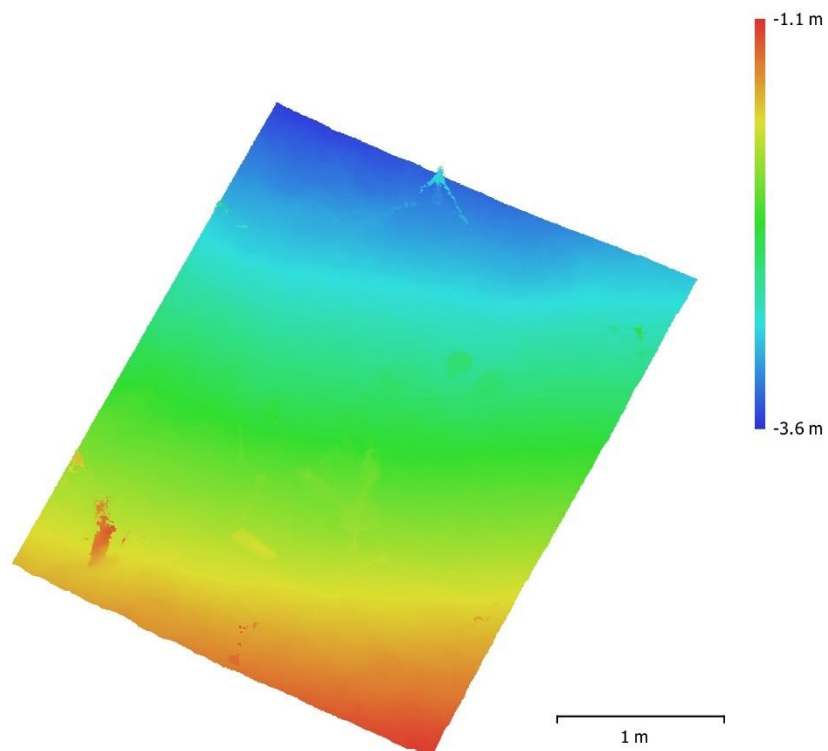


Fig. 3. Reconstructed digital elevation model.

Resolution: unknown
Point density: unknown

Processing Parameters

General

| | |
|-------------------|-----------------------|
| Cameras | 120 |
| Aligned cameras | 120 |
| Markers | 12 |
| Scale bars | 4 |
| Coordinate system | Local Coordinates (m) |
| Rotation angles | Yaw, Pitch, Roll |

Point Cloud

| | |
|--------------------------------|------------------------|
| Points | 64,636 of 930,701 |
| RMS reprojection error | 0.11752 (0.345247 pix) |
| Max reprojection error | 0.376068 (2.34113 pix) |
| Mean key point size | 2.88496 pix |
| Point colors | 3 bands, uint8 |
| Key points | No |
| Average tie point multiplicity | 2.57995 |

Alignment parameters

| | |
|-------------------------------|-----------------------|
| Accuracy | High |
| Generic preselection | Yes |
| Key point limit | 100,000 |
| Tie point limit | 40,000 |
| Adaptive camera model fitting | No |
| Matching time | 24 minutes 26 seconds |
| Alignment time | 8 minutes 45 seconds |

Optimization parameters

| | |
|-------------------------------|---------------------------------|
| Parameters | f, b1, b2, cx, cy, k1-k4, p1-p4 |
| Adaptive camera model fitting | No |
| Optimization time | 7 seconds |
| Software version | 1.5.5.9097 |

Depth Maps

| | |
|-------|-----|
| Count | 112 |
|-------|-----|

Depth maps generation parameters

| | |
|------------------|-------------------|
| Quality | High |
| Filtering mode | Aggressive |
| Processing time | 9 hours 7 minutes |
| Software version | 1.5.5.9097 |

Dense Point Cloud

| | |
|--------------|----------------|
| Points | 32,096,970 |
| Point colors | 3 bands, uint8 |

Depth maps generation parameters

| | |
|-----------------|-------------------|
| Quality | High |
| Filtering mode | Aggressive |
| Processing time | 9 hours 7 minutes |

Dense cloud generation parameters

| | |
|------------------|--------------------|
| Processing time | 2 hours 53 minutes |
| Software version | 1.5.5.9097 |

Model

| | |
|---------------|-------------------------------|
| Faces | 2,994,321 |
| Vertices | 1,501,925 |
| Vertex colors | 3 bands, uint8 |
| Texture | 8,192 x 8,192, 4 bands, uint8 |

General**Depth maps generation parameters**

| | |
|-----------------|-------------------|
| Quality | High |
| Filtering mode | Aggressive |
| Processing time | 9 hours 7 minutes |

Reconstruction parameters

| | |
|-------------------------|-----------------------|
| Surface type | Arbitrary |
| Source data | Dense cloud |
| Interpolation | Enabled |
| Strict volumetric masks | No |
| Processing time | 42 minutes 49 seconds |

Texturing parameters

| | |
|------------------------|----------------------|
| Mapping mode | Generic |
| Blending mode | Mosaic |
| Texture size | 8,192 |
| Enable hole filling | Yes |
| Enable ghosting filter | No |
| UV mapping time | 3 minutes 29 seconds |
| Blending time | 13 minutes 5 seconds |
| Software version | 1.5.5.9097 |

Orthomosaic

| | |
|-------------------|-----------------------|
| Size | 8,768 x 6,409 |
| Coordinate system | Local Coordinates (m) |
| Colors | 3 bands, uint8 |

Reconstruction parameters

| | |
|---------------------|----------------------|
| Blending mode | Mosaic |
| Surface | Mesh |
| Enable hole filling | Yes |
| Processing time | 7 minutes 44 seconds |
| Software version | 1.5.5.9097 |

Software

| | |
|----------|------------------|
| Version | 1.5.5 build 9097 |
| Platform | Windows 64 |

Model 1A-1

Agisoft Metashape

Processing Report
10 June 2021



Survey Data

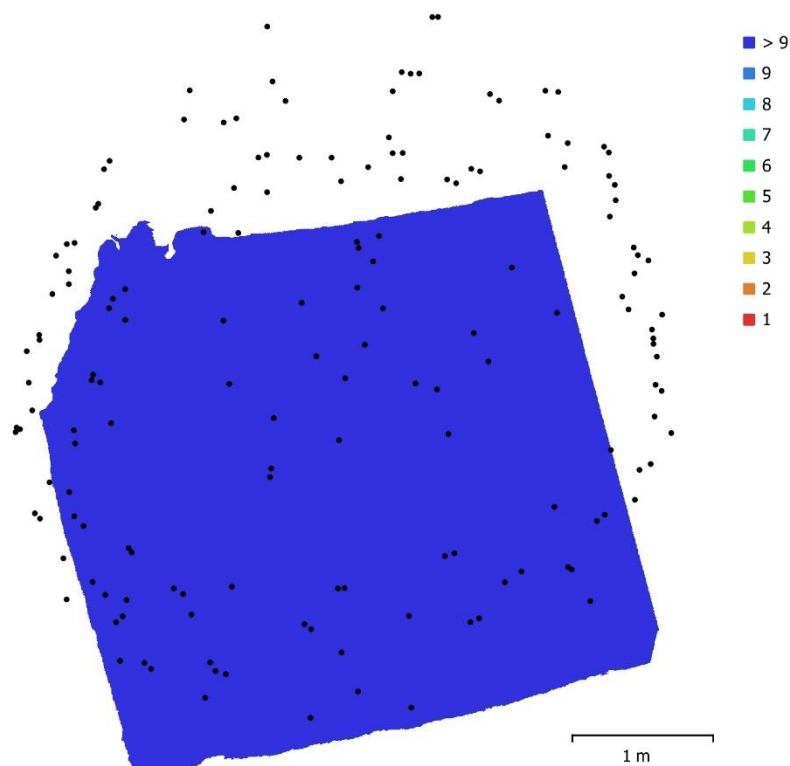


Fig. 1. Camera locations and image overlap.

| | | | |
|--------------------|---------------------|---------------------|-----------|
| Number of images: | 162 | Camera stations: | 162 |
| Flying altitude: | 2 m | Tie points: | 13,227 |
| Ground resolution: | 0.428 mm/pix | Projections: | 34,069 |
| Coverage area: | 13.7 m ² | Reprojection error: | 0.292 pix |

| Camera Model | Resolution | Focal Length | Pixel Size | Precalibrated |
|--------------------|-------------|--------------|----------------|---------------|
| NIKON D7200 (18mm) | 6000 x 4000 | 18 mm | 3.91 x 3.91 μm | No |

Table 1. Cameras.

Camera Calibration

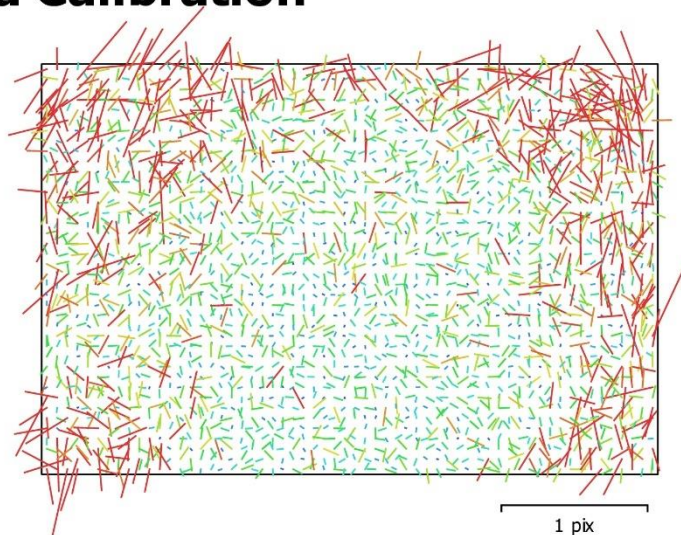


Fig. 2. Image residuals for NIKON D7200 (18mm).

NIKON D7200 (18mm)

162 images

| Type | Resolution | Focal Length | Pixel Size |
|-------|-------------|--------------|----------------|
| Frame | 6000 x 4000 | 18 mm | 3.91 x 3.91 μm |
| F: | 4661.05 | | |
| Cx: | 6.40754 | B1: | -1.48176 |
| Cy: | 15.4807 | B2: | 0.328149 |
| K1: | -0.155108 | P1: | 0.000298039 |
| K2: | 0.117451 | P2: | 0.000644699 |
| K3: | -0.0336486 | P3: | 0.15979 |
| K4: | 0.0279118 | P4: | 0.283438 |

Scale Bars

| Label | Distance (m) | Error (m) |
|---------------------|--------------|--------------------|
| target 73_target 75 | 1.00021 | -9.5612e-006 |
| target 52_target 54 | 0.499627 | -0.000292706 |
| target 57_target 59 | 0.999853 | -0.000247452 |
| target 68_target 70 | 0.499204 | 7.39925e-005 |
| Total | | 0.000195241 |

Table 2. Control scale bars.

Digital Elevation Model

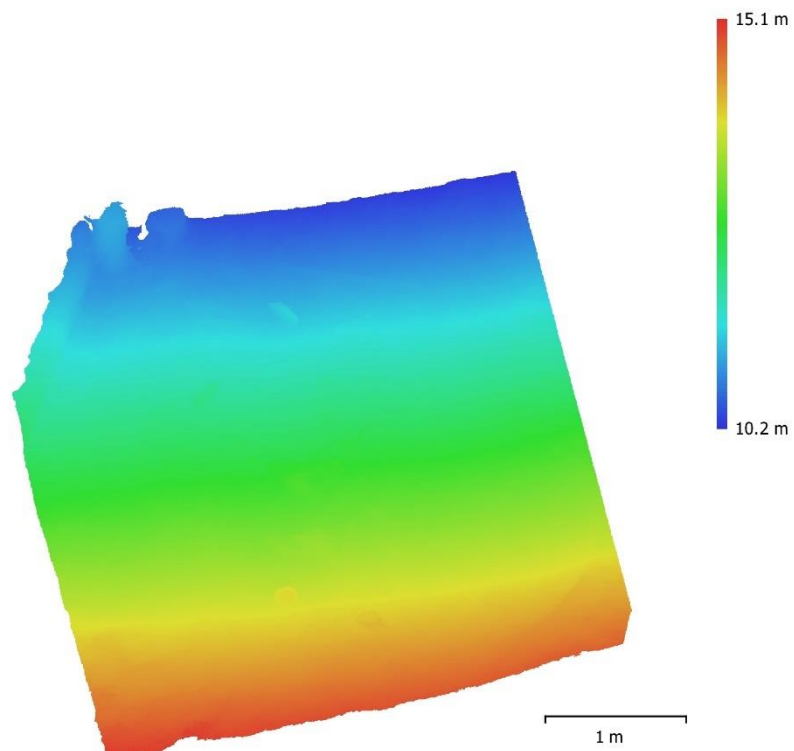


Fig. 3. Reconstructed digital elevation model.

| | |
|----------------|---------|
| Resolution: | unknown |
| Point density: | unknown |

Processing Parameters

General

| | |
|-------------------|-----------------------|
| Cameras | 162 |
| Aligned cameras | 162 |
| Markers | 24 |
| Scale bars | 4 |
| Coordinate system | Local Coordinates (m) |
| Rotation angles | Yaw, Pitch, Roll |

Point Cloud

| | |
|--------------------------------|-------------------------|
| Points | 13,227 of 966,198 |
| RMS reprojection error | 0.130668 (0.291802 pix) |
| Max reprojection error | 0.46922 (1.12038 pix) |
| Mean key point size | 2.21231 pix |
| Point colors | 3 bands, uint8 |
| Key points | No |
| Average tie point multiplicity | 2.47751 |

Alignment parameters

| | |
|-------------------------------|-----------------------|
| Accuracy | High |
| Generic preselection | No |
| Key point limit | 100,000 |
| Tie point limit | 40,000 |
| Adaptive camera model fitting | Yes |
| Matching time | 4 hours 9 minutes |
| Alignment time | 11 minutes 15 seconds |

Optimization parameters

| | |
|-------------------------------|---------------------------------|
| Parameters | f, b1, b2, cx, cy, k1-k4, p1-p4 |
| Adaptive camera model fitting | No |
| Optimization time | 4 seconds |
| Software version | 1.5.5.9097 |

Depth Maps

| | |
|-------|-----|
| Count | 133 |
|-------|-----|

Depth maps generation parameters

| | |
|------------------|--------------------|
| Quality | High |
| Filtering mode | Aggressive |
| Processing time | 2 hours 16 minutes |
| Software version | 1.5.5.9097 |

Dense Point Cloud

| | |
|--------------|----------------|
| Points | 34,610,228 |
| Point colors | 3 bands, uint8 |

Depth maps generation parameters

| | |
|-----------------|--------------------|
| Quality | High |
| Filtering mode | Aggressive |
| Processing time | 2 hours 16 minutes |

Dense cloud generation parameters

| | |
|------------------|--------------------|
| Processing time | 3 hours 20 minutes |
| Software version | 1.5.5.9097 |

Model

| | |
|---------------|-------------------------------|
| Faces | 3,947,261 |
| Vertices | 1,978,038 |
| Vertex colors | 3 bands, uint8 |
| Texture | 8,192 x 8,192, 4 bands, uint8 |

General**Depth maps generation parameters**

| | |
|-----------------|--------------------|
| Quality | High |
| Filtering mode | Aggressive |
| Processing time | 2 hours 16 minutes |

Reconstruction parameters

| | |
|-------------------------|-----------------------|
| Surface type | Arbitrary |
| Source data | Dense cloud |
| Interpolation | Enabled |
| Strict volumetric masks | No |
| Processing time | 45 minutes 47 seconds |

Texturing parameters

| | |
|------------------------|----------------------|
| Mapping mode | Generic |
| Blending mode | Mosaic |
| Texture size | 8,192 |
| Enable hole filling | Yes |
| Enable ghosting filter | No |
| UV mapping time | 4 minutes 21 seconds |
| Blending time | 16 minutes 1 seconds |
| Software version | 1.5.5.9097 |

Orthomosaic

| | |
|-------------------|-----------------------|
| Size | 11,600 x 7,750 |
| Coordinate system | Local Coordinates (m) |
| Colors | 3 bands, uint8 |

Reconstruction parameters

| | |
|---------------------|-----------------------|
| Blending mode | Mosaic |
| Surface | Mesh |
| Enable hole filling | Yes |
| Processing time | 12 minutes 20 seconds |
| Software version | 1.5.5.9097 |

Software

| | |
|----------|------------------|
| Version | 1.5.5 build 9097 |
| Platform | Windows 64 |

Model 2B-1

Agisoft Metashape

**Processing Report
10 June 2021**



Survey Data

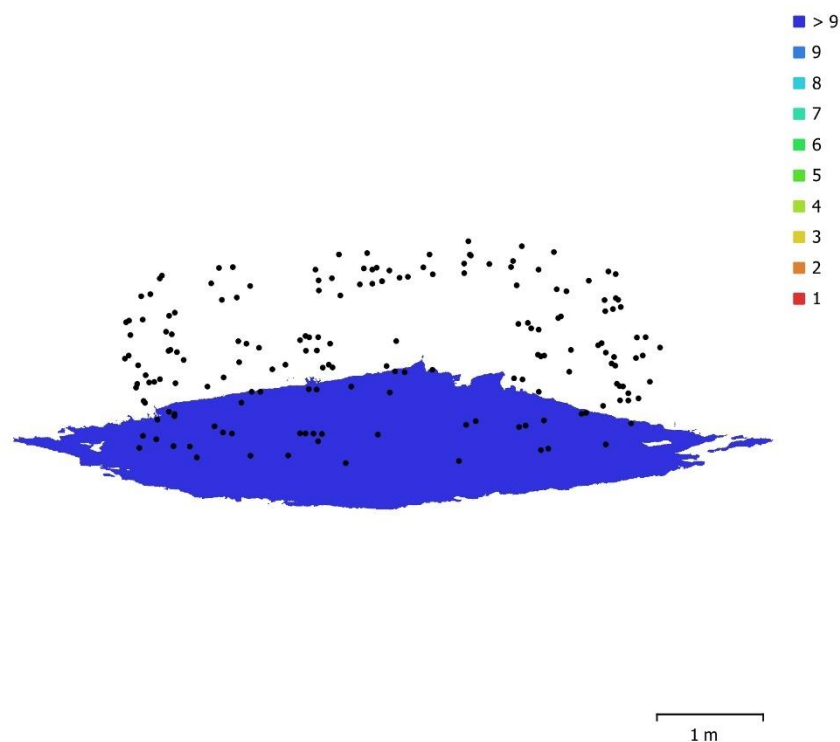


Fig. 1. Camera locations and image overlap.

| | | | |
|--------------------|---------------------|---------------------|-----------|
| Number of images: | 175 | Camera stations: | 175 |
| Flying altitude: | 2.12 m | Tie points: | 21,411 |
| Ground resolution: | 0.456 mm/pix | Projections: | 62,456 |
| Coverage area: | 5.32 m ² | Reprojection error: | 0.334 pix |

| Camera Model | Resolution | Focal Length | Pixel Size | Precalibrated |
|--------------------|-------------|--------------|----------------|---------------|
| NIKON D7200 (18mm) | 6000 x 4000 | 18 mm | 3.91 x 3.91 μm | No |

Table 1. Cameras.

Scale Bars

| Label | Distance (m) | Error (m) |
|---------------------|--------------|-------------------|
| target 52_target 54 | 0.499753 | -0.000167155 |
| target 57_target 59 | 0.999527 | -0.000573118 |
| target 68_target 70 | 0.499294 | 0.000163976 |
| target 73_target 75 | 1.0008 | 0.000576502 |
| Total | | 0.00042298 |

Table 2. Control scale bars.

Digital Elevation Model

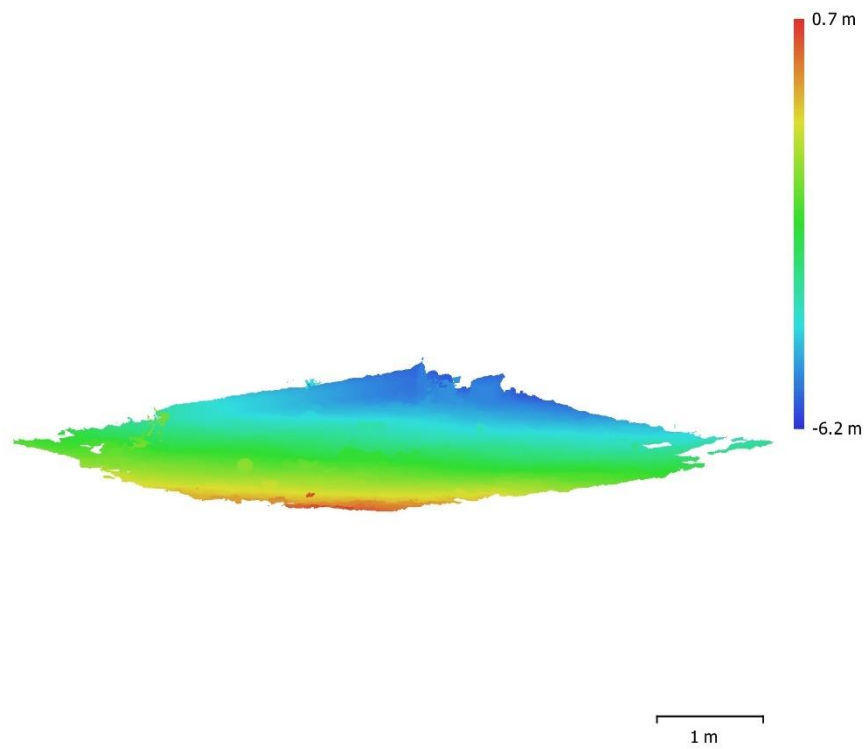


Fig. 3. Reconstructed digital elevation model.

Resolution: unknown
Point density: unknown

Processing Parameters

General

| | |
|-------------------|-----------------------|
| Cameras | 175 |
| Aligned cameras | 175 |
| Markers | 24 |
| Scale bars | 4 |
| Coordinate system | Local Coordinates (m) |
| Rotation angles | Yaw, Pitch, Roll |

Point Cloud

| | |
|--------------------------------|-------------------------|
| Points | 21,411 of 1,011,355 |
| RMS reprojection error | 0.135435 (0.333939 pix) |
| Max reprojection error | 0.332047 (1.18478 pix) |
| Mean key point size | 2.43657 pix |
| Point colors | 3 bands, uint8 |
| Key points | No |
| Average tie point multiplicity | 2.69469 |

Alignment parameters

| | |
|-------------------------------|----------------------|
| Accuracy | High |
| Generic preselection | No |
| Key point limit | 100,000 |
| Tie point limit | 40,000 |
| Adaptive camera model fitting | Yes |
| Matching time | 4 hours 43 minutes |
| Alignment time | 8 minutes 32 seconds |

Optimization parameters

| | |
|-------------------------------|---------------------------------|
| Parameters | f, b1, b2, cx, cy, k1-k4, p1-p4 |
| Adaptive camera model fitting | No |
| Optimization time | 6 seconds |
| Software version | 1.5.5.9097 |

Depth Maps

| | |
|-------|-----|
| Count | 147 |
|-------|-----|

Depth maps generation parameters

| | |
|------------------|--------------------|
| Quality | High |
| Filtering mode | Aggressive |
| Processing time | 7 hours 12 minutes |
| Software version | 1.5.5.9097 |

Dense Point Cloud

| | |
|--------------|----------------|
| Points | 30,423,249 |
| Point colors | 3 bands, uint8 |

Depth maps generation parameters

| | |
|-----------------|--------------------|
| Quality | High |
| Filtering mode | Aggressive |
| Processing time | 7 hours 12 minutes |

Dense cloud generation parameters

| | |
|------------------|--------------------|
| Processing time | 6 hours 23 minutes |
| Software version | 1.5.5.9097 |

Model

| | |
|---------------|-------------------------------|
| Faces | 6,084,595 |
| Vertices | 3,050,118 |
| Vertex colors | 3 bands, uint8 |
| Texture | 8,192 x 8,192, 4 bands, uint8 |

General**Depth maps generation parameters**

| | |
|-----------------|--------------------|
| Quality | High |
| Filtering mode | Aggressive |
| Processing time | 7 hours 12 minutes |

Reconstruction parameters

| | |
|-------------------------|--------------------|
| Surface type | Arbitrary |
| Source data | Dense cloud |
| Interpolation | Enabled |
| Strict volumetric masks | No |
| Processing time | 1 hours 58 minutes |

Texturing parameters

| | |
|------------------------|-----------------------|
| Mapping mode | Generic |
| Blending mode | Mosaic |
| Texture size | 8,192 |
| Enable hole filling | Yes |
| Enable ghosting filter | No |
| UV mapping time | 7 minutes 25 seconds |
| Blending time | 22 minutes 18 seconds |
| Software version | 1.5.5.9097 |

Orthomosaic

| | |
|-------------------|-----------------------|
| Size | 13,834 x 14,544 |
| Coordinate system | Local Coordinates (m) |
| Colors | 3 bands, uint8 |

Reconstruction parameters

| | |
|---------------------|-----------------------|
| Blending mode | Mosaic |
| Surface | Mesh |
| Enable hole filling | Yes |
| Processing time | 33 minutes 56 seconds |
| Software version | 1.5.5.9097 |

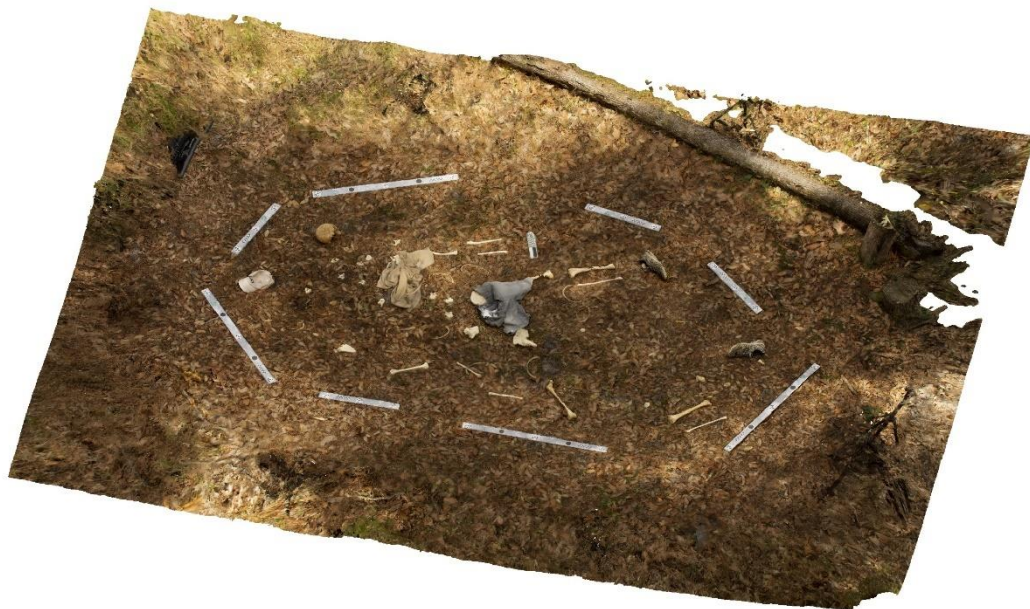
Software

| | |
|----------|------------------|
| Version | 1.5.5 build 9097 |
| Platform | Windows 64 |

Model 1C-2

Agisoft Metashape

Processing Report
15 July 2021



Survey Data

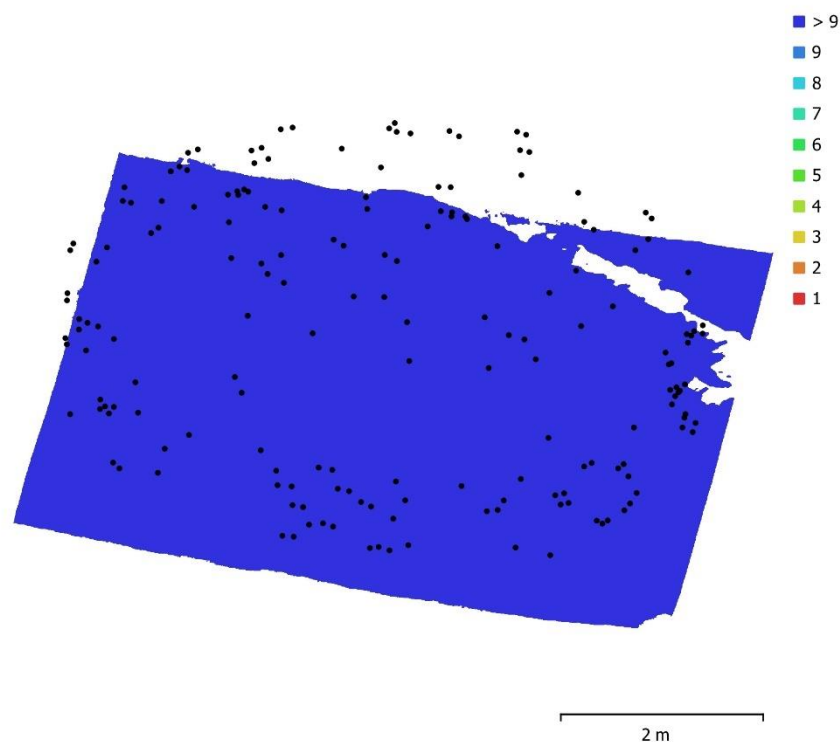


Fig. 1. Camera locations and image overlap.

| | | | |
|--------------------|---------------------|---------------------|-----------|
| Number of images: | 180 | Camera stations: | 180 |
| Flying altitude: | 2.22 m | Tie points: | 69,724 |
| Ground resolution: | 0.477 mm/pix | Projections: | 166,502 |
| Coverage area: | 24.8 m ² | Reprojection error: | 0.275 pix |

| Camera Model | Resolution | Focal Length | Pixel Size | Precalibrated |
|--------------------|-------------|--------------|----------------|---------------|
| NIKON D7200 (18mm) | 6000 x 4000 | 18 mm | 3.91 x 3.91 μm | No |

Table 1. Cameras.

Camera Calibration

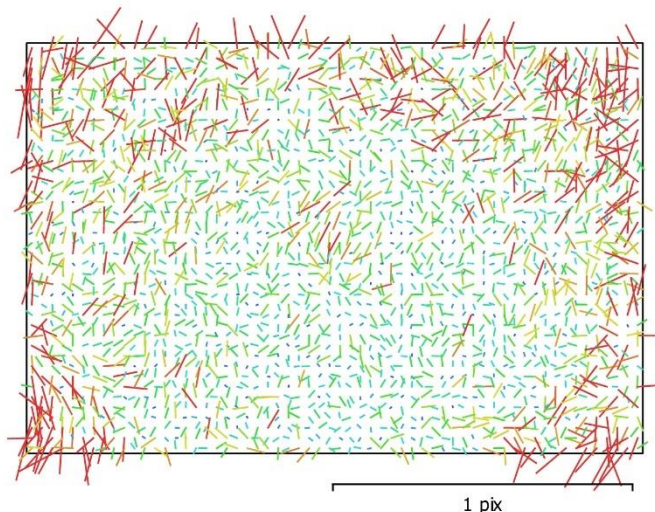


Fig. 2. Image residuals for NIKON D7200 (18mm).

NIKON D7200 (18mm)

180 images

| Type | Resolution | Focal Length | Pixel Size |
|--------------|--------------------|--------------|---|
| Frame | 6000 x 4000 | 18 mm | 3.91 x 3.91 μm |
| F: | 4658.02 | | |
| Cx: | 1.26087 | B1: | 1.7343 |
| Cy: | 1.25163 | B2: | -0.947816 |
| K1: | -0.153651 | P1: | 0.000276646 |
| K2: | 0.104498 | P2: | 0.000278314 |
| K3: | 0.000994533 | P3: | 1.05133 |
| K4: | -0.000377253 | P4: | -0.489557 |

Scale Bars

| Label | Distance (m) | Error (m) |
|---------------------|--------------|--------------------|
| target 52_target 54 | 0.499788 | -0.000131634 |
| target 57_target 59 | 1.00041 | 0.000314165 |
| target 68_target 70 | 0.499125 | -4.74839e-006 |
| target 73_target 75 | 0.999975 | -0.000245349 |
| Total | | 0.000209908 |

Table 2. Control scale bars.

Digital Elevation Model

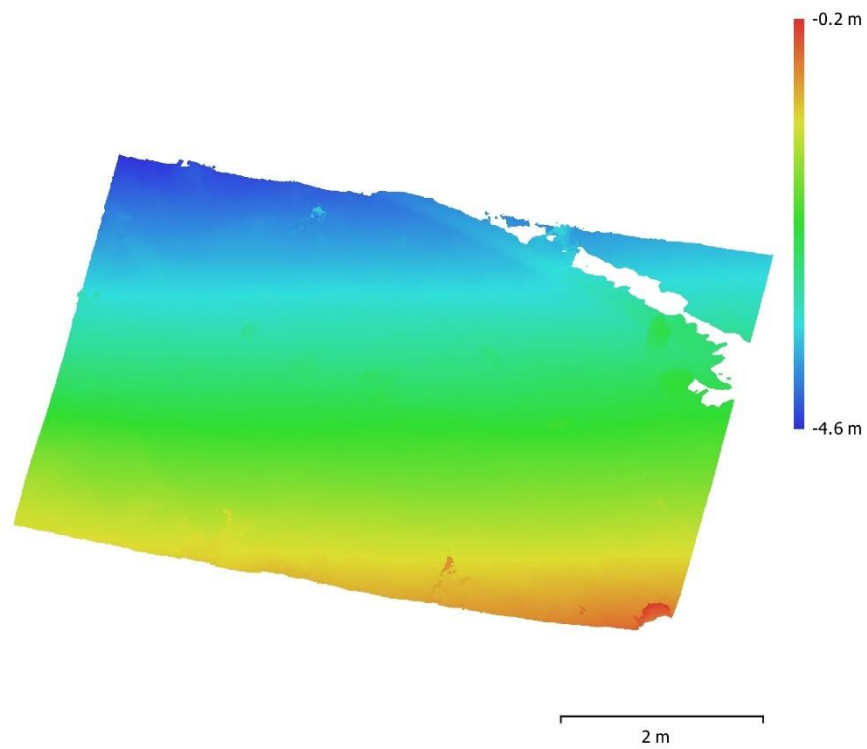


Fig. 3. Reconstructed digital elevation model.

Resolution: unknown
Point density: unknown

Processing Parameters

General

| | |
|-------------------|-----------------------|
| Cameras | 180 |
| Aligned cameras | 180 |
| Markers | 24 |
| Scale bars | 4 |
| Coordinate system | Local Coordinates (m) |
| Rotation angles | Yaw, Pitch, Roll |

Point Cloud

| | |
|--------------------------------|-------------------------|
| Points | 69,724 of 941,989 |
| RMS reprojection error | 0.101935 (0.274857 pix) |
| Max reprojection error | 0.472427 (1.57001 pix) |
| Mean key point size | 2.64798 pix |
| Point colors | 3 bands, uint8 |
| Key points | No |
| Average tie point multiplicity | 2.41065 |

Alignment parameters

| | |
|-------------------------------|-----------------------|
| Accuracy | High |
| Generic preselection | No |
| Key point limit | 100,000 |
| Tie point limit | 40,000 |
| Adaptive camera model fitting | Yes |
| Matching time | 7 hours 56 minutes |
| Alignment time | 18 minutes 15 seconds |

Optimization parameters

| | |
|-------------------------------|---------------------------------|
| Parameters | f, b1, b2, cx, cy, k1-k4, p1-p4 |
| Adaptive camera model fitting | No |
| Optimization time | 5 seconds |
| Software version | 1.5.5.9097 |

Depth Maps

| | |
|-------|-----|
| Count | 173 |
|-------|-----|

Depth maps generation parameters

| | |
|------------------|--------------------|
| Quality | High |
| Filtering mode | Aggressive |
| Processing time | 5 hours 44 minutes |
| Software version | 1.5.5.9097 |

Dense Point Cloud

| | |
|--------------|----------------|
| Points | 39,636,067 |
| Point colors | 3 bands, uint8 |

Depth maps generation parameters

| | |
|-----------------|--------------------|
| Quality | High |
| Filtering mode | Aggressive |
| Processing time | 5 hours 44 minutes |

Dense cloud generation parameters

| | |
|------------------|--------------------|
| Processing time | 7 hours 42 minutes |
| Software version | 1.5.5.9097 |

Model

| | |
|---------------|-------------------------------|
| Faces | 7,927,136 |
| Vertices | 3,973,670 |
| Vertex colors | 3 bands, uint8 |
| Texture | 8,192 x 8,192, 4 bands, uint8 |

General**Depth maps generation parameters**

| | |
|-----------------|--------------------|
| Quality | High |
| Filtering mode | Aggressive |
| Processing time | 5 hours 44 minutes |

Reconstruction parameters

| | |
|-------------------------|--------------------|
| Surface type | Arbitrary |
| Source data | Dense cloud |
| Interpolation | Enabled |
| Strict volumetric masks | No |
| Processing time | 2 hours 11 minutes |

Texturing parameters

| | |
|------------------------|-----------------------|
| Mapping mode | Generic |
| Blending mode | Mosaic |
| Texture size | 8,192 |
| Enable hole filling | Yes |
| Enable ghosting filter | Yes |
| UV mapping time | 7 minutes 38 seconds |
| Blending time | 37 minutes 41 seconds |
| Software version | 1.5.5.9097 |

Orthomosaic

| | |
|-------------------|-----------------------|
| Size | 13,274 x 10,167 |
| Coordinate system | Local Coordinates (m) |
| Colors | 3 bands, uint8 |

Reconstruction parameters

| | |
|---------------------|-----------------------|
| Blending mode | Mosaic |
| Surface | Mesh |
| Enable hole filling | Yes |
| Processing time | 40 minutes 22 seconds |
| Software version | 1.5.5.9097 |

Software

| | |
|----------|------------------|
| Version | 1.5.5 build 9097 |
| Platform | Windows 64 |

Model 1D-1

Agisoft Metashape

**Processing Report
10 June 2021**



Survey Data

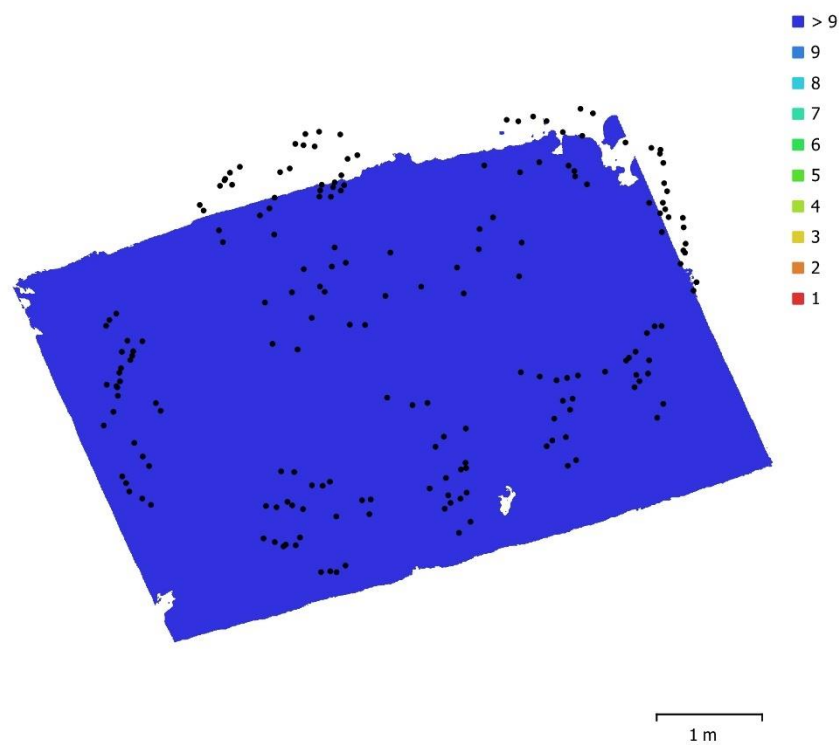


Fig. 1. Camera locations and image overlap.

| | | | |
|--------------------|---------------------|---------------------|-----------|
| Number of images: | 190 | Camera stations: | 190 |
| Flying altitude: | 1.96 m | Tie points: | 135,666 |
| Ground resolution: | 0.421 mm/pix | Projections: | 348,623 |
| Coverage area: | 22.1 m ² | Reprojection error: | 0.351 pix |

| Camera Model | Resolution | Focal Length | Pixel Size | Precalibrated |
|--------------------|-------------|--------------|---------------------|---------------|
| NIKON D7200 (18mm) | 6000 x 4000 | 18 mm | 3.91 x 3.91 μ m | No |

Table 1. Cameras.

Camera Calibration

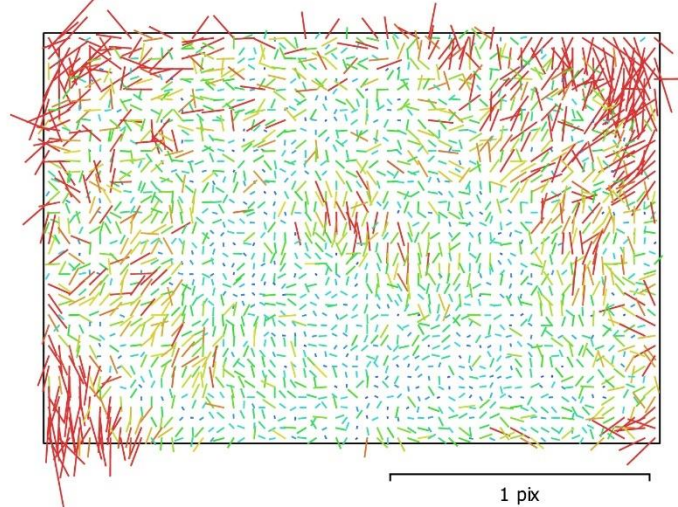


Fig. 2. Image residuals for NIKON D7200 (18mm).

NIKON D7200 (18mm)

190 images

| | | | |
|--------------|--------------------|--------------|--------------------------------------|
| Type | Resolution | Focal Length | Pixel Size |
| Frame | 6000 x 4000 | 18 mm | 3.91 x 3.91 μm |

| | Value | Error | F | Cx | Cy | B1 | B2 | K1 | K2 | K3 | K4 | P1 | P2 | P3 | P4 |
|-----------|--------------------|----------|------|-------|-------|-------|-------|-------|-------|-------|-------|-------|-------|-------|-------|
| F | 4666.79 | 0.097 | 1.00 | -0.04 | -0.08 | -0.10 | -0.10 | -0.16 | 0.19 | -0.17 | 0.17 | -0.01 | 0.16 | -0.00 | -0.02 |
| Cx | 13.4419 | 0.13 | | 1.00 | 0.04 | 0.19 | 0.17 | 0.03 | -0.02 | 0.02 | -0.02 | 0.67 | 0.01 | -0.01 | 0.06 |
| Cy | 10.3745 | 0.13 | | | 1.00 | -0.26 | 0.15 | -0.02 | 0.02 | -0.01 | 0.01 | 0.06 | 0.39 | -0.01 | 0.03 |
| B1 | -0.946997 | 0.023 | | | | 1.00 | -0.08 | 0.04 | -0.04 | 0.03 | -0.02 | 0.11 | 0.10 | -0.01 | 0.00 |
| B2 | -1.36662 | 0.021 | | | | | 1.00 | 0.01 | -0.00 | 0.01 | -0.01 | 0.03 | -0.15 | 0.01 | 0.04 |
| K1 | -0.152976 | 9.5e-005 | | | | | | 1.00 | -0.97 | 0.92 | -0.87 | -0.03 | -0.04 | 0.05 | -0.03 |
| K2 | 0.104379 | 0.00062 | | | | | | | 1.00 | -0.99 | 0.95 | 0.04 | 0.03 | -0.07 | 0.05 |
| K3 | 0.00171564 | 0.0015 | | | | | | | | 1.00 | -0.99 | -0.04 | -0.03 | 0.06 | -0.05 |
| K4 | -0.00199987 | 0.0013 | | | | | | | | | 1.00 | 0.03 | 0.02 | -0.05 | 0.03 |
| P1 | 0.000736583 | 5.6e-006 | | | | | | | | | | 1.00 | 0.44 | -0.65 | 0.58 |
| P2 | 0.000683683 | 5.6e-006 | | | | | | | | | | | 1.00 | -0.58 | 0.48 |
| P3 | 0.33081 | 0.028 | | | | | | | | | | | | 1.00 | -0.96 |
| P4 | 0.590226 | 0.036 | | | | | | | | | | | | | 1.00 |

Table 2. Calibration coefficients and correlation matrix.

Scale Bars

| Label | Distance (m) | Error (m) |
|---------------------|--------------|--------------------|
| target 52_target 54 | 0.499077 | -0.000842601 |
| target 57_target 59 | 0.999941 | -0.000159018 |
| target 68_target 70 | 0.49941 | 0.000279925 |
| target 73_target 75 | 1.00066 | 0.00044043 |
| Total | | 0.000501896 |

Table 3. Control scale bars.

Digital Elevation Model

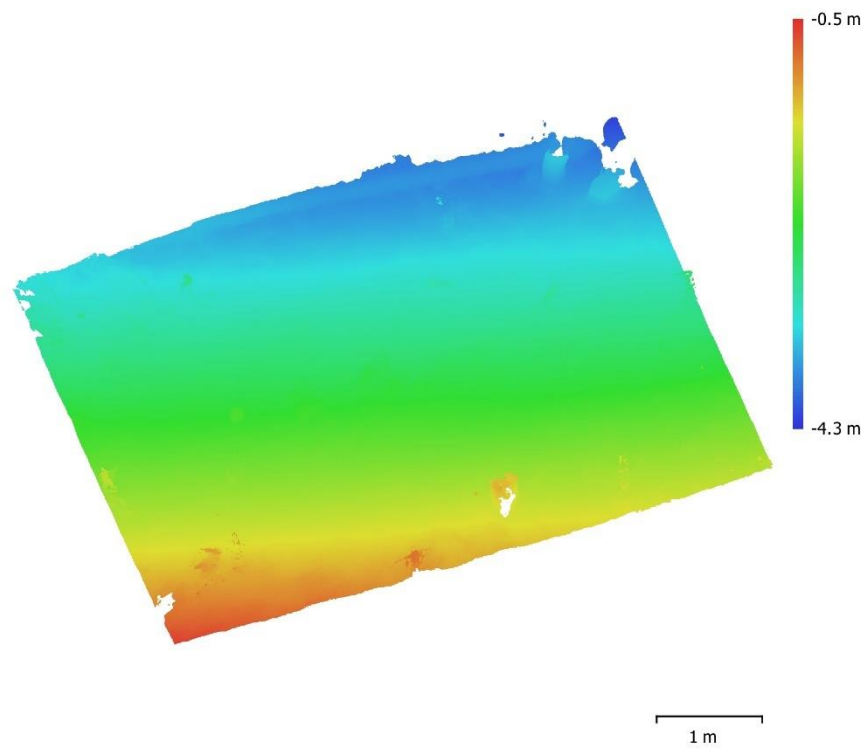


Fig. 3. Reconstructed digital elevation model.

Resolution: unknown
Point density: unknown

Processing Parameters

General

| | |
|-------------------|-----------------------|
| Cameras | 190 |
| Aligned cameras | 190 |
| Markers | 24 |
| Scale bars | 4 |
| Coordinate system | Local Coordinates (m) |
| Rotation angles | Yaw, Pitch, Roll |

Point Cloud

| | |
|--------------------------------|-------------------------|
| Points | 135,666 of 1,235,934 |
| RMS reprojection error | 0.128723 (0.350717 pix) |
| Max reprojection error | 0.517319 (2.83383 pix) |
| Mean key point size | 2.67853 pix |
| Point colors | 3 bands, uint8 |
| Key points | No |
| Average tie point multiplicity | 2.622 |

Alignment parameters

| | |
|-------------------------------|-----------------------|
| Accuracy | High |
| Generic preselection | No |
| Key point limit | 100,000 |
| Tie point limit | 40,000 |
| Adaptive camera model fitting | Yes |
| Matching time | 8 hours 34 minutes |
| Alignment time | 14 minutes 13 seconds |

Optimization parameters

| | |
|-------------------------------|---------------------------------|
| Parameters | f, b1, b2, cx, cy, k1-k4, p1-p4 |
| Adaptive camera model fitting | No |
| Optimization time | 8 seconds |
| Software version | 1.5.5.9097 |

Depth Maps

| | |
|-------|-----|
| Count | 188 |
|-------|-----|

Depth maps generation parameters

| | |
|------------------|--------------------|
| Quality | High |
| Filtering mode | Aggressive |
| Processing time | 5 hours 52 minutes |
| Software version | 1.5.5.9097 |

Dense Point Cloud

| | |
|--------------|----------------|
| Points | 51,257,551 |
| Point colors | 3 bands, uint8 |

Depth maps generation parameters

| | |
|-----------------|--------------------|
| Quality | High |
| Filtering mode | Aggressive |
| Processing time | 5 hours 52 minutes |

Dense cloud generation parameters

| | |
|------------------|--------------------|
| Processing time | 8 hours 21 minutes |
| Software version | 1.5.5.9097 |

Model

| | |
|---------------|-------------------------------|
| Faces | 10,251,407 |
| Vertices | 5,138,422 |
| Vertex colors | 3 bands, uint8 |
| Texture | 8,192 x 8,192, 4 bands, uint8 |

General**Depth maps generation parameters**

| | |
|-----------------|--------------------|
| Quality | High |
| Filtering mode | Aggressive |
| Processing time | 5 hours 52 minutes |

Reconstruction parameters

| | |
|-------------------------|--------------------|
| Surface type | Arbitrary |
| Source data | Dense cloud |
| Interpolation | Enabled |
| Strict volumetric masks | No |
| Processing time | 1 hours 21 minutes |

Texturing parameters

| | |
|------------------------|-----------------------|
| Mapping mode | Generic |
| Blending mode | Mosaic |
| Texture size | 8,192 |
| Enable hole filling | Yes |
| Enable ghosting filter | No |
| UV mapping time | 12 minutes 3 seconds |
| Blending time | 22 minutes 54 seconds |
| Software version | 1.5.5.9097 |

Orthomosaic

| | |
|-------------------|-----------------------|
| Size | 14,579 x 12,156 |
| Coordinate system | Local Coordinates (m) |
| Colors | 3 bands, uint8 |

Reconstruction parameters

| | |
|---------------------|-----------------------|
| Blending mode | Mosaic |
| Surface | Mesh |
| Enable hole filling | Yes |
| Processing time | 37 minutes 11 seconds |
| Software version | 1.5.5.9097 |

Software

| | |
|----------|------------------|
| Version | 1.5.5 build 9097 |
| Platform | Windows 64 |

Model 1E-1

Agisoft Metashape

**Processing Report
15 June 2021**



Survey Data

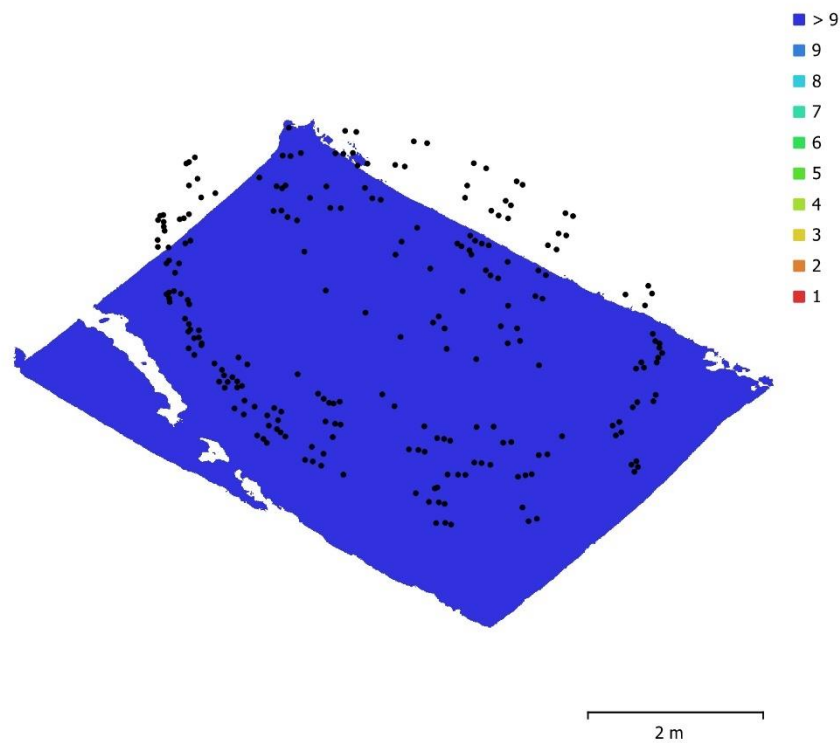


Fig. 1. Camera locations and image overlap.

| | | | |
|--------------------|-------------------|---------------------|-----------|
| Number of images: | 233 | Camera stations: | 233 |
| Flying altitude: | 2.15 m | Tie points: | 253,133 |
| Ground resolution: | 0.462 mm/pix | Projections: | 643,683 |
| Coverage area: | 24 m ² | Reprojection error: | 0.347 pix |

| Camera Model | Resolution | Focal Length | Pixel Size | Precalibrated |
|--------------------|-------------|--------------|----------------|---------------|
| NIKON D7200 (18mm) | 6000 x 4000 | 18 mm | 3.91 x 3.91 μm | No |

Table 1. Cameras.

Camera Calibration

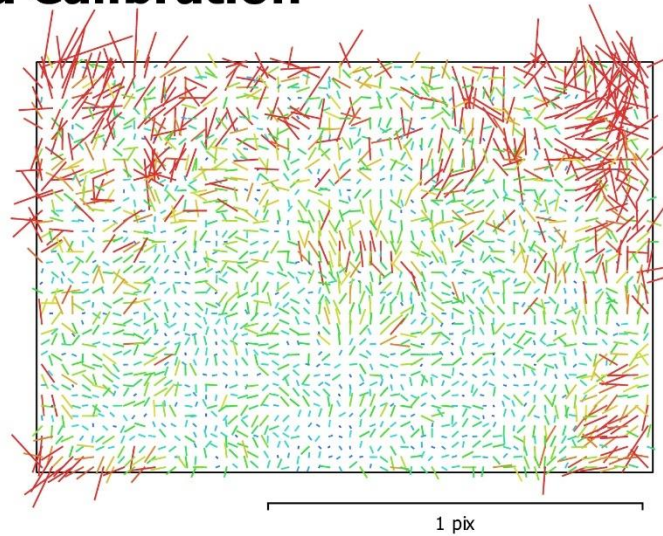


Fig. 2. Image residuals for NIKON D7200 (18mm).

NIKON D7200 (18mm)

233 images

| | | | |
|--------------|--------------------|--------------|--------------------------------------|
| Type | Resolution | Focal Length | Pixel Size |
| Frame | 6000 x 4000 | 18 mm | 3.91 x 3.91 μm |

| | Value | Error | F | Cx | Cy | B1 | B2 | K1 | K2 | K3 | K4 | P1 | P2 | P3 | P4 |
|-----------|---------------------|----------|------|------|-------|-------|-------|-------|-------|-------|-------|-------|-------|-------|-------|
| F | 4665.88 | 0.068 | 1.00 | 0.07 | 0.10 | -0.46 | 0.02 | -0.16 | 0.19 | -0.17 | 0.16 | 0.02 | 0.16 | 0.02 | 0.00 |
| Cx | -6.21377 | 0.059 | | 1.00 | -0.01 | -0.04 | 0.17 | 0.02 | -0.00 | -0.01 | 0.02 | 0.82 | 0.02 | 0.02 | -0.02 |
| Cy | 4.66617 | 0.099 | | | 1.00 | -0.52 | -0.31 | -0.02 | 0.02 | -0.01 | 0.01 | 0.12 | 0.16 | 0.04 | 0.09 |
| B1 | -2.18074 | 0.035 | | | | 1.00 | 0.02 | 0.01 | -0.01 | 0.01 | -0.01 | -0.02 | 0.05 | -0.10 | 0.02 |
| B2 | 0.22184 | 0.028 | | | | | 1.00 | 0.00 | -0.00 | -0.00 | 0.01 | -0.09 | -0.01 | -0.02 | -0.02 |
| K1 | -0.154361 | 6.2e-005 | | | | | | 1.00 | -0.97 | 0.92 | -0.87 | 0.01 | -0.19 | 0.18 | -0.16 |
| K2 | 0.111489 | 0.0004 | | | | | | | 1.00 | -0.99 | 0.95 | 0.01 | 0.17 | -0.21 | 0.18 |
| K3 | -0.0144529 | 0.00099 | | | | | | | | 1.00 | -0.99 | -0.02 | -0.15 | 0.18 | -0.17 |
| K4 | 0.0123771 | 0.00082 | | | | | | | | | 1.00 | 0.03 | 0.12 | -0.15 | 0.13 |
| P1 | 1.43681e-005 | 2.7e-006 | | | | | | | | | | 1.00 | 0.02 | -0.01 | 0.03 |
| P2 | 0.000601703 | 5.2e-006 | | | | | | | | | | | 1.00 | -0.68 | 0.66 |
| P3 | -0.202778 | 0.031 | | | | | | | | | | | | 1.00 | -0.97 |
| P4 | -0.296237 | 0.047 | | | | | | | | | | | | | 1.00 |

Table 2. Calibration coefficients and correlation matrix.

Scale Bars

| Label | Distance (m) | Error (m) |
|---------------------|--------------|--------------------|
| target 52_target 54 | 0.499693 | -0.000227471 |
| target 57_target 59 | 1.00067 | 0.000574327 |
| target 68_target 70 | 0.498974 | -0.000155719 |
| target 73_target 75 | 0.999837 | -0.000383109 |
| Total | | 0.000371691 |

Table 3. Control scale bars.

Digital Elevation Model

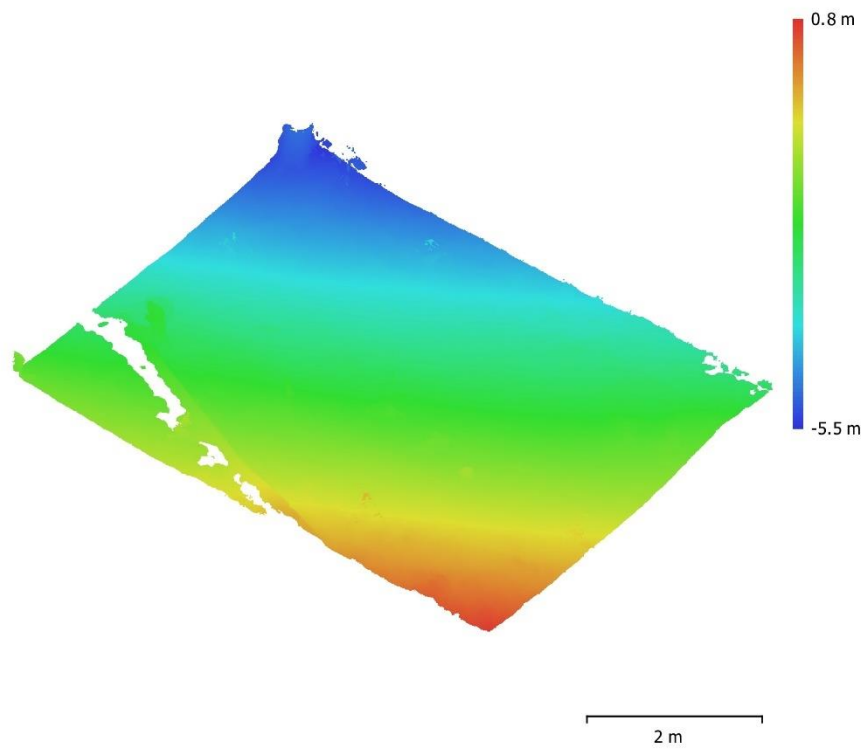


Fig. 3. Reconstructed digital elevation model.

Resolution: unknown
Point density: unknown

Processing Parameters

General

| | |
|-------------------|-----------------------|
| Cameras | 233 |
| Aligned cameras | 233 |
| Markers | 24 |
| Scale bars | 4 |
| Coordinate system | Local Coordinates (m) |
| Rotation angles | Yaw, Pitch, Roll |

Point Cloud

| | |
|--------------------------------|-------------------------|
| Points | 253,133 of 1,418,441 |
| RMS reprojection error | 0.100095 (0.346847 pix) |
| Max reprojection error | 0.435508 (2.60992 pix) |
| Mean key point size | 3.40217 pix |
| Point colors | 3 bands, uint8 |
| Key points | No |
| Average tie point multiplicity | 2.47854 |

Alignment parameters

| | |
|-------------------------------|-----------------------|
| Accuracy | High |
| Generic preselection | No |
| Key point limit | 100,000 |
| Tie point limit | 40,000 |
| Adaptive camera model fitting | Yes |
| Matching time | 15 hours 13 minutes |
| Alignment time | 12 minutes 30 seconds |

Optimization parameters

| | |
|-------------------------------|---------------------------------|
| Parameters | f, b1, b2, cx, cy, k1-k4, p1-p4 |
| Adaptive camera model fitting | No |
| Optimization time | 19 seconds |
| Software version | 1.5.5.9097 |

Depth Maps

| | |
|-------|-----|
| Count | 233 |
|-------|-----|

Depth maps generation parameters

| | |
|------------------|---------------------|
| Quality | High |
| Filtering mode | Aggressive |
| Processing time | 10 hours 33 minutes |
| Software version | 1.5.5.9097 |

Dense Point Cloud

| | |
|--------------|----------------|
| Points | 56,129,032 |
| Point colors | 3 bands, uint8 |

Depth maps generation parameters

| | |
|-----------------|---------------------|
| Quality | High |
| Filtering mode | Aggressive |
| Processing time | 10 hours 33 minutes |

Dense cloud generation parameters

| | |
|------------------|--------------------|
| Processing time | 6 hours 14 minutes |
| Software version | 1.5.5.9097 |

Model

| | |
|---------------|-------------------------------|
| Faces | 11,225,694 |
| Vertices | 5,626,620 |
| Vertex colors | 3 bands, uint8 |
| Texture | 8,192 x 8,192, 4 bands, uint8 |

General**Depth maps generation parameters**

| | |
|-----------------|---------------------|
| Quality | High |
| Filtering mode | Aggressive |
| Processing time | 10 hours 33 minutes |

Reconstruction parameters

| | |
|-------------------------|--------------------|
| Surface type | Arbitrary |
| Source data | Dense cloud |
| Interpolation | Enabled |
| Strict volumetric masks | No |
| Processing time | 1 hours 30 minutes |

Texturing parameters

| | |
|------------------------|-----------------------|
| Mapping mode | Generic |
| Blending mode | Mosaic |
| Texture size | 8,192 |
| Enable hole filling | Yes |
| Enable ghosting filter | No |
| UV mapping time | 7 minutes 17 seconds |
| Blending time | 26 minutes 32 seconds |
| Software version | 1.5.5.9097 |

Software

| | |
|----------|------------------|
| Version | 1.5.5 build 9097 |
| Platform | Windows 64 |

5.14 Nothing Try 1

Processing Report
01 June 2021



Survey Data

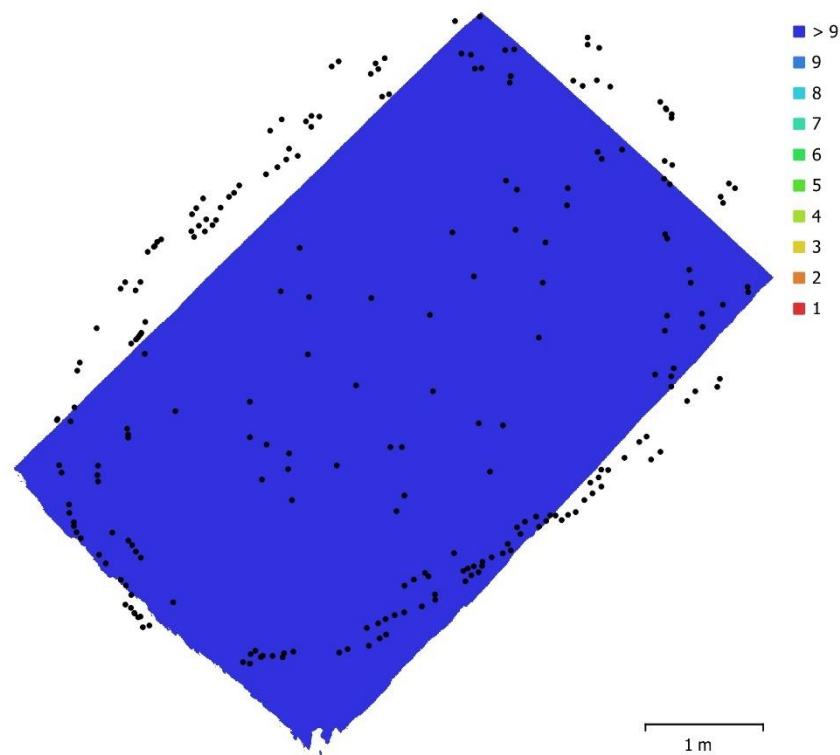


Fig. 1. Camera locations and image overlap.

| | | | |
|--------------------|---------------------|---------------------|-----------|
| Number of images: | 240 | Camera stations: | 240 |
| Flying altitude: | 2.18 m | Tie points: | 530,344 |
| Ground resolution: | 0.468 mm/pix | Projections: | 1,371,789 |
| Coverage area: | 19.7 m ² | Reprojection error: | 0.269 pix |

| Camera Model | Resolution | Focal Length | Pixel Size | Precalibrated |
|--------------------|-------------|--------------|----------------|---------------|
| NIKON D7200 (18mm) | 6000 x 4000 | 18 mm | 3.91 x 3.91 μm | No |

Table 1. Cameras.

Camera Calibration

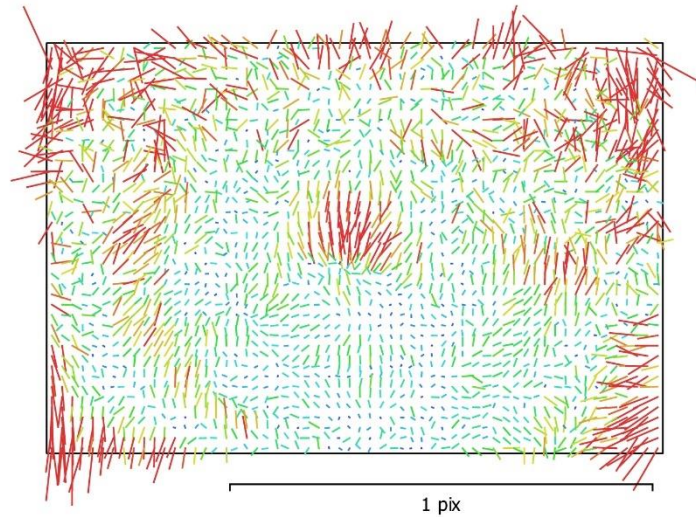


Fig. 2. Image residuals for NIKON D7200 (18mm).

NIKON D7200 (18mm)

240 images

| | | | |
|--------------|--------------------|--------------|---|
| Type | Resolution | Focal Length | Pixel Size |
| Frame | 6000 x 4000 | 18 mm | 3.91 x 3.91 μm |

| | Value | Error | F | Cx | Cy | B1 | B2 | K1 | K2 | K3 | K4 | P1 | P2 | P3 | P4 |
|-----------|--------------------|----------|------|-------|-------|-------|-------|-------|-------|-------|-------|-------|-------|-------|-------|
| F | 4664.54 | 0.054 | 1.00 | -0.06 | -0.38 | 0.08 | -0.10 | -0.06 | 0.13 | -0.12 | 0.12 | -0.03 | 0.11 | -0.01 | -0.03 |
| Cx | -17.1278 | 0.05 | | 1.00 | 0.11 | 0.04 | 0.20 | 0.01 | 0.01 | -0.01 | 0.01 | 0.65 | -0.14 | 0.03 | 0.07 |
| Cy | 31.1917 | 0.065 | | | 1.00 | -0.51 | 0.26 | -0.05 | 0.03 | -0.02 | 0.01 | 0.08 | -0.02 | -0.01 | 0.10 |
| B1 | 0.104326 | 0.01 | | | | 1.00 | -0.19 | 0.04 | -0.04 | 0.03 | -0.02 | 0.03 | 0.28 | -0.01 | -0.05 |
| B2 | -0.696738 | 0.009 | | | | | 1.00 | -0.01 | 0.01 | -0.01 | 0.00 | -0.03 | -0.10 | 0.04 | 0.02 |
| K1 | -0.152534 | 3.3e-005 | | | | | | 1.00 | -0.96 | 0.92 | -0.86 | -0.07 | -0.08 | 0.12 | -0.10 |
| K2 | 0.106085 | 0.00022 | | | | | | | 1.00 | -0.99 | 0.95 | 0.08 | 0.06 | -0.13 | 0.12 |
| K3 | -0.00713874 | 0.00057 | | | | | | | | 1.00 | -0.99 | -0.08 | -0.05 | 0.11 | -0.10 |
| K4 | 0.00872714 | 0.00049 | | | | | | | | | 1.00 | 0.06 | 0.04 | -0.07 | 0.06 |
| P1 | 0.000364845 | 2e-006 | | | | | | | | | | 1.00 | 0.28 | -0.53 | 0.52 |
| P2 | 0.000519901 | 2.5e-006 | | | | | | | | | | | 1.00 | -0.61 | 0.48 |
| P3 | 0.268838 | 0.017 | | | | | | | | | | | | 1.00 | -0.95 |
| P4 | 0.222157 | 0.023 | | | | | | | | | | | | | 1.00 |

Table 2. Calibration coefficients and correlation matrix.

Scale Bars

| Label | Distance (m) | Error (m) |
|---------------------|--------------|--------------------|
| target 73_target 75 | 0.999702 | -0.000517968 |
| target 68_target 70 | 0.499235 | 0.00010462 |
| target 57_target 59 | 1.00058 | 0.000476053 |
| target 52_target 54 | 0.499902 | -1.8211e-005 |
| Total | | 0.000355737 |

Table 3. Control scale bars.

Digital Elevation Model

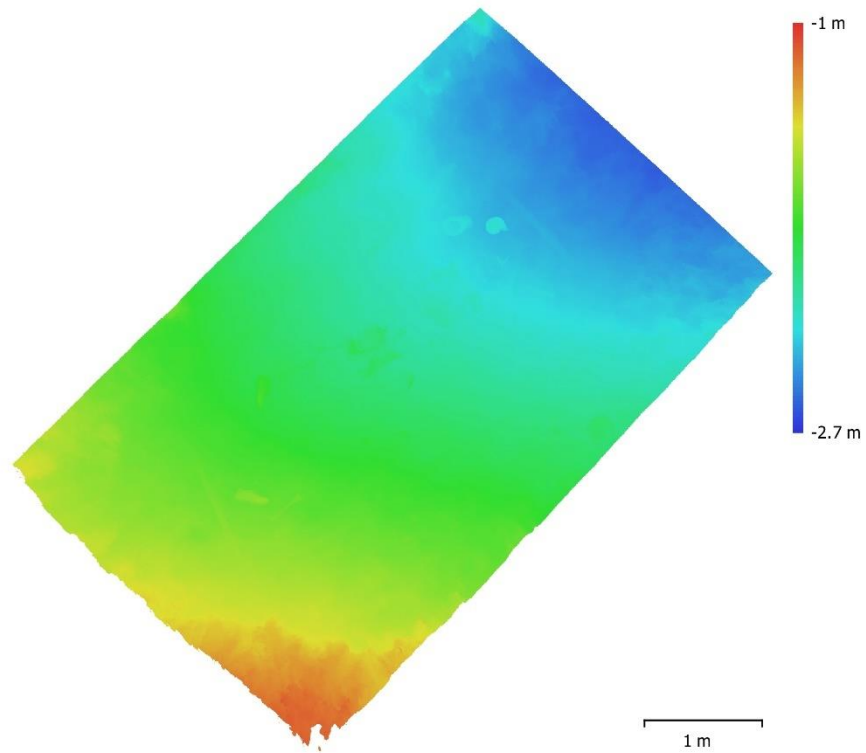


Fig. 3. Reconstructed digital elevation model.

Resolution: unknown
Point density: unknown

Processing Parameters

General

| | |
|-------------------|-----------------------|
| Cameras | 240 |
| Aligned cameras | 240 |
| Markers | 24 |
| Scale bars | 4 |
| Coordinate system | Local Coordinates (m) |
| Rotation angles | Yaw, Pitch, Roll |

Point Cloud

| | |
|--------------------------------|------------------------|
| Points | 530,344 of 1,964,616 |
| RMS reprojection error | 0.100699 (0.26855 pix) |
| Max reprojection error | 2.09817 (8.37755 pix) |
| Mean key point size | 2.60986 pix |
| Point colors | 3 bands, uint8 |
| Key points | No |
| Average tie point multiplicity | 2.58868 |

Alignment parameters

| | |
|-------------------------------|-----------------------|
| Accuracy | High |
| Generic preselection | No |
| Key point limit | 100,000 |
| Tie point limit | 40,000 |
| Adaptive camera model fitting | Yes |
| Matching time | 7 hours 50 minutes |
| Alignment time | 16 minutes 20 seconds |

Optimization parameters

| | |
|-------------------------------|---------------------------------|
| Parameters | f, b1, b2, cx, cy, k1-k4, p1-p4 |
| Adaptive camera model fitting | No |
| Optimization time | 35 seconds |
| Software version | 1.5.5.9097 |

Depth Maps

| | |
|-------|-----|
| Count | 237 |
|-------|-----|

Depth maps generation parameters

| | |
|------------------|--------------------|
| Quality | High |
| Filtering mode | Aggressive |
| Processing time | 9 hours 41 minutes |
| Software version | 1.5.5.9097 |

Dense Point Cloud

| | |
|--------------|----------------|
| Points | 61,053,106 |
| Point colors | 3 bands, uint8 |

Depth maps generation parameters

| | |
|-----------------|--------------------|
| Quality | High |
| Filtering mode | Aggressive |
| Processing time | 9 hours 41 minutes |

Dense cloud generation parameters

| | |
|------------------|--------------------|
| Processing time | 6 hours 10 minutes |
| Software version | 1.5.5.9097 |

Model

| | |
|---------------|-------------------------------|
| Faces | 6,578,828 |
| Vertices | 3,297,717 |
| Vertex colors | 3 bands, uint8 |
| Texture | 8,192 x 8,192, 4 bands, uint8 |

General**Depth maps generation parameters**

| | |
|-----------------|--------------------|
| Quality | High |
| Filtering mode | Aggressive |
| Processing time | 9 hours 41 minutes |

Reconstruction parameters

| | |
|-------------------------|-------------------|
| Surface type | Arbitrary |
| Source data | Dense cloud |
| Interpolation | Enabled |
| Strict volumetric masks | No |
| Processing time | 1 hours 7 minutes |

Texturing parameters

| | |
|------------------------|-----------------------|
| Mapping mode | Generic |
| Blending mode | Mosaic |
| Texture size | 8,192 |
| Enable hole filling | Yes |
| Enable ghosting filter | No |
| UV mapping time | 11 minutes 18 seconds |
| Blending time | 27 minutes 4 seconds |
| Software version | 1.5.5.9097 |

Orthomosaic

| | |
|-------------------|-----------------------|
| Size | 11,960 x 7,417 |
| Coordinate system | Local Coordinates (m) |
| Colors | 3 bands, uint8 |

Reconstruction parameters

| | |
|---------------------|-----------------------|
| Blending mode | Mosaic |
| Surface | Mesh |
| Enable hole filling | Yes |
| Processing time | 19 minutes 46 seconds |
| Software version | 1.5.5.9097 |

Software

| | |
|----------|------------------|
| Version | 1.5.5 build 9097 |
| Platform | Windows 64 |

Model 2B-1

5.14 Sheet Only Try 1

**Processing Report
01 June 2021**



Survey Data

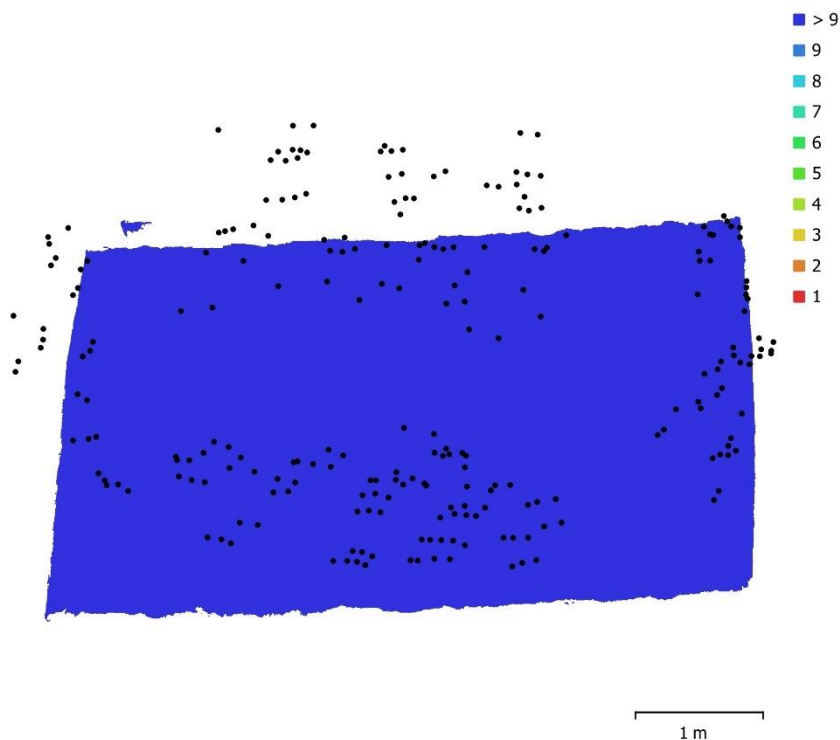


Fig. 1. Camera locations and image overlap.

| | | | |
|--------------------|---------------------|---------------------|-----------|
| Number of images: | 240 | Camera stations: | 240 |
| Flying altitude: | 2 m | Tie points: | 233,675 |
| Ground resolution: | 0.43 mm/pix | Projections: | 650,870 |
| Coverage area: | 15.6 m ² | Reprojection error: | 0.289 pix |

| Camera Model | Resolution | Focal Length | Pixel Size | Precalibrated |
|--------------------|-------------|--------------|----------------|---------------|
| NIKON D7200 (18mm) | 6000 x 4000 | 18 mm | 3.91 x 3.91 μm | No |

Table 1. Cameras.

Camera Calibration

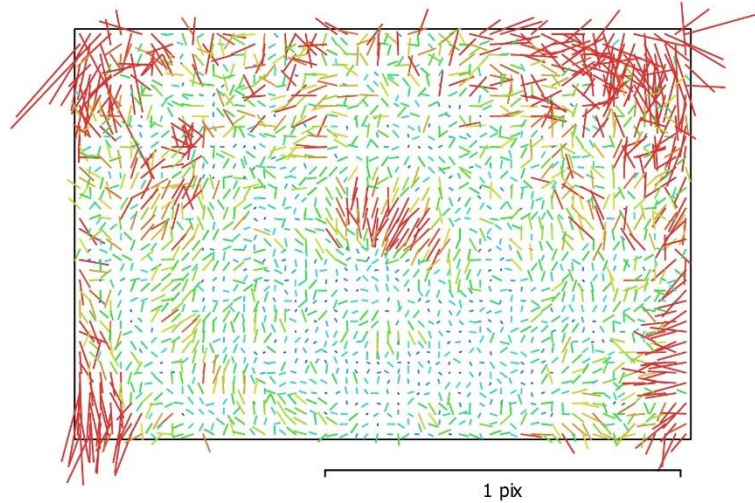


Fig. 2. Image residuals for NIKON D7200 (18mm).

NIKON D7200 (18mm)

240 images

| | | | |
|--------------|--------------------|--------------|---|
| Type | Resolution | Focal Length | Pixel Size |
| Frame | 6000 x 4000 | 18 mm | 3.91 x 3.91 μm |

| | Value | Error | F | Cx | Cy | B1 | B2 | K1 | K2 | K3 | K4 | P1 | P2 | P3 | P4 |
|-----------|--------------------|----------|------|------|-------|-------|-------|-------|-------|-------|-------|-------|-------|-------|-------|
| F | 4659.94 | 0.063 | 1.00 | 0.05 | -0.27 | -0.09 | -0.04 | -0.12 | 0.15 | -0.14 | 0.13 | 0.05 | 0.09 | 0.01 | -0.03 |
| Cx | -11.0935 | 0.078 | | 1.00 | -0.05 | -0.11 | 0.36 | 0.01 | 0.00 | -0.00 | 0.00 | 0.67 | -0.15 | 0.03 | 0.04 |
| Cy | 25.6841 | 0.087 | | | 1.00 | -0.46 | -0.06 | -0.04 | 0.03 | -0.02 | 0.02 | -0.01 | 0.29 | 0.01 | 0.02 |
| B1 | -0.24567 | 0.016 | | | | 1.00 | 0.02 | 0.03 | -0.04 | 0.03 | -0.03 | -0.04 | 0.16 | -0.05 | -0.01 |
| B2 | -0.369301 | 0.014 | | | | | 1.00 | 0.01 | 0.00 | -0.00 | 0.00 | 0.10 | -0.13 | 0.02 | 0.03 |
| K1 | -0.15326 | 4.9e-005 | | | | | | 1.00 | -0.97 | 0.92 | -0.87 | -0.01 | -0.05 | 0.02 | -0.00 |
| K2 | 0.105419 | 0.00032 | | | | | | | 1.00 | -0.99 | 0.95 | 0.03 | 0.02 | -0.03 | 0.01 |
| K3 | -0.0042086 | 0.0008 | | | | | | | | 1.00 | -0.99 | -0.02 | -0.01 | 0.01 | 0.01 |
| K4 | 0.00428624 | 0.00068 | | | | | | | | | 1.00 | 0.01 | -0.00 | 0.01 | -0.04 |
| P1 | 0.000407401 | 3e-006 | | | | | | | | | | 1.00 | 0.30 | -0.58 | 0.52 |
| P2 | 0.000434259 | 3.1e-006 | | | | | | | | | | | 1.00 | -0.58 | 0.45 |
| P3 | 0.187976 | 0.024 | | | | | | | | | | | | 1.00 | -0.95 |
| P4 | 0.831822 | 0.031 | | | | | | | | | | | | | 1.00 |

Table 2. Calibration coefficients and correlation matrix.

Scale Bars

| Label | Distance (m) | Error (m) |
|---------------------|--------------|---------------------|
| target 52_target 54 | 0.500018 | 9.80004e-005 |
| target 57_target 59 | 1.00007 | -2.79174e-005 |
| target 68_target 70 | 0.499196 | 6.56419e-005 |
| target 73_target 75 | 1.00017 | -5.21875e-005 |
| Total | | 6.59846e-005 |

Table 3. Control scale bars.

Digital Elevation Model

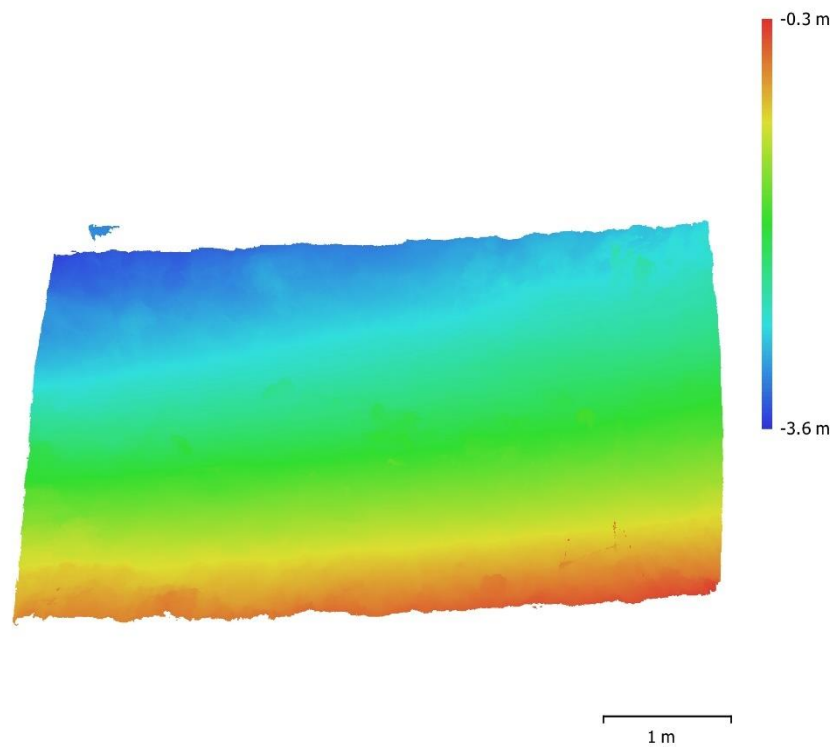


Fig. 3. Reconstructed digital elevation model.

Resolution: unknown
Point density: unknown

Processing Parameters

General

| | |
|-------------------|-----------------------|
| Cameras | 240 |
| Aligned cameras | 240 |
| Markers | 24 |
| Scale bars | 4 |
| Coordinate system | Local Coordinates (m) |
| Rotation angles | Yaw, Pitch, Roll |

Point Cloud

| | |
|--------------------------------|-------------------------|
| Points | 233,675 of 1,676,283 |
| RMS reprojection error | 0.120419 (0.288932 pix) |
| Max reprojection error | 0.401002 (1.715 pix) |
| Mean key point size | 2.36937 pix |
| Point colors | 3 bands, uint8 |
| Key points | No |
| Average tie point multiplicity | 2.67294 |

Alignment parameters

| | |
|-------------------------------|-----------------------|
| Accuracy | High |
| Generic preselection | Yes |
| Key point limit | 100,000 |
| Tie point limit | 40,000 |
| Adaptive camera model fitting | No |
| Matching time | 51 minutes 17 seconds |
| Alignment time | 22 minutes 33 seconds |

Optimization parameters

| | |
|-------------------------------|---------------------------------|
| Parameters | f, b1, b2, cx, cy, k1-k4, p1-p4 |
| Adaptive camera model fitting | No |
| Optimization time | 15 seconds |
| Software version | 1.5.5.9097 |

Depth Maps

| | |
|-------|-----|
| Count | 240 |
|-------|-----|

Depth maps generation parameters

| | |
|------------------|---------------------|
| Quality | High |
| Filtering mode | Aggressive |
| Processing time | 22 hours 40 minutes |
| Software version | 1.5.5.9097 |

Dense Point Cloud

| | |
|--------------|----------------|
| Points | 53,670,979 |
| Point colors | 3 bands, uint8 |

Depth maps generation parameters

| | |
|-----------------|---------------------|
| Quality | High |
| Filtering mode | Aggressive |
| Processing time | 22 hours 40 minutes |

Dense cloud generation parameters

| | |
|------------------|--------------------|
| Processing time | 5 hours 52 minutes |
| Software version | 1.5.5.9097 |

Model

| | |
|---------------|-------------------------------|
| Faces | 7,740,361 |
| Vertices | 3,879,495 |
| Vertex colors | 3 bands, uint8 |
| Texture | 8,192 x 8,192, 4 bands, uint8 |

General**Depth maps generation parameters**

| | |
|-----------------|---------------------|
| Quality | High |
| Filtering mode | Aggressive |
| Processing time | 22 hours 40 minutes |

Reconstruction parameters

| | |
|-------------------------|-------------------|
| Surface type | Arbitrary |
| Source data | Dense cloud |
| Interpolation | Enabled |
| Strict volumetric masks | No |
| Processing time | 1 hours 3 minutes |

Texturing parameters

| | |
|------------------------|-----------------------|
| Mapping mode | Generic |
| Blending mode | Mosaic |
| Texture size | 8,192 |
| Enable hole filling | Yes |
| Enable ghosting filter | No |
| UV mapping time | 9 minutes 7 seconds |
| Blending time | 24 minutes 45 seconds |
| Software version | 1.5.5.9097 |

Orthomosaic

| | |
|-------------------|-----------------------|
| Size | 11,901 x 8,592 |
| Coordinate system | Local Coordinates (m) |
| Colors | 3 bands, uint8 |

Reconstruction parameters

| | |
|---------------------|-----------------------|
| Blending mode | Mosaic |
| Surface | Mesh |
| Enable hole filling | Yes |
| Processing time | 34 minutes 22 seconds |
| Software version | 1.5.5.9097 |

Software

| | |
|----------|------------------|
| Version | 1.5.5 build 9097 |
| Platform | Windows 64 |

5.14 Lights Only Try 3

Processing Report
01 June 2021



Survey Data

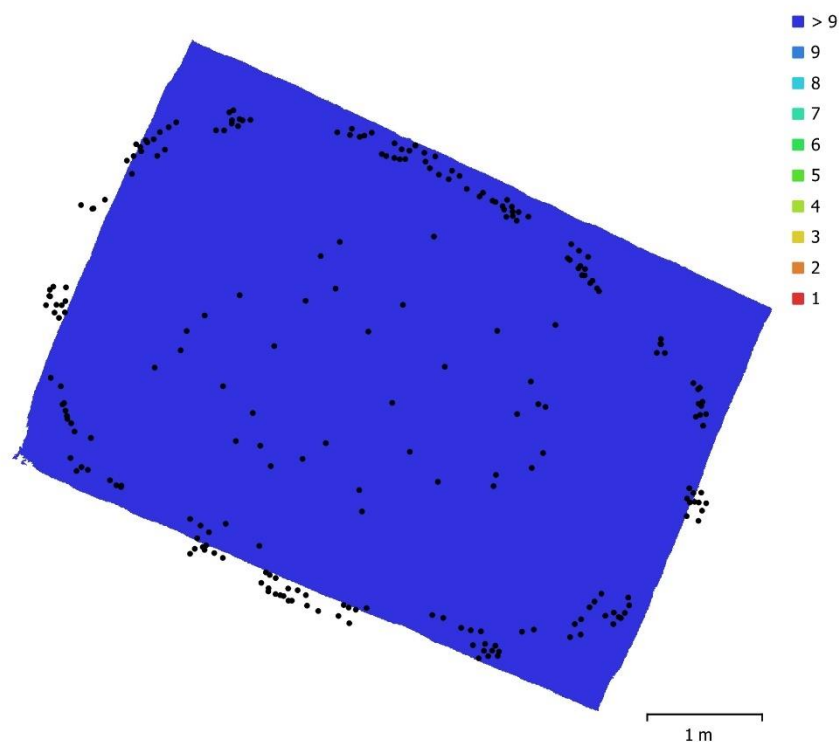


Fig. 1. Camera locations and image overlap.

| | | | |
|--------------------|-------------------|---------------------|-----------|
| Number of images: | 240 | Camera stations: | 240 |
| Flying altitude: | 2.29 m | Tie points: | 523,853 |
| Ground resolution: | 0.488 mm/pix | Projections: | 1,348,956 |
| Coverage area: | 22 m ² | Reprojection error: | 0.264 pix |

| Camera Model | Resolution | Focal Length | Pixel Size | Precalibrated |
|--------------------|-------------|--------------|----------------|---------------|
| NIKON D7200 (18mm) | 6000 x 4000 | 18 mm | 3.91 x 3.91 μm | No |

Table 1. Cameras.

Camera Calibration

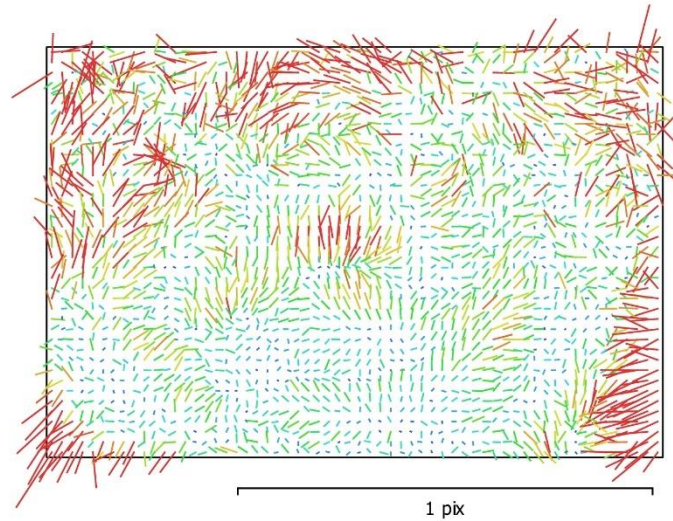


Fig. 2. Image residuals for NIKON D7200 (18mm).

NIKON D7200 (18mm)

240 images

| | | | |
|--------------|--------------------|--------------|--------------------------------------|
| Type | Resolution | Focal Length | Pixel Size |
| Frame | 6000 x 4000 | 18 mm | 3.91 x 3.91 μm |

| | Value | Error | F | Cx | Cy | B1 | B2 | K1 | K2 | K3 | K4 | P1 | P2 | P3 | P4 |
|-----------|--------------------|----------|------|-------|-------|-------|-------|-------|-------|-------|-------|-------|-------|-------|-------|
| F | 4680.69 | 0.04 | 1.00 | -0.01 | -0.12 | -0.12 | 0.01 | -0.13 | 0.17 | -0.15 | 0.15 | -0.03 | 0.15 | 0.02 | -0.04 |
| Cx | -20.7423 | 0.037 | | 1.00 | 0.06 | -0.05 | 0.27 | 0.02 | -0.00 | -0.01 | 0.01 | 0.76 | -0.08 | 0.06 | 0.01 |
| Cy | 26.8936 | 0.059 | | | 1.00 | -0.60 | -0.00 | -0.01 | 0.01 | -0.01 | 0.01 | 0.09 | 0.05 | 0.05 | 0.09 |
| B1 | 0.310324 | 0.014 | | | | 1.00 | -0.02 | -0.00 | -0.01 | 0.01 | -0.01 | -0.07 | 0.26 | -0.05 | -0.03 |
| B2 | -1.40417 | 0.011 | | | | | 1.00 | 0.01 | -0.01 | 0.00 | 0.00 | -0.04 | 0.02 | 0.02 | 0.00 |
| K1 | -0.151766 | 3.3e-005 | | | | | | 1.00 | -0.97 | 0.92 | -0.87 | -0.01 | -0.13 | 0.13 | -0.09 |
| K2 | 0.109233 | 0.00022 | | | | | | | 1.00 | -0.99 | 0.95 | 0.03 | 0.12 | -0.14 | 0.12 |
| K3 | -0.0110716 | 0.00057 | | | | | | | | 1.00 | -0.99 | -0.04 | -0.09 | 0.12 | -0.10 |
| K4 | 0.0123286 | 0.00049 | | | | | | | | | 1.00 | 0.03 | 0.07 | -0.08 | 0.06 |
| P1 | 0.000135668 | 1.8e-006 | | | | | | | | | | 1.00 | -0.00 | -0.15 | 0.19 |
| P2 | 0.000752915 | 2.9e-006 | | | | | | | | | | | 1.00 | -0.58 | 0.53 |
| P3 | -0.589038 | 0.013 | | | | | | | | | | | | 1.00 | -0.95 |
| P4 | 0.584264 | 0.019 | | | | | | | | | | | | | 1.00 |

Table 2. Calibration coefficients and correlation matrix.

Scale Bars

| Label | Distance (m) | Error (m) |
|---------------------|--------------|--------------------|
| target 73_target 75 | 1.00029 | 6.78735e-005 |
| target 68_target 70 | 0.499105 | -2.53078e-005 |
| target 57_target 59 | 0.999976 | -0.00012446 |
| target 52_target 54 | 0.500096 | 0.000176361 |
| Total | | 0.000113843 |

Table 3. Control scale bars.

Digital Elevation Model

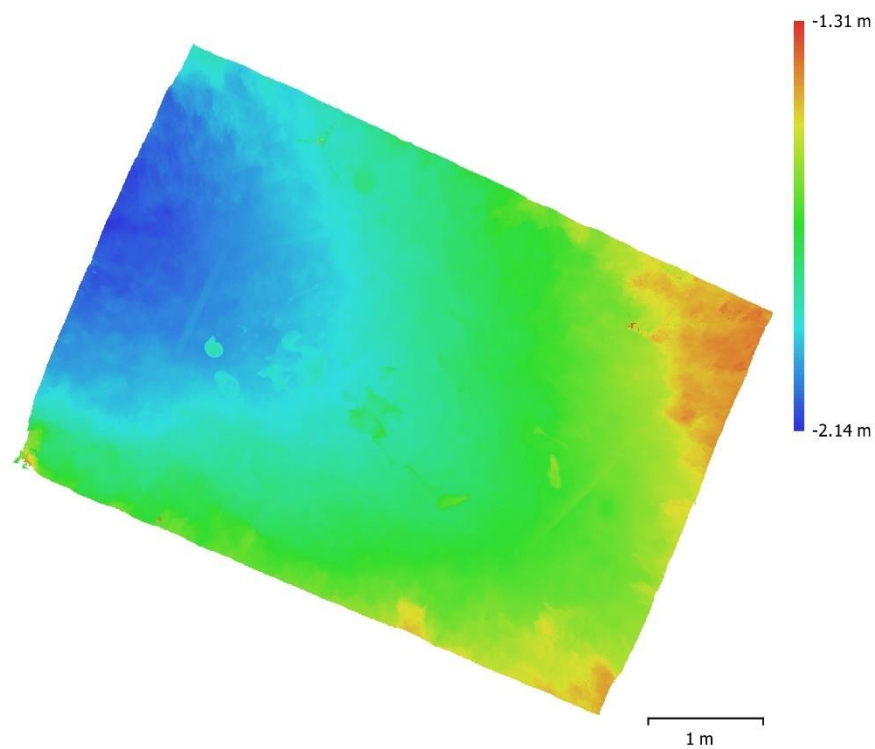


Fig. 3. Reconstructed digital elevation model.

Resolution: unknown
Point density: unknown

Processing Parameters

General

| | |
|-------------------|-----------------------|
| Cameras | 240 |
| Aligned cameras | 240 |
| Markers | 24 |
| Scale bars | 4 |
| Coordinate system | Local Coordinates (m) |
| Rotation angles | Yaw, Pitch, Roll |

Point Cloud

| | |
|--------------------------------|--------------------------|
| Points | 523,853 of 1,751,801 |
| RMS reprojection error | 0.0995281 (0.264188 pix) |
| Max reprojection error | 0.477241 (2.45496 pix) |
| Mean key point size | 2.60623 pix |
| Point colors | 3 bands, uint8 |
| Key points | No |
| Average tie point multiplicity | 2.51986 |

Alignment parameters

| | |
|-------------------------------|-----------------------|
| Accuracy | High |
| Generic preselection | Yes |
| Key point limit | 100,000 |
| Tie point limit | 40,000 |
| Adaptive camera model fitting | No |
| Matching time | 1 hours 9 minutes |
| Alignment time | 11 minutes 14 seconds |

Optimization parameters

| | |
|-------------------------------|---------------------------------|
| Parameters | f, b1, b2, cx, cy, k1-k4, p1-p4 |
| Adaptive camera model fitting | No |
| Optimization time | 21 seconds |
| Software version | 1.5.5.9097 |

Depth Maps

| | |
|-------|-----|
| Count | 240 |
|-------|-----|

Depth maps generation parameters

| | |
|------------------|--------------------|
| Quality | High |
| Filtering mode | Aggressive |
| Processing time | 9 hours 22 minutes |
| Software version | 1.5.5.9097 |

Dense Point Cloud

| | |
|--------------|----------------|
| Points | 61,266,200 |
| Point colors | 3 bands, uint8 |

Depth maps generation parameters

| | |
|-----------------|--------------------|
| Quality | High |
| Filtering mode | Aggressive |
| Processing time | 9 hours 22 minutes |

Dense cloud generation parameters

| | |
|------------------|-------------------|
| Processing time | 6 hours 3 minutes |
| Software version | 1.5.5.9097 |

Model

| | |
|---------------|-------------------------------|
| Faces | 8,136,224 |
| Vertices | 4,077,543 |
| Vertex colors | 3 bands, uint8 |
| Texture | 8,192 x 8,192, 4 bands, uint8 |

General**Depth maps generation parameters**

| | |
|-----------------|--------------------|
| Quality | High |
| Filtering mode | Aggressive |
| Processing time | 9 hours 22 minutes |

Reconstruction parameters

| | |
|-------------------------|--------------------|
| Surface type | Arbitrary |
| Source data | Dense cloud |
| Interpolation | Enabled |
| Strict volumetric masks | No |
| Processing time | 2 hours 46 minutes |

Texturing parameters

| | |
|------------------------|-----------------------|
| Mapping mode | Generic |
| Blending mode | Mosaic |
| Texture size | 8,192 |
| Enable hole filling | Yes |
| Enable ghosting filter | No |
| UV mapping time | 21 minutes 1 seconds |
| Blending time | 30 minutes 52 seconds |
| Software version | 1.5.5.9097 |

Orthomosaic

| | |
|-------------------|-----------------------|
| Size | 11,518 x 8,107 |
| Coordinate system | Local Coordinates (m) |
| Colors | 3 bands, uint8 |

Reconstruction parameters

| | |
|---------------------|----------------------|
| Blending mode | Mosaic |
| Surface | Mesh |
| Enable hole filling | Yes |
| Processing time | 43 minutes 3 seconds |
| Software version | 1.5.5.9097 |

Software

| | |
|----------|------------------|
| Version | 1.5.5 build 9097 |
| Platform | Windows 64 |

5.14 Lights & Sheet Try 1

Processing Report
01 June 2021



Survey Data

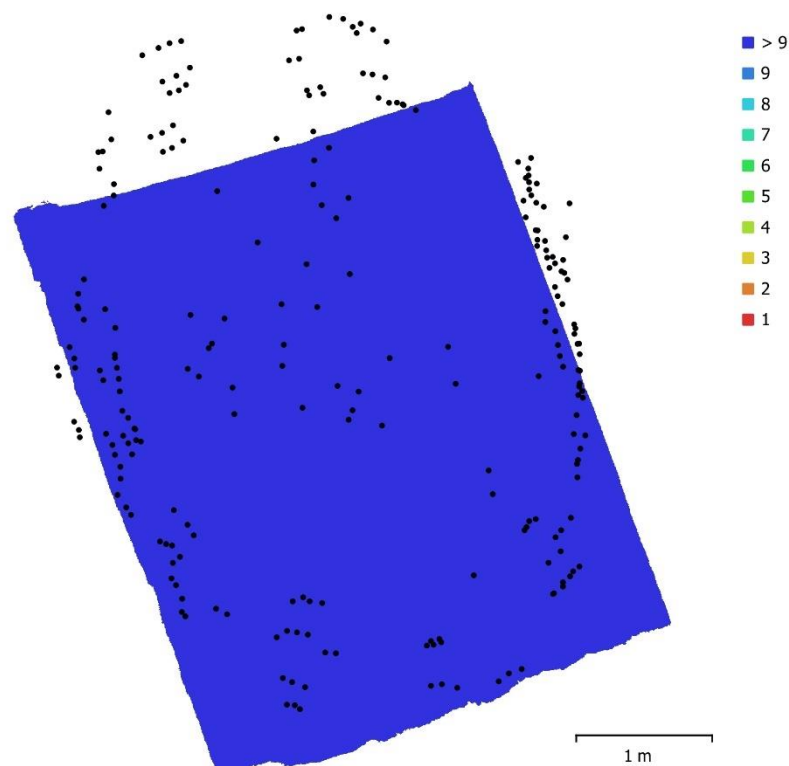


Fig. 1. Camera locations and image overlap.

| | | | |
|--------------------|---------------------|---------------------|-----------|
| Number of images: | 240 | Camera stations: | 240 |
| Flying altitude: | 2.03 m | Tie points: | 136,604 |
| Ground resolution: | 0.433 mm/pix | Projections: | 419,888 |
| Coverage area: | 15.3 m ² | Reprojection error: | 0.315 pix |

| Camera Model | Resolution | Focal Length | Pixel Size | Precalibrated |
|--------------------|-------------|--------------|----------------|---------------|
| NIKON D7200 (18mm) | 6000 x 4000 | 18 mm | 3.91 x 3.91 μm | No |

Table 1. Cameras.

Camera Calibration

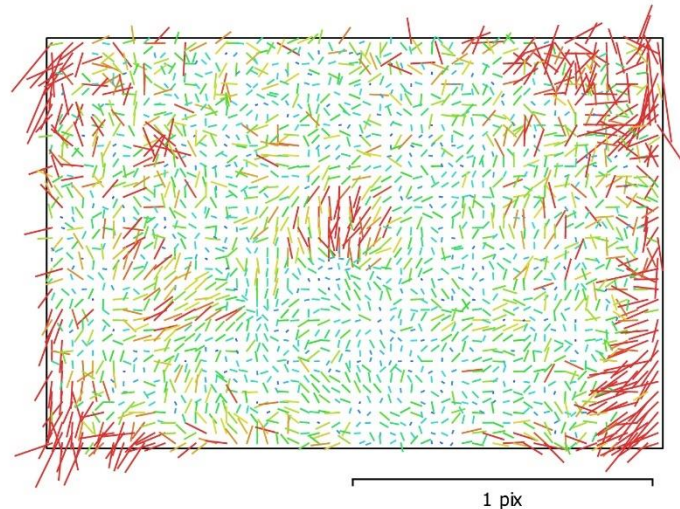


Fig. 2. Image residuals for NIKON D7200 (18mm).

NIKON D7200 (18mm)

240 images

| | | | |
|--------------|--------------------|--------------|--------------------------------------|
| Type | Resolution | Focal Length | Pixel Size |
| Frame | 6000 x 4000 | 18 mm | 3.91 x 3.91 μm |

| | Value | Error | F | Cx | Cy | B1 | B2 | K1 | K2 | K3 | K4 | P1 | P2 | P3 | P4 |
|-----------|--------------------|----------|------|------|-------|-------|-------|-------|-------|-------|-------|-------|-------|-------|-------|
| F | 4679.12 | 0.07 | 1.00 | 0.07 | -0.36 | -0.01 | 0.05 | -0.16 | 0.18 | -0.16 | 0.16 | 0.05 | 0.07 | -0.01 | -0.02 |
| Cx | -13.9941 | 0.073 | | 1.00 | 0.00 | -0.01 | 0.30 | 0.01 | 0.00 | -0.00 | -0.00 | 0.66 | -0.08 | 0.01 | 0.06 |
| Cy | 23.8958 | 0.08 | | | 1.00 | -0.54 | -0.12 | -0.01 | 0.01 | -0.01 | 0.00 | 0.02 | -0.00 | -0.02 | 0.09 |
| B1 | -0.126845 | 0.018 | | | | 1.00 | 0.05 | -0.00 | -0.01 | 0.01 | -0.01 | 0.07 | 0.29 | -0.03 | -0.03 |
| B2 | 0.733562 | 0.015 | | | | | 1.00 | -0.00 | 0.00 | -0.00 | 0.00 | 0.01 | 0.07 | 0.02 | 0.01 |
| K1 | -0.152058 | 6e-005 | | | | | | 1.00 | -0.97 | 0.92 | -0.87 | -0.01 | -0.08 | 0.03 | -0.02 |
| K2 | 0.108065 | 0.0004 | | | | | | | 1.00 | -0.99 | 0.95 | 0.02 | 0.05 | -0.04 | 0.02 |
| K3 | -0.00865655 | 0.001 | | | | | | | | 1.00 | -0.99 | -0.02 | -0.04 | 0.03 | -0.01 |
| K4 | 0.00996049 | 0.00089 | | | | | | | | | 1.00 | 0.01 | 0.02 | -0.01 | -0.01 |
| P1 | 0.00037552 | 3.1e-006 | | | | | | | | | | 1.00 | 0.37 | -0.54 | 0.50 |
| P2 | 0.000630374 | 3.8e-006 | | | | | | | | | | | 1.00 | -0.71 | 0.59 |
| P3 | -0.146512 | 0.024 | | | | | | | | | | | | 1.00 | -0.95 |
| P4 | 0.7099 | 0.033 | | | | | | | | | | | | | 1.00 |

Table 2. Calibration coefficients and correlation matrix.

Scale Bars

| Label | Distance (m) | Error (m) |
|---------------------|--------------|--------------------|
| target 52_target 54 | 0.500018 | 9.84698e-005 |
| target 57_target 59 | 0.999731 | -0.000369039 |
| target 73_target 75 | 1.00039 | 0.000171339 |
| target 68_target 70 | 0.499473 | 0.000343107 |
| Total | | 0.000270632 |

Table 3. Control scale bars.

Digital Elevation Model

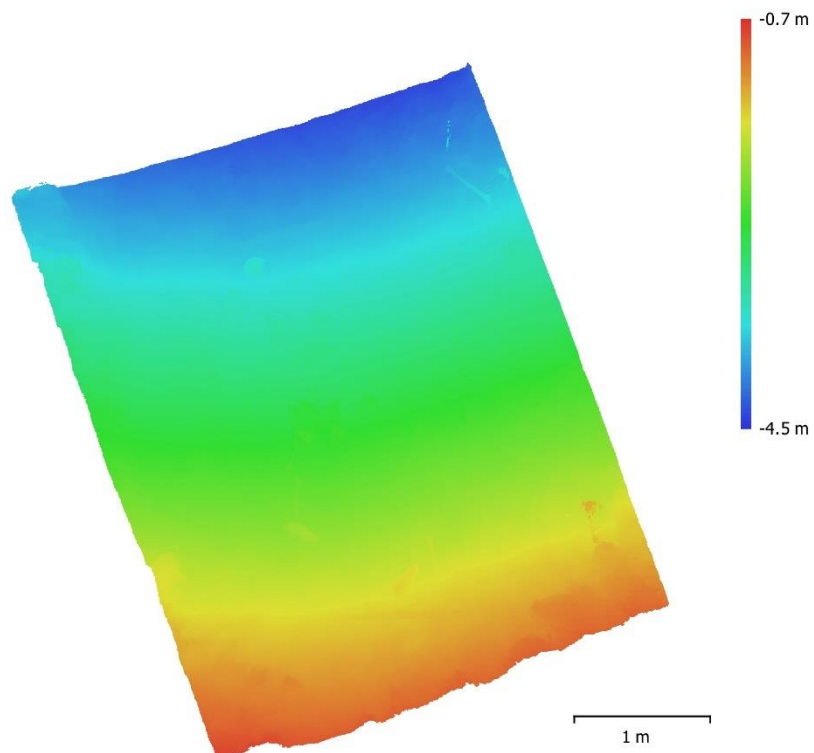


Fig. 3. Reconstructed digital elevation model.

Resolution: unknown
Point density: unknown

Processing Parameters

General

| | |
|-------------------|-----------------------|
| Cameras | 240 |
| Aligned cameras | 240 |
| Markers | 24 |
| Scale bars | 4 |
| Coordinate system | Local Coordinates (m) |
| Rotation angles | Yaw, Pitch, Roll |

Point Cloud

| | |
|--------------------------------|-------------------------|
| Points | 136,604 of 1,736,743 |
| RMS reprojection error | 0.130227 (0.314765 pix) |
| Max reprojection error | 0.289998 (1.69748 pix) |
| Mean key point size | 2.38239 pix |
| Point colors | 3 bands, uint8 |
| Key points | No |
| Average tie point multiplicity | 2.66722 |

Alignment parameters

| | |
|-------------------------------|-----------------------|
| Accuracy | High |
| Generic preselection | Yes |
| Key point limit | 100,000 |
| Tie point limit | 40,000 |
| Adaptive camera model fitting | No |
| Matching time | 39 minutes 35 seconds |
| Alignment time | 11 minutes 38 seconds |

Optimization parameters

| | |
|-------------------------------|---------------------------------|
| Parameters | f, b1, b2, cx, cy, k1-k4, p1-p4 |
| Adaptive camera model fitting | No |
| Optimization time | 10 seconds |
| Software version | 1.5.5.9097 |

Depth Maps

| | |
|-------|-----|
| Count | 238 |
|-------|-----|

Depth maps generation parameters

| | |
|------------------|---------------------|
| Quality | High |
| Filtering mode | Aggressive |
| Processing time | 11 hours 35 minutes |
| Software version | 1.5.5.9097 |

Dense Point Cloud

| | |
|--------------|----------------|
| Points | 60,022,726 |
| Point colors | 3 bands, uint8 |

Depth maps generation parameters

| | |
|-----------------|---------------------|
| Quality | High |
| Filtering mode | Aggressive |
| Processing time | 11 hours 35 minutes |

Dense cloud generation parameters

| | |
|------------------|--------------------|
| Processing time | 5 hours 46 minutes |
| Software version | 1.5.5.9097 |

Model

| | |
|---------------|-------------------------------|
| Faces | 7,563,667 |
| Vertices | 3,791,229 |
| Vertex colors | 3 bands, uint8 |
| Texture | 8,192 x 8,192, 4 bands, uint8 |

General**Depth maps generation parameters**

| | |
|-----------------|---------------------|
| Quality | High |
| Filtering mode | Aggressive |
| Processing time | 11 hours 35 minutes |

Reconstruction parameters

| | |
|-------------------------|-------------------|
| Surface type | Arbitrary |
| Source data | Dense cloud |
| Interpolation | Enabled |
| Strict volumetric masks | No |
| Processing time | 1 hours 4 minutes |

Texturing parameters

| | |
|------------------------|-----------------------|
| Mapping mode | Generic |
| Blending mode | Mosaic |
| Texture size | 8,192 |
| Enable hole filling | Yes |
| Enable ghosting filter | No |
| UV mapping time | 9 minutes 45 seconds |
| Blending time | 25 minutes 18 seconds |
| Software version | 1.5.5.9097 |

Orthomosaic

| | |
|-------------------|-----------------------|
| Size | 12,109 x 7,857 |
| Coordinate system | Local Coordinates (m) |
| Colors | 3 bands, uint8 |

Reconstruction parameters

| | |
|---------------------|-----------------------|
| Blending mode | Mosaic |
| Surface | Mesh |
| Enable hole filling | Yes |
| Processing time | 33 minutes 57 seconds |
| Software version | 1.5.5.9097 |

Software

| | |
|----------|------------------|
| Version | 1.5.5 build 9097 |
| Platform | Windows 64 |

Windy Model

Agisoft Metashape

**Processing Report
30 June 2021**



Survey Data

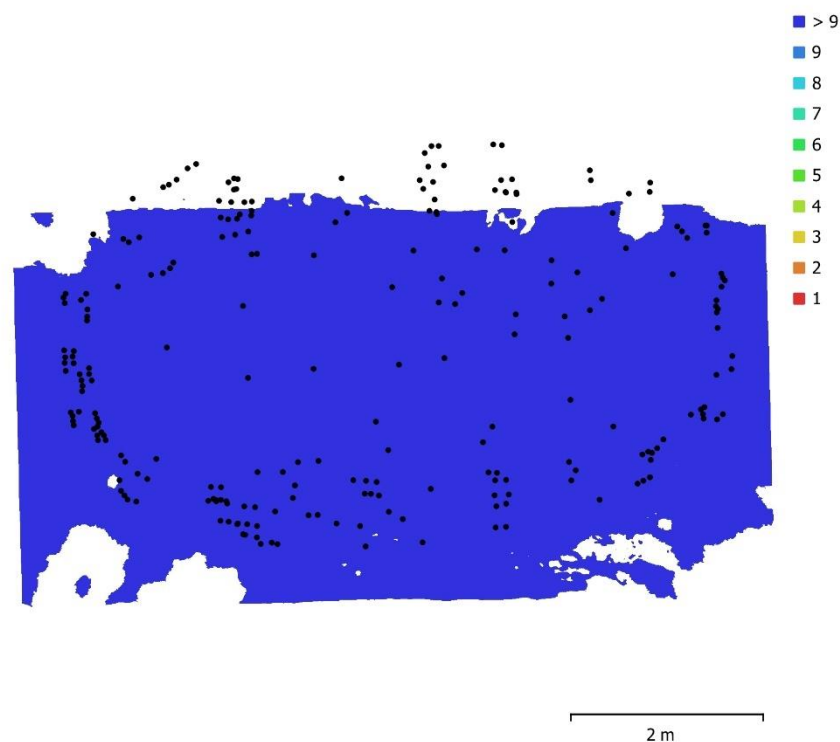


Fig. 1. Camera locations and image overlap.

| | | | |
|--------------------|---------------------|---------------------|-----------|
| Number of images: | 240 | Camera stations: | 238 |
| Flying altitude: | 2.55 m | Tie points: | 296,222 |
| Ground resolution: | 0.546 mm/pix | Projections: | 686,582 |
| Coverage area: | 29.4 m ² | Reprojection error: | 0.374 pix |

| Camera Model | Resolution | Focal Length | Pixel Size | Precalibrated |
|--------------------|-------------|--------------|----------------|---------------|
| NIKON D7200 (18mm) | 6000 x 4000 | 18 mm | 3.91 x 3.91 μm | No |

Table 1. Cameras.

Camera Calibration

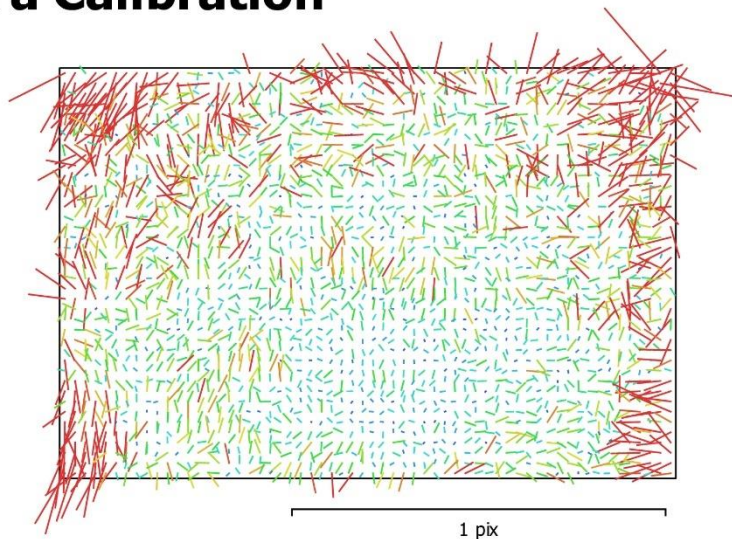


Fig. 2. Image residuals for NIKON D7200 (18mm).

NIKON D7200 (18mm)

240 images

| Type | Resolution | Focal Length | Pixel Size |
|-------|-------------|--------------|----------------|
| Frame | 6000 x 4000 | 18 mm | 3.91 x 3.91 μm |
| F: | 4672.48 | | |
| Cx: | -12.881 | B1: | -2.14728 |
| Cy: | 33.0382 | B2: | -0.215398 |
| K1: | -0.153338 | P1: | 0.000240938 |
| K2: | 0.110756 | P2: | 0.000835159 |
| K3: | -0.0153068 | P3: | 0.100359 |
| K4: | 0.0142017 | P4: | 0.107439 |

Scale Bars

| Label | Distance (m) | Error (m) |
|---------------------|--------------|--------------------|
| target 49_target 51 | 0.998712 | -0.00126763 |
| target 57_target 59 | 1.00034 | 0.000236445 |
| target 65_target 67 | 1.00036 | 0.000449679 |
| target 73_target 75 | 1.00068 | 0.000483074 |
| Total | | 0.000724287 |

Table 2. Control scale bars.

Digital Elevation Model

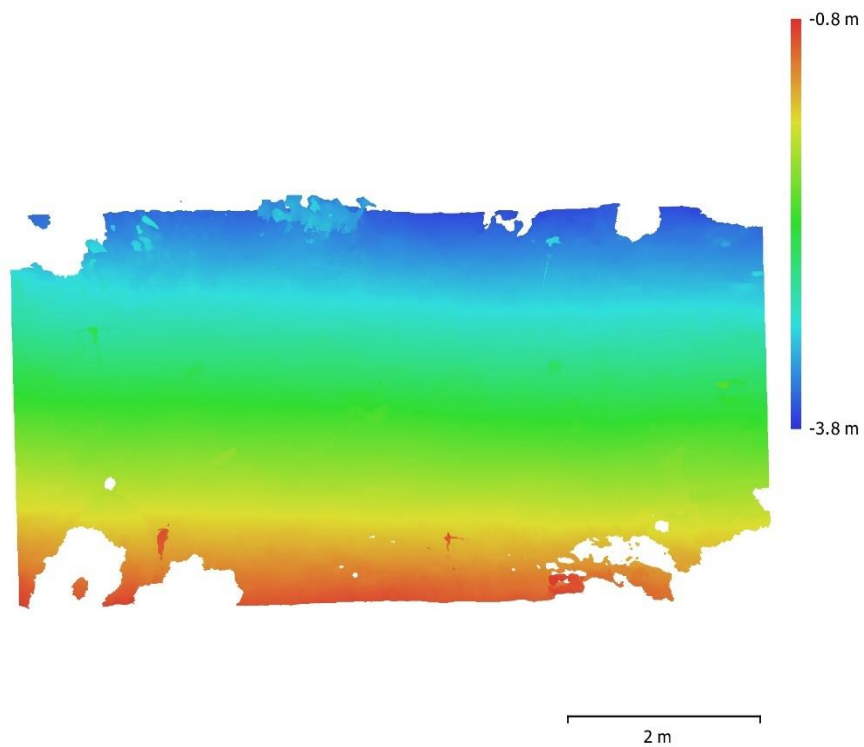


Fig. 3. Reconstructed digital elevation model.

Resolution: unknown
Point density: unknown

Processing Parameters

General

| | |
|-------------------|---------------------|
| Cameras | 240 |
| Aligned cameras | 238 |
| Markers | 24 |
| Scale bars | 4 |
| Coordinate system | WGS 84 (EPSG::4326) |
| Rotation angles | Yaw, Pitch, Roll |

Point Cloud

| | |
|--------------------------------|-------------------------|
| Points | 296,222 of 932,528 |
| RMS reprojection error | 0.113203 (0.373979 pix) |
| Max reprojection error | 0.68566 (3.91772 pix) |
| Mean key point size | 3.24414 pix |
| Point colors | 3 bands, uint8 |
| Key points | No |
| Average tie point multiplicity | 2.36537 |

Alignment parameters

| | |
|-------------------------------|----------------------|
| Accuracy | High |
| Generic preselection | No |
| Key point limit | 100,000 |
| Tie point limit | 50,000 |
| Adaptive camera model fitting | Yes |
| Matching time | 10 hours 11 minutes |
| Alignment time | 8 minutes 14 seconds |

Optimization parameters

| | |
|-------------------------------|---------------------------------|
| Parameters | f, b1, b2, cx, cy, k1-k4, p1-p4 |
| Adaptive camera model fitting | No |
| Optimization time | 37 seconds |
| Software version | 1.5.5.9097 |

Depth Maps

| | |
|-------|-----|
| Count | 223 |
|-------|-----|

Depth maps generation parameters

| | |
|------------------|-------------------|
| Quality | High |
| Filtering mode | Mild |
| Processing time | 6 hours 1 minutes |
| Software version | 1.5.5.9097 |

Dense Point Cloud

| | |
|--------------|----------------|
| Points | 63,934,390 |
| Point colors | 3 bands, uint8 |

Depth maps generation parameters

| | |
|-----------------|--------------------|
| Quality | High |
| Filtering mode | Aggressive |
| Processing time | 5 hours 55 minutes |

Dense cloud generation parameters

| | |
|------------------|-------------------|
| Processing time | 5 hours 4 minutes |
| Software version | 1.5.5.9097 |

Model

| | |
|---------------|-------------------------------|
| Faces | 13,363,672 |
| Vertices | 6,686,726 |
| Vertex colors | 3 bands, uint8 |
| Texture | 8,192 x 8,192, 4 bands, uint8 |

General**Depth maps generation parameters**

| | |
|-----------------|-------------------|
| Quality | High |
| Filtering mode | Mild |
| Processing time | 6 hours 1 minutes |

Reconstruction parameters

| | |
|-------------------------|-----------------|
| Surface type | Arbitrary |
| Source data | Depth maps |
| Interpolation | Enabled |
| Strict volumetric masks | No |
| Processing time | 1 days 15 hours |

Texturing parameters

| | |
|------------------------|----------------------|
| Mapping mode | Generic |
| Blending mode | Mosaic |
| Texture size | 8,192 |
| Enable hole filling | Yes |
| Enable ghosting filter | Yes |
| UV mapping time | 2 minutes 48 seconds |
| Blending time | 51 minutes 7 seconds |
| Software version | 1.5.5.9097 |

Orthomosaic

| | |
|-------------------|---------------------|
| Size | 28,353 x 18,164 |
| Coordinate system | WGS 84 (EPSG::4978) |
| Colors | 3 bands, uint8 |

Reconstruction parameters

| | |
|---------------------|-----------------------|
| Blending mode | Mosaic |
| Surface | Mesh |
| Enable hole filling | Yes |
| Processing time | 44 minutes 43 seconds |
| Software version | 1.5.5.9097 |

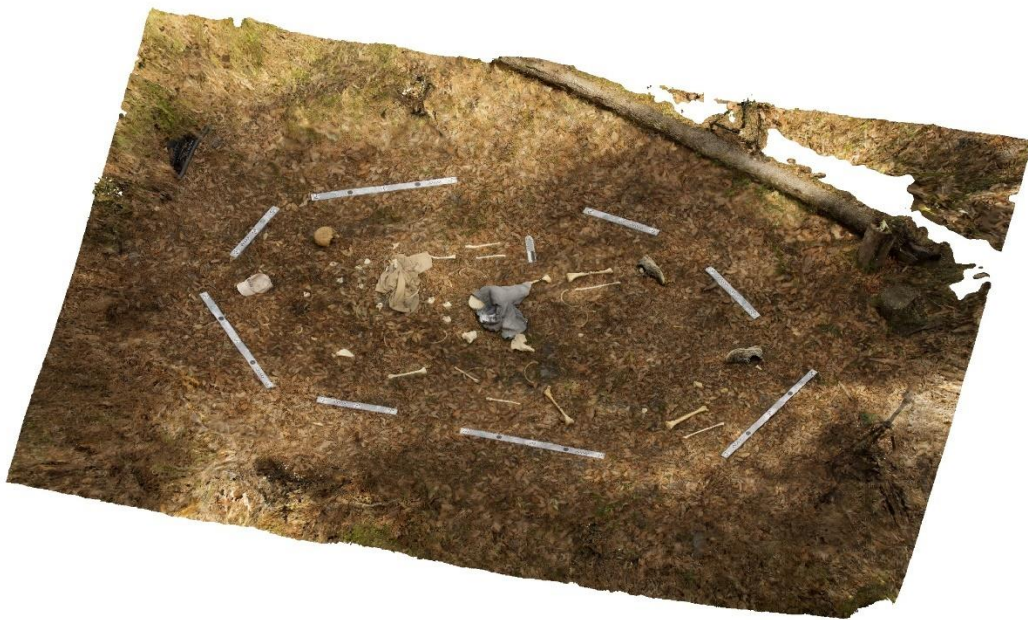
Software

| | |
|----------|------------------|
| Version | 1.5.5 build 9097 |
| Platform | Windows 64 |

Model 1C-1

Agisoft Metashape

Processing Report
15 July 2021



Survey Data

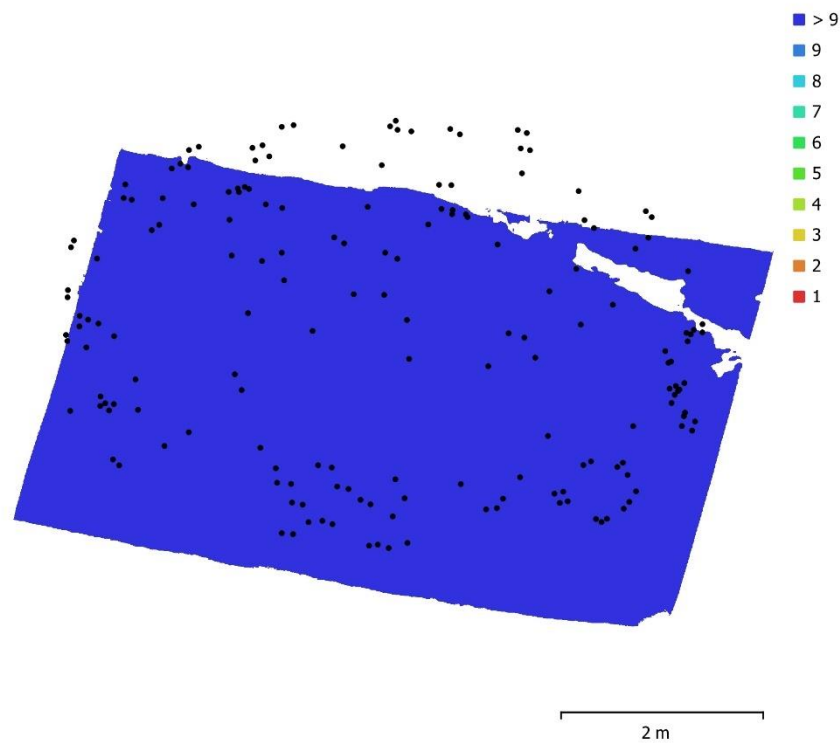


Fig. 1. Camera locations and image overlap.

| | | | |
|--------------------|---------------------|---------------------|-----------|
| Number of images: | 173 | Camera stations: | 173 |
| Flying altitude: | 2.2 m | Tie points: | 174,099 |
| Ground resolution: | 0.472 mm/pix | Projections: | 409,759 |
| Coverage area: | 24.9 m ² | Reprojection error: | 0.313 pix |

| Camera Model | Resolution | Focal Length | Pixel Size | Precalibrated |
|--------------------|-------------|--------------|----------------|---------------|
| NIKON D7200 (18mm) | 6000 x 4000 | 18 mm | 3.91 x 3.91 μm | No |

Table 1. Cameras.

Camera Calibration

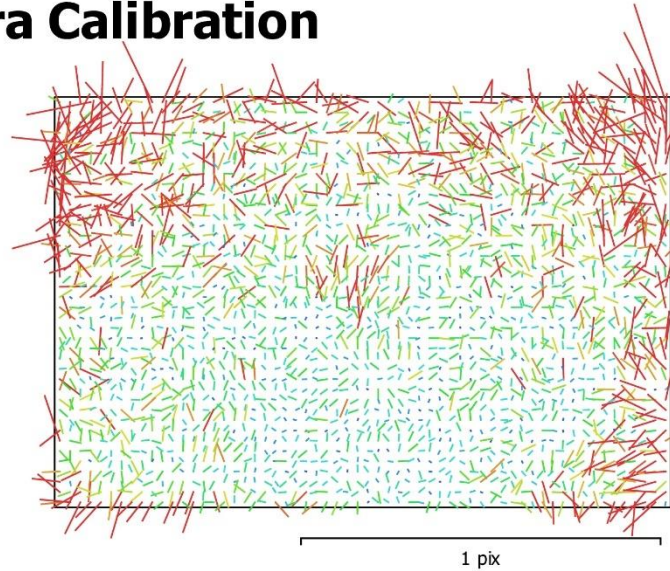


Fig. 2. Image residuals for NIKON D7200 (18mm).

NIKON D7200 (18mm)

173 images

| | | | |
|--------------|--------------------|--------------|--------------------------------------|
| Type | Resolution | Focal Length | Pixel Size |
| Frame | 6000 x 4000 | 18 mm | 3.91 x 3.91 μm |

| | Value | Error | F | Cx | Cy | B1 | B2 | K1 | K2 | K3 | K4 | P1 | P2 | P3 | P4 |
|-----------|---------------------|----------|------|------|-------|-------|-------|-------|-------|-------|-------|-------|-------|-------|-------|
| F | 4657.99 | 0.094 | 1.00 | 0.07 | -0.04 | -0.34 | 0.01 | -0.17 | 0.19 | -0.17 | 0.17 | -0.01 | 0.19 | 0.04 | -0.01 |
| Cx | -7.39044 | 0.072 | | 1.00 | -0.05 | -0.01 | 0.22 | 0.02 | -0.01 | -0.00 | 0.01 | 0.70 | 0.03 | 0.04 | -0.05 |
| Cy | -1.9427 | 0.14 | | | 1.00 | -0.55 | -0.21 | -0.02 | 0.01 | -0.00 | -0.00 | 0.10 | 0.15 | 0.04 | 0.10 |
| B1 | 2.6951 | 0.041 | | | | 1.00 | 0.09 | 0.01 | 0.00 | -0.00 | 0.00 | 0.01 | 0.02 | -0.10 | 0.01 |
| B2 | -1.0775 | 0.033 | | | | | 1.00 | 0.01 | -0.01 | 0.00 | -0.00 | -0.12 | 0.08 | -0.01 | -0.01 |
| K1 | -0.154077 | 8.4e-005 | | | | | | 1.00 | -0.97 | 0.92 | -0.87 | 0.04 | -0.15 | 0.16 | -0.14 |
| K2 | 0.107433 | 0.00054 | | | | | | | 1.00 | -0.99 | 0.95 | -0.02 | 0.14 | -0.19 | 0.17 |
| K3 | -0.00475111 | 0.0013 | | | | | | | | 1.00 | -0.99 | 0.00 | -0.12 | 0.17 | -0.15 |
| K4 | 0.00357357 | 0.0011 | | | | | | | | | 1.00 | 0.01 | 0.10 | -0.13 | 0.12 |
| P1 | 1.91299e-006 | 3.5e-006 | | | | | | | | | | 1.00 | -0.05 | 0.03 | -0.04 |
| P2 | 0.000483374 | 7.3e-006 | | | | | | | | | | | 1.00 | -0.63 | 0.67 |
| P3 | -0.27865 | 0.053 | | | | | | | | | | | | 1.00 | -0.96 |
| P4 | -0.509155 | 0.081 | | | | | | | | | | | | | 1.00 |

Table 2. Calibration coefficients and correlation matrix.

Scale Bars

| Label | Distance (m) | Error (m) |
|---------------------|--------------|--------------------|
| target 52_target 54 | 0.499707 | -0.000212757 |
| target 57_target 59 | 1.00073 | 0.000634276 |
| target 68_target 70 | 0.499098 | -3.17059e-005 |
| target 73_target 75 | 0.999708 | -0.00051181 |
| Total | | 0.000421464 |

Table 3. Control scale bars.

Digital Elevation Model

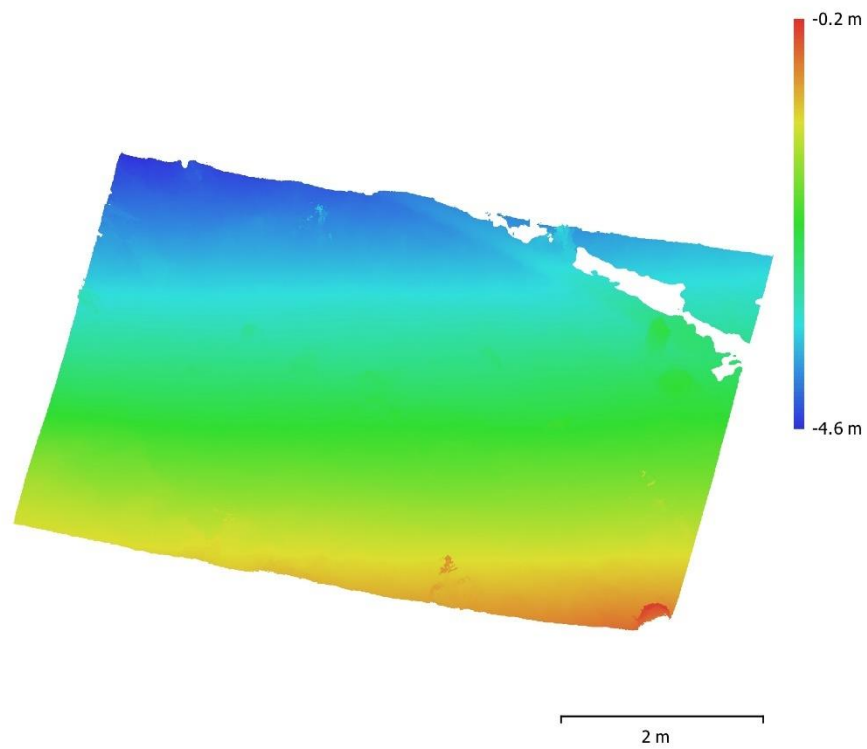


Fig. 3. Reconstructed digital elevation model.

Resolution: unknown
Point density: unknown

Processing Parameters

General

| | |
|-------------------|-----------------------|
| Cameras | 173 |
| Aligned cameras | 173 |
| Markers | 24 |
| Scale bars | 4 |
| Coordinate system | Local Coordinates (m) |
| Rotation angles | Yaw, Pitch, Roll |

Point Cloud

| | |
|--------------------------------|-------------------------|
| Points | 174,099 of 940,029 |
| RMS reprojection error | 0.109688 (0.313369 pix) |
| Max reprojection error | 0.692462 (1.96931 pix) |
| Mean key point size | 2.80169 pix |
| Point colors | 3 bands, uint8 |
| Key points | No |
| Average tie point multiplicity | 2.40501 |

Alignment parameters

| | |
|-------------------------------|-----------------------|
| Accuracy | High |
| Generic preselection | No |
| Key point limit | 100,000 |
| Tie point limit | 40,000 |
| Adaptive camera model fitting | Yes |
| Matching time | 10 hours 43 minutes |
| Alignment time | 41 minutes 48 seconds |

Optimization parameters

| | |
|-------------------------------|---------------------------------|
| Parameters | f, b1, b2, cx, cy, k1-k4, p1-p4 |
| Adaptive camera model fitting | No |
| Optimization time | 5 seconds |
| Software version | 1.5.5.9097 |

Depth Maps

| | |
|-------|-----|
| Count | 172 |
|-------|-----|

Depth maps generation parameters

| | |
|------------------|--------------------|
| Quality | High |
| Filtering mode | Aggressive |
| Processing time | 6 hours 10 minutes |
| Software version | 1.5.5.9097 |

Dense Point Cloud

| | |
|--------------|----------------|
| Points | 40,502,103 |
| Point colors | 3 bands, uint8 |

Depth maps generation parameters

| | |
|-----------------|--------------------|
| Quality | High |
| Filtering mode | Aggressive |
| Processing time | 6 hours 10 minutes |

Dense cloud generation parameters

| | |
|------------------|-------------------|
| Processing time | 6 hours 0 minutes |
| Software version | 1.5.5.9097 |

Model

| | |
|---------------|-------------------------------|
| Faces | 8,100,336 |
| Vertices | 4,060,678 |
| Vertex colors | 3 bands, uint8 |
| Texture | 8,192 x 8,192, 4 bands, uint8 |

General**Depth maps generation parameters**

| | |
|-----------------|--------------------|
| Quality | High |
| Filtering mode | Aggressive |
| Processing time | 6 hours 10 minutes |

Reconstruction parameters

| | |
|-------------------------|--------------------|
| Surface type | Arbitrary |
| Source data | Dense cloud |
| Interpolation | Enabled |
| Strict volumetric masks | No |
| Processing time | 5 hours 35 minutes |

Texturing parameters

| | |
|------------------------|-----------------------|
| Mapping mode | Generic |
| Blending mode | Mosaic |
| Texture size | 8,192 |
| Enable hole filling | Yes |
| Enable ghosting filter | No |
| UV mapping time | 8 minutes 55 seconds |
| Blending time | 20 minutes 16 seconds |
| Software version | 1.5.5.9097 |

Orthomosaic

| | |
|-------------------|-----------------------|
| Size | 13,519 x 10,330 |
| Coordinate system | Local Coordinates (m) |
| Colors | 3 bands, uint8 |

Reconstruction parameters

| | |
|---------------------|-----------------------|
| Blending mode | Mosaic |
| Surface | Mesh |
| Enable hole filling | Yes |
| Processing time | 17 minutes 47 seconds |
| Software version | 1.5.5.9097 |

Software

| | |
|----------|------------------|
| Version | 1.5.5 build 9097 |
| Platform | Windows 64 |

LIST OF REFERENCES

- Agisoft LLC. (2019a). Agisoft Metashape Professional Version 1.5 [Computer Software]. St. Petersburg, RU; Agisoft LLC.
- Agisoft LLC. (2019b). *Agisoft Metashape User Manual: Professional Edition, Version 1.5*. St. Petersburg, RU; Agisoft LLC.
- Al-kheder, S., Al-shawebkeh, Y., & Haala, N. (2008). Developing a documentation system for desert palaces in Jordan using 3D laser scanning and digital photogrammetry. *Journal of Archaeological Science* 36(2):537-546.
- Baier, W., & Rando, C. (2016). Developing the use of Structure-from-Motion in mass grave documentation. *Forensic Science International* 261: 19-25.
- Baltsavias E.P. (1999). A comparison between photogrammetry and laser scanning. *ISPRS Journal of Photogrammetry and Remote Sensing* 54:83–94.
- Barazzetti, L., Binda, L., Scaioni, M., & Taranto, P. (2011a). Photogrammetric survey of complex geometries with low-cost software: Application to the ‘G1’ temple in MySon Vietnam. *Journal of Cultural Heritage*, 12, 253-262.
- Barazzetti, L., Mussio, L., Remondino, R., & Scaioni, M. (2011b). Targetless camera calibration. *International Archives of the Photogrammetry, Remote Sensing and Spatial Information Sciences*, 38, 335-342.
- Barazzetti, L., Sala, R., Scaioni, M., Cattaneo, C., Gibelli, D., Giussani, A., Poppa, P., Roncoroni, F., & Vandone, A. (2012). 3D scanning and imaging for quick documentation of crime and accident scenes. *Proc. SPIE 8359, Sensors, and Command, Control, Communications, and Intelligence (C3I) Technologies for Homeland Security and Homeland Defense XI*, 835910; doi: 10.1117/12.920728.

- Benavides López, J.A., Aranda Jiménez, G., Sánchez Romero, M., Alarcón García, E.,
Fernández Martín, S., Lozano Medina, A., & Esquivel Guerrero, J.A. (2016). 3D
modelling in archaeology: The application of Structure from Motion methods to the study
of the megalithic necropolis of Panoria (Granada, Spain). *Journal of Archaeological
Science*, 10, 495-506.
- Burdziakowski P, Bobkowska K. (2021). UAV Photogrammetry under Poor Lighting
Conditions—Accuracy Considerations. *Sensors*. 21(10):3531.
<https://doi.org/10.3390/s21103531>
- Burtch, R. (2008) History of Photogrammetry. *The Center for Photogrammetric Training,
Surveying Engineering Department, Ferris State University*.
- Campana, S., Sordini, M., Bianchi, G., Fichera, G.A., Lai, L. (2012). 3D Recording and Total
Archaeology: From Landscapes to Historical Buildings. *International Journal of
Heritage in the Digital Era* 1:443–460.
- Carbonnell, M. (1968) L'Histoire et la situation presente des applications de la pho a
l'architecture. *11th Congress of the International Society for Photogrammetry:*
Commission V. Lausanne.1-42.
- Christensen, A.M., Passalacqua, N.V., & Bartelink, E.J. (2014). *Forensic Anthropology: Current
Methods and Practice*. Oxford, UK: Academic Press.
- Church E. (2019). *The forensic utility of photogrammetry in surface scene documentation*.
Boston University Libraries [Internet]. Available from:
<https://open.bu.edu/handle/2144/38598>
- Colwill S. (2016). Low-cost crime scene mapping: reviewing emerging freeware, low-cost
methods of 3D mapping and applying them to crime scene investigation and forensic

- evidence. Murdoch University Research Repository [Internet]. Available from:
<https://researchrepository.murdoch.edu.au/id/eprint/35143/>
- Cultural Heritage Imaging. (2021). *Guidelines for Calibrated Scale Bar Placement and Processing, Version 2.0*. San Francisco, CA: Cultural Heritage Imaging.
- De Reu, J., De Smedt, P., Herremans, D., Van Meirvenne, M., Laloo, P., De Clercq, W., (2014). On introducing an image-based 3D reconstruction method in archaeological excavation practice. *Journal of Archaeological Science*, 41, 251-262.
- Dirkmaat, D.C., & Adovasio, J.M. (1997). The role of archaeology in the recovery and interpretation of human remains from an outdoor forensic setting. In W.D. Haglund, & M.H. Sorg (Eds.), *Forensic taphonomy and the postmortem fate of human remains*. CRC Press.
- Dirkmaat, D.C., & Cabo, L.L. (2012). Forensic anthropology: Embracing the new paradigm. In D.C. Dirkmaat (Ed.), *A companion to forensic anthropology*. Blackwell Publishing.
- Dirkmaat D.C. (2015). *A companion to forensic anthropology*. Malden, MA: Wiley-Blackwell.
- Doneus, M., Verhoeven, G., Fera, M., Briese, Ch., Kcera, M., & Neubauer, W. (2011). From deposit to point cloud – a study of low-cost computer vision approaches for the straightforward documentation of archaeological excavation. *Geoinformatics CTU FCE*, 6, 81-88.
- Douglass, M., Lin, S., & Chodoronek, M. (2015). The application of 3D photogrammetry for in-field documentation of archaeological features. *Advances in Archaeological Practices*, 3(2), 136-152.
- Dupras, T.L., Schultz, J.J., Wheeler, S.J., & Williams, L.J. (2012). *Forensic Recovery of Human Remains: Archaeological Approaches* 2nd edition. Boca Raton, Florida: CRC Press.

- Edelman, G.J., & Aalders, M.C. (2018). Photogrammetry using visible, infrared, hyperspectral and thermal imaging of crime scenes. *Forensic Science International* 292:181-189.
- Ferrell, M. J. (2020). *Applications of Close-range Photogrammetry for Documenting Human Skeletal Remains in Obstructed Wooded Environments*. University of Central Florida STARS: Master's Thesis.
- Ferrell M, & Schultz J. (2021). Documenting Skeletal Scatters in Obstructed Wooded Environments Using Close-Range Photogrammetry. *Forensic Anthropology*.
- Forte M, Dell'Unto, N., Issavi, J., Onsurez, L., Lercari, N. (2012). 3D Archaeology at Catalhöyük. *International Journal of Heritage in the Digital Era* 1:351–378.
- Fussell A. (1982). Terrestrial photogrammetry in archaeology. *World Archaeology* 14:157–172.
- Gidusko, K.A. (2018). *Testing the Capability of Close-Range Photogrammetry to Document Outdoor Forensic Scenes with Skeletal Remains Using Mock Scenarios*. University of Central Florida STARS: Master's Thesis.
- Gonizzi Barsanti, S., Remondino, F., Visintini D. (2013). 3D SURVEYING AND MODELING OF ARCHAEOLOGICAL SITES – SOME CRITICAL ISSUES –. *ISPRS Annals of the Photogrammetry, Remote Sensing and Spatial Information Sciences* II-5/W1:145–150.
- Gonzalez-Jorge, H., Solla, M., Martinez-Sanchez, J., & Arias, P. (2012). Comparison between laser scanning, single-image rectification and ground-penetrating radar technologies in forensic science. *Measurement* 45:836-843.
- Granshaw, S.I. (2016). Photogrammetric terminology: Third edition. *The Photogrammetric Record*, 31(154), 210-251.

- Green, S., Bevan, A., & Shapland, M. (2014). A comparative assessment of structure from motion methods for archaeological research. *Journal of Archaeological Science* 46:173-181.
- Hochrein MJ. 2003. A bibliography related to crime scene interpretation: with emphases in forensic geotaphonomic and forensic archaeological field techniques. Washington, D.C.: U.S. Dept. of Justice, Federal Bureau of Investigation.
- Howard, P. (2007). *Archaeological surveying and mapping: Recording and depicting the landscape*. Routledge.
- Howland, M.D., Kuester, F., & Levy, T.E. (2014). Photogrammetry in the field: Documenting, recording, and presenting archaeology. *Mediterranean Archaeology and Archaeometry*, 14(4), 101-108.
- Linder, W. (2003). *Digital photogrammetry: Theory and applications*. Springer.
- Mayer, C., Gomes Pereira, L.M., & Kersten, T.P. (2018). A comprehensive workflow to process UAV images for the efficient production of accurate geo-information. *Proceedings of the IX National Conference on Cartography and Geodesy*, Amafia, Portugal, 1-8.
- McCollum, M.L. (2020). *Refining the Data Collection Methodology of Outdoor Forensic Scenes Involving Scattered Human Remains Using Close-Range Photogrammetry*. University of Central Florida STARS: Master's Thesis.
- McPherron, S. P., Gernat, T., & Hublin, J.-J. (2009). *Structured light scanning for high-resolution documentation of in situ archaeological finds*. *Journal of Archaeological Science*. <https://www.sciencedirect.com/science/article/pii/S030544030800160X>.
- Mikhail, E.M., Bethel, J.S., & McGlone, J.C. (2001). *Introduction to modern photogrammetry*. John Wiley & Sons, Inc.

- National Forensic Science Technology Center. (2013). *Crime scene investigation: A guide for law enforcement*. National Institute of Justice, U.S. Department of Justice.
<https://shop.nfstc.org/crime-scene-investigation-guide/>
- Nedergaard, N.J., Heinen, F., Sloth, S., Hébert-Losier, K., Holmberg, H-C., Kersting, U.G.. (2013). The effect of light reflections from the snow on kinematic data collected using stereo-photogrammetry with passive markers. *Sports Engineering* 17:97–102.
- Nikon Inc. (2020). *AF-S DX NIKKOR 18-140mm f/3.5-5.6G ED VR*.
<https://www.nikonusa.com/en/nikon-products/product/camera-lenses/af-s-dx-nikkor-18-140mm-f%252f3.5-5.6g-ed-vr.html#tab-ProductDetail-ProductTabs-TechSpecs>
- Olson, B.R., Placchetti, R.A., Quartermaine, J., Killebrew, A.E. (2013). The Tel Akko Total Archaeology Project (Akko, Israel): Assessing the suitability of multi-scale 3D field recording in archaeology. *Journal of Field Archaeology* 38:244–262.
- Ozbek, M., Rixen, D.J., Erne, O., Sanow, G. (2010). Feasibility of monitoring large wind turbines using photogrammetry. *Energy* 35:4802–4811.
- Partsinevelos, P., Mertikas, S., Agioutantis, Z., Tsioukas, V., Tripolitsiotis, A., Zervos, P. (2014). Rockfall detection along road networks using close range photogrammetry. *Second International Conference on Remote Sensing and Geoinformation of the Environment (RSCy2014)*.
- Portalés, C., Lerma, J.L., Pérez, C. (2009). Photogrammetry and augmented reality for cultural heritage applications. *The Photogrammetric Record* 24:316–331.
- Porter, S.T., Huber, N., Hoyer, C., Floss, H. (2016). Portable and low-cost solutions to the imaging of Paleolithic art objects: A comparison of photogrammetry and reflectance transformation imaging. *Journal of Archaeological Science: Reports* 10:859–863.

- Randles, B., Jones, B., Welcher, J., Szabo, T. et al., 2010 "The Accuracy of Photogrammetry vs. Hands-on Measurement Techniques used in Accident Reconstruction," *SAE Technical Paper 2010-01-0065*, 2010, <https://doi.org/10.4271/2010-01-0065>.
- Sapirstein, P., & Murray, S. (2017). Establishing best practices for photogrammetric recording during archaeological fieldwork. *Journal of Field Archaeology*, 42(4), 337-350.
- Sapirstein, P. (2016). Accurate measurements with photogrammetry at large sites. *Journal of Archaeological Science* 66: 137-145.
- Schultz, J. J., & Dupras, T. L. (2008). The Contribution of Forensic Archaeology to Homicide Investigations. *Homicide Studies* 12(4):399-413.
- Teza G, Pesci A, Ninfo A. 2016. Morphological Analysis for Architectural Applications: Comparison between Laser Scanning and Structure-from-Motion Photogrammetry. *Journal of Surveying Engineering* 142:04016004.
- USGS National UAS Project Office (2017). *Unmanned Aircraft Systems Data Post-Processing: Structure-from-Motion Photogrammetry*. Reston, VA: USGS.
- Willis, M.D., Koenig, C.W., Black, S.L., & Castañeda, A.M. (2016). Archaeological 3D mapping: the structure from motion revolution. *Journal of Texas Archaeology and History*, 3, 1-36.